Eco-evolutionary modeling of soil microbial decomposition in a warming climate

Elsa Abs

▶ **To cite this version:**

Elsa Abs. Eco-evolutionary modeling of soil microbial decomposition in a warming climate. Symbiosis. Université Sorbonne Paris Cité, 2019. English. NNT : 2019USPCC029 . tel-02614092

HAL Id: tel-02614092
https://theses.hal.science/tel-02614092

Submitted on 20 May 2020

HAL is a multi-disciplinary open access archive for the deposit and dissemination of scientific research documents, whether they are published or not. The documents may come from teaching and research institutions in France or abroad, or from public or private research centers.

L'archive ouverte pluridisciplinaire **HAL**, est destinée au dépôt et à la diffusion de documents scientifiques de niveau recherche, publiés ou non, émanant des établissements d'enseignement et de recherche français ou étrangers, des laboratoires publics ou privés.

Thèse de doctorat
de l'Université Sorbonne Paris Cité
Préparée à l'Université Paris Diderot

Ecole doctorale 474 Frontière du Vivant

Institut de Biologie de l'Ecole Normale Supérieure de Paris
Unité Mixte Internationale iGLOBES

Eco-evolutionary modeling of soil microbial decomposition in a warming climate

Par Elsa Abs

Thèse de doctorat d'Ecologie

Dirigée par Pr. Régis Ferrière et Pr. Scott Saleska

Présentée et soutenue publiquement à Paris le 8 janvier 2019

Pr. Pakdaman Khashayar (Université Paris Diderot)	Président du jury
Pr. Steven Allison (UC Irvine)	Rapporteur
Dr. Sonia Kéfi (CNRS Montpellier)	Rapporteure
Dr. Claire de Mazancourt (CNRS Moulis)	Examinatrice
Dr. Florence Débarre (CNRS Paris)	Examinatrice
Pr. Régis Ferrière (ENS & Université d'Arizona)	Directeur de thèse
Pr. Scott Saleska (Université d'Arizona)	Co-directeur de thèse

Except where otherwise noted, this work is licensed under
http://creativecommons.org/licenses/by-nc-nd/3.0/

Remerciements

Mes remerciements vont d'abord à Régis Ferrière qui m'a transmis à la fois rigueur et goût du risque, qui m'a appris à ne jamais dire non, qui a partagé avec la générosité qui le caractérise sa communauté scientifique des deux côtés de l'Atlantique.

Scott Saleska, thank you for accompanying me all along. Thank you for those long brainstorming sessions, for letting me teach in your class these past 3 years, for your great feedbacks and being such a fun advisor.

Hélène Leman, mathématicienne à l'INRIA de l'ENS Lyon, merci d'avoir été une collaboratrice sur le travail constituant le chapitre 3 de cette thèse, merci d'avoir été ma professeure personnelle de mathématiques et de code, merci pour tes visites et les Skypes et Whatsapp à toute heure.

Je voudrais remercier également les institutions et les personnes que j'y ai croisées qui ont accompagné ces trois années de recherche. L'IBENS, qui m'a toujours accueillie comme si je n'étais jamais partie à chacun de mes passages, pour ses séminaires, ses déjeuners familiaux, sa vue, sa lumière et la fontaine de sa voisine du 45. Je voudrais remercier en particulier l'équipe "Mathématique Eco-Evolutive". Stéphane Legendre, avec qui j'ai fait les premiers tests de mon modèle sur son logiciel ZEN et parlé musique, ciné, BD et politique pendant que ça tournait. David Claessen, parce que c'est toi qui a enseigné à ma cohorte mastérienne la dynamique adaptative, et en anglais. Je remercie aussi Bernard Cazelles, Minus van Baalen et Silvia de Monte, pour nos discussions, pour vos recommandations. J'y ai trouvé de super-pairs : Célian Colon, pour ces déjeuners sur la science sur la vie et pour l'article dédicacé qui m'a tenu compagnie, perché au-dessus de mon bureau de Tucson, Boris Sauterey, pour le plaisir de refaire la science et la politique à l'heure du café ou de l'apéro. J'ai adoré y croiser Orso Romano, petit soleil d'Italie, Clara Champagne, toujours prête à donner un coup de main, Phuong Nguyen, pour l'organisation des séminaires, Guilhem Doulcier, pour avoir été mon acolyte à Montpellier. The University of Arizona, which has hosted me as a visiting scholar and that I have way more than just visited over the five past years. Thank you for the Monday and

Tuesday seminars, for giving me the opportunity to present my work every year, for the meetings at Biosphere 2, for the "hot papers" meetings. Thank you to the Saleska lab, my adoptive lab, Moira Hough, Loren Albert, Marielle Smith, Tyeen Taylor, thank you to the Martinez, the Bronstein labs and the Masel group for brainstorming over my work and the regular meetings that we shared at different times. Special thanks to Rachel Gallery and Dave Moore. I loved attending your class on terrestrial ecosystems ecology, thank you Rachel for beeing part of my thesis committee, for creating and leading the 500 WS Tucson POD, thank you both for advising me and for being awesome human beings. Super special thanks to the best mentor and friend Laura Meredith. Thank you for listening to so many of my talks and for your feedbacks, always to the point, for reviewing my applications, for singing (shouting?) with me at the protests for science, for women, for climate change. Special thanks finally to all the women of 500 WS Tucson POD, and to Natasha MacBean, Aditi Sengupta, Soumaya Belmecheri and Fernanda Valdovinos, who on top of being awesome scientists, have been supportive of askWOT since day 1. Merci à l'UMI iGLOBES de m'avoir accueillie dans vos bureaux ce dernier semestre. Ruth Gosset, pour ton rire si communicatif, François-Michel Le Tourneau, de nous embarquer à la recherche des orpailleurs guyanais. Côté français, Paris Diderot pour la prise en charge administrative de ma thèse. Le programme Frontières du Vivant du CRI pour son équipe de visionnaires enthousiastes, pour m'avoir permis de rencontrer J, ma cagole from another mother, Jo, Paul, Hippolyte, Ignacio, Nadine et tous les autres. Merci à Sofie Leon d'avoir été une super coordinatrice durant ma première année et un géant merci à Elodie Kaslikowski d'avoir tout géré cette année. Merci à la chaire Véolia qui m'a toujours accueillie à bras ouverts, malgré mes retours en France en pointillé, aux journées de séminaires et surtout aux écoles d'été d'Aussois. J'y ai rencontré des chercheurs trop top, Sylvain Billiard, Colin Fontaine, Diala Abu Awad, Coralie Fritsch et retrouvé Hélène Leman, Nicolas Loeuille, Aurore Picot. Beaucoup sont derrière l'organisation de ces rencontres géniales, avec en première ligne Sylvie Méléard, merci.

Pierre-Henri Gouyon, merci de me suivre depuis le début, de mon premier stage d'agro jusqu'à mon comité de thèse, de me pousser à explorer sans sourciller. Nicolas Loeuille, merci pour tes précieux conseils, ta finesse et ta générosité.

J’envoie au quatre coins du monde mes pensées reconnaissantes à mes copains de master. Aurore Picot, petit bijou, merci Aussois de nous avoir permis de nous recroiser. Léa Blondel, j’arrive à Montréal, prépare-toi. Pierre Quévreux et Thomas Koffel, quel plaisir de vous retrouver en conf’ sur le sol américain.

Je veux remercier aussi les professeurs de ma très lointaine jeunesse. Juliette Yilmazian, ma professeure de piano. Sylviane Lemmi, qui me faisait lire Georges Sand pour comprendre Chopin. Joachim Martin, Patrick Vargas, Marc Parenti, pépites de l’enseignement des mathématiques et de la physique.

Laurent Ripoll, ça fait des années que j’attends de pouvoir te mettre dans mes crédits. Je te remercie énormément d’être ce que tu es. Sarah Khoubbaz, Kela Vidal, Elia Lesourt, mes trois mousquetaires, mes trois bombes. Trop fière d’être votre pote. Martin Prieur-Bley (et oui Tinmar c’est très sérieux), Noémie Monnier, mes amours rencontrés à l’agro, maintenant amours pour la vie. Justine Cavanié, mon boubou, mon rock, mon soleil. Juliette, def my sister from another mother. Clara Bastid, ma plus vieille amie, force de la nature. Saba Ijadi, thank you for sharing so many adventures. Serena Sahajian, Josh Wysocki, Edgar van Tinkle, mes coeurs de coeur. Cora and Will, my loves. Kayla Hale-Sale, my best friend in this adventure. Erika D’Souza, thank you for listening to so many of my talks even though you could not care less about microbes. Bérénice Geoffray, Clem Alba, Margaux Stypak, Flora Vincent vous êtes des meufs de ouf. Margaux Guyon, merci pour les correcs, à bientôt à Mexico. Adrien, le seul qui a réussi à m’apprendre la ponctualité, mon coach perso pendant un an, mon petit loup, merci. Merci à la team SF, Robin, Rico, Laetouch, Nato pour les bureaux de travail et le kiff. My American coeurs: the whole askWOT crew, Cora, Serena, Lizzy, Ellie, Jeanne, Mega, Eddika, Caitlin, Andrea, Maxine, Luna. The espresso crew: Nate, Daniel (and Jenna), Danny, Will, Paul, Domino, Isaiah, Kim, Miranda. My climbing team: Don, Karen, Cat, Abel, Gus, Kelli, Kim, Annette. Ysa, Alex, Soumaya, Paul. Thank you all for making my life in Tucson.

Enfin, le plus chaud, le plus intense, le plus drama pour la fin. Mom, dad, Alice, Robin, vous êtes le sang. Je vous aime à la mort. En toute sobriété.

Abstract – Résumé

Keywords

Climate change - Carbon cycle – Decomposition - Global predictions - Microbial evolution - Adaptive dynamics - Soil-climate feedbacks - Evolution of cooperation - Individual-based models

Abstract

One major source of uncertainty in global climate predictions is the extent to which global warming will increase atmospheric CO_2 concentrations through enhanced microbial decomposition of soil organic matter. There is therefore a critical need for models that mechanistically link decomposition to the dynamics of microbial communities, and integration of these mechanistic models in global projection models of the Earth system. Mathematical models of soil microbial decomposition models have recently been introduced to predict soil C stocks and heterotrophic soil respiration, especially in the context of climate change. Thus far, models focused on physiological and ecological mechanisms of microbial responses, leaving the role of evolutionary adaptation poorly understood. My thesis addresses this gap and evaluates the hypothesis that microbial evolutionary adaptation to warming can have a significant impact on the global carbon cycle. After reviewing mechanistic, non-evolutionary microbial models of decomposition, I construct an eco-evolutionary spatially explicit, stochastic model, scaling up from microscopic processes acting at the level of cells and extracellular molecules. I use an approximated version of the model (spatially implicit, deterministic) to investigate the eco-evolutionary response of a soil microbe-enzyme system to warming, under three possible scenarios for the influence of temperature on microbial activity. In the absence of microbial evolution, warming results in soil carbon loss to the atmosphere (an amplification of climate change) in all scenarios. Microbial evolutionary adaptation generally aggravates soil carbon loss in cold ecosystems, and may aggravate, buffer or even reverse carbon loss in warm ecosystems. Constraining the model with observations from five contrasting

biomes reveals evolutionary aggravation of soil carbon loss to be the most likely outcome. Earth-scale projections of carbon stocks that integrate my eco-evolutionary model support the prediction of a significant global aggravation of soil C loss due to microbial evolution. Dormant soils, in which microbial activity is very low, play a special role in the long-term eco-evolutionary dynamics of global soil carbon, since in these regions, the negative effect of evolution on soil carbon stocks may not kick in until the microbial community shifts from dormant to active, and may thus be delayed by decades. Overall, my work is a first step toward predictive modeling of eco-evolutionary dynamics of carbon cycling; it also lays the ground for a broad future research program that will empirically test model predictions about the role of evolutionary mechanisms in different systems across the globe, by leveraging the growing global archive of soil metagenomics data to quantify variations in microbial metabolic functions and their response to selection.

Mots clés

Changement climatique - Cycle du carbone – Décomposition - Projections globales - Evolution microbienne - Dynamiques adaptatives - Rétroaction sol-climat - Evolution de la coopération - Modèles individu-centrés

Résumé

L'une des principales sources d'incertitude des projections climatiques globales tient à l'activité microbienne des sols : dans quelle mesure le réchauffement de la planète entraînera-t-il une augmentation des concentrations de CO_2 dans l'atmosphère du fait d'une décomposition accrue de la matière organique par les communautés microbiennes des sols ? Mieux évaluer, voire réduire, cette incertitude requiert le développement de modèles mathématiques mécanistes reliant la décomposition à la dynamique des communautés microbiennes et l'intégration de ces modèles dans les simulations globales. Les modèles mathématiques de décomposition de la matière organique du sol représentent explicitement le compartiment microbien et sont donc à même de mettre en relation biomasse microbienne, production d'enzymes de dégradation de la matière organique, stocks de carbone du sol. Formulés dans le contexte du changement climatique, ces modèles se sont concentrés sur les mécanismes physiologiques et écologiques des réponses microbiennes à l'augmentation de la température, ignorant les effets possibles de l'adaptation évolutive. Ma thèse vise à combler cette lacune, en évaluant l'hypothèse selon laquelle l'adaptation évolutive microbienne au réchauffement peut avoir un impact significatif sur le cycle global du carbone. Après avoir passé en revue des modèles de décomposition microbienne mécanistes et non évolutifs, je construis un modèle stochastique spatialement explicite et éco-évolutif, basé sur des processus microscopiques des cellules et des molécules extracellulaires. J'utilise une approximation du modèle (spatialement implicite, déterministe) pour étudier la réponse éco-évolutive au réchauffement d'un système microbe-enzyme du sol, dans trois scénarios possibles d'influence de la température sur l'activité

microbienne. En l'absence d'évolution microbienne, le réchauffement entraîne une perte de carbone dans le sol (une accélération du changement climatique) dans tous les scénarios. L'adaptation évolutive microbienne aggrave généralement la perte de carbone du sol dans les écosystèmes froids et peut aggraver, amortir ou même inverser la perte de carbone (et donc augmenter la séquestration du carbone) dans les écosystèmes chauds. En contraignant le modèle avec les observations de cinq biomes distincts je montre que l'aggravation évolutive de la perte de carbone du sol est l'issue la plus probable. Enfin, en intégrant mon modèle éco-évolutif dans une projection globale des stocks de carbone du sol à l'échelle de la Terre, je confirme la prévision d'une aggravation mondiale significative de la perte de carbone dans le sol due à l'évolution microbienne. Les sols dormants, dans lesquels l'activité microbienne est très faible, jouent un rôle particulier dans la dynamique éco-évolutive à long terme du carbone du sol global, car dans ces régions, l'effet négatif de l'évolution sur les stocks de carbone du sol ne se manifesterait pas avant la sortie de la dormance microbienne et pourrait de fait s'en trouvé différé de plusieurs décennies. En conclusion, mes travaux constituent un premier pas vers des modèles de prédiction de la dynamique éco-évolutive du cycle du carbone. Ils ouvrent la voie à un programme de recherche qui testerait de manière empirique les prédictions des modèles sur le rôle des mécanismes évolutifs dans différents types d'écosystèmes terrestres, en exploitant les archives de plus en plus riches de données métagénomiques des sols pour quantifier les variations des fonctions métaboliques microbiennes et leurs réponses à la sélection.

Contents

Chapter 1. Thesis Overview

1. Contexte et objectifs de la thèse

1.1. Les processus de décomposition de la matière organique du sol

La décomposition complète de la matière organique du sol consiste en la transformation d'éléments ou d'organismes entiers morts (plantes, animaux) en CO_2 et en nutriments inorganiques (Falkowski *et al.* 2008, Waksman & Starkey 1931). Cette transformation est le produit de la combinaison de processus physiques (lessivage, fragmentation), et chimiques (Chapin *et al.* 2011). Les eaux de lessivage emportent avec elles les éléments solubles de la matière organique en décomposition. Les animaux, par ingestion puis excrétion, fragmentent les grands composés organiques en de la matière fraiche organique de taille réduite, surface privilégiée de colonisation microbienne. Les champignons et les bactéries sont les principaux acteurs de la dégradation chimique de la matière organique morte, bien que certaines réactions aient lieu spontanément, en l'absence d'action directe des microorganismes ou de leurs produits catalytiques.

élément sous droit, diffusion non autorisée

Le taux de décomposition est déterminé par la composition chimique de la matière organique, les propriétés physico-chimiques du sol (humidité, composition minérale), ainsi que les espèces de microorganismes présents dans le sol qui produisent des composés catalytiques différents (Coûteaux *et al.* 1995). Les composés organiques simples, tels que les glucides et les protéines, sont décomposés plus rapidement que les composés organiques plus complexes comme la lignine ou les protéines membranaires. La litière issue des plantes des milieux riches en nutriments est généralement plus facile à décomposer que celle des sols plus pauvres. Les composés organiques simples présents dans la litière sont les premiers à être décomposés, ce qui

explique la diminution de la vitesse de décomposition de la litière plus l'état de décomposition est avancé (Fig. 1). Les animaux présents dans le sol ont un effet sur la vitesse de décomposition de la matière organique morte par l'intermédiaire de la fragmentation, de la prédation de microorganismes et de l'effet de leurs mouvements sur les interactions entre matière organique et composés minéraux (Verhoef & Brussaard 1990, Beare *et al.* 1992). La décomposition est également plus rapide dans la rhizosphère, autour des racines des plantes, parce que les cellules racinaires excrètent des composés organiques simples, les exsudats, qui stimulent la croissance des populations microbiennes, ce qui entraîne à son tour l'accélération de la décomposition de composés organiques plus complexes (effet de « priming ») (Cheng *et al.* 2003). Les conditions environnementales de forte production végétale (chaleur, humidité, richesse en nutriments) sont aussi celles d'une décomposition rapide, et la décomposition microbienne est aussi le mécanisme privilégié de formation des sols (Bradford *et al.* 2016). Si les différents processus biotiques et abiotiques impliqués dans la décomposition sont bien caractérisés, il est néanmoins difficile d'établir une relation entre productivité végétale, taux de décomposition de la matière morte et quantité de carbone dans le sol.

1.2. Les rétroactions (*feedbacks*) des microorganismes du sol sur le climat

Il est reconnu que les microorganismes ont joué un rôle essentiel dans la composition chimique actuelle de l'atmosphère (Falkowski et al. 2008). Ce qui est en revanche moins clair est le rôle qu'ils vont jouer dans le contexte du changement climatique actuel, en fonction de la vitesse, direction et amplitude de leurs réponses. La question des feedbacks des microorganismes vers l'atmosphère et le climat a longtemps été séparée de celle du changement climatique. Un tournant scientifique a été pris lorsque les premiers modèles incluant les dynamiques microbiennes de la décomposition ont été construits et analysés ; ces modèles révélaient l'impact global que l'activité microbienne des sols pouvaient avoir sur le cycle du carbone (Allison *et al.* 2010). Ainsi, les réponses microbiennes qui conduisent à l'augmentation de la production de gaz à effet de serre, comme une respiration accrue du fait de la dégradation plus rapide des protéines à plus haute température, pourraient contribuer à l'accélération du changement climatique. A l'inverse, les réponses qui réduisent la production de gaz à effet de serre, comme la production de protéines adaptées à des températures plus élevées, pourraient ralentir le changement climatique.

Les systèmes terrestres sont une énorme interface d'échange de gaz à effet de serre, à hauteur de 240 milliards de CO_2 échangés chaque année, dont la moitié est mobilisée par les plantes par photosynthèse, et l'autre moitié émise dans l'atmosphère par la respiration autotrophe (des plantes) et hétérotrophe (des animaux terrestres et microorganismes du sol) (Fig. 2). Le changement climatique devrait modifier les fonctions microbiennes associées au cycle du carbone à travers les effets directs et indirects de l'augmentation de la concentration atmosphérique en CO_2, de l'augmentation de température et de la modification des régimes de précipitation (Singh *et al.* 2010).

Les effets de l'augmentation de la concentration atmosphérique en CO_2 sur le fonctionnement écosystémique des microorganismes du sol sont essentiellement indirects, conséquences de l'augmentation initiale de la productivité des plantes. A plus haute concentration de l'air en CO_2, la photosynthèse est stimulée, entraînant une production accrue de litière à la surface des sols et une excrétion plus importante dans les sols d'exsudats racinaires composés de sucres simples, d'acides aminés faciles à ingérer par les microorganismes du sol (Bardgett *et al.* 2009). Dans les sols riches en nutriments, l'enrichissement en composés organiques simples devrait entraîner une prolifération microbienne à l'origine d'émissions plus importantes de CO_2, établissant une boucle rétroactive positive entre atmosphère et biosphère. Cet effet devrait cependant être limité dans les sols pauvres en nutriments (Janssens & Luyssaert 2009) et dans les sols dont la communauté microbienne est majoritairement composée d'oligotrophes, comme les champignons, efficaces dans la conversion de la matière organique et dont la structure cellulaire est composée de polymères complexes de carbone, parce qu'ils favorisent une décomposition de la litière plutôt que de composés carbonés simples, avec une respiration plus lente et donc une plus grande séquestration du carbone dans

le sol (Six *et al.* 2006) (Fig. 3). La modification des apports carbonés due à l'augmentation de la concentration atmosphérique en CO_2 pourrait aussi entraîner des réponses individuelles physiologiques des microorganismes et des changements dans la composition de la communauté, ce qui pourraient accentuer ou à l'inverse limiter les feedbacks précédemment évoqués (Balser & Wixon 2009).

L'augmentation de température associée au changement climatique est estimée entre +1.1 et +6.4°C d'ici à 2100 (IPCC, Pachauri *et al.* 2014). Les tests sur cultures microbiennes en laboratoire et les expériences de réchauffement en mésocosmes montrent une accélération initiale de la décomposition dans le sol et une respiration du sol accrue (Steinweg *et al.* 2008, Frey *et al.* 2013). Cette réponse est due à l'accélération des activités des enzymes intra et extracellulaires microbienne responsables de la décomposition et de l'acquisition des ressources par les microorganismes (Davidson *et al.* 2006, Allison *et al.* 2010). Ces dernières pourraient entraîner une augmentation des émissions de carbone du sol de 10 Pg pour une augmentation de température globale de 2°C (Bond-Lamberty & Thompson 2010). L'intensification de la décomposition et de la respiration du sol pourrait être critique à hautes latitudes, en particulier dans les régions à permafrost, où des grandes quantités de composés organiques simples gelés deviennent accessibles à la décomposition microbienne (Schuur *et al.* 2009). Cependant, les différents groupes fonctionnels microbiens ayant différentes températures optimales, une augmentation de température pourrait entraîner dans

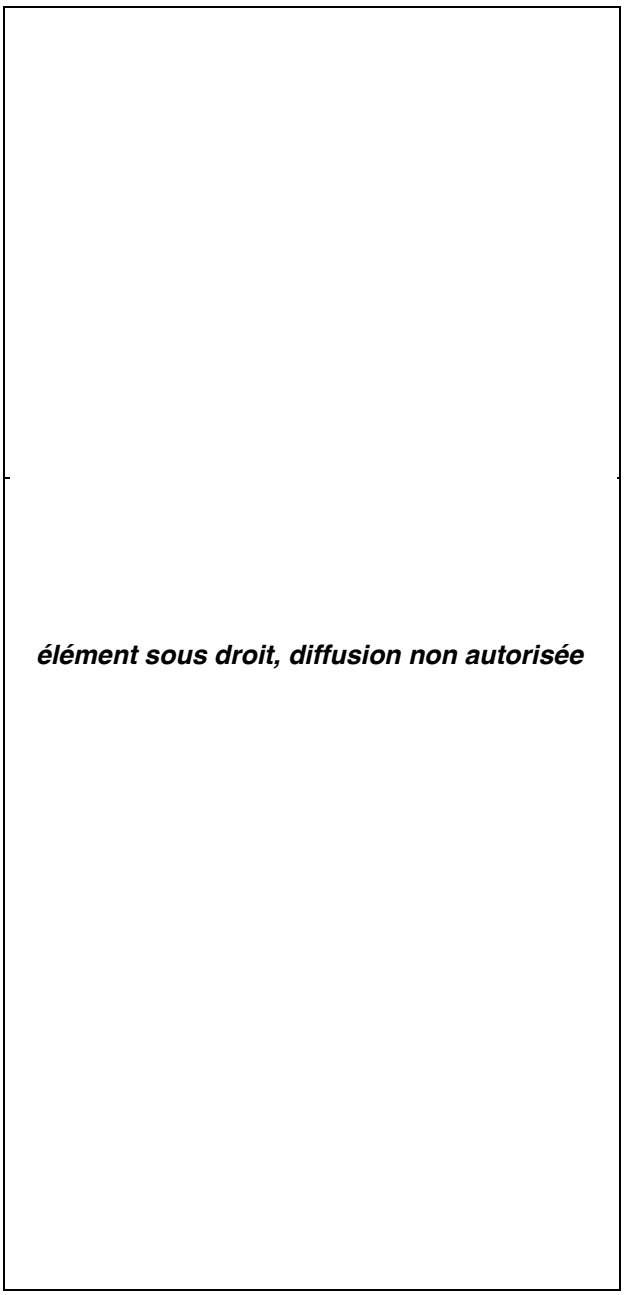

certaines écosystèmes la modification de la composition de la communauté microbienne, voire même l'extinction des populations les moins acclimatées, qui entraîneraient une décomposition et respiration plus lentes et une séquestration du carbone dans le sol en réponse au réchauffement (Monson *et al.* 2006). Enfin une augmentation de température est susceptible de modifier, comme l'augmentation de la concentration atmosphérique en CO_2, la nature de la matière organique entrante et les interactions organo-minérales dans le sol.

Le changement climatique global pourrait aussi se traduire par une variation de 20% du régime de précipitation avec le changement climatique (IPCC, Pachauri *et al.* 2014). L'effet direct d'une diminution des précipitations serait de ralentir les activités microbiennes, mais aurait pour effet indirect d'accélérer la diffusion des gaz, en particulier CO_2 et O_2, dont l'augmentation de concentration pourrait accélérer métabolisme microbien et réactions chimiques dans le sol. On s'attend à des changements de régime de précipitation et de leurs effets très différents selon les régions du globe. Par exemple, les sécheresses californiennes pourraient voir l'activité microbienne de leurs sols considérablement ralentie, tandis que l'assèchement en zones humides où les sols sont saturés en eau permettrait une réoxygénation des sols et ainsi un réveil microbien (Freeman *et al.* 2002).

Prédire les rétroactions sol-climat globales en réponse au changement climatique implique de comprendre comment ces rétroactions fonctionnent aux échelles écologiques régionales. Les grandes éco-régions du globe diffèrent notamment par l'amplitude et la dynamique des variations climatiques, par la végétation et donc les flux et la composition de la litière et des exsudats racinaires, ainsi que par la nature chimique des sols qui contrôlent le transport des éléments et les interactions entre composés organiques et composés minéraux (Fig. 4). De surcroît, j'ai concentré cette brève présentation des rétroactions sol-climat sur les effets liés aux émissions de CO_2 ; mais ces rétroactions sont aussi alimentées par les flux de méthane (CH_4) et d'oxyde d'azote (N_2O), produits du métabolisme

élément sous droit, diffusion non autorisée

des mêmes organismes ou d'organismes en interaction dans les mêmes environnements, qu'il conviendrait d'appréhender également à l'échelle régionale.

1.3. L'évolution adaptative dans les populations microbiennes naturelles

L'évolution des microorganismes est le grand oublié de l'histoire de l'évolution néo-Darwinienne du fait des difficultés techniques rencontrées jusqu'à une époque récente pour les identifier (Dykhuizen 1990). Si des expériences de transplantation ou de comparaison de différents systèmes ont permis de caractériser l'adaptation de population naturelles, la connaissance des mécanismes évolutifs des microorganismes vient essentiellement d'expériences réalisées in vitro (Koskella & Vos 2015). Il est essentiel cependant de poursuivre les études évolutives en conditions écologiques plus complexes mais plus réalistes, parce qu'elles ont montré à de nombreuses reprises des résultats divergents avec celles réalisées en laboratoire, comme l'illustre la dynamique co-évolutive de la bactérie *Pseudomonas fluorescens* et d'un phage en présence et absence des concurrents naturels de la bactérie (Gomez & Buckling 2011).

L'adaptation, au sens darwinien du terme, met en jeu des agents de sélection, dans l'environnement biotique et/ou abiotique d'une population, qui s'appliquent à la variation héritable d'un phénotype. La diversité génétique sur laquelle s'exerce la sélection est à la fois contrainte par l'histoire phylogénétique de la population et alimentée par les processus de migration et de modification aléatoire du génome (mutations, délétions, duplications, transferts horizontaux intra et interspécifiques). La vitesse d'adaptation d'une population exposée à une modification de son environnement dépend donc des agents de sélection associés à ce nouvel environnement, ainsi que de la diversité génétique en présence et de la fréquence des modifications génétiques.

Les mutations (infra-chromosomiques) constituent la source de variation génétique la mieux connue. Dans le cas le plus simple, la mutation affecte une base nucléotidique de la partie codante d'un gène, entraînant la synthèse d'un nouvel acide aminé dans la chaîne protéique qui modifie sa fonction cellulaire originelle et conduit à l'acquisition par la cellule d'un nouveau trait. C'est le cas du polymorphisme du gène *rpoB* responsable de la résistance d'*Escherichia coli* à l'antibiotique rifampicine (Jin & Gross 1988). Les mutations sont généralement rares, leur fréquence est estimée à une toutes les mille générations par génome

(Lee *et al.* 2012, Sung *et al.* 2012). Cependant, les taux de mutation peuvent être de plusieurs ordres de grandeur supérieurs chez certaines lignées « hypermutatrices », chez lesquelles le système de réparation de l'ADN est altéré (Oliver *et al.* 2000). Ces lignées ont souvent un avantage sélectif en environnement variable et sont contre-sélectionnées en environnement stable, en particulier lorsque les lignées non mutantes parviennent à acquérir la fonction avantageuse par transfert horizontal (Giraud *et al.* 2001b). Les délétions et les duplications peuvent jouer un rôle important dans l'adaptation rapide en environnement changeant, ces dernières permettant de cumuler les fonctions originelle et nouvelle du gène dupliqué. Le sort d'une mutation rare au sein d'une population est déterminé par l'influence cumulée de deux forces, sélection naturelle et dérive génétique, cette dernière étant d'autant plus forte que la taille (efficace) de la population est petite.

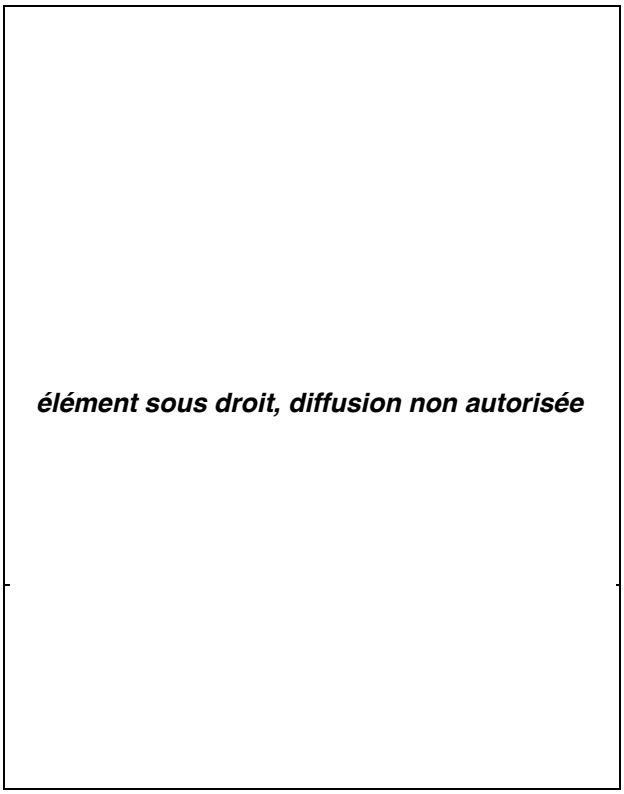

L'idée que toute la diversité génétique est déjà présente et que la sélection naturelle n'a qu'à y piocher les gènes les mieux adaptés (Becking 1934) est encore une idée répandue en microbiologie (De Wit & Bouvier 2006), en particulier marine. Il a été montré cependant que même en milieu océanique, la dispersion des microorganismes n'est pas illimitée (e.g. Bell 2010, Finkel *et al.* 2012, Östman *et al.* 2010, Telford *et al.* 2006), et que les populations ont la capacité de d'adapter localement et de se différencier rapidement. Par exemple le cas des cyanobactéries *Mastigocladus laminosus* adaptées à un gradient naturel de température de 15°C sur 1 km démontre l'effet que peut avoir une interaction entre environnement local et dispersion sur l'adaptation de cette population bactérienne (Miller *et al.* 2009).

Les expériences de transplantation suivie de la comparaison des taux de croissance de populations retransplantées dans leur environnement d'origine ou dans un nouvel environnement sont la méthode privilégiée pour tester l'étendue spatiale d'adaptation d'une population (Kawecki & Ebert 2004). Elles nécessitent de connaître a priori le gradient spatial de la force de sélection. Une étude de l'adaptation locale d'une population bactérienne au sol

d'une forêt ancienne a pu ainsi montré une diminution de la fitness de 6% par mètre de distance de leur site d'échantillonnage (Belotte *et al.* 2003). L'adaptation locale des populations microbiennes du sol est dans certains cas fortement corrélée à la communauté végétale, par exemple dans les cas des bactéries fixatrices d'azote en symbiose avec les légumineuses, alors qu'elle peut-être davantage déterminée par des facteurs climatiques (Macel *et al.* 2007). L'échelle spatiale d'adaptation peut être très variable, du millimètre au kilomètre (Fig. 5a), en fonction de la vitesse de dispersion des individus, de l'hétérogénéité spatiale du sol et de potentielles autres forces de sélection (Vos *et al.* 2009, Koskella *et al.* 2011).

Les populations microbiennes étant caractérisées par des temps de génération courts, de grandes tailles de population et des génomes généralement plus variables que ceux des macroorganismes, leur temps d'adaptation peut être très court, inférieur à un an dans les quelques expériences conduites sur populations naturelles (Lieberman *et al.* 2011) et de seulement quelques jours en laboratoire (Buckling & Rainey 2002, Lenski & Travisano 1994).

L'adaptation des populations microbiennes peut avoir lieu sur des échelles de temps allant de la minute à plusieurs années en fonction de la durée et de la vitesse du changement environnemental relativement au temps de génération de la population (Fig 5b). Les changements rapides et à court-terme (par exemple de température, d'apport de composés organiques et de lumière entre le jour et la nuit) sélectionneront souvent des réponses plastiques (physiologiques individuelles), tandis que l'adaptation génétique est attendue en réponse à des changements maintenus dans le temps (par exemple une prolongation de la saison de croissance des plantes). Parce qu'elles modifient leur environnement, notamment par l'immobilisation et l'excrétion de composés organiques et inorganiques, les populations microbiennes peuvent modifier le changement environnemental lui-même et ainsi leur propre processus adaptatif. C'est le cas par exemple des sidérophores dont l'évolution adaptative est accélérée par la consommation du fer du sol (Wandersman & Delepelaire 2004).

1.4. Dynamiques éco-évolutives du carbone et réchauffement climatique

Les flux de carbone globaux étant essentiellement des processus biotiques, étudier les effets du changement climatique sur le cycle du carbone nécessite de comprendre les potentielles

réponses écologiques et évolutives des organismes impliqués. La photosynthèse et la respiration sont les flux les plus importants du cycle du carbone ; si tous les autres flux de carbone étaient maintenus constants, une augmentation du flux net photosynthétique de 2% suffirait à compenser entièrement l'augmentation récente de la concentration atmosphérique de CO_2. De faibles changements peuvent avoir de forts effets du fait des rétroactions des écosystèmes sur le climat. Les émissions anthropiques de carbone ne représentent qu'1.5% des flux de carbone globaux, et sont pourtant à l'origine du réchauffement climatique, de changements de régime de précipitation, de l'acidification des océans, des altérations, phénologiques par exemple, des cycles de vie des espèces et de leur viabilité, au cours de ces dernières décennies.

La concentration atmosphérique en CO_2, principal moteur du changement climatique, résulte du bilan entre émissions dans l'atmosphère et stockage du carbone dans les sols et les océans. Les traits fonctionnels potentiellement impliqués dans le maillon « organismes » des rétroactions des écosystèmes sur le climat, sont ceux associés à la machinerie photosynthétique, à la machinerie métabolique responsable des réactions d'anabolisme (synthèse de nouvelles protéines) et de catabolisme (production d'énergie) et aux traits impliqués dans le stockage du carbone dans les sols (par exemple, la croissance racinaire et la production de composés organiques stables par décomposition microbienne) ou dans les océans (par exemple, la calcification) (Fig. 6). Une expérience de réchauffement en mésocosme sur 10 ans a montré une adaptation vers une augmentation du taux net photosynthétique (différence entre photosynthèse et respiration) chez l'algue verte unicellulaire *Chlamydomonas reinhardtii* (Schaum *et al.* 2017). Dans les sols, qui contiennent deux à trois fois plus de carbone que l'atmosphère sans

élément sous droit, diffusion non autorisée

être encore saturés en carbone (Kell 2012), il a été estimé qu'une augmentation de la longueur des racines des plantes d'un mètre sur moins de 4% des terres cultivables permettraient de compenser complètement les émissions annuelles de CO_2 liées aux combustibles fossiles (Kell 2011).

L'évolution des traits fonctionnels impliqués dans le cycle du carbone a joué un rôle historique dans la constitution de notre climat actuel. L'évolution des organismes photosynthétiques a profondément transformé l'atmosphère terrestre, l'évolution et la diversification des organismes décomposeurs ont modifié les capacités et vitesses de décomposition de la matière organique, et on estime que l'évolution des angiospermes a réduit de 10 à 20 fois la concentration atmosphérique en CO_2. Il est probable que les changements environnementaux actuels modifient les agents de la sélection naturelle qui s'exercent sur de multiples systèmes écologiques. Mais en pratique, prédire les trajectoires évolutives des traits associés au cycle du carbone nécessite d'identifier les agents de sélection en cause et d'estimer leur variation ; et de mesurer la diversité génétique sur laquelle ces agents s'exercent, et l'amplitude des réponses , à des échelles spatiales qui ne sont pas elles-mêmes clairement définies *a priori*.

Une grande variation génétique additive de certains traits impliqués dans le cycle du carbone a été démontrée chez certaines espèces de plantes et de phytoplancton. Par exemple les traits associés à la production racinaire et à la réponse à la sécheresse sont fortement héritables chez l'espèce *Brachypodium distachyon* (Des Marais *et al.* 2017). On en sait moins sur la variation génétique des traits du cycle du carbone des microorganismes hétérotrophes parce que les études se sont plus souvent portées sur leur variabilité interspécifique plutôt qu'intraspécifique (Wallenstein & Hall 2012). Cependant des études récentes ont mis en évidence une variation génétique associée à la production des enzymes de décomposition (Alster *et al.* 2016, Trivedi *et al.* 2016). La signature de la sélection peut être détectée directement grâce au séquençage de sous-populations adaptées à leur environnement local (Yeaman *et al.* 2016, Thomas *et al.* 2012, Oliviero *et al.* 2017, Yampolsky *et al.* 2014). Ces études permettent notamment de comparer différentes combinaisons de facteurs climatiques, dont les effets sur la sélection ne sont pas simplement additifs.

La marque d'adaptations évolutives au changement climatique actuel a été trouvée sur le taux de fixation du carbone du phytoplancton (Jin *et al.* 2013), sur le taux de fixation de l'azote et la croissance des cyanobactéries (Hutchins *et al.* 2015, Walworth *et al.* 2016), et la

conductance des stomates des plantes (Grossman & Rice 2014) en réponse à l'augmentation de la concentration de CO_2 ; et chez des bactéries hétérotrophes en réponse à l'augmentation de la température (Kileen *et al.* 2017). Ces adaptations peuvent se produire sur une échelle de temps écologique. Des populations naturelles de zooplancton *Daphnia magna* s'adaptent en moins de 2 ans (Geerts *et al.* 2015) et le phytoplancton *Chlorella vulgaris* en moins de 100 générations à une augmentation de température (Padfield *et al.* 2016), tandis que des adaptations à la sécheresse chez la plante annuelle *Brassica rapa* ont été détectées en moins de 10 ans.

La réponse du cycle du carbone global au changement climatique intègre les réponses des différentes communautés écologiques distribuées sur l'ensemble du globe. Si les espèces autotrophes s'adaptent par une augmentation de leur activité photosynthétique, elles pourraient entraîner un ralentissement du changement climatique ; si les adaptations des espèces hétérotrophes se traduisent par des taux de respiration plus élevés, elles sont susceptibles de contribuer à l'accélération du changement climatique global (Monroe *et al.* 2018). Il est à noter que les réponses évolutives ne suivent pas toujours la même direction que les réponses plastiques. Par exemple, les espèces phytoplanctoniques réduisent leur taux photosynthétique en cas d'acidification à court-terme, tandis qu'ils s'adaptent par une augmentation de leur production photosynthétique après plusieurs générations en conditions d'acidification (Collins *et al.* 2014). Analyser empiriquement la direction globale des réponses au changement climatique nécessite donc de combiner de multiples approches : manipulation expérimentale d'un ou plusieurs facteurs climatiques agissant sur des communautés-modèles en environnement contrôlé, expériences de transplantation, séquençage le long de gradients spatiaux naturels… Dans un programme d'une telle ampleur, la modélisation a un rôle crucial à jouer, en générant des prédictions quantitatives, et en rendant possible l'intégration et la simulation à grande échelle de temps et d'espace des mécanismes mis en évidence aux échelles – généralement locales, voire microscopiques – des études empiriques.

1.5. Objectifs de la thèse

L'objectif central de la thèse est de comprendre, par une approche essentiellement théorique, comment l'évolution des bactéries hétérotrophes du sol contribue à la réponse du

cycle du carbone terrestre au réchauffement climatique global. Les bactéries hétérotrophes constituent un modèle idéal d'étude d'interactions éco-évolutives entre une population et son environnement, pour trois raisons principales : (1) elles jouent un rôle écologique majeur au travers de la décomposition de la matière organique du sol et de la respiration ; (2) elles sont présentes dans tous les écosystèmes terrestres et aquatiques du globe ; (3) elles sont susceptibles d'évoluer sur des échelles de temps courtes (quelques jours en culture) du fait de leur grande taille de population, de leur grande variabilité génétique potentielle et de leur temps de génération court (Monroe *et al.* 2018). Des études récentes suggèrent un rôle crucial pour les communautés microbiennes dans la réponse globale des écosystèmes au changement climatique (e.g. Wieder *et al.* 2013) mais on connaît encore très mal la nature de ces réponses (changement de l'abondance relative de groupes fonctionnels bactériens, plasticité individuelle ou adaptation évolutive) et leur importance relative. Les modèles les plus avancés d'interaction entre populations bactériennes et matière organique tentent d'intégrer des réponses physiologiques rapides dont on suppose qu'elles assurent l'homéostasie des traits métaboliques des bactéries face au réchauffement. Aucun de ces modèles n'a considéré l'adaptation des populations bactériennes, au sens darwinien du terme. Ainsi, c'est dans le champ de l'étude des dynamiques éco-évolutives intégrant l'effet du réchauffement sur les énergies cinétiques des réactions, la distribution du carbone dans le sol et les réponses physiologiques des bactéries, que s'inscrit ma thèse.

Quatre objectifs principaux ont guidé mes travaux :

1) Réaliser une synthèse des travaux de modélisation des dynamiques de populations bactériennes du sol. J'ai focalisé ma compilation bibliographique sur l'effet des dynamiques de populations bactériennes sur le taux de décomposition du carbone dans le sol et sur la respiration du sol dans le contexte du réchauffement climatique global.
2) Développer un nouveau modèle de la dynamique de décomposition de la matière organique du sol couplant l'écologie et l'évolution de la population bactérienne. Ce modèle déterministe intègre explicitement un *trade-off* dans l'allocation des ressources entre la croissance individuelle bactérienne et la production des enzymes extracellulaires impliqués dans la décomposition de la matière organique du sol. Le modèle intègre également le caractère spatialement localisé de la compétition entre bactéries pour le carbone organique dissous.
3) Utiliser ce modèle pour analyser la réponse éco-évolutive des décomposeurs bactériens au réchauffement climatique. Cette analyse vise à (i) prédire la direction et l'amplitude des

réponses évolutives de traits bactériens au réchauffement climatique ; (ii) évaluer l'impact écologique de ces réponses sur le carbone du sol ; et (iii) comparer cet impact aux prédictions des modèles écologiques sans évolution. La production d'enzymes extracellulaires peut s'interpréter comme un investissement dans une forme de coopération entre bactéries. Mon étude s'inscrit donc dans le contexte de deux questions fondamentales de la biologie de l'évolution, celui du maintien évolutif d'interactions coopératives et celui de la coexistence de plusieurs stratégies d'acquisition des ressources dans un système à ressource unique.

4) Intégrer le modèle éco-évolutif comme module dans un modèle numérique planétaire de projection des stocks de carbone du sol, de façon à étudier l'effet global potentiel de l'évolution des décomposeurs microbiens terrestres sur le cycle du carbone dans le contexte du réchauffement climatique.

Modélisation des dynamiques adaptatives

L'évolution à long terme de la communauté microbienne est modélisée par la « dynamique adaptative » du système, qui consiste mathématiquement en un « processus de saut » dans un espace phénotypique prédéfini (Metz *et al.* 1996, Champagnat *et al.* 2006). Ce processus de saut est gouverné par des événements de mutation (phénomène génétique rare) et de sélection (phénomène écologique rapide, dans l'échelle de temps des mutations). Ainsi, lorsque qu'une lignée microbienne mutante apparaît, présentant une différence légère de phénotype, au sein d'une communauté microbienne « résidente », on considère que le taux de mutation est assez faible de façon à ce que cette population mutante ait soit déjà totalement envahi le système ou disparu lorsque le mutant suivant apparaît. Autrement dit, le système écologique atteint son équilibre (ou plus généralement, son attracteur ou état stationnaire) avant qu'une nouvelle stratégie mutante survienne. Ainsi, les échelles de temps écologique et évolutif sont séparées (Dieckmann & Law 1996, Metz *et al.* 1996, Marrow *et al.* 1996, Law *et al.* 1997, Geritz *et al.* 1998, Doebeli & Dieckmann 2000).

Fonction de fitness et condition d'invasion

La fitness d'invasion est le taux de croissance exponentielle à long terme d'un phénotype mutant de trait x' dans un environnement façonné par la population résidente de trait x (Metz

et al. 1992, 1996, Geritz *et al.* 1998). Une fois qu'une population a atteint son équilibre écologique, sa démographie est stationnaire ; les fitness de toutes les populations présentes dans le système à l'équilibre sont donc toutes égales à zéro.

Le sort d'une population mutante initialement rare est déterminé par sa fonction de fitness. Sous l'hypothèse de grandes populations (qui s'applique naturellement aux systèmes microbiens considéré ici), les mutants tels que $s_x(x') < 0$ sont condamnés à l'extinction, tandis que ceux au $s_x(x') > 0$ ont une probabilité non nulle d'envahir la population résidente (mais ne l'envahissent pas nécessairement du fait du phénomène d'extinction aléatoire due à la faible densité de leur population initiale). Si $s_x(x') > 0$ mais $s_{x'}(x) < 0$, le mutant peut envahir mais le résident d'origine ne serait pas capable d'envahir une population de ce même mutant. Il ne peut alors y avoir dimorphisme (i.e. coexistence de deux lignées de microbes différentes) et la population mutante envahit la population résidente jusqu'à extinction de cette dernière (remplacement).

Singularités évolutives

Pour connaître le sens d'évolution du trait à partir de la valeur de trait résident x, on étudie le signe du gradient de sélection :

$$[(\partial s_x(x'))/(\partial x')]_{(x'=x)}$$

Si le gradient est de signe positif x augmente, s'il est négatif x diminue, en considérant ici qu'invasion implique remplacement (Geritz *et al.* 2002, Diekmann 2004). Lorsque le gradient atteint la valeur nulle, x se trouve alors sur un point singulier, c'est-à-dire que le gradient de sélection de premier ordre ne peut nous renseigner sur le sens d'évolution du trait à partir de cette valeur de trait résident x*.

Conditions de convergence et stabilité évolutive

Nous voulons à présent connaître la nature de ce point singulier x*. Si aucun mutant de stratégies proches de x* ne peut envahir une population résidente de trait x*, alors ce point singulier est une ESS locale (Evolutionarily Stable Strategy), ou « stratégie imbattable » (Hamilton 1967, Maynard Smith & Price 1973). Graphiquement, $s_x(x')$ est une fonction concave de x' au voisinage de x*. L'appellation « stable » est cependant un abus de langage car ce point peut être un « répulseur ». Un point singulier est un « répulseur » local lorsque, dans une population résidente de stratégie x proche de x*, un mutant de stratégie x' compris entre x et x* ne peut envahir. Dans ce cas, seule une population présentant initialement le trait

x* peut permettre l'existence de cette valeur de trait, par définition de la théorie de dynamique adaptative qui impose de très petites mutations (Hofbauer & Sigmund 1988, Nowak 1990). Une ESS est localement stable si c'est aussi un « attracteur », c'est-à-dire que pour tout x suffisamment proche de x*, les x' compris entre x et x* envahissent x ; une telle stratégie x* est alors appelée Convergent Stable Strategy (ou Continuously Stable Strategy) (Diekmann 2004). Dans ce cas, sans perturbation extérieure (par exemple un changement de conditions environnementales, un flux d'individus immigrants…), le système est à l'équilibre évolutif et écologique.

Il est possible qu'une singularité soit attractive mais pas ESS. Le « branchement évolutionnaire » peut alors se produire : une série de remplacements par mutation sur le trait x peut nous amener au voisinage de x* avec une population monomorphe ; la sélection devient alors disruptive et la coexistence de deux valeurs du trait, de part et d'autre de x*, est alors possible. Un tel point singulier est appelé « point de branchement » (branching point) et indique la transition d'un monomorphisme à un dimorphisme ; mais il est à noter que l'existence d'un point de branchement ne garantit pas en elle-même la divergence du polymorphisme et son maintien à long terme.

Algébriquement, un point singulier x* est un « attracteur » si et seulement si il répond à la condition :

$$[(\partial^2 s_x(x))/\partial x'^2]_{(x'=x=x^*)} < [(\partial^2 s_x(x'))/\partial x^2]_{(x'=x=x^*)}$$

Un point singulier x* n'est pas une ESS si et seulement si il répond à la condition :

$$[(\partial^2 s_x(x'))/\partial x'^2]_{(x'=x=x^*)} > 0$$

D'autre part, nous pouvons montrer que si le système n'admet qu'un seul point de singularité et que cette singularité est attractive localement, alors elle est nécessaire attractive globalement. En effet, en raisonnant par l'absurde, si cette unique singularité est attractive localement mais pas globalement, c'est soit qu'il existe une autre singularité attractive et alors elle n'est pas unique, soit qu'une valeur extrême du trait (par exemple 0 pour un trait toujours positif) est attractive mais dans ce cas, il doit exister entre la singularité attractive et cet extrême une singularité répulsive et alors ici encore la singularité n'est pas unique.

2. Revue des modèles mathématiques « microbes-exoenzymes » de la décomposition et de la respiration hétérotrophique du sol

Mes recherches bibliographiques m'ont permis d'identifier et classifier les principaux types de modèles mécanistes représentant l'influence des décomposeurs microbiens sur le cycle du carbone. Placés dans le contexte du réchauffement climatique, ces modèles décrivent les effets du réchauffement sur les stocks de carbone et sur la respiration du sol, et leurs prédictions sont significativement différentes entre elles (Fig. 7). A titre d'exemple, la plupart des modèles du début des années 2000, qui n'intègrent pas la dynamique de la communauté microbienne du sol, prédisent une perte de carbone du sol et une augmentation de la respiration en réponse à une augmentation soutenue de la température globale. En rendant un seul trait des bactéries dépendant de la température, la deuxième génération de modèles (e.g. Allison *et al.* 2010, Hagerty *et al.* 2014) renverse complètement cette prédiction. Mon travail de synthèse m'a permis de comprendre de façon systématique l'origine de telles différences.

élément sous droit, diffusion non autorisée

De cette compréhension se dégagent trois messages principaux. En premier lieu, la diversité des modèles existants s'organise selon leur niveau de complexité (nombre de variables, nombre de mécanismes, type de fonctions associées aux mécanismes), leur nature statistique ou mécanistique, et la disponibilité des données nécessaires à leur paramétrage. Il apparaît par exemple que les modèles de décomposition les plus simples sont plus performants que ceux explicitant les dynamiques microbiennes pour prédire les flux et stocks de carbone en environnement stable, parce qu'un grand nombre d'expériences permettent une meilleure paramétrisation. En revanche leur pouvoir prédictif devient faible lorsque l'environnement est changeant, notamment dans le contexte du changement climatique. En second lieu, un clivage existe entre modèles selon l'importance relative qu'ils donnent aux réponses physico-chimiques (adsorption/désorption, décomposition physico-chimique) aux changements

environnementaux par rapport aux réponses biotiques (changements de composition et activité (métabolisme, production d'enzyme, dormance) de la communauté microbienne). Enfin, ma synthèse souligne l'absence de modélisation rigoureuse des réponses plastiques et évolutives de traits bactériens au changement climatique et résume les approches possibles pour dépasser cette frontière.

Ce travail, présenté dans le chapitre 2 de la thèse, est en cours de publication sous la forme d'un chapitre de livre publié par la American Geophysical Union:

Abs E. & Ferriere R. Modeling Microbial Dynamics and Soil Respiration, Effect of Climate Change. In *Biogeochemical Cycles: Anthropogenic and Ecological Drivers*. Edited by K. Dontsova, Z. Balogh-Brunstad and G. Le Roux. American Geophysical Union.

3. Dynamiques éco-évolutives de la décomposition: Modélisation spatialement explicite de la coopération microbienne pour des biens communs diffusifs

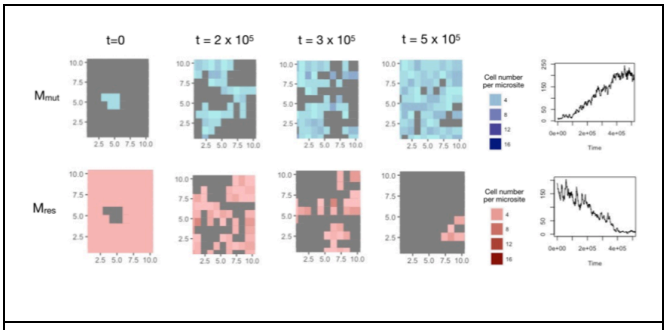

Figure 8. Invasion d'un mutant « fort producteur » d'enzymes (*en haut*) apparaissant dans la population résidente d'un « faible producteur » (*en bas*). *A gauche*, états de la grille à quatre temps différents. *A droite*, dynamique agrégée de la population de microbes.

Les modèles déterministes écologiques ou éco-évolutifs font des hypothèses fortes sur les échelles de temps et d'espace des phénomènes modélisés. Avec Hélène Leman, mathématicienne chargée de recherche INRIA au sein de l'Unité de Mathématiques Pures et Appliquées de l'ENS Lyon, j'ai entrepris d'explorer les fondements mathématiques et la validité des échelles spatio-temporelles des modèles déterministes de décomposition. Pour ce faire, nous avons redéfini en termes de processus stochastiques le modèle d'interactions locales entre bactéries, enzymes, litière et carbone organique dissous (COD).

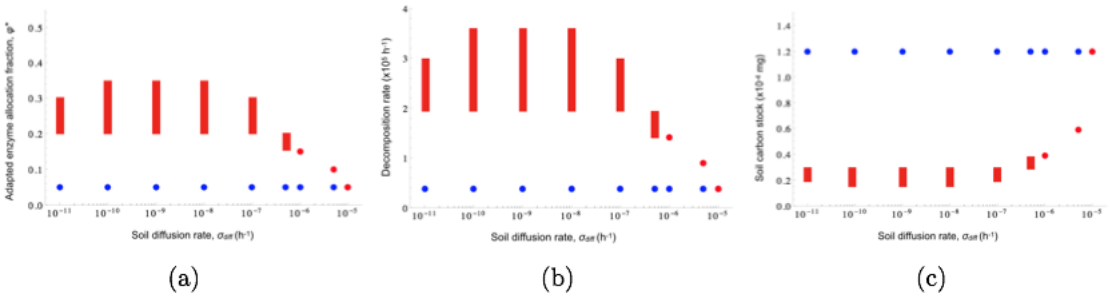

(a) (b) (c)

Figure 9. Effet de la diffusivité des ressources sur l'évolution de la coopération microbienne et ses conséquences écosystémiques. (a) Investissement microbien dans la production d'enzymes, (b) Taux de décomposition, (c) Quantité de carbone (SOC) dans l'habitat. *En bleu*, réponse du système à la variation de la diffusivité, en l'absence d'évolution bactérienne. *En rouge*, réponse du système à la variation de la diffusivité, avec évolution bactérienne.

L'analyse du modèle stochastique nous montre qu'il ne peut y avoir survie d'un petit nombre de bactéries partageant leurs ressources qu'en modélisant une consommation progressive des ressources et un mécanisme de stockage de ces ressources dans les bactéries.

Deuxièmement, lorsque l'on autorise l'apparition de mutants rares, nous obtenons systématiquement la diminution de la coopération jusqu'à production nulle d'enzymes et extinction de la population bactérienne du fait de l'absence de ressources (cas de suicide évolutif). Notre travail intègre la explicitement la structure spatiale du système, nous montrons la possible stabilisation évolutive du système à une valeur non nulle de l'investissement cellulaire dans la production d'exoenzymes de dégradation (Fig. 8).

Nous montrons également l'effet important de la diffusivité des ressources sur cette valeur et donc sur le taux de décomposition et la quantité de carbone moyens du système (Fig. 9).

Ce travail est présenté dans le chapitre 3 sous forme d'un article en préparation ;

Abs E., Ferriere R. & Leman, H. Eco-evolutionary dynamics of decomposition: emergence and stability of microbial cooperation for diffusive goods. To be submitted to *INTERFACE Journal of the Royal Society*.

4. Prédictions: Impact de l'évolution microbienne sur la rétroaction carbone du sol – climat

Pour intégrer la dynamique éco-évolutive des décomposeurs bactériens dans le cycle du carbone terrestre, j'ai utilisé le modèle introduit par Allison et al. (2010) dans lequel j'ai explicité la stratégie microbienne d'allocation des ressources entre croissance et production d'enzymes (Fig. 10). La théorie des dynamiques adaptatives m'a permis d'analyser l'évolution d'un trait bactérien mesurant la fraction des ressources assimilées investie par la cellule dans la production d'enzymes extracellulaires.

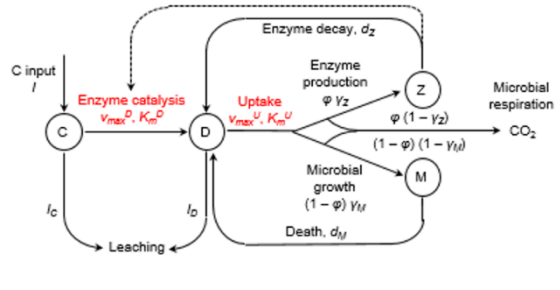

Figure 10. Structure du modèle. En rouge, les paramètres dépendant de la température dans le scenario 1.

J'ai montré premièrement que ce trait ne peut être évolutivement stable sans mécanisme de « récompense » de la coopération face aux stratégies « tricheuses ». Un tel mécanisme peut se conceptualiser de façon générale comme un avantage acquis par les souches coopératives dans l'accès aux ressources produites par la coopération (i.e. carbone organique dissous). J'ai introduit dans le modèle une représentation mathématique simple d'un tel avantage compétitif, dont l'intensité peut varier selon les propriétés locales de l'environnement, telle que l'humidité ou la porosité locales du sol. J'ai conduit l'analyse mathématique et numérique des dynamiques écologiques et éco-évolutives de ce système.

Pour étudier l'effet de l'évolution des décomposeurs bactériens sur la réponse du carbone du sol au réchauffement climatique, j'ai comparé les dynamiques écologique et éco-évolutives du modèle sous trois scénarios de sensibilité des paramètres à la température : (1) seules les vitesses de décomposition enzymatique et d'assimilation des ressources par les microorganismes augmentent avec la température ; (2) les vitesses de décomposition et d'assimilation augmentent, ainsi que le taux de mortalité bactérien; (3) les vitesses de décomposition et d'assimilation augmentent mais l'efficacité de croissance microbienne diminue.

Mes résultats (Fig. 11) montrent que, dans le cas général, les bactéries investissent davantage dans la production d'enzymes après réchauffement dans le scénario 1, que cette réponse s'inverse dans le scénario 2 et qu'elle dépend de la température initiale dans le scénario 3. Je montre également que, dans le cas général sans évolution, le réchauffement entraîne une perte de carbone dans le sol dans les trois scénarios. J'en déduis donc que l'adaptation évolutive des bactéries au réchauffement peut entraîner tous les types de réponses, des pertes de carbone dans le sol plus importantes que sans évolution à l'enrichissement du sol en carbone.

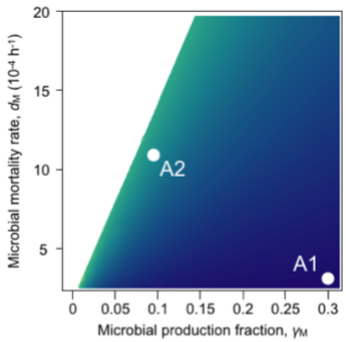

Figure 11. Un résultat central : amplitude de l'effet de l'évolution sur la réponse du stock du carbone du sol à un réchauffement de 5°C. L'effet est évalué en fonction de l'efficacité de croissance et du taux de mortalité microbiens. Les tons plus sombres indiquent un effet plus important.

Afin d'évaluer l'importance des effets de l'évolution des décomposeurs bactériens dans la réponse du cycle du carbone au réchauffement climatique, j'ai appliqué mon modèle général au cas de cinq biomes contrastés pour lequel les données nécessaires (dépendance des cinétiques enzymatiques de décomposition à la température) étaient disponible (*cf.* German *et al.* 2012). J'ai montré que les résultats de l'analyse générale s'appliquent aux cinq biomes (Fig. 12). Les effets évolutifs les plus forts sont attendus dans les biomes froids et où les conditions du sol limitent l'évolution de la coopération. L'évolution aggrave les pertes de carbone dans le sol prédites par les modèles écologiques dans les biomes froids et à l'inverse les réduit dans les biomes chauds.

Ce travail est présenté dans le chapitre 4 de la thèse, sous la forme d'un manuscrit actuellement soumis à *Nature Ecology & Evolution* :

Abs E., Saleska S. & Ferriere R. Eco-evolutionary dynamics can mediate microbial carbon cycle feedbacks to climate change. Submitted to *Nature Ecology & Evolution*.

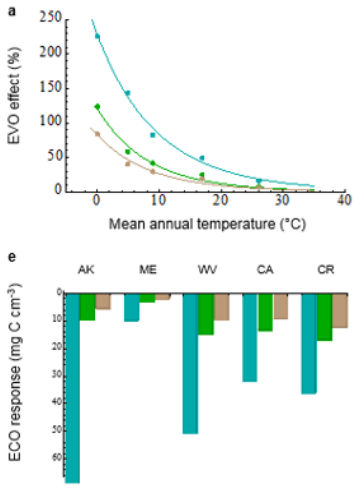

Figure 12. Effet de l'évolution (a) et réponse écologique (b) prédits par le modèle dans cinq biomes. AK, forêt boréale d'Alaska; ME, forêt tempérée du Maine ; WV, forêt tempérée de West Virginia ; CA, prairie de Californie ; CR, forêt tropicale du Costa Rica. Les couleurs correspondent à trois valeurs d'un paramètre de diffusion du COD.

5. Le futur des stocks de carbone du sol : Impact de l'évolution microbienne sur les projections globales

Afin d'évaluer l'effet potentiel de l'évolution des décomposeurs bactériens à l'échelle planétaire, j'ai utilisé le modèle avec évolution du chapitre 4 et le premier scénario de sensibilité à la température pour établir la carte de distribution du carbone du sol actuelle, avant réchauffement climatique, considérant ainsi que les populations microbiennes sont initialement adaptées à leur environnement. L'environnement est caractérisé par la température de la surface du sol (première couche d'1 cm), l'apport en litière (matière organique non décomposée), les caractéristiques cinétiques initiales de l'activité de décomposition des enzymes, ainsi que leur sensibilité à la température. Pour les deux premiers paramètres, j'ai utilisé les projections d'un des modèles de carbone globaux (« Community Earth System Model ») prédites par le scénario RCP8.5 (réchauffement global moyen de 3°C à l'horizon 2100) moyennées sur 15 ans (entre 2006 et 2021). La carte des températures m'a permis de dresser celle des valeurs d'investissement microbien à la production d'enzymes. Pour les paramètres enzymatiques, j'ai regroupé les 14 écorégions

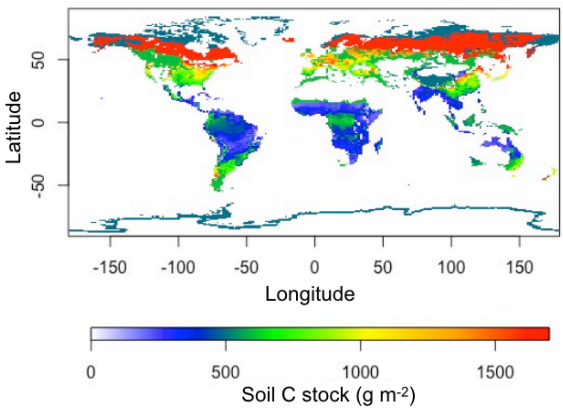

Figure 13. Distribution globale des stocks de carbone terrestre. Estimations produites par simulation numérique de mon modèle.

terrestres en 5 biomes et j'ai utilisé les données enzymatiques de German *et al.* (2012) exploitées dans le chapitre 4. J'ai montré premièrement qu'il existe des régions non viables pour les microbes (en particulier dans les régions froides), que j'ai interprétées comme des sites « dormants ». Pour quantifier la quantité de carbone dans le sol dans ces régions, j'ai utilisé les observations fournies par la World Soil Data Base (Wieder *et al.* 2013) (Fig. 13).

En utilisant ces mêmes projections de température du sol et d'apport en litière cette fois par année entre 2010 et 2100, j'ai montré que les prédictions du chapitre 4 sont confirmées à l'échelle globale : l'évolution accentue les pertes de carbone du sol prédites par le modèle écologique là où les microbes sont actifs (Fig. 14a) et l'effet de l'évolution est particulièrement important dans les biomes froids. Dans les sols « dormants », le carbone s'accumule dans le sol lorsqu'il n'y a pas adaptation microbienne, tandis que les microbes deviennent actifs dans certains sites à partir d'une certaine température du sol. Ce phénomène entraîne à l'échelle globale pour ces sites dormants une décélération de l'accumulation de carbone initiale suivie de la perte de carbone de sol retardée prédite dans les sols actifs (Fig. 14b).

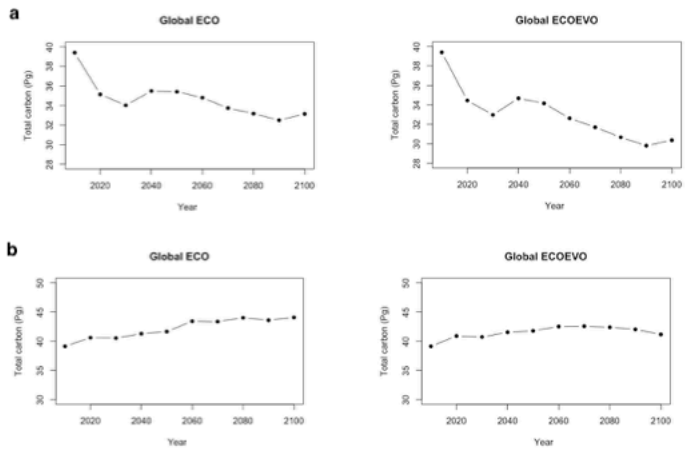

Figure 14. Projections globales des stocks de carbone du sol en réponse au réchauffement, sans évolution microbienne (*à gauche*) et avec évolution microbienne (*à droite*). (a) Sites actifs, (b) Sites dormants.

Ces résultats sont présentés dans le chapitre 5 de la thèse, sous forme d'un manuscrit en cours de préparation :

Abs E., Saleska S.R., & Ferriere R. Impact of microbial evolution on soil carbon global projections. To be submitted to *Nature Climate Change.*

6. Perspectives

Mon travail de thèse s'est focalisé sur le cas d'une stratégie microbienne stable évolutivement afin de pouvoir étudier un cas simple d'effet d'effets rétroactifs éco-évolutifs sur le cycle du carbone en réponse au réchauffement climatique. On pourra exploiter le cas où la stratégie microbienne est attractive mais non stable, cas d'un point de branchement, dans lequel il peut y avoir divergence et donc apparition d'un polymorphisme de trait dans la population microbienne en un système de type « producteur fort-producteur faible ». Durant mon stage de master 2, pendant lequel j'avais travaillé sur un modèle déterministe très similaire à celui présenté dans le chapitre 4, je m'étais intéressée à ce cas de divergence en me demandant si elle pouvait conduire à la coexistence éco-évolutive stable d'au moins deux phénotypes microbiens. Pour ce faire, j'avais construit un modèle écologique de coexistence de deux lignées microbiennes, dans lequel la représentation phénoménologique des effets écologiques des interactions locales utilisée dans le modèle mutant-résident, était remplacée par un coefficient de diffusion de façon à modéliser la séparation spatiale des deux lignées microbiennes. Les individus de la lignée 1 avaient ainsi accès à la quantité de ressources moyenne issue de la décomposition enzymatique réalisée par les enzymes produites par leur lignée et à une fraction de celle issue de la décomposition réalisée par les enzymes produites par la lignée 2 (et vice-versa pour les individus de la lignée 2). En étudiant un cas numérique remplissant les conditions de branchement évolutif, j'avais pu montrer qu'il existait une région de combinaisons de valeurs d'effet local entre mutants et résidents et du coefficient de diffusion pour lesquelles existait un polymorphisme stable mais je n'avais pas trouvé de conditions pour lesquelles des trajectoires convergeaient du point de branchement à ce point de polymorphisme stable (Fig. 15). Il devrait être possible de trouver de telles trajectoires en généralisant ce cas numérique.

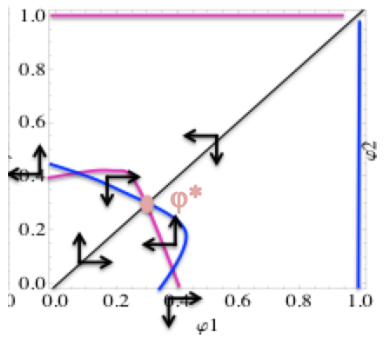

Figure 15. Modèle d'évolution (dynamiques adaptatives) de deux lignées microbiennes en compétition. Chaque lignée est caractérisée par son investissement (φ_1, φ_2, respectivement) dans la production d'enzymes. Les trajectoires évolutives conduisent l'une des deux lignées vers l'extinction.

Ce type de travail est nécessaire pour appréhender la complexité du processus d'assemblage de communautés fonctionnellement diverses.

Le modèle de coexistence n'impliquait qu'une séparation dans l'espace des espèces chimiques issues des deux lignées microbiennes. On pourrait redéfinir certains traits (par exemple l'efficacité de conversion, ou l'efficacité d'assimilation des ressources) et autoriser l'évolution de plusieurs traits à la fois, de façon à décrire une diversification vers des espèces chimiques (enzymes, DOC) différenciées. En incluant également une diversité de substrats, on étendrait ainsi avec une approche éco-évolutive rigoureuse le type d'approche de modèles multi-traits (« trait-based model ») qui cherchent à rendre compte de la diversité fonctionnelle des systèmes du sol réels (Allison 2005, Allison 2012, Folse & Allison 2012, Kaiser *et al.* 2014, 2015). En outre, les modèles à plusieurs types microbiens permettent la représentation de regroupements spatiaux de types microbiens qui augmentent leur fitness individuelle en se répartissant la production des différents types d'enzymes extracellulaires nécessaires à la décomposition de la litière (Folse & Allison 2012). Ces modèles montrent des relations complexes entre diversité, interactions sociales et taux de décomposition. On voudrait étendre l'espace discret de types microbiens que ces modèles proposent par des espaces continus sur un ou plusieurs traits. Intégrer l'évolution sur espace phénotypique continu soulèvera la question de la modélisation des *trade-offs* qui peuvent exister entre ces traits (en particulier sur les traits de type « efficacité de conversion »), par exemple entre type d'enzymes produits et types de ressources accessibles (Allison 2012). La construction d'un tel modèle s'apparenterait à l'analyse, par Kisdi et Liu (2006), de la dynamique adaptative d'une population de consommateurs soumis à un *trade-off* entre temps de manipulation et efficacité de conversion.

Certains des modèles multi-traits précédemment cités intègrent des contraintes de stœchiométrie entre nutriments (en général carbone, azote, phosphore) qui régissent les taux d'assimilation des ressources par les microbes en fonction de la composition chimique cellulaire (Folse & Allison 2012, Kaiser *et al.* 2015). Ces contraintes sont d'autant plus importantes qu'elles peuvent être étroitement associées au type fonctionnel microbien, les cellules riches en azote étant généralement celles de microorganismes à croissance rapide et à faible efficacité de conversion (comme les bactéries), tandis que les cellules riches en carbone sont typiquement celles d'organismes à croissance plus lente, à structure chimique plus complexe et à plus grande efficacité de conversion (comme les champignons). Les interactions entre microorganismes régies par les contraintes stœchiométriques de ces derniers

ainsi que par les contraintes de limitation en nutriments amèneraient à considérer des interactions interspécifiques sur la base des mêmes contraintes, celles entre microorganismes du sol et plantes. Harte et Kinzig avaient déjà décrit en 1993 un modèle à quatre compartiments fonctionnels incluant microorganismes et plantes. Les expériences d'évolution rapide de traits de plantes, comme l'adaptation à la sécheresse en quelques années de la production racinaire de l'espèce *Brassica rapa* (Franks *et al.* 2007), justifierait de tester l'évolution de traits de plantes également, et d'étudier les conséquences de dynamiques de coévolution entre microorganismes et plantes sur le taux de décomposition sur l'échelle des « temps climatiques ».

Enfin, je me suis concentrée au cours de ce travail de thèse sur la décomposition microbienne et donc sur la matière organique accessible à la décomposition, afin de prouver l'influence potentielle de l'évolution microbienne sur le taux de décomposition et le stock de carbone dans le sol. Cependant, les interactions entre climat et carbone du sol se produisent à des échelles de temps de l'ordre d'années ou siècles qui nécessitent d'intégrer les mécanismes de formation et stabilisation du sol (Davidson & Janssens 2006, Bradford *et al.* 2016, Abramoff et al. 2018) (Fig. 16). Des études récentes ont prouvé que la matière constitutive du carbone stable du sol était davantage le produit de l'association de minéraux aux produits secondaires de la décomposition microbienne plutôt que celui de la « sédimentation » des composés récalcitrants à la décomposition de la matière organique (Bradford *et al.* 2016). Ces micro-agrégats peuvent s'associer en macro-agrégats qui se désagrègent au cours du temps dû à un stress physique ou à la dégradation lente de ses constituants liants, libérant ainsi lentement la matière organique protégée dans ces complexes minéro-organiques (Sollins *et al*

1996). Les modèles globaux les plus récents (Abramoff *et al.* 2018, Sulman *et al.* 2014, Wieder *et al.* 2014) montrent l'effet de l'intégration de tels processus. Parce que la décomposition microbienne jouent un rôle déterminant dans la formation du carbone du sol et que les expériences de réchauffement en conditions naturelles évaluent l'adaptation microbienne à des échelles de temps similaires (une dizaine d'années pour les champignons et à une vingtaine d'années pour les bactéries, voir Melillo *et al.* 2017), la prochaine étape est de coupler stabilisation du sol et évolution dans un même modèle.

7. Références

1. Falkowski, P. G., Fenchel, T. & Delong, E. F. The microbial engines that drive Earth's biogeochemical cycles. *Science* **320,** 1034–1039 (2008).
2. Waksman, S. A. & Starkey, R. L. *The soil and the microbe*. (John Wiley And Sons; New York, 1931).
3. Chapin, F. S., Matson, P. A. & Vitousek, P. M. Landscape Heterogeneity and Ecosystem Dynamics. in *Principles of Terrestrial Ecosystem Ecology* (eds. Chapin, F. S., Matson, P. A. & Vitousek, P. M.) 369–397 (Springer New York, 2011).
4. Coûteaux, M. M., Bottner, P. & Berg, B. Litter decomposition, climate and liter quality. *Trends Ecol. Evol.* **10,** 63–66 (1995).
5. Verhoef, H. A. & Brussaard, L. Decomposition and nitrogen mineralization in natural and agroecosystems: the contribution of soil animals. *Biogeochemistry* **11,** 175 (1990).
6. Beare, M. H. *et al.* Microbial and Faunal Interactions and Effects on Litter Nitrogen and Decomposition in Agroecosystems. *Ecol. Monogr.* **62,** 569–591 (1992).
7. Cheng, W., Johnson, D. W. & Fu, S. Rhizosphere Effects on Decomposition. *Soil Sci. Soc. Am. J.* **67,** 1418–1427 (2003).
8. Bradford, M. A. *et al.* Managing uncertainty in soil carbon feedbacks to climate change. *Nat. Clim. Chang.* **6,** 751 (2016).
9. Allison, S. D., Wallenstein, M. D. & Bradford, M. A. Soil-carbon response to warming dependent on microbial physiology. *Nat. Geosci.* **3,** 336 (2010).
10. Singh, B. K., Bardgett, R. D., Smith, P. & Reay, D. S. Microorganisms and climate change: terrestrial feedbacks and mitigation options. *Nat. Rev. Microbiol.* **8,** 779–790 (2010).
11. Bardgett, R. D., De Deyn, G. B. & Ostle, N. J. Plant--soil interactions and the carbon cycle. *J. Ecol.* **97,** 838–839 (2009).

12. Janssens, I. A. & Luyssaert, S. Carbon cycle: nitrogen's carbon bonus. *Nat. Geosci.* **2,** 318 (2009).
13. Six, J., Frey, S. D., Thiet, R. K. & Batten, K. M. Bacterial and Fungal Contributions to Carbon Sequestration in Agroecosystems. doi:10.2136/sssaj2004.0347
14. Balser, T. C. & Wixon, D. L. Investigating biological control over soil carbon temperature sensitivity. *Glob. Chang. Biol.* **15,** 2935–2949 (2009).
15. Pachauri, R. K. *et al. Climate Change 2014: Synthesis Report. Contribution of Working Groups I, II and III to the Fifth Assessment Report of the Intergovernmental Panel on Climate Change*. 151 (IPCC, 2014).
16. Steinweg, J. M., Plante, A. F., Conant, R. T., Paul, E. A. & Tanaka, D. L. Patterns of substrate utilization during long-term incubations at different temperatures. *Soil Biol. Biochem.* **40,** 2722–2728 (2008).
17. Frey, S. D., Lee, J., Melillo, J. M. & Six, J. The temperature response of soil microbial efficiency and its feedback to climate. *Nat. Clim. Chang.* **3,** 395 (2013).
18. Davidson, E. A., Janssens, I. A. & Luo, Y. On the variability of respiration in terrestrial ecosystems: moving beyond Q10. *Glob. Chang. Biol.* **12,** 154–164 (2006).
19. Bond-Lamberty, B. & Thomson, A. A global database of soil respiration data. *Biogeosciences* **7,** 1915–1926 (2010).
20. Schuur, E. A. G. *et al.* The effect of permafrost thaw on old carbon release and net carbon exchange from tundra. *Nature* **459,** 556–559 (2009).
21. Monson, R. K. *et al.* Winter forest soil respiration controlled by climate and microbial community composition. *Nature* **439,** 711–714 (2006).
22. Freeman, C. *et al.* Contrasted effects of simulated drought on the production and oxidation of methane in a mid-Wales wetland. *Soil Biol. Biochem.* **34,** 61–67 (2002).
23. Dykhuizen, D. E. Experimental Studies of Natural Selection in Bacteria. *Annu. Rev. Ecol. Syst.* **21,** 373–398 (1990).
24. Koskella, B. & Vos, M. Adaptation in Natural Microbial Populations. *Annu. Rev. Ecol. Evol. Syst.* **46,** 503–522 (2015).
25. Gómez, P. & Buckling, A. Bacteria-phage antagonistic coevolution in soil. *Science* **332,** 106–109 (2011).
26. Jin, D. J. & Gross, C. A. Mapping and sequencing of mutations in the Escherichia coli rpoB gene that lead to rifampicin resistance. *J. Mol. Biol.* **202,** 45–58 (1988).

27. Lee, H., Popodi, E., Tang, H. & Foster, P. L. Rate and molecular spectrum of spontaneous mutations in the bacterium Escherichia coli as determined by whole-genome sequencing. *Proc. Natl. Acad. Sci. U. S. A.* **109,** E2774–83 (2012).
28. Sung, W., Ackerman, M. S., Miller, S. F., Doak, T. G. & Lynch, M. Drift-barrier hypothesis and mutation-rate evolution. *Proc. Natl. Acad. Sci. U. S. A.* **109,** 18488–18492 (2012).
29. Oliver, A., Cantón, R., Campo, P., Baquero, F. & Blázquez, J. High frequency of hypermutable Pseudomonas aeruginosa in cystic fibrosis lung infection. *Science* **288,** 1251–1254 (2000).
30. Giraud, A., Radman, M., Matic, I. & Taddei, F. The rise and fall of mutator bacteria. *Curr. Opin. Microbiol.* **4,** 582–585 (2001).
31. Becking, L. B. *Geobiologie of inleiding tot de milieukunde*. (WP Van Stockum & Zoon, 1934).
32. de Wit, R. & Bouvier, T. 'Everything is everywhere, but, the environment selects'; what did Baas Becking and Beijerinck really say? *Environ. Microbiol.* **8,** 755–758 (2006).
33. Bell, T. Experimental tests of the bacterial distance-decay relationship. *ISME J.* **4,** 1357–1365 (2010).
34. Finkel, O. M. *et al.* Distance-decay relationships partially determine diversity patterns of phyllosphere bacteria on Tamarix trees across the Sonoran Desert [corrected]. *Appl. Environ. Microbiol.* **78,** 6187–6193 (2012).
35. Östman, Ö. *et al.* Regional invariance among microbial communities. *Ecol. Lett.* **13,** 118–127 (2010).
36. Telford, R. J., Vandvik, V. & Birks, H. J. B. Dispersal limitations matter for microbial morphospecies. *Science* **312,** 1015 (2006).
37. Miller, S. R., Williams, C., Strong, A. L. & Carvey, D. Ecological specialization in a spatially structured population of the thermophilic cyanobacterium Mastigocladus laminosus. *Appl. Environ. Microbiol.* **75,** 729–734 (2009).
38. Kawecki, T. J. & Ebert, D. Conceptual issues in local adaptation. *Ecol. Lett.* **7,** 1225–1241 (2004).
39. Belotte, D., Curien, J.-B., Maclean, R. C. & Bell, G. An experimental test of local adaptation in soil bacteria. *Evolution* **57,** 27–36 (2003).
40. Macel, M. *et al.* Climate vs. soil factors in local adaptation of two common plant species. *Ecology* **88,** 424–433 (2007).
41. Vos, M., Birkett, P. J., Birch, E., Griffiths, R. I. & Buckling, A. Local adaptation of bacteriophages to their bacterial hosts in soil. *Science* **325,** 833 (2009).

42. Koskella, B., Thompson, J. N., Preston, G. M. & Buckling, A. Local biotic environment shapes the spatial scale of bacteriophage adaptation to bacteria. *Am. Nat.* **177,** 440–451 (2011).
43. Lieberman, T. D. *et al.* Parallel bacterial evolution within multiple patients identifies candidate pathogenicity genes. *Nat. Genet.* **43,** 1275–1280 (2011).
44. Buckling, A. & Rainey, P. B. Antagonistic coevolution between a bacterium and a bacteriophage. *Proc. Biol. Sci.* **269,** 931–936 (2002).
45. Lenski, R. E. & Travisano, M. Dynamics of adaptation and diversification: a 10,000-generation experiment with bacterial populations. *Proc. Natl. Acad. Sci. U. S. A.* **91,** 6808–6814 (1994).
46. Wandersman, C. & Delepelaire, P. Bacterial iron sources: from siderophores to hemophores. *Annu. Rev. Microbiol.* **58,** 611–647 (2004).
47. Schaum, C.-E. *et al.* Adaptation of phytoplankton to a decade of experimental warming linked to increased photosynthesis. *Nat Ecol Evol* **1,** 94 (2017).
48. Kell, D. B. Large-scale sequestration of atmospheric carbon via plant roots in natural and agricultural ecosystems: why and how. *Philos. Trans. R. Soc. Lond. B Biol. Sci.* **367,** 1589–1597 (2012).
49. Kell, D. B. Breeding crop plants with deep roots: their role in sustainable carbon, nutrient and water sequestration. *Ann. Bot.* **108,** 407–418 (2011).
50. Des Marais, D. L., Lasky, J. R., Verslues, P. E., Chang, T. Z. & Juenger, T. E. Interactive effects of water limitation and elevated temperature on the physiology, development and fitness of diverse accessions of Brachypodium distachyon. *New Phytol.* **214,** 132–144 (2017).
51. Wallenstein, M. D. & Hall, E. K. A trait-based framework for predicting when and where microbial adaptation to climate change will affect ecosystem functioning. *Biogeochemistry* **109,** 35–47 (2012).
52. Alster, C. J., Baas, P., Wallenstein, M. D., Johnson, N. G. & von Fischer, J. C. Temperature Sensitivity as a Microbial Trait Using Parameters from Macromolecular Rate Theory. *Front. Microbiol.* **7,** 1821 (2016).
53. Trivedi, P. *et al.* Microbial regulation of the soil carbon cycle: evidence from gene-enzyme relationships. *ISME J.* **10,** 2593–2604 (2016).
54. Yeaman, S. *et al.* Convergent local adaptation to climate in distantly related conifers. *Science* **353,** 1431–1433 (2016).
55. Thomas, M. K., Kremer, C. T., Klausmeier, C. A. & Litchman, E. A global pattern of thermal adaptation in marine phytoplankton. *Science* **338,** 1085–1088 (2012).

56. Oliverio, A. M., Bradford, M. A. & Fierer, N. Identifying the microbial taxa that consistently respond to soil warming across time and space. *Glob. Chang. Biol.* **23,** 2117–2129 (2017).
57. Yampolsky, L. Y., Schaer, T. M. M. & Ebert, D. Adaptive phenotypic plasticity and local adaptation for temperature tolerance in freshwater zooplankton. *Proc. Biol. Sci.* **281,** 20132744 (2014).
58. Jin, P., Gao, K. & Beardall, J. Evolutionary responses of a coccolithophorid Gephyrocapsa oceanica to ocean acidification. *Evolution* **67,** 1869–1878 (2013).
59. Hutchins, D. A. *et al.* Irreversibly increased nitrogen fixation in Trichodesmium experimentally adapted to elevated carbon dioxide. *Nat. Commun.* **6,** 8155 (2015).
60. Walworth, N. G., Lee, M. D., Fu, F.-X., Hutchins, D. A. & Webb, E. A. Molecular and physiological evidence of genetic assimilation to high CO2 in the marine nitrogen fixer Trichodesmium. *Proc. Natl. Acad. Sci. U. S. A.* **113,** E7367–E7374 (2016).
61. Grossman, J. D. & Rice, K. J. Contemporary evolution of an invasive grass in response to elevated atmospheric CO2 at a Mojave Desert FACE site. *Ecol. Lett.* **17,** 710–716 (2014).
62. Killeen, J., Gougat-Barbera, C., Krenek, S. & Kaltz, O. Evolutionary rescue and local adaptation under different rates of temperature increase: a combined analysis of changes in phenotype expression and genotype frequency in Paramecium microcosms. *Mol. Ecol.* **26,** 1734–1746 (2017).
63. Geerts, A. N. *et al.* Rapid evolution of thermal tolerance in the water flea Daphnia. *Nat. Clim. Chang.* **5,** 665 (2015).
64. Padfield, D., Yvon-Durocher, G., Buckling, A., Jennings, S. & Yvon-Durocher, G. Rapid evolution of metabolic traits explains thermal adaptation in phytoplankton. *Ecol. Lett.* **19,** 133–142 (2016).
65. Monroe, J. G. *et al.* Ecoevolutionary Dynamics of Carbon Cycling in the Anthropocene. *Trends Ecol. Evol.* **33,** 213–225 (2018).
66. Collins, S., Rost, B. & Rynearson, T. A. Evolutionary potential of marine phytoplankton under ocean acidification. *Evol. Appl.* **7,** 140–155 (2014).
67. Wieder, W. R., Bonan, G. B. & Allison, S. D. Global soil carbon projections are improved by modelling microbial processes. *Nat. Clim. Chang.* **3,** 909 (2013).
68. Metz, J. A. J., Geritz, S. A. H., Meszena, G., Jacobs, F. J. A. & Heerwaarden, J. S. van. Adaptive Dynamics: A Geometrical Study of the Consequences of Nearly Faithful Reproduction. 50 (1995).
69. Champagnat, N., Ferrière, R. & Méléard, S. Unifying evolutionary dynamics: from individual stochastic processes to macroscopic models. *Theor. Popul. Biol.* **69,** 297–321 (2006).

70. Dieckmann, U. & Law, R. The dynamical theory of coevolution: a derivation from stochastic ecological processes. *J. Math. Biol.* **34,** 579–612 (1996).
71. Geritz, S. A. H., Kisdi, E., Mesze´NA, G. & Metz, J. A. J. Evolutionarily singular strategies and the adaptive growth and branching of the evolutionary tree. *Evol. Ecol.* **12,** 35–57 (1998).
72. Doebeli, M. & Dieckmann, U. Evolutionary Branching and Sympatric Speciation Caused by Different Types of Ecological Interactions. *Am. Nat.* **156,** S77–S101 (2000).
73. Law, R., Marrow, P. & Dieckmann, U. On evolution under asymmetric competition. *Evol. Ecol.* **11,** 485–501 (1997).
74. Marrow, P., Dieckmann, U. & Law, R. Evolutionary dynamics of predator-prey systems: an ecological perspective. *J. Math. Biol.* **34,** 556–578 (1996).
75. Metz, J. A. J., Nisbet, R. M. & Geritz, S. A. H. How should we define 'fitness' for general ecological scenarios? *Trends Ecol. Evol.* **7,** 198–202 (1992).
76. Geritz, S. A. H., Gyllenberg, M., Jacobs, F. J. A. & Parvinen, K. Invasion dynamics and attractor inheritance. *J. Math. Biol.* **44,** 548–560 (2002).
77. Diekmann, O. A beginner's guide to adaptive dynamics. in *Mathematical Modelling of Population Dynamics* (2003). doi:10.4064/bc63-0-2
78. Smith, J. M. & Price, G. R. The Logic of Animal Conflict. *Nature* **246,** 15 (1973).
79. Hamilton, W. D. Extraordinary sex ratios. *Science* **156,** 477–488 (1967).
80. Hofbauer, J., Sigmund, K. & Others. *The theory of evolution and dynamical systems: mathematical aspects of selection*. (1988).
81. Nowak, M. An evolutionarily stable strategy may be inaccessible. *J. Theor. Biol.* **142,** 237–241 (1990).
82. Hagerty, S. B. *et al.* Accelerated microbial turnover but constant growth efficiency with warming in soil. *Nat. Clim. Chang.* **4,** 903 (2014).
83. German, D. P., Marcelo, K. R. B., Stone, M. M. & Allison, S. D. The Michaelis-Menten kinetics of soil extracellular enzymes in response to temperature: a cross-latitudinal study. *Glob. Chang. Biol.* **18,** 1468–1479 (2012).
84. Allison, S. D. Cheaters, diffusion and nutrients constrain decomposition by microbial enzymes in spatially structured environments: Constraints on enzymatic decomposition. *Ecol. Lett.* **8,** 626–635 (2005).
85. Allison, S. D. A trait-based approach for modelling microbial litter decomposition. *Ecol. Lett.* **15,** 1058–1070 (2012).

86. Folse, H. J., 3rd & Allison, S. D. Cooperation, competition, and coalitions in enzyme-producing microbes: social evolution and nutrient depolymerization rates. *Front. Microbiol.* **3,** 338 (2012).
87. Kaiser, C., Franklin, O., Dieckmann, U. & Richter, A. Microbial community dynamics alleviate stoichiometric constraints during litter decay. *Ecol. Lett.* **17,** 680–690 (2014).
88. Kaiser, C., Franklin, O., Richter, A. & Dieckmann, U. Social dynamics within decomposer communities lead to nitrogen retention and organic matter build-up in soils. *Nat. Commun.* **6,** 8960 (2015).
89. Kisdi, E. & Liu, S. Evolution of handling time can destroy the coexistence of cycling predators. *J. Evol. Biol.* **19,** 49–58 (2006).
90. Harte, J. & Kinzig, A. P. Mutualism and competition between plants and decomposers: implications for nutrient allocation in ecosystems. *Am. Nat.* **141,** 829–846 (1993).
91. Franks, S. J., Sim, S. & Weis, A. E. Rapid evolution of flowering time by an annual plant in response to a climate fluctuation. *Proc. Natl. Acad. Sci. U. S. A.* **104,** 1278–1282 (2007).
92. Abramoff, R. *et al.* The Millennial model: in search of measurable pools and transformations for modeling soil carbon in the new century. *Biogeochemistry* **137,** 51–71 (2018).
93. Sollins, P., Homann, P. & Caldwell, B. A. Stabilization and destabilization of soil organic matter: mechanisms and controls. *Geoderma* **74,** 65–105 (1996).
94. Sulman, B. N., Phillips, R. P., Oishi, A. C., Shevliakova, E. & Pacala, S. W. Microbe-driven turnover offsets mineral-mediated storage of soil carbon under elevated CO2. *Nat. Clim. Chang.* **4,** 1099 (2014).
95. Wieder, W. R., Boehnert, J. & Bonan, G. B. Evaluating soil biogeochemistry parameterizations in Earth system models with observations: Soil Biogeochemistry in ESMs. *Global Biogeochem. Cycles* **28,** 211–222 (2014).
96. Melillo, J. M. *et al.* Long-term pattern and magnitude of soil carbon feedback to the climate system in a warming world. *Science* **358,** 101–105 (2017).

Modeling Microbial Dynamics and Heterotrophic Soil Respiration – Effect of Climate Change

Elsa Abs[1,2] & Régis Ferrière[1,2,3]

1 Department of Ecology & Evolutionary Biology, University of Arizona, Tucson, AZ 85721, USA

2 Institut de Biologie de l'Ecole Normale Supérieure (IBENS), Ecole Normale Supérieure, CNRS, INSERM, PSL University, 75005 Paris, France

3 International Center for Interdisciplinary and Global Environmental Studies (iGLOBES), CNRS, ENS, University of Arizona, Tucson, AZ 85721, USA

Abstract

One major source of uncertainty in global climate predictions is the extent to which global warming will increase atmospheric CO_2 concentrations through enhanced microbial decomposition of soil organic matter. There is therefore a critical need for models that mechanistically link decomposition to the dynamics of microbial communities, and integration of these mechanistic models in global projection models of the Earth system. This chapter gives a brief introduction to mathematical models of soil microbial decomposition models and how these models can be used to predict soil C stocks and heterotrophic soil respiration, especially in the context of climate change. The chapter focuses on the microbial and enzymatic processes driving the decomposition of soil organic matter. We present the construction of fine-scale models that capture fundamental processes without excessive mathematical complexity. We show how the effect of climate change can be incorporated in these models. We then review some key insights that have been gained from these models regarding the effect of climate change on the soil C cycle. Finally, we discuss the challenge of upscaling mechanistic microbial decomposition models and integrating them into Earth system models for global projections of soil C-climate feedbacks.

Introduction

One major source of uncertainty in global climate predictions is the extent to which global warming will increase atmospheric CO_2 concentrations through enhanced microbial decomposition of soil organic carbon. Through microbial respiration, the decomposition of soil organic matter releases ten times more CO_2 to the atmosphere than human-caused emissions (Schlesinger 1997). Furthermore, soils store ~ 2,300 Pg C, nearly four times the amount of C in plant biomass (Jobbágy & Jackson, 2000). Therefore, even small changes in soil C turnover could have large consequences for atmospheric CO_2 concentrations and the stability of the global climate system. Yet most current global models do not represent direct microbial control over decomposition. Instead, all of the coupled climate models reviewed in the last Intergovernmental Panel on Climate Change (IPCC) report (Pachauri et al., 2014) assume that decomposition is a first-order decay process, proportional to the size of the soil carbon pool. There is therefore a critical need for models that mechanistically link decomposition to the size and activity of microbial communities, and integration of these mechanistic models in global projection models of the Earth system (Todd-Brown et al., 2012).

This chapter gives a brief introduction to mathematical models of soil microbial dynamics and how these models can be used to predict soil respiration, especially in the context of climate change. We recognize the importance of abiotic controls on soil carbon accessibility (through soil physical structure, mineral-organic associations, soil moisture, see sections 3 and 4) (Bradford et al., 2016; Dungait et al., 2012; Schimel & Schaeffer, 2012; Van Veen & Kuikman, 1990), however our presentation focuses on the microbial and enzymatic processes driving litter decomposition (Fontaine & Barot, 2005; Moorhead & Sinsabaugh, 2006; Schimel & Weintraub, 2003). In section 1, we present the construction of fine-scale models of soil microbial decomposition that capture fundamental processes without excessive mathematical complexity. In section 2, we show how the effect of climate change can be incorporated in these models, and address the issue of parameterization. In section 3, we review some key insights that have been gained from these models regarding the effect of climate change on soil C cycle. In section 4, we highlight some major challenges faced by current and future research. Finally, section 5 provides a summary of the chapter's key points.

1. From first-order kinetics to 4-pool *CDMZ* soil microbial models

Early models of soil organic matter (SOM) decomposition, that are still widely used in Earth system models, assume first order decomposition kinetics and take the form:

(1) $$\frac{dC}{dt} = -K\,C$$

where C is the size of a soil carbon pool, and K is a first-order rate constant which may differ among SOM pools depending on their "quality". Such first-order kinetics models assume that SOM decomposition is controlled by microbial activity, but that the rate of decomposition is independent of microbial biomass (Bradford & Fierer, 2012; J. Schimel, 2001; Wieder et al., 2015). In reality, SOM breakdown is catalyzed by extracellular enzymes that are produced by microorganisms, and its rate should therefore vary with the abundance of active microbes and microbial enzyme production. To more accurately describe the kinetics of catalyzed reactions the concentration of the catalyst *must* be part of the rate equation (Roberts, 1977). This can be done using the Michaelis–Menten relation:

(2) $$\frac{dC}{dt} = \frac{K\,Z}{K_m + C}\,C$$

where K is the fundamental kinetic constant as defined by the quality of the substrate, Z the concentration of enzymes, and K_m is the half-saturation constant of the enzymatic reaction. If we assume that Z is constant, as commonly done, then Z can be combined with K into a v_{max} term, the maximum reaction rate. Under some conditions (e.g. low C), this relationship can be

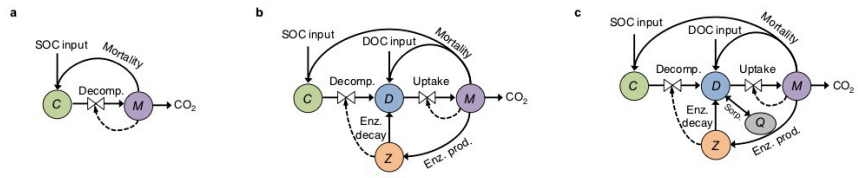

Figure 1. Structure of microbial decomposition models compared in this review. a, *CM* model: two-pool microbial model with SOC (*C*) and microbial biomass (*M*) pools. **b**, *CDMZ* model. This four-pool microbial model includes enzymatic (*Z*) decomposition of SOC and subsequent assimilation (uptake) of DOC (*D*). **c**, *CDMZ* model with soil C stabilization. This five-pool microbial model includes sorption of DOC (*D*) onto mineral surfaces to form mineral-associated DOC (*Q*) that is protected from enzymatic attack. (Adapted from Georgiou et al. 2017)

effectively simplified to a pseudo-first order equation, but even in that case, the enzyme concentration *Z* remains part of the rate (D. Schimel, 2001).

While the rate at which accessible SOM is processed is strongly controlled by the quality of the material (the fundamental *K* value), how much carbon is available locally to the microorganisms is controlled by the activity of extracellular (exo) enzymes. To model this, we need to introduce the pool of small dissolved organic carbon molecules (DOC, with concentration denoted by *D*) as an additional compartment besides soil organic carbon (SOC, concentration *C*), exoenzymes (concentration *Z*) and soil microbes (biomass *M*) (all variables being measured in C mass per soil volume unit). DOC molecules can be taken up and used by microbes to provide for their needs (in order of priority): exoenzyme synthesis; cellular maintenance (respired as CO_2); biomass production.

The production of exoenzymes and cell biomass both require energy. Some fraction of the available C pool is assimilated and respired to provide that energy. The processes shown in Fig. 1b can be translated into time-continuous differential equations that govern the change rate of *C*, *D*, *M* and *Z*. The resulting set of equations varies depending on specific assumptions on the process rates. Here we use a slightly simpler model of microbe resource allocation to present the different versions that Schimel & Weintraub (2003) derived for their model. Our simplification amounts to assuming that at low resource availability, rather than dying, microbes can reduce their maintenance cost by tuning down their metabolism (He et al., 2015; Salazar et al., 2018; G. Wang et al., 2014, 2015).

In their simplest model, Schimel & Weintraub (2003) assume that the SOM pool is large and relatively unchanging on the microbial time scale. As a consequence, the SOC pool is treated as constant, hence $\frac{dC}{dt} = 0$. Microbes uptake DOC, and uptake is assumed to be fast, so that the total uptake rate, *U*, is assumed to be constantly equal to the total production rate of DOC from SOC by decomposition. By treating the decomposition kinetics as first-order with respect to both substrate (*C*) and exoenzymes (*Z*), this can be written as $K_D\ Z\ C$. Thus, $U = K_D\ Z\ C$ at any time, and $\frac{dD}{dt} = 0$. Using our notation for resource allocation parameters, Schimel & Weintraub's (2003) simplest model has only two state variables (*M* and *Z*) and reads

(3a) $\frac{dM}{dt} = (1 - \varphi)\ \gamma_M\ \widetilde{K}_D\ Z\ -\ d_M M$

(3b) $\frac{dZ}{dt} = \varphi\, \gamma_Z\, \widetilde{K}_D\, Z\, -\, d_Z Z$

where $\widetilde{K}_D$ is the "decomposition constant" K_D for a particular SOM pool, multiplied by the constant SOC concentration (C). Microbial death is modeled as due primarily to external factors (predation, infection, and accidental abiotic causes) and is assumed to occur at a constant rate, d_M. Exoenzymes decay at a constant rate, d_Z.

This simplest model predicts either unbounded population growth, or extinction. To obtain a stable system, Schimel & Weintraub (2003) consider the possibility of competition among enzymes for binding substrates. This leads to model decomposition kinetics with a "reverse Michaelis-Menten" model, with total decomposition rate equal to $\frac{K_D\, C\, Z}{K_{es}+Z}$, where K_{es} is the half saturation constant for enzymes on substrate. Keeping the assumption that C is approximately constant, this also writes as $\frac{\widetilde{K}_D\, Z}{K_{es}+Z}$. The "reverse" Michaelis-Menten model assumes that there is functionally a saturating level of enzymes on the substrate, rather than a saturating level of substrates on the enzyme; see Vetter et al. (1998) for empirical support. The corresponding model is:

(4a) $\frac{dM}{dt} = (1-\varphi)\, \gamma_M\, \frac{\widetilde{K}_D\, Z}{K_{es}+Z}\, -\, d_M M$

(4b) $\frac{dZ}{dt} = \varphi\, \gamma_Z\, \frac{\widetilde{K}_D\, Z}{K_{es}+Z}\, -\, d_Z Z$

With such nonlinear kinetics, the system is stabilized and converges to a stable equilibrium (Moorhead & Weintraub, 2018; Sihi et al., 2016).

The fully dynamical version of the Schimel-Weintraub model relaxes the assumptions of constant SOC and DOC pools. Time variation of C, D, M, and Z obey equations 5a-d, hereafter dubbed "*CDMZ* model":

(5a) $\frac{\mathrm{dC}}{\mathrm{d}t} = \mathrm{I} - \frac{\mathrm{v}^{\mathrm{D}}_{\mathrm{max}}\,\mathrm{C}}{\mathrm{K}^{\mathrm{D}}_{\mathrm{m}}+\mathrm{C}}\mathrm{Z} + (1-p)\mathrm{d}_{\mathrm{M}}\mathrm{M} - \mathrm{e}_{\mathrm{C}}\mathrm{C}$

(5b) $\frac{\mathrm{dD}}{\mathrm{dt}} = \frac{\mathrm{v}^{\mathrm{D}}_{\mathrm{max}}\,\mathrm{C}}{\mathrm{K}^{\mathrm{D}}_{\mathrm{m}}+\mathrm{C}}\mathrm{Z} + p\mathrm{d}_{\mathrm{M}}\mathrm{M} + \mathrm{d}_{\mathrm{Z}}\mathrm{Z} - \frac{\mathrm{v}^{\mathrm{U}}_{\mathrm{max}}\,\mathrm{D}}{\mathrm{K}^{\mathrm{U}}_{\mathrm{m}}+\mathrm{D}}\mathrm{M} - \mathrm{e}_{\mathrm{D}}\mathrm{D}$

(5c) $\frac{\mathrm{dM}}{\mathrm{dt}} = (1-\varphi)\gamma_{\mathrm{M}}\frac{\mathrm{v}^{\mathrm{U}}_{\mathrm{max}}\,\mathrm{D}}{\mathrm{K}^{\mathrm{U}}_{\mathrm{m}}+\mathrm{D}}\mathrm{M} - \mathrm{d}_{\mathrm{M}}\mathrm{M}$

(5d) $\frac{\mathrm{dZ}}{\mathrm{dt}} = \varphi\,\gamma_{\mathrm{Z}}\frac{\mathrm{v}^{\mathrm{U}}_{\mathrm{max}}\,\mathrm{D}}{\mathrm{K}^{\mathrm{U}}_{\mathrm{m}}+\mathrm{D}}\mathrm{M} - \mathrm{d}_{\mathrm{Z}}\mathrm{Z}$

In equation 5a, decomposition follows from Michaelis-Menten kinetics of Z binding substrate C; there is a constant input, I, of soil organic (non decomposed) carbon from aboveground

litter, an input from microbial necromass (fraction $1 - p$ of necromass produced per unit time, at constant rate d_M), and a loss due to leaching at constant rate e_C. In equation 5b, D is produced by decomposition and the recycling of microbial necromass (fraction p of necromass produced per unit time) and inactive enzymes; D is consumed by microbial uptake, and lost by leaching at constant rate e_D. In equation 5c, growth of microbial biomass M is driven by the rate of DOC uptake (a Monod function of D) times the fraction of uptaken DOC turned into biomass, $(1 - j)\, g_M$, minus microbial death at rate d_M. In equation 5d, enzyme variation is driven by the rate of DOC uptake times the fraction allocated to enzyme production, j, and production efficiency, g_Z, minus enzyme decay at constant rate, d_Z.

Depending on parameter values (Box 2), the *CDMZ* model (5) possesses either one globally stable equilibrium, or three equilibria (one of which is always unstable). There are thresholds j_{min} and j_{max} such that the globally stable equilibrium exists for $j < j_{min}$ or $j > j_{max}$ and is given by $M = 0$, $Z = 0$, $C = I/e_C$, $D = 0$. Thus, at this equilibrium, the microbial

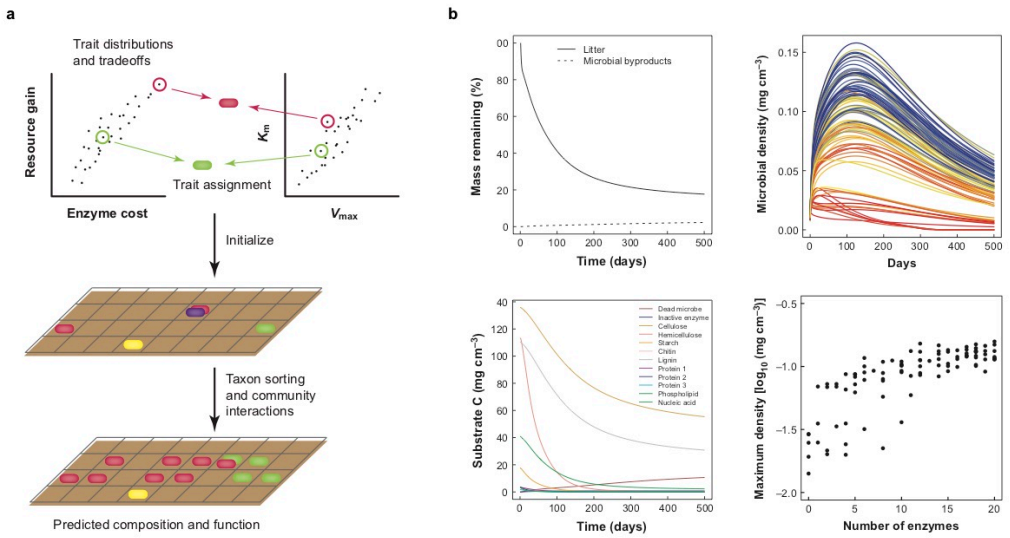

Figure 2. Structure of Allison's (2012) trait-based model DEMENT (left) and examples of outputs (middle and right). Left, Structure of the model. Multiple strains with different traits are sampled in a set of feasible trait values constrained by trade-offs (top). Initialization: strain-specific microbial biomass is randomly distributed across the microsites of a spatial grid. Dynamics: The state of all microsites is updated as within-site and between-sites processes are iterated. (Reproduced from Allison 2012)

population is extinct and no decomposition occurs. For $j_{min} < j < j_{max}$, the microbial population can either go extinct (then the system stabilizes at the same equilibrium as before) or persists at or around a non-trivial equilibrium, which can be solved for analytically. Note that j_{min} and j_{max} depend on all microbial and model parameters.

Variants of the basic *CDMZ* model (5) have been introduced (Steven D. Allison et al., 2010; Tang & Riley, 2014; G. Wang et al., 2013; Y. Wang et al., 2014; Zhang et al., 2014). All these models greatly simplify the spatial structure of soil and treat soil carbon and microbial pools as spatially and chemically homogenous. In reality, soil microbes and substrates interact at micro-scales, and at any point in time, state variables may vary greatly among micro-sites. Moreover, heterogeneity exists in the physiological and biochemical traits present in the system, which results in a distribution of parameters controlling microbial growth, extracellular enzyme production, and enzyme affinity. Trait-based computational models have been developed to account for such spatial and functional heterogeneity. Trait-based models trade off mathematical formalism for biological complexity. By explicitly representing diversity, trait-based models can simulate ecosystem processes based on spatial and functional trait distributions in a community.

Allison (2012) constructed a trait-based model that links microbial community composition with physiological and enzymatic traits to predict litter decomposition rates. The model, dubbed DEMENT, is spatially explicit and integrates processes from micrometer to millimeter scale (Box 1,

). Microbial cells interact on a square grid. The grid is analogous to the surface of a decomposing leaf, and multiple microbial cells may occupy the same grid box. The microbial community is made up of multiple strains. Each strain is characterized by phenotypic traits including: the enzymes that the strain produces, the rates at which the strain produces them, the strain's MGE. There is a given list of enzymes and substrates, and each enzyme is characterized by its substrates' binding affinities and kinetics parameters. The trait-based model captures the interaction between the diversity of enzymes and substrates, and how this interaction feeds back on the community of microbial strains and shape their diversity and abundances. For example, in response to an input of litter this "chemo-ecological" feedback determines the time trajectory of each substrate, when different strains peak in density, what densities they actually reach, and how these properties depend on the strains' trait values (Fig. 2b). The system state variables (e.g., litter, strain abundances) can then be aggregated at the

scale of the whole grid to characterize the dynamics of total microbial biomass and organic matter at that scale.

Parameterization of the *CDMZ* models (Box 2) have been based on observational measurements and incubation experiments (e.g. German et al., 2012; Sulman et al., 2014), involving in some cases inverse modeling and parameter optimization (German et al., 2012). Trait-based models can also tap into 'omics' data to assess the diversity of microbial and enzyme communities, estimate relative abundances, and measure activity and specificity (Trivedi et al., 2013; Fierer et al., 2014).

Box 1. Microbial and decomposition processes in trait-based models

Here we summarize some important details of Allison's (2012) trait-based model DEMENT.

- Microbial cells interact on a 2-dimensional square grid. Boundary conditions are periodic, i.e. the grid edges contact each other, forming a torus. The grid is initialised with a homogeneous distribution of each substrate and monomer. Each grid box is colonised at random by each taxon with a 1% probability, meaning that each strain is expected to occupy ~ 100 grid boxes on the 100 x 100 grid. Each strain in an occupied grid box is initialised with biomass C concentration 1 mg cm^{-3}, such that the average biomass density across the grid is ~ 1 mg cm^{-3} with 100 different strains.
- Each polymeric substrate can be degraded into monomers by multiple (randomly chosen) enzymes, and each enzyme can degrade at least one substrate. Substrate degradation obeys Michaelis-Menten regulation.
- Microbial uptake rates are also modeled as Michaelis-Menten functions of monomer concentrations and microbial strain biomass. Each strain is characterized by its transporters; each transporter binds to at least one monomer, and each monomer corresponds to at least one transporter. Uptake is measured first per transporter and then scaled up to strain biomass. When If the monomer pool size is limiting, the available monomer is partitioned among strains in proportion to their calculated uptake rates.
- Microbial growth is represented implicitly as the difference between uptake and loss processes. Microbial growth is modeled within each grid box, where the microbes present have the first opportunity to take up DOC (monomers). Microbes respire a fraction of C upon uptake, representing the energy cost of monomer metabolism, and additional respiration occurs as a consequence of processing a fraction of biomass and uptaken monomers to produce enzymes (the use of a biomass fraction represents constitutive

enzyme production). There is also a daily maintenance cost for each uptake transporter, expressed as a fraction of microbial biomass C.

- C, N, P stoichiometry is explicit. There are thresholds on microbial biomass C, N, P such that excess elements are mineralized into CO_2 or inorganic nutrients. Stoichiometry is assumed constant across all enzymes.
- The state variables of each grid box are updated on a daily timescale. Typical runs are 500 time steps, i.e. the simulations describe the system dynamics over 500 days.
- Grid boxes are spatially connected by (i) diffusion of excess monomers after uptake by microbes within each grid box. Diffusion is instantaneous and excess monomers from any grid box are uniformly distributed across the entire grid; (ii) biomass dispersal, which occurs when local (i.e. within a grid box) biomass of a given strain reaches some threshold; then that biomass splits and one half disperses to a grid box in any direction up to some maximum dispersal distance. Dispersal is independent of whether or not the destination grid box is occupied.
- The distribution of feasible traits is constrained by physiological tradeoffs. Three tradeoffs are considered: (i) between enzyme substrate generalism and maximum reaction rate (i.e. more generalist enzymes have lower v_{max}^D); (ii) between v_{max}^D and binding affinity (resulting in a positive correlation between v_{max}^D and K_m^D); (iii) between microbial growth and enzyme production (the strain position along this tradeoff is measured by j in our formalism, *cf.* Fig. 1b).

In Allison (2012)'s model, microbial stoichiometry is flexible and enzymes are randomly attributed to microbial taxa and substrates, and therefore distinct traits among microbial taxa (enzyme types and quantities produced, and C, N, P stoichiometry) are an emerging property of the model. Kaiser et al. (2014) specifically address the question of the link between C and N availability community dynamics and decay rates, and they build on Allison (2012)'s model by adding the following features.

- They initialize their model with pre-selected microbial functional groups with distinct life-history traits: maximal cell size, maximum turnover rate, cell chemical composition and C : N ratio, and enzyme production rate and types).
- Secondary substrates are divided into C-rich (C: N ratio of 150) and N-rich (C: N ratio of 5) microbial products.
- Diffusion is not instantaneous but is instead modeled using Brownian motion.

- A fraction of enzyme production is constitutive but a fraction of it is resource dependent, such as growth, after maintenance and constitutive production are completed.
- Nutrient excess released from cells is mineralized for both C and N.

2. Incorporating climate parameters

Three climate-change drivers that may alter soil biogeochemistry and change future soil respiration and C stocks are changing temperature, altered precipitation regime, and elevated CO_2 (Wieder et al., 2015). Mathematical models that include explicit microbial traits and parameters provide the opportunity to mechanistically represent the effect of such abiotic factors on decomposition. Then the response of decomposition and soil respiration to climate change becomes an emerging property, integrated across the individual physiological responses of microorganisms and up-scaled by individual interactions through population and community levels. As a consequence, the response of microbial biomass and respiration to climate change may be decoupled (Todd-Brown et al. 2012). Numerous laboratory studies support the assumption that microbial respiration increases exponentially with temperature (Davidson et al., 2006; Lloyd and Taylor, 1994). But even though biomass-specific respiration tend to increase with temperature, community-level respiration is ultimately mediated by the emerging response (increase or decrease) of microbial biomass (Steven D. Allison et al., 2010).

Temperature

In the models reviewed in Section 1, the v_{max} parameter of Michaelis-Menten kinetics represents the proportionality constant between enzyme concentration and process rate (hydrolysis, uptake and metabolism). This general parameter has a well-established dependence on temperature as defined by the Arrhenius equation, which has an exponential form:

$$(6) \qquad v_{max} = v_0 \, e^{-\frac{E_a}{R(T+273)}}$$

where v_0 is a pre-exponential coefficient, Ea is the activation energy for the reaction, and R is the ideal gas constant. The activation energy represents the temperature sensitivity and biochemical resistance of the substrate to catalysis.

The temperature response of half-saturation constants K_m is uncertain. There is some evidence from animal physiology literature that enzyme K_m values tend to increase with

temperature, thereby reducing affinity for substrate and slowing catalysis (Hochochka & Somero, 2002; Somero, 1978; Somero, 2004). Although recent work showed a declining response of K_m of multiple enzymes, probably due the production of isoenzymes (Sihi et al., 2019), K_m has most commonly been hypothesized to increase with temperature in soil (Davidson et al., 2006; Davidson and Janssens, 2006). Todd-Brown et al. (2012) suggested representing K_m for extracellular enzymes as a linear function of temperature, whereas German et al. (2012) opted for an exponential function, leading to an Arrhenius-like model of K_m sensitivity to temperature.

Because intracellular enzymatic catalysis is limited by the availability of DOC whereas availability of SOC limits extracellular catalysis, models of temperature dependence need to use parameters that are specific to extracellular enzymatic catalysis vs. microbial uptake and metabolism (Todd-Brown et al. 2012). Consistently with model choices made by Allison et al. (2010) and German et al. (2012), this leads to the following set of equations that can be incorporated in the *CDMZ* model (5):

(7a) $$v_{max}^{D} = v_0^{D}\, e^{-\frac{E_V^{D}}{R(T+273)}}$$

(7b) $$K_m^{D} = K_0^{D}\, e^{-\frac{E_K^{D}}{R(T+273)}}$$

(7c) $$v_{max}^{U} = v_0^{U}\, e^{-\frac{E_V^{U}}{R(T+273)}}$$

(7d) $$K_m^{U} = K_0^{U}\, e^{-\frac{E_K^{U}}{R(T+273)}}$$

where T is temperature in Celsius, R is the ideal gas constant, and the E parameters denote the corresponding activation energies.

By increasing kinetic energy, warming accelerates enzyme-catalyzed reactions and stimulates C consumption by soil microbes. Thus, the response of microbial respiration to warming is determined by the abundance (microbial biomass M in the models introduced in the previous section) and function of the microbial community. For a given mass-specific uptake rate, warming may affect M through two demographic mechanisms:

- decreasing MGE, as a consequence of increasing the energy cost of maintaining existing biomass (Sinsabaugh et al., 2013);
- increasing the microbial death rate (Hagerty et al., 2014; Joergensen et al., 1990).

The effect of temperature on maintenance energy cost, resulting in MGE decreasing with warming, has been observed in pure culture experiments (Crowther & Bradford, 2013;

Manzoni et al., 2012). However, responses of MGE to warming are generally equivocal, possibly due to methodological reasons, or to actual processes related to substrate type (Frey et al., 2013), or to physiological acclimation (Steven D. Allison, 2014), or to the magnitude of warming (Sihi et al., 2018). Hagerty et al. (2014) reported data from short-term laboratory soil incubation showing a significant increase in turnover rate of microbial biomass with warming, but no sensitivity of MGE to temperature. To represent a negative effect of temperature on MGE, Allison et al. (2010), German et al. (2012), Wang et al. (2013) used a linear relationship (see also Todd-Brown et al. 2012, Li et al. (2014)):

(8) $$\gamma_M = \gamma_{M,ref} - m(T - T_{ref})$$

with T_{ref} = 20 °C. To represent a positive effect of temperature on microbial mortality, Hagerty et al. (2014) used the Arrhenius model:

(9) $$d_M = d_{M0}\, e^{-\frac{E_{dM}}{R(T+273)}}$$

Soil moisture and precipitation regime

With climate change, frequency and intensity of precipitation will become increasingly variable (Pachauri et al., 2014). Variation in soil moisture can have strong transient effects on soil respiration that have long been observed in laboratory as well as field experiments. The

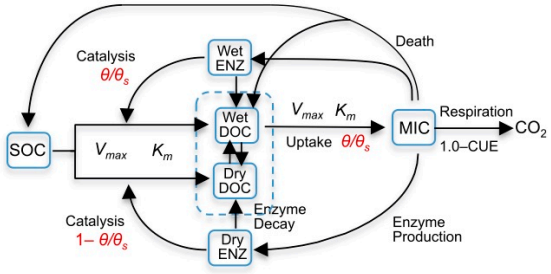

Figure 3. *CDMZ* model extended to account for variation in soil moisture. SOC decomposition and microbial uptake rates are controlled by water saturation, ϑ/ϑ_s, where q is volumetric water content and ϑ_s is porosity (dependent on soil texture). The model splits DOC and enzyme pools into two, respectively, one for the wet zone and the other for the dry zone of soil pore space. Microbial uptake of DOC occurs only in the wet zone, and the uptake is linearly related to ϑ/ϑ_s. The enzyme catalytic rate is proportional to ϑ/ϑ_s in the wet zone, and to $1 - \vartheta/\vartheta_s$ in the dry zone. (Reproduced from Zhang et al. 2014)

well-known "Birch effect" (Birch, 1958) refers to the dramatic increase in soil respiration caused by pulsed wetting after drought periods. To include the effect of variation in soil moisture due to variable precipitation in *CDMZ* models, Zhang et al. (2014) introduced controls of enzyme activity and DOC uptake by water saturation (ϑ/ϑ_s in

), and distinct pools of wet vs. dry enzymes and DOC (Fig. 3). These pools reflect the heterogeneous soil structure, in particular pore size distribution and wet and dry zones within soil pores. Microbes can only access DOC in the wet pores. SOC decomposition occurs in the dry pores at a reduced efficiency due to enzyme immobilization; enzymes in the dry pores are also expected to have a lower deactivation rate due to protection from decay (Alster et al., 2013).

It remains unclear whether soil moisture constrains microbial activity primarily through direct (via desiccation stress) or indirect (via its impact on diffusion of substrates or enzymes) mechanisms. Zhang et al. (2014) used linear functions to relate enzyme and uptake rates to soil moisture. However, at very low and high moisture levels, the relationship is likely nonlinear (Davidson et al., 2012; Lawrence et al., 2009; Moyano et al., 2013). For example, at high water content, O_2 becomes a limiting factor, whereas at low water content, diffusion is constrained by thin and discontinuous water films (Abramoff et al., 2017; Davidson et al., 2012; D. Sihi et al., 2018). On the other hand, Homyak et al. (2018) argue that dry periods increase C substrate availability through abiotic processes.

Elevated CO_2

Many field studies have found that elevated atmospheric CO_2 (eCO_2) leads to higher carbon assimilation by plants leading to higher carbon storage in soils, through higher root production, higher litter production and enhanced root exudation (Liu et al., 2005; Norby et al., 2005; Phillips et al., 2011; Pregitzer et al., 2008), and even more so in surface soils (Hicks Pries et al., 2018). Individual microbes have shown no response to eCO_2 in lab experiments (Carney et al., 2007; Norby et al., 2001), in which case soils should accumulate carbon at eCO_2. However, enhanced litter and root exudate inputs can increase soil respiration and SOC decay rates (called "priming effect") and induce soil C losses (Kuzyakov, 2010; Pendall et al., 2014), through enhanced production of enzymes decomposing recalcitrant substrates (Phillips et al., 2011), or changes in the microbial community composition (Blagodatskaya et al., 2010; Carney et al., 2007; Cheng et al., 2012). Blagodatskaya et al. (2010) found a linear relationship between microbial growth rate and atmospheric CO_2 concentration. This

relationship has not been included in soil microbial models, but priming effect has been modeled with higher litter inputs (J. E. Drake et al., 2013; Sulman et al., 2014).

In Sulman *et al.* (2014)'s model, three classes of soil C compounds are included (simple, chemically resistant plant-derived, chemically resistant microbe-derived), characterized by different maximum decomposition and microbial uptake rates, and each existing in both unprotected and protected forms (Fig. 4). Only unprotected carbon is accessible to microbes. The model shed light on the role played by priming effects in the response of C stocks to warming. This was done by comparing a rhizosphere model with increasing root exudation (calibrated with data from eCO_2 field experiments), and a bulk soil model without root exudates. At regional scale, the model predicted either net loss of soil C or sequestration, depending on litter quality (determined by the plant community) and soil texture. At global scale, the model predicted a loss of soil C.

First-order models would fail to account for priming effects (Zaehle et al., 2014). This is because without microbial-driven decomposition, soil C increases linearly with inputs (Li et al., 2014). Recent non-microbial models have tried phenomenologically to capture priming effects by representing multiple SOC pools for which decay rates vary with litter inputs, using observed responses of plant growth and microbial respiration for parameterization (van Groenigen et al., 2015; Z. Luo et al., 2017). However, priming effects might not persist over

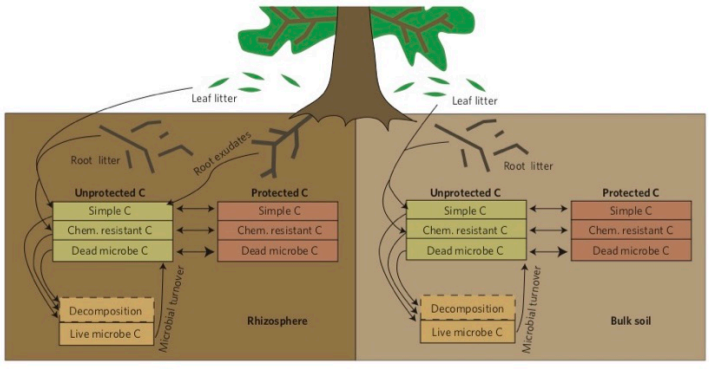

Figure 4. Structure of Sulman *et al.* (2014)'s model. Soil carbon is divided into three chemical classes, which can be protected or unprotected. Decomposition is mediated by microbial biomass, which takes up a portion of decomposed carbon and loses carbon to CO2 and the dead microbial C pool over time. Soil is separated into the rhizosphere, which receives root exudate inputs, and bulk soil, which does not. (Reproduced from Sulman *et al.* 2014)

time in certain ecosystems (John E. Drake et al., 2018), raising the need for more long-term experiments to better represent priming effects over time across biomes.

If enhanced root exudation in eCO_2 leads to stimulated root and microbial respiration, eCO_2 may also result in enhanced weathering because higher soil CO_2 concentration from respiration supplies more protons for dissolution reactions (Goddéris et al., 2006). Root exudates also promote weathering because they contain organic acids (e.g. oxalic acid) and organic phenolic compounds (Keiluweit et al., 2015; McGill, 1996; Natali et al., 2009) that disrupt mineral-organic associations. The breakdown of mineral-associated organic compounds releases previously inaccessible organic C and inorganic nutrients such as phosphorus (Amundson, 2003) that could further stimulate microbial activity in nutrient-limiting conditions. Although some studies provide strong indication that eCO_2 will promote weathering (Karberg et al., 2005), specific experiments are needed to predict the magnitude of the feedbacks between atmospheric CO_2, microbial activity and weathering in different ecosystems over time (Brantley et al., 2011).

3. What do we learn from *CDMZ* models?

In this section we focus on what models of soil microbial dynamics tell us about the response of soil respiration to climate warming. Field experiments have documented an initial increase in CO_2 efflux from soils, followed by a decline in CO_2 loss, down to control levels within a few years (see e.g. Y. Luo et al., 2001; Melillo et al., 2002; Oechel et al., 2000). Recent long-term warming experiments show that the response might be more complex over time (Melillo et al., 2017). Can models help us explain explain empirical patterns and their variation? How can models help us explain the Birch effect, i.e. the sudden pulse of soil respiration after precipitation pulses? And moving up to larger scales (Huang et al., 2018; D. Sihi et al., 2018; K. Wang et al., 2017), how can mechanistic models of microbial dynamics and soil respiration be used to improve coupled projections of the C cycle and Earth climate?

Box 2. Model parameterization

Using *CDMZ* models to extrapolate short-term empirical results and assess their significance for long-term ecosystem states requires model parameterization with realistic values. Parameter values are obtained from the empirical literature, derived from experiments specifically designed to measure them (e.g. German et al. 2012), or constrained to promote

model stability and reasonable quantitative outputs. Allison et al. (2010), Allison (2012), German et al. (2012) and Kaiser et al. (2014, 2015) provide useful list of values and ranges to parameterize *CDMZ* models and their trait-based extensions.

- *Target outputs*. The target C is of the order of 100 mg cm^{-3}, biomass *M* is about 2% of C, *Z* is about 1% of *M* and *D* is limiting, hence close to 0. 60% of the microbial biomass is estimated to be in the first 5cm, 70% in the first 10cm and 80% in the first 20cm below surface (Fierer et al., 2009), therefore the vertical resolution of microbial processes is not as relevant as for other processes of soil formation.
- *Carbon inputs.* Using global predictions of the fraction of NPP that goes into litter from the CMIP5 averaged over 2005-2020, litter inputs range between 0 (e.g. in high latitudes) and ~1700 gC cm^{-2} y^{-1} (e.g. in tropical forests). Most mechanistic microbial models do not include coarse wooden debris in litter inputs and litter inputs are therefore usually below 100 gC cm^{-2} y^{1} (Allison 2010; German et al, 2012; Wang et al., 2012, 2013).
- *Microbial parameters.* The microbial death rate is typically fixed between 0.05 and 0.0002 h^{-1} corresponding an expected lifespan of between 1 and 200 days (Allison et al., 2010; German et al., 2010; Sulman et al., 2014; Wieder et al., 2013). Dead biomass is recycled in equal proportion between SOC and DOC. The uptake kinetics are poorly known and are therefore assumed to follow enzymatic properties. Assuming that DOC substrate is close to 0 and does not saturate the uptake rate, K_m^U is fixed to 0.3 mg cm^{-3}. The temperature sensitivity function for K_m^U is assumed to be linear positive and the proportional factor is fixed to 0.01 mg cm^{-3} $°C^{-1}$. The 20°C value and Arrhenius relation for v_{max}^U are the same as for v_{max}^D (Allison et al., 2010). In models integrating rules of stoichiometry with nitrogen and phosphorous, predicted stoichiometry is compared with the empirical ratios of 8.6 for C: N and 7 for N: P (Cleveland & Liptzin, 2007).
- *MGE temperature dependence.* Empirical studies in soils suggest that MGE declines by at least 0.009 $°C^{-1}$ (Steinweg et al., 2008). Allison et al. (2010) assumed MGE = 0.63 – 0.016 *T* for temperature *T* between 0 and 25 °C and they tested as well decreasing its sensitivity to half.
- *Enzyme production.* In Allison et al.'s (2010) *CDMZ* model, the microbial rate of enzyme production is fixed at 0.012% of microbial biomass per day. In models where enzyme production is a fraction of resources taken, this fraction ranges between 0.0005 and 0.2 (Burns et al., 2013; Kaiser et al., 2014, 2015; Schimel & Weintraub, 2003). Models integrating N and P assume no cost in these nutrients for enzymes.

- *Enzyme parameters.* The deactivation rate is typically fixed around 0.02 d^{-1}, corresponding to an expected lifespan of 50 days (Allison et al., 2010; Allison, 2012; Kaiser et al., 2014, 2015; Wang et al., 2013). Assuming that the SOC substrate does not saturate enzyme reactions, K_m^D is fixed to 600 mg cm^{-3}. The temperature sensitivity function for K_m is assumed to be linear positive and the proportional factor is fixed to 5 mg cm^{-3} $°C^{-1}$. The pre-exponential coefficient in the Arrhenius relation for v_{max}^D was constrained by equilibrium stability at 20 °C. Activation energies for soil hydrolytic enzymes vary from 13 to 94 kJ mol^{-1} with most values in the range of 20–50 kJ mol^{-1} (McClaugherty & Linkins, 1990; Trasar-Cepeda et al., 2007).

Explaining empirical patterns of soil respiration responses to climate change

Short-term laboratory and field experiments have shown consistently that soil respiration increases exponentially with temperature. On longer timescales, soil respiration tends to decline, but it has been very difficult to tease apart possible explanatory mechanisms, such as a decreasing SOC stock, a decreasing microbial biomass, or a reduced production of enzyme that may be caused by individual-level physiological acclimation, or population-level genetic adaptation, or community-level ecological shift (Karhu et al., 2014).

Allison *et al.* (2010) sought to explain the nonlinear, hump-shaped pattern of soil CO_2 loss with warming by using the basic *CDMZ* model with constant or temperature-dependent MGE. Their goal was to evaluate the model's ability to reproduce the transitory increase in soil respiration as well as generate plausible changes in *C*, *M* and *Z*. They focused on ecosystems for which no dramatic changes in SOC pools had been reported (Schuur et al., 2009) while microbial biomass declined with warming (Steven D. Allison & Treseder, 2008; Bradford et al., 2008; Rinnan et al., 2007). This pattern may not be general (T. W. Crowther et al. (2016) and van Gestel et al. (2018) reported significant losses of soil C under warming), however Allison et al.'s (2010) analysis is a first attempt to understand the mechanistic link between heterotrophic respiration and soil C loss in response to climate warmong. Specifically, Allison et al. (2010) simulated the consequences over time, with a 30-year horizon, of 5 °C warming. Warming was abrupt (instantaneous) and represented a perturbation of the model's parameters (previously set at 20 °C). Transient dynamics over 30 years were simulated by monitoring the state variables initialized at their equilibrium value at 20 °C. Their baseline model assumes that temperature affects the microbial uptake rate and

the exoenzyme catalysis rate. They compare model simulations run (Fig. 5) under the following scenarios:

- MGE may be constant, decrease with warming, or "acclimate" i.e. show reduced sensitivity to temperature (Fig. 5a).
- The temperature sensitivity of enzymes itself may be constant, or "acclimate" i.e. decrease with warming through a 50% reduction in maximal activity (v_{max}^{D}) and 50% increase in the half-saturation constant (K_m^D) (Fig. 5b).

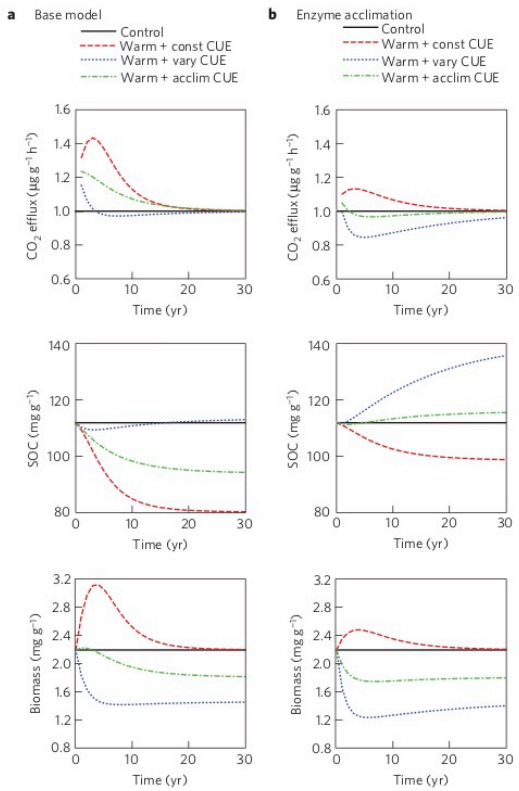

Figure 5. Response of microbial dynamics and soil respiration to 5 °C warming predicted by Allison et al.'s (2010) *CDMZ* model. a, Enzyme sensitivity to temperature is fixed. **b**, Enzyme parameters v_{max}^{D} and K_m^D are ajusted to compensate their intrinsic response to warming. Scenario "vary CUE" assumes a constant temperature-dependence of Carbon Use Efficiency (*sensu* Allison et al. 2010). Scenario "acclim CUE" assumes that CUE responded to warming with reduced temperature sensitivity. (Adapted from Allison *et al.* 2010)

The conclusion from these simulations is that, without enzyme "acclimation" (Fig. 5a), only the temperature-dependent MGE scenario (dotted line in Fig. 5a) can produce the target pattern of transient increase in the soil CO_2 loss rate, little change in the SOC pool, and reduced microbial biomass. Assuming that enzyme activity can acclimate (Fig. 5b), the best match of the empirical target is achieved by the "acclimating" MGE scenario.

What happens if we use simpler models in which the enzyme pool is not explicitly represented ("*CDM* models"), to predict the effect of warming on soil CO2 loss, SOC stock,

and microbial biomass? In these models (such as the "conventional model" *sensu* Allison et al. 2010), microbial processes, including degradative enzyme production and activity, are not explicitly coupled to soil C turnover, so temperature-driven changes in microbial biomass and enzymes cannot interact with the response of decomposition to warming. Allison et al. (2010) report simulations of a *CDM* model for constant, temperature-dependent or "acclimating" MGE. The *CDM* model can predict the transient rise in respiration along with the decline in microbial biomass, but in all cases the *CDM* model predicts strong SOC stock decline, which, according to Allison et al. (2010) is at odds with empirical observations.

Li et al. (2014) reported a model comparison encompassing Allison et al.'s (2010) "conventional" (*CDM*) and *CDMZ* models and Wang et al. (2013) *CDMZ* model with multiple SOC and enzyme pools (and also German et al.'s (2012) simplified "*CM* model" (Fig. 1a), which does not explicitely represent the DOC and enzyme pools). Like Allison et al. (2010), they assume initial equilibrium at 20 °C and instantaneous + 5 °C warming, and they monitor the subsequent system dynamics under different scenarios of MGE temperature dependence (no dependence, constant decline, reduced decline). Whereas the main effect of warming in the "conventional" microbial model is to reduce the equilibrium SOC pool, the direction of SOC change in the *CDMZ* models depends on the balance between increases in K_m parameters and declines in MGE with warming, both of which tend to increase SOC; and increases in v_{max} coefficients, which tend to reduce SOC (Li et al., 2014). Li et al. (2014) model comparison also shows that in all *CDMZ* models and scenarios, there is a critical temperature that minimizes the equilibrium SOC stock. This critical temperature, T_{crit}, determines whether warming causes a gain or loss of soil C in a given ecosystem. Cooler ecosystems with mean temperature below T_{crit} are expected to lose soil C in response to warming, whereas warmer ecosystems with mean temperature above T_{crit} are predicted to store more C in response to warming. The critical temperature depends on the temperature dependence scenario and model complexity.

The temperature-dependence of the microbial death rate was ignored in the models that Li et al. (2014) compared. In a laboratory study, Hagerty et al. (2014) documented the case of a forest soil in which MGE is temperature-independent while microbial turnover (death rate) accelerates with warming. By using Allison et al.'s (2010) *CDMZ* model with either constant or temperature-dependent MGE and microbial death rate, Hagerty et al. (2014) evaluated the long term consequences of increasing microbial mortality with warming. Focusing on equilibrium SOC sampled at 3 °C and incubated in temperatures between 5 and 20 °C, they

found that temperature-dependent mortality results in significant decrease in microbial biomass (equilibrium *M*) and increase SOC (equilibrium *C*), these effects being similar in direction but much larger than in the temperature-dependent MGE/temperature-independent mortality scenario.

Wang et al. (2013) built on Allison et al.'s (2010) *CDMZ* model by considering two SOC pools (particulate organic carbon, POC, and mineral-associated organic carbon, MOC) and associated exoenzymes. It is the first *CDMZ* model to account for the soil C stabilization mechanisms of DOC adsorption and SOC association with minerals. In this model, only adsorbed DOC is protected, i.e. inaccessible to microbes; MOC can still be decomposed but at slower rate than POC. Their model can reproduce the response of total SOC to warming predicted by Allison et al.'s (2010) *CDMZ* model. As climate change affects water availability and therefore accessibility of microbes to SOC and mineral-organic matter interactions, Wang et al.'s (2013) model is well suited to study the effect of multivariate climate change.

Tang and Riley (2015) introduced another *CDMZ* model accounting for mineral-organic interactions. The model does not account explicitely for adsorbed or mineral-associated carbon pools, instead mineral associations with enzymes and DOC are represented as competing reactions at equilibrium, in which enzymes bind with SOC and microbes bind with DOC. This mechanism alters the fraction of accessible SOC for enzymes and DOC for microbes. Additionally, Tang and Riley's (2015) model represents daily and seasonal change of temperature. This makes their model well design to investigate the consequences of dynamical climate variation across multiple timescales.

Zhang et al. (2014) used the extended *CDMZ* model (Fig. 3) to investigate the causes of Birch pulses of soil respiration in response to episodic rainfall pulses. Their approach goes beyond the kind of model-based extrapolation of empirical data that studies such as Allison et al. (2010) and Hagerty et al. (2014) implemented. They evaluated alternate hypotheses by constructing *CDMZ* models corresponding to their different hypotheses and fitting these models to a set of field measurements of soil respiration from a semiarid savannah ecosystem driven by episodic rainfall pulses (Fig. 6). They used some known parameter values (see previous section) and performed Bayesian parameter estimation of MGE, enzyme production rate, microbial death rate, and enzyme deactivation rate. They evaluated and compared the models using three assessment criteria considering both goodness of fit and model complexity. The best model turns out to be the one depicted in Fig. 3; this model accounts for

the moisture-dependence of enzyme activity and microbial uptake rates, and for the processes of accumulation and storage of DOC in the dry soil pores during dry periods (that is temporarily inaccessible to microbes), along with the facilitation of SOC decomposition

during dry periods by enzymes localized in dry soil pores (Homyak et al., 2018). Soil microbial models are also effective in reproducing drought events in primarily temperature-limited system like that in temperate and boreal forests (Sihi et al., 2018).These results emphasize the need to better understand and quantify the mechanisms of DOC accumulation in dry soil pores.

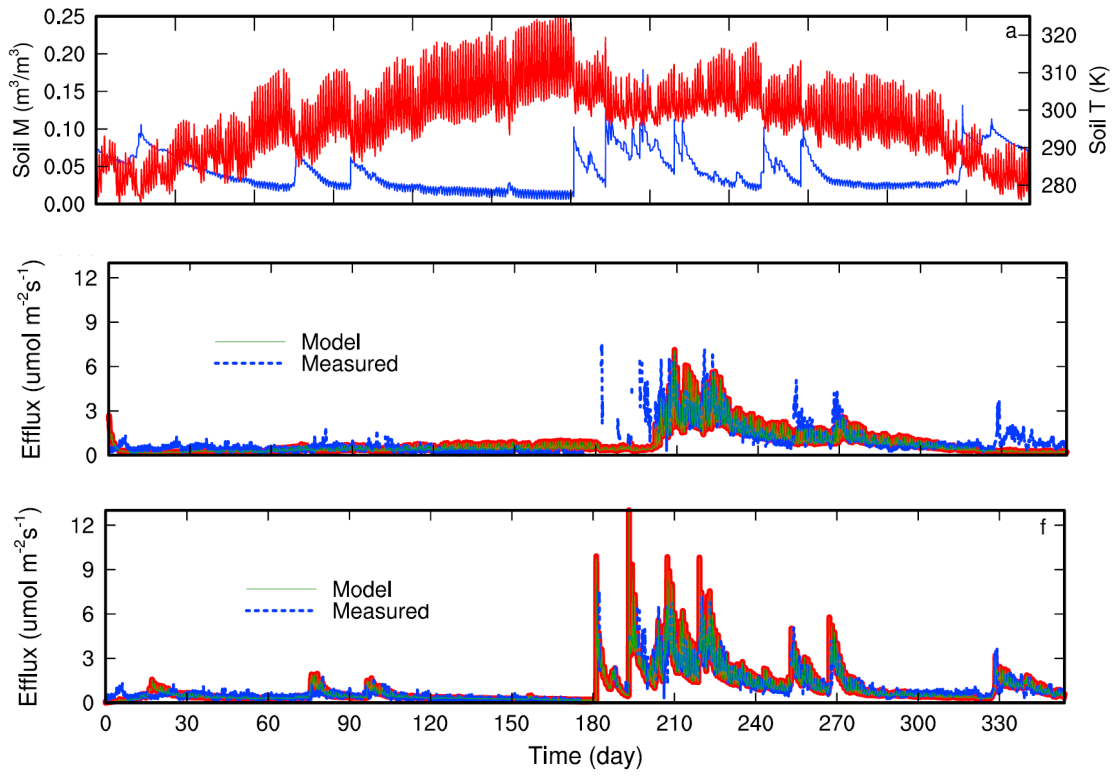

Figure 6. Data assimilation and model selection for the effect of rainfall pulses on soil respiration. Top, Observed half-hourly volumetric soil moisture (in m3 m^{-3}) and temperature (in K) at 10 cm. **Middle and Bottom**, CO2 efflux measured half hourly at the soil surface (in µmol m^{-2} s^{-1}) compared with (**Middle**) the basic *CDMZ* model of Fig. 1b, and (**Bottom**) the six-pool *CDMZ* model shown in Fig. 3. The shaded area (in red) represents the 95% credible interval, while the green line is for the best realization. (Reproduced from Zhang *et al.* 2014)

Projecting global soil C stocks in a changing climate

Mechanistic models are useful to investigate the significance of short-term experimental results to long-term ecosystem states, and to evaluate alternative hypotheses for explaining empirical data. They also exhibit two general properties that are relevant for scaling up microbial processes to the global Earth system.

- First, the C stock response to warming depends on the initial temperature. Soil carbon losses are expected in cold biomes, such as Arctic tundra; minimal carbon losses or even carbon gains are predicted in warm regions such as the tropics.
- Second, the C stock at steady state appears to be decoupled from inputs. In Allison et al.'s (2010) *CDMZ* model, equilibrium C depends on the ratio of SOC to DOC inputs, not the total amount (Li et al., 2014). This result is consistent with experiments which demonstrate that increased plant inputs and SOC responses are not linearly related (Lajtha et al., 2014, 2015).

The actual integration of microbial models of soil respiration into broad-scale land models remains a challenge. Different model structures and parameterization lead to different patterns of soil C response to warming. Continuous change in climate over time may prevent soils from reaching equilibrium and require considering transient dynamics (which are prone to develop strong oscillations, e.g. Li et al., 2014; Wang et al., 2014). Properly describing even the short-term response of soil C dynamics to warming may raise the need to account for mechanisms such as physicochemical changes, priming, and the interaction of C and N cycles (e.g. S. Fontaine et al., 2003). Microbial model complexity will need to be optimized before integration into larger-scale models.

In the first attempt to represent soil microbial dynamics in Earth system models (ESMs), Wieder and contributors built a temperature-dependent *CM* model into the Community Land Model (CLM) and thus produced a "CLM microbial model" (Wieder et al., 2013). This model represents aboveground and belowground processes. Two belowground layers are included, surface (0-30 cm) and subsurface (30-100 cm). Microbial biomass is the source of enzymatic activity, but degradative enzymes are not modeled explicitly (no Z pool); rather, microbes

directly catalyzes the mineralization of litter and SOC according to Michaelis-Menten kinetics, hence the model CM structure applied to all three layers (above-ground and two below-ground horizons). The parameterization of the CLM microbial model uses German et al.'s (2012) data (*cf.* Box 2). Temperature affects microbial uptake parameters and MGE. To validate the model, global simulations were run using globally gridded data: observed (rather

than simulated) litter inputs and mean annual soil temperature. Model outputs were compared with observations from the Harmonized World Soils Database. The CLM model explains 50% of the spatial variation in observed soil C stock, contra 28-30% for the best traditional, non-microbial models. They concluded then that models with explicit microbes should show greater agreement with actual measurements of soil C than models without them. To simulate soil C responses to global warming, control simulations were run using observationally derived litter inputs distributed throughout the year and mean monthly soil temperature data from 1985 to 2005 from a single community ESM (CESM) ensemble member from archived Coupled Model Intercomparison Project Phase 5 (CMIP5) experiments. Projections of the CLM microbial model were run from 2006 to 2100 by using CESM projected soil temperature (obtained from ensemble member one of CESM simulations for the Representative Concentration Pathway 8.5 (RCP 8.5)) corresponding to a 4.8 °C increase in mean global temperature by 2100. The salient result is a massive soil C loss (~300 Pg C by

year 2100) in the case of temperature-independent MGE (Fig. 7a). In a temperature-dependent MGE scenario, this effect can be completely offset (Fig. 7a). These results emphasised that microbial processes and their temperature dependence should be critical to

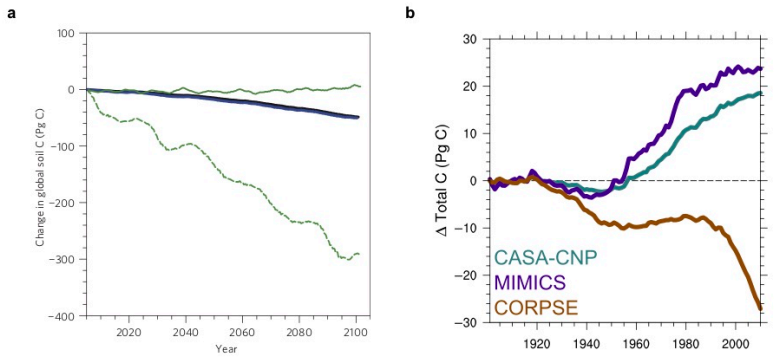

Figure 7. Predictions of cumulative change of soil carbon stocks by structurally different models. (a) Future predictions in response to a 4.8 °C warming scenario over 2006-2100. Thick lines (black and blue): conventional CLM models. Green lines: CLM microbial model, with temperature-dependent MGE (dotted line) or temperature-independent MGE (plain line). (b) Historical predictions in response to a 1.1°C warming over 1910-2010. Cyan line: first-order CASA-CNP. Purple line: MIMICS. Brown line: CORPSE. See text for details. ((a) and (b) reproduced from Wieder *et al.* 2013 and 2018 respectively)

model global soil carbon responses to warming on decadal to century-long timescales and to properly evaluate the uncertainties of model projections.

In a more recent study comparing a first-order model (CASA-CNP) and two microbial models (MIMICS and CORPSE), Wieder et al. (2018) pointed to limits of ranking models based on their capacity to simulate the spatial distribution of soil carbon stocks, especially considering that different models are not calibrated similarly. Rather, they highlighted and embraced the diversity of projections generated by alternate models, and focused on explaining the mechanistic causes of such differences. Considering transient dynamics, the three models were forced with litterfall inputs calculated by running the CASA-CNP vegetation model, and used historical data of temperature and moisture from 1901 to 2010 (instead of projected data). According to these data, global mean annual soil temperature increased by 1.1°C and mean annual soil moisture by 0.5%, relative the initial conditions. Again, the three models showed dramatically different patterns of soil carbon gains and losses despite identical litter inputs and climate forcing, with a net accumulation of soil carbon in CASA-CNP (+18.1 Pg C) and MIMICS (+24.1 Pg C), and a net loss in CORPSE (-21.7 Pg C) over the same period (Fig. 7b).

Ultimately, the development, validation, and verification of models crucially depends on our ability to constrain them with empirical data, but we face a lack of relevant global data sets. Table 1 provides a short list of global data sets that can be used to initialize global projections that incorporate *CDMZ* models. As the analysis of Wieder et al. (2013) demonstrates, explicitly incorporating microbial dynamics into ESMs will increase the uncertainty of the projections. This is not a negative result: comparing multiple structurally different models to better assess the uncertainties of coupled C-climate projections is highly desirable (Bradford et al., 2016; Wieder et al., 2015, 2018). In addition, moving beyond first-order models is required for a mechanistic and quantitative understanding of soil C-climate feedbacks in the context of multivariate climate change (Abramoff et al., 2018; Monroe et al., 2018).

4. Challenges and perspectives

The development of microbial models of soil respiration and the application of these models to improve our projections of climate and ecosystem change face multiple challenges, all revolving around the general issue of scaling in ecology (Levin, 1992). Mechanistic models of

the *CDMZ* family capture processes at a spatial scale that is intermediate between the microscopic (micro) scale of cellular and physicochemical processes at which SOM decomposition and stabilization occur (10^{-6} to 10^{-3} m) and the mesoscale at which these processes are commonly measured (10^{-2} to 1 m). Projections of ecosystem rates of soil respiration involve macro-scales that are relevant to global climate projections (10^{3} to 10^{14} m) (Hinckley et al. 2014). There are thus two major scaling issues when considering the derivation and application of *CDMZ* models (Bradford & Fierer, 2012; Burd et al., 2016; Davidson et al., 2014; Hararuk et al., 2015; Ise & Moorcroft, 2006; Sulman et al., 2014, Wieder et al., 2013, 2015). First, we need *CDMZ* models that are consistent with micro scale processes and can be integrated with mesoscale empirical data (Kaiser et al., 2014, 2015). Second, we need to integrate *CDMZ* models in ESMs and validate their projections at macro-scales (Todd-Brown et al., 2012; Wieder et al., 2013, 2015). What is at stake here ultimately is a better understanding of how soil microbial processes and dynamics influence the global, long-term (decadal to centennial) dynamics of Earth coupled C-climate, and how global effects feed back and shape soil microbial communities and function across temporal and spatial scales.

Consistency of* CDMZ *models with micro-scale decomposition processes

CDMZ models typically assume a 10^{-2} m spatial scale and iterate over hourly or daily time steps. The underlying processes, in contrast, involve individual cells with characteristic length of order 1 mm and interaction range of order 10 mm (Raynaud & Nunan, 2014). Microbial accessibility to substrates on this micro-scale is key to the timescale of microbial influence on SOM decomposition (J. P. Schimel & Schaeffer, 2012). The C that is associated with mineral fractions and that is not available for decomposition may be irrelevant for short-term soil respiration dynamics, whereas on a longer timescale, the dynamics of mineral adsorption/desorption will change substrate accessibility and impact microbial activity and respiration. In addition, the physical diffusion of labile compounds (enzymes, DOC) couples the micro-scale dynamics of their production with accessibility on longer spatial and temporal scales.

Ultimately to describe measurable soil C dynamics on the mesoscale, scaling up from micro to meso scales requires to (i) integrate microbial functional and enzyme chemical diversity across microsite variations in substrate availability and environmental conditions (temperature, water content, CO_2, pH…) while (ii) accounting for spatial environmental

correlations induced by physical diffusion among microsites. Computational trait-based modeling as done by Allison (2012) and Kaiser et al. (2014, 2015) (see Section 1, Box 1) represents seminal steps in this direction, where numerical simulations of the micro-scale processes are used to derive the dynamics of aggregate variables. This is illustrated by the run shown in Fig. 8, where considerable heterogeneity in the spatial distribution of microbes (Fig. 8, top) and SOC (Fig. 8, bottom) collapses into aggregated variables that vary smoothly over time (Fig. 8, right panels). Considering the aggregated dynamics also informs us on the characteristic timescale (1 year) of decomposition at that scale. The critical question that such work raises is, how should micro-scale parameters of C-D-M-Z activity and interaction be rescaled for a mesoscale *CDMZ* model to fit the aggregated variables dynamics precisely?

Trait-based models as constructed and analysed by Allison (2012) and Kaiser et al. (2014, 2015) are fundamentally designed to investigate the consequences of diverse functional types in the soil microbial community (as illustrated in Fig. 2 and Fig. 8). Because exoenzyme production is key to the decomposition function of soil microbes, it is essential to understand how variation in exoenzyme production across strains influences decomposition and soil respiration. In particular, "cheater" strains that invest little resource or none in exoenzyme production may still reap off the benefits of decomposition, i.e. access to DOC, brought about by "cooperative" strains that pay the cost of producing exoenzymes.

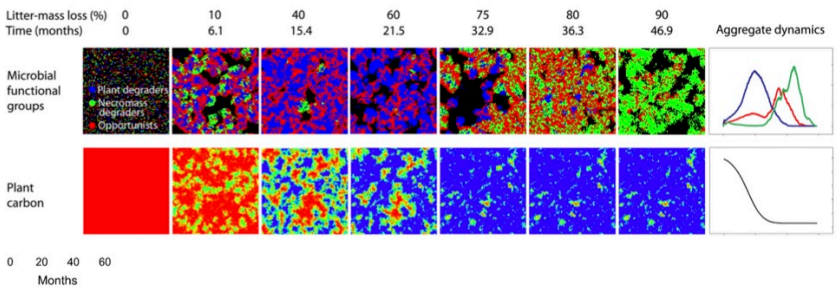

Figure 8. Spatio-temporal dynamics of microbial decomposition emerging from micro-scale processes. Each square shows a 100 x 100 grid of microsites, each 10 mm of side length, corresponding to a 1 x 1 mm area of leaf litter. Top row, spatial distribution of individual microbes of three functional groups (blue: Plant degrader, green: Microbial-necromass degrader, red: Opportunists). Bottom row, spatial distribution of litter material (SOC). Quantity ranges from low (blue) to high (red); sites empty of microbes appear in black. Panels on the right show the aggregated sizes of the respective pools. (Reproduced from Kaiser *et al.* 2014)

The ecological stability of such a "social" system of cooperation and cheating was studied by Allison (2005); Kaiser et al. (2015) explored the consequences of cooperator-cheater social dynamics for decomposition of a given amount of organic matter (Fig. 8). It turns out that the equilibrium ratio between enzyme producers and cheaters down-regulates to a minimum the total amount of enzymes produced per total microbial biomass, thus slowing down decomposition and causing an accumulation of soil carbon (and nitrogen). To explore consequences on longer time and spatial scales, one challenge now is to consider a fully evolutionary version of this model, which will account for genetic mutation generating variation in enzyme production, and natural selection arising from spatial and temporal variation in environmental conditions. Mathematical and modeling techniques exist to achieve this goal (e.g. Champagnat et al., 2006).

There are other micro-scale processes that are potentially critical for soil respiration dynamics at meso-scale, which need to be incorporated in *CDMZ*-type models. One such process involves how soil moisture affects the supply of substrates at the microscopic scale, for which we need a mechanistic representation. This could be achieved by explicitly modeling water transport of the substrates at the scale of soil pores. Also, a spatial representation of soil heterogeneous structure could account for the distribution of available substrates in the pore network. This is important because substrate concentrations vary enormously in the pore network and microbes may not be collocated with the available C (Baldock & Skjemstad, 2000; Van Veen & Kuikman, 1990).

Accounting for interactions among the carbon, nitrogen, and phosphorus cycles is another challenge. Community-level competition for C and N sources is likely to be important for determining the overall response of soil respiration to warming (Conant et al., 2011). For example, if the temperature sensitivity of key N-cycle processes are greater than some C-cycle processes, then it is possible that N availability limits microbial activity. This could influence plastic responses or evolutionary adaptations in microbial allocation to N versus C acquisition. Trait-based models are ideally suited to address the microbial dynamics of C, N and P simultaneously (Steven D. Allison, 2012). On the mathematical side, we need to build further on models such as J.P. Schimel & Weintraub's (2003) to represent N availability, C: N soil and microbial stoichiometry, and the coupling of C cycling to N. These models will require additional parameterization of the enzymatic processes that convert organic N to forms (Abramoff et al., 2017; S. D. Allison, 2012; Averill & Waring, 2018; Kaiser et al., 2014, 2015; Moorhead et al., 2012; J.P. Schimel & Bennett, 2004).

Incorporating soil C stabilization in CDMZ *models*

Soil C-climate feedbacks involve timescales (year to century) over which mechanisms of soil C stabilization may not be ignored (Abramoff et al., 2017). Using *CDMZ* models to improve long-term and large-scale climate forecasting requires to incorporate such mechanisms. Soil C is stabilized by interacting with minerals, through sorption (physical or chemical binding of organic matter with mineral), occlusion (blocking of organic matter within a mineral frame), or aggregation (association of mix of minerals and organic compounds including pores and live microbes) (Keil & Mayer, 2014). Microaggregates break down over time due to mechanical stresses or the gradual degradation of binding agents, and carbon in chemically protected organo-mineral complexes is slowly released through desorption (Sollins et al., 1996).

As presented earlier, there have been few attempts to incorporate organic-mineral interactions in *CDMZ* models. Wang et al.'s (2013) model includes the slower decomposable mineral-associated SOC and the non-decomposable adsorbed-DOC. Adsorption and desorption are first-order temperature-dependent functions.In Tang and Riley (2015), mineral-associated C pools are not explicit, however SOC "compete" with mineral surface to bind enzymes, while microbes compete with mineral surface to bind DOC.

Recent microbial models intended to be used in global numerical models usually simplify the decomposition process (*CM* instead of *CDMZ* models, i.e. no explicit enzymes or DOC), but they do account for processes of C stabilization (Abramoff et al., 2018; Sulman et al., 2014; Wieder et al., 2014). What makes "stabilised SOC" conceptually different from "recalcitrant SOC" with slower decomposition kinetics, is that it is mainly formed at the end of the microbial decomposition chain and is little or not accessible to microbial decomposition. In Sulman et al. (2014)'s model (cf. section 2), there are three chemically distinct classes of SOC (simple, chemically resistant, and dead microbes), each of them divided into an accessible form and a fully inaccessible form. Carbon moves from accessible to inaccessible forms at a class-specific protection rate that also depends on soil texture (clay content); inaccessible carbon moves back to the accessible form after 45 years. In Wieder et al. (2014)'s model, formation of inaccessible SOC is, like decomposition, a microbial process. Most aboveground to belowground carbon inputs start as accessible SOC, then are converted into microbial biomass (through decomposition, uptake and growth captured with one reaction). Microbial residues then form the bulk of stabilised SOC (not fully inaccessible to

decomposition). Only a small fraction of carbon inputs bypasses accessible SOC and microbial biomass and is transformed directly into stabilised SOC. Abramoff et al. (2018) synthesizes both Sulman and Wieder's models by including two pools of stabilised SOC: one fully inaccessible pool formed by mineral sorption of microbial products ("mineral-associated organic C"), and one little-accessible pool formed by aggregation of accessible SOC and microbial residues ("aggregate C"). They compared their predictions with the non-microbial Century model, which has long been a standard for large-scale simulations of soil C stocks (Bonan et al., 2013; Parton et al., 1987, 1995; Paustian et al., 1992). The microbial model exhibits distinct nonlinear responses due to the choice of functions affecting SOC in the pool; importantly, the two models diverge regarding the direction of SOC change (sink vs. source) in case of multiple varying environmental factors.

Integrating* CDMZ *models in global C-climate projections

To scale up the ecosystem effects of micro-scale microbial dynamics to continental and global scales, the general principle is to use statistical distributions of parameters, such as v_{max}, K_m, and the death rates of microbes and decay rates of exoenzymes and assemble them across ecosystems and soil types. The spatial resolution of ESMs then dictates the spatial scale at which projections must be run (German et al., 2012; Sinsabaugh et al., 2008). In addition to climate drivers, vegetation and soil physico-chemical variables are well-characterized at that scale; for example, soil texture and pH data have been shown to be effective at scaling microbial respiration rates across landscapes (Pansu et al., 2010).

Seminal attempts of global scaling such as Wieder et al. (2013) pave the way forward. Further developments could draw from progress in global modeling of vegetation dynamics:

- Williams et al. (1997) developed a protocol for scaling up models of gross primary productivity. A fine-scale mechanistic model is used to predict productivity across a wide range of conditions, and these predictions are then aggregated across time and space. A broad-scale model with simplified equations is then developed to replicate the aggregated output from the fine-scale model. Projections from the broad-scale model of gross primary productivity across disparate ecosystems using broad environmental drivers, such as daily irradiance and leaf area index, can be successfully validated.
- The "Ecosystem Demography" (Moorcroft et al., 2001) and "Perfect-Plasticity Approximation" (Strigul et al., 2008) models apply individual-based forest gap dynamics

to derive properties of size and age-classes at larger ecosystem scale, which can be related to forest structure, productivity, and C storage (Fischer et al., 2015).

- Likewise, scaling terrestrial photosynthesis from leaf to Earth scale is now achieved by scaling leaf traits within plant canopies and across plant functional types while still using micro-scale enzyme kinetics to model aboveground C balance and project its response to climate change (G. B. Bonan et al., 2011, 2012, 2014).

Similar developments are needed for modeling soil microbial dynamics across scales (see Bond-Lamberty et al. (2016) for a discussion of how modeling approaches to decomposition functional types differ from, and complement models of plant functional types). A critical issue when moving up from meso- to global scales is to account for the multiple exogenous and endogenous processes that generate variation at spatial and temporal scales above that of mechanistic *CDMZ* models, including:

- The quantity and quality of organic matter inputs, which are determined primarily by vegetation type and productivity at scales larger than the meso-scale of decomposition. Temperature as well as its indirect effects via soil moisture will alter plant production, partitioning of that carbon to roots and leaves and to litter, and litter quality (Conant et al., 2011),
- Large scale and long-term ecological feedbacks of small-scale, short-term physiological, ecological, and evolutionary processes. Increased C inputs, as might occur with CO_2 or nutrient fertilization, may cause little change to soil C stock, yet microbial respiration will return more CO_2 to the atmosphere. This could be a significant influence of global warming, which would then feed back to the micro-scale dynamics of respiration.
- Environmental correlates of global warming, such as extreme climatic events (droughts and floods) and changes in their distribution, frequency, and intensity, are likely to generate wide variation at regional scale in soil properties and microbial responses. Physiological consequences may include microbial dormancy, while episodes of severe ecological filtering on community composition and strong natural selection on genetic variation of microbial traits can be expected.

Validating soil microbial models of decomposition at the global scale is the ultimate challenge. Global datasets on soil carbon stocks and fluxes offer promising opportunities to validate the emerging ESM microbial models. Many of the land submodels from current Global Circulation Models (GCMs) are tested at continental scales, and a similar approach could be applied to microbial ESM projections, possibly using CO_2 flux data from networks

such as the North American Carbon Program and CarboEurope (Schwalm et al., 2010; Suzuki & Ichii, 2010). As we tackle challenges in scaling, parameterization, and validation, a new generation of microbially-based decomposition models will eventually improve predictions of carbon-climate feedbacks in the Earth system and help quantify projection uncertainty.

5. Summary

Here we provide a brief recap of the chapter key points.

- As the flaws of first-order decay kinetics still used in most coupled C-climate models were recognized, a new generation of SOC decomposition models have been developed to link SOC turnover to microbial eco-physiology and degradative enzyme kinetics. The basic processes represented are: litter input, microbial enzyme production, enzymatic SOC degradation, microbial DOC uptake and assimilation, microbial death, and enzyme deactivation. The models take the form of systems of non-linear ordinary differential equations with at least four state variables corresponding to the main four pools represented at a mesoscale of space and time: *C* (measuring SOC), *D* (measuring DOC), *M* (microbial biomass), *Z* (enzyme concentration). Trait-based models are computational in essence and allow representing a diversity of microbial functional types, that high-throughput sequencing and "omics" data can help monitor in real systems.
- To investigate how soil microbes and exoenzymes mediate the effects of environmental (e.g. climate) change on soil respiration and C stock, these models implement the Dual Arrhenius and Michaelis-Menten kinetics. The Arrhenius function represents dependence of microbial and enzyme activity on temperature and substrate quality (through activation energy); the Michaelis-Menten function represents the limitation of substrates availability and chemical affinity of substrates on temperature sensitivity.
- Accounting for climate factors other than temperature (moisture, CO_2 concentration) allows to distinguish the "apparent" vs. "intrinsic" temperature sensitivity of SOC decomposition and soil heterotrophic respiration. The effect of variation in soil moisture due to variable precipitation can be addressed by including controls of enzyme activity and DOC uptake by water saturation, and possibly distinguishing pools of wet vs. dry enzymes and DOC.
- Temperature-dependent *CDMZ* models of decomposition and soil respiration are used to explain observational and experimental responses of soil respiration to warming. They can explain a pattern of increasing respiration, decreasing microbial biomass, and relatively

stable SOC.Temperature-dependent *CDMZ* can be integrated in ESMs. Processes that need to be integrated in large-scale models include microbial evolutionary adaptation and eco-evolutionary feedbacks between soil C and climate.

- Microbial respiration is the largest flux of C out of the soil. Inclusion of explicit microbial processes of decomposition in ESMs will likely increase the inter-model range of soil C projections in model intercomparison projects, which may in fact provide a more accurate assessment of uncertainty in future carbon cycle projections.

Acknowledgements

We thank the Editors for their invitation to write this chapter, and Rachel Gallery, Pierre-Henri Gouyon, Hélène Leman, Nicolas Loeuille, Scott Saleska and Will Wieder for discussion. E.A. received support for the graduate program Frontières du Vivant (University Paris 7), Chaire Modélisation Mathématique de la Biodiversité, PSL University, Laboratory of Excellence (LabEx) MemoLife (PIA-10-LABX-54). This work was also supported by CNRS Pépinière de site PSL "Eco-Evo-Devo") and the Partner University Fund for ENS-University of Arizona cooperation.

References

1. Abramoff, R. Z., Davidson, E. A., & Finzi, A. C. (2017). A parsimonious modular approach to building a mechanistic belowground carbon and nitrogen model. *Journal of Geophysical Research: Biogeosciences*, *122*(9), 2418–2434.
2. Allison, S. D. (2012). A trait-based approach for modelling microbial litter decomposition. *Ecology Letters*, *15*(9), 1058–1070.
3. Allison, S. D. (2014). Modeling adaptation of carbon use efficiency in microbial communities. *Frontiers in Microbiology*, *5*, 571.
4. Allison, S. D., & Treseder, K. K. (2008). Warming and drying suppress microbial activity and carbon cycling in boreal forest soils. *Global Change Biology*, *14*(12), 2898–2909.
5. Allison, S. D., & Vitousek, P. M. (2004). Extracellular Enzyme Activities and Carbon Chemistry as Drivers of Tropical Plant Litter Decomposition. *Biotropica*, *36*(3), 285–296.
6. Allison, S. D., Wallenstein, M. D., & Bradford, M. A. (2010). Soil-carbon response to warming dependent on microbial physiology. *Nature Geoscience*, *3*, 336.
7. Alster, C. J., German, D. P., Lu, Y., & Allison, S. D. (2013). Microbial enzymatic responses to drought and to nitrogen addition in a southern California grassland. *Soil Biology & Biochemistry*, *64*, 68–79.
8. Amundson, R. (2003). Soil Formation. *Treatise on Geochemistry*, *5*, 605.
9. Averill, C., & Waring, B. (2018). Nitrogen limitation of decomposition and decay: How can it occur? *Global Change Biology*, *24*(4), 1417–1427.
10. Baldock, J. A., & Skjemstad, J. O. (2000). Role of the soil matrix and minerals in protecting natural organic materials against biological attack. *Organic Geochemistry*, *31*(7), 697–710.
11. Birch, H. F. (1958). The effect of soil drying on humus decomposition and nitrogen availability. *Plant and Soil*, *10*(1), 9–31.
12. Blagodatskaya, E., Blagodatsky, S., Dorodnikov, M., & Kuzyakov, Y. (2010). Elevated atmospheric CO2 increases microbial growth rates in soil: results of three CO2 enrichment experiments. *Global Change Biology*, *16*(2), 836–848.
13. Bonan, G. B., Lawrence, P. J., Oleson, K. W., Levis, S., Jung, M., Reichstein, M., et al. (2011). Improving canopy processes in the Community Land Model version 4 (CLM4)

using global flux fields empirically inferred from FLUXNET data. *Journal of Geophysical Research*, *116*(G2), GB1008.

14. Bonan, G. B., Oleson, K. W., Fisher, R. A., Lasslop, G., & Reichstein, M. (2012). Reconciling leaf physiological traits and canopy flux data: Use of the TRY and FLUXNET databases in the Community Land Model version 4. *Journal of Geophysical Research: Biogeosciences*, *117*(G2). Retrieved from https://onlinelibrary.wiley.com/doi/abs/10.1029/2011JG001913
15. Bonan, G. B., Williams, M., Fisher, R. A., & Oleson, K. W. (2014). Modeling stomatal conductance in the earth system: linking leaf water-use efficiency and water transport along the soil–plant–atmosphere continuum. *Geoscientific Model Development*, *7*(5), 2193–2222.
16. Bond-Lamberty, B., & Thomson, A. (2010). A global database of soil respiration data. *Biogeosciences* , *7*(6), 1915–1926.
17. Bond-Lamberty, B., Epron, D., Harden, J., Harmon, M. E., Hoffman, F., Kumar, J., et al. (2016). Estimating heterotrophic respiration at large scales: challenges, approaches, and next steps. *Ecosphere* , *7*(6), e01380.
18. Bradford, M. A., & Fierer, N. (2012). The biogeography of microbial communities and ecosystem processes: implications for soil and ecosystem models. *Soil Ecology and Ecosystem Services*, *18*. Retrieved from https://books.google.com/books?hl=en&lr=&id=w_o0obAFdLQC&oi=fnd&pg=PA189&dq=The+biogeography+of+microbial+communities+and+ecosystem+processes+Implications+for+soil+and+ecosystem+models&ots=Z9ibKwdUHU&sig=2Kg5u_gGg74lO0N96unOPqirJyA
19. Bradford, M. A., Davies, C. A., Frey, S. D., Maddox, T. R., Melillo, J. M., Mohan, J. E., et al. (2008). Thermal adaptation of soil microbial respiration to elevated temperature. *Ecology Letters*, *11*(12), 1316–1327.
20. Bradford, M. A., Wieder, W. R., Bonan, G. B., Fierer, N., Raymond, P. A., & Crowther, T. W. (2016). Managing uncertainty in soil carbon feedbacks to climate change. *Nature Climate Change*, *6*, 751.
21. Brantley, S. L., Megonigal, J. P., Scatena, F. N., Balogh-Brunstad, Z., Barnes, R. T., Bruns, M. A., et al. (2011). Twelve testable hypotheses on the geobiology of weathering. *Geobiology*, *9*(2), 140–165.

22. Burd, A. B., Frey, S., Cabre, A., Ito, T., Levine, N. M., Lønborg, C., et al. (2016). Terrestrial and marine perspectives on modeling organic matter degradation pathways. *Global Change Biology*, *22*(1), 121–136.
23. Carney, K. M., Hungate, B. A., Drake, B. G., & Patrick Megonigal, J. (2007). Altered soil microbial community at elevated CO2 leads to loss of soil carbon. *Proceedings of the National Academy of Sciences of the United States of America*, *104*(12), 4990–4995.
24. Champagnat, N., Ferrière, R., & Méléard, S. (2006). Unifying evolutionary dynamics: from individual stochastic processes to macroscopic models. *Theoretical Population Biology*, *69*(3), 297–321.
25. Cheng, L., Booker, F. L., Tu, C., Burkey, K. O., Zhou, L., Shew, H. D., et al. (2012). Arbuscular mycorrhizal fungi increase organic carbon decomposition under elevated CO2. *Science*, *337*(6098), 1084–1087.
26. Christiansen, T., & Nielsen, J. (2002). Production of extracellular protease and glucose uptake in Bacillus clausii in steady-state and transient continuous cultures. *Journal of Biotechnology*, *97*(3), 265–273.
27. Cleveland, C. C., & Liptzin, D. (2007). C:N:P stoichiometry in soil: is there a "Redfield ratio" for the microbial biomass? *Biogeochemistry*, *85*(3), 235–252.
28. Conant, R. T., Ryan, M. G., Ågren, G. I., Birge, H. E., Davidson, E. A., Eliasson, P. E., et al. (2011). Temperature and soil organic matter decomposition rates - synthesis of current knowledge and a way forward. *Global Change Biology*, *17*(11), 3392–3404.
29. Crowther, T. W., & Bradford, M. A. (2013). Thermal acclimation in widespread heterotrophic soil microbes. *Ecology Letters*, *16*(4), 469–477.
30. Crowther, T. W., Todd-Brown, K. E. O., Rowe, C. W., Wieder, W. R., Carey, J. C., Machmuller, M. B., et al. (2016). Quantifying global soil carbon losses in response to warming. *Nature*, *540*(7631), 104–108.
31. Davidson, E. A., & Janssens, I. A. (2006). Temperature sensitivity of soil carbon decomposition and feedbacks to climate change. *Nature*, *440*(7081), 165–173.
32. Davidson, E. A., Janssens, I. A., & Luo, Y. (2006). On the variability of respiration in terrestrial ecosystems: moving beyond Q10. *Global Change Biology*, *12*(2), 154–164.
33. Davidson, E. A., Samanta, S., Caramori, S. S., & Savage, K. (2012). The D ual A rrhenius and M ichaelis--M enten kinetics model for decomposition of soil organic matter at hourly to seasonal time scales. *Global Change Biology*, *18*(1), 371–384.
34. Davidson, E. A., Savage, K. E., & Finzi, A. C. (2014). A big-microsite framework for soil carbon modeling. *Global Change Biology*, *20*(12), 3610–3620.

35. Drake, J. E., Darby, B. A., Giasson, M.-A., Kramer, M. A., Phillips, R. P., & Finzi, A. C. (2013). Stoichiometry constrains microbial response to root exudation- insights from a model and a field experiment in a temperate forest. *Biogeosciences* , *10*(2), 821–838.
36. Drake, J. E., Macdonald, C. A., Tjoelker, M. G., Reich, P. B., Singh, B. K., Anderson, I. C., & Ellsworth, D. S. (2018). Three years of soil respiration in a mature eucalypt woodland exposed to atmospheric CO2 enrichment. *Biogeochemistry*, *139*(1), 85–101.
37. Dungait, J. A. J., Hopkins, D. W., Gregory, A. S., & Whitmore, A. P. (2012). Soil organic matter turnover is governed by accessibility not recalcitrance. *Global Change Biology*, *18*(6), 1781–1796.
38. Falkowski, P. G., Fenchel, T., & Delong, E. F. (2008). The microbial engines that drive Earth's biogeochemical cycles. *Science*, *320*(5879), 1034–1039.
39. Fierer, N., Strickland, M. S., Liptzin, D., Bradford, M. A., & Cleveland, C. C. (2009). Global patterns in belowground communities. *Ecology Letters*, *12*(11), 1238–1249.
40. Fierer, N., Barberán, A., & Laughlin, D. C. (2014). Seeing the forest for the genes: using metagenomics to infer the aggregated traits of microbial communities. *Frontiers in Microbiology*, *5*, 614.
41. Fischer, R., Ensslin, A., Rutten, G., Fischer, M., Schellenberger Costa, D., Kleyer, M., et al. (2015). Simulating carbon stocks and fluxes of an African tropical montane forest with an individual-based forest model. *PloS One*, *10*(4), e0123300.
42. Fontaine, S., & Barot, S. (2005). Size and functional diversity of microbe populations control plant persistence and long-term soil carbon accumulation: Modelling long-term SOM dynamics. *Ecology Letters*, *8*(10), 1075–1087.
43. Fontaine, S., Mariotti, A., & Abbadie, L. (2003). The priming effect of organic matter: a question of microbial competition? *Soil Biology & Biochemistry*. Retrieved from https://www.sciencedirect.com/science/article/pii/S0038071703001238
44. Frey, S. D., Lee, J., Melillo, J. M., & Six, J. (2013). The temperature response of soil microbial efficiency and its feedback to climate. *Nature Climate Change*, *3*, 395.
45. German, D. P., Marcelo, K. R. B., Stone, M. M., & Allison, S. D. (2012). The Michaelis-Menten kinetics of soil extracellular enzymes in response to temperature: a cross-latitudinal study. *Global Change Biology*, *18*(4), 1468–1479.
46. van Gestel, N., Shi, Z., van Groenigen, K. J., Osenberg, C. W., Andresen, L. C., Dukes, J. S., et al. (2018). Predicting soil carbon loss with warming. *Nature*, *554*(7693), E4–E5.

47. Goddéris, Y., François, L. M., Probst, A., Schott, J., Moncoulon, D., Labat, D., & Viville, D. (2006). Modelling weathering processes at the catchment scale: The WITCH numerical model. *Geochimica et Cosmochimica Acta*, *70*(5), 1128–1147.
48. van Groenigen, K. J., Xia, J., Osenberg, C. W., Luo, Y., & Hungate, B. A. (2015). Application of a two-pool model to soil carbon dynamics under elevated CO2. *Global Change Biology*, *21*(12), 4293–4297.
49. Hagerty, S. B., van Groenigen, K. J., Allison, S. D., Hungate, B. A., Schwartz, E., Koch, G. W., et al. (2014). Accelerated microbial turnover but constant growth efficiency with warming in soil. *Nature Climate Change*, *4*, 903.
50. Hararuk, O., Smith, M. J., & Luo, Y. (2015). Microbial models with data-driven parameters predict stronger soil carbon responses to climate change. *Global Change Biology*, *21*(6), 2439–2453.
51. Hengl, T., de Jesus, J. M., MacMillan, R. A., Batjes, N. H., Heuvelink, G. B. M., Ribeiro, E., et al. (2014). SoilGrids1km—global soil information based on automated mapping. *PloS One*, *9*(8), e105992.
52. He, Y., Yang, J., Zhuang, Q., Harden, J. W., McGuire, A. D., Liu, Y., et al. (2015). Incorporating microbial dormancy dynamics into soil decomposition models to improve quantification of soil carbon dynamics of northern temperate forests. *Journal of Geophysical Research: Biogeosciences*, *120*(12), 2596–2611.
53. Hinckley, E.-L. S., Wieder, W., Fierer, N., & Paul, E. (2014). Digging Into the World Beneath Our Feet: Bridging Across Scales in the Age of Global Change. *Eos, Transactions American Geophysical Union*, *95*(11), 96–97.
54. Hochochka, P. W., & Somero, G. N. (2002). Biochemical adaptation. Oxford University Press, Oxford.
55. Homyak, P. M., Blankinship, J. C., Slessarev, E. W., Schaeffer, S. M., Manzoni, S., & Schimel, J. P. (2018). Effects of altered dry season length and plant inputs on soluble soil carbon. *Ecology*, *99*(10), 2348–2362.
56. Huang, Y., Guenet, B., Ciais, P., Janssens, I. A., Soong, J. L., Wang, Y., et al. (2018). ORCHIMIC (v1.0), a microbe-mediated model for soil organic matter decomposition. *Geoscientific Model Development*, *11*(6), 2111–2138.
57. Ise, T., & Moorcroft, P. R. (2006). The global-scale temperature and moisture dependencies of soil organic carbon decomposition: an analysis using a mechanistic decomposition model. *Biogeochemistry*, *80*(3), 217–231.

58. Jobbágy, E. G., & Jackson, R. B. (2000). THE VERTICAL DISTRIBUTION OF SOIL ORGANIC CARBON AND ITS RELATION TO CLIMATE AND VEGETATION. *Ecological Applications: A Publication of the Ecological Society of America*, *10*(2), 423–436.
59. Joergensen, R. G., Brookes, P. C., & Jenkinson, D. S. (1990). Survival of the soil microbial biomass at elevated temperatures. *Soil Biology & Biochemistry*, *22*(8), 1129–1136.
60. Kaiser, C., Franklin, O., Dieckmann, U., & Richter, A. (2014). Microbial community dynamics alleviate stoichiometric constraints during litter decay. *Ecology Letters*, *17*(6), 680–690.
61. Kaiser, C., Franklin, O., Richter, A., & Dieckmann, U. (2015). Social dynamics within decomposer communities lead to nitrogen retention and organic matter build-up in soils. *Nature Communications*, *6*, 8960.
62. Karberg, N. J., Pregitzer, K. S., King, J. S., Friend, A. L., & Wood, J. R. (2005). Soil carbon dioxide partial pressure and dissolved inorganic carbonate chemistry under elevated carbon dioxide and ozone. *Oecologia*, *142*(2), 296–306.
63. Karhu, K., Auffret, M. D., Dungait, J. A. J., Hopkins, D. W., Prosser, J. I., Singh, B. K., et al. (2014). Temperature sensitivity of soil respiration rates enhanced by microbial community response. *Nature*, *513*(7516), 81–84.
64. Keiluweit, M., Bougoure, J. J., Nico, P. S., Pett-Ridge, J., Weber, P. K., & Kleber, M. (2015). Mineral protection of soil carbon counteracted by root exudates. *Nature Climate Change*, *5*, 588.
65. Kuzyakov, Y. (2010). Priming effects: Interactions between living and dead organic matter. *Soil Biology & Biochemistry*, *42*(9), 1363–1371.
66. Lajtha, K., Townsend, K. L., Kramer, M. G., Swanston, C., Bowden, R. D., & Nadelhoffer, K. (2014). Changes to particulate versus mineral-associated soil carbon after 50 years of litter manipulation in forest and prairie experimental ecosystems. *Biogeochemistry*, *119*(1), 341–360.
67. Lajtha, K., Peterson, F., Nadelhoffer, K., & Bowden, R. D. (2015). Twenty years of litter and root manipulations: insights into multi-decadal som dynamics. *Soil Science Society of America Journal. Soil Science Society of America*. Retrieved from https://dspace.allegheny.edu/handle/10456/37712
68. Lawrence, C. R., Neff, J. C., & Schimel, J. P. (2009). Does adding microbial mechanisms of decomposition improve soil organic matter models? A comparison of

four models using data from a pulsed rewetting experiment. *Soil Biology & Biochemistry*, *41*(9), 1923–1934.

69. Levin, S. A. (1992). The Problem of Pattern and Scale in Ecology: The Robert H. MacArthur Award Lecture. *Ecology*, *73*(6), 1943–1967.
70. Li, J., Wang, G., Allison, S. D., Mayes, M. A., & Luo, Y. (2014). Soil carbon sensitivity to temperature and carbon use efficiency compared across microbial-ecosystem models of varying complexity. *Biogeochemistry*, *119*(1), 67–84.
71. Liu, L., King, J. S., & Giardina, C. P. (2005). Effects of elevated concentrations of atmospheric CO2 and tropospheric O3 on leaf litter production and chemistry in trembling aspen and paper birch communities. *Tree Physiology*, *25*(12), 1511–1522.
72. Lloyd, J., & Taylor, J. A. (1994). On the Temperature Dependence of Soil Respiration. *Functional Ecology*, *8*(3), 315–323.
73. Luo, Y., Wan, S., Hui, D., & Wallace, L. L. (2001). Acclimatization of soil respiration to warming in a tall grass prairie. *Nature*, *413*(6856), 622–625.
74. Luo, Z., Baldock, J., & Wang, E. (2017). Modelling the dynamic physical protection of soil organic carbon: Insights into carbon predictions and explanation of the priming effect. *Global Change Biology*, *23*(12), 5273–5283.
75. Manzoni, S., Taylor, P., Richter, A., Porporato, A., & Ågren, G. I. (2012). Environmental and stoichiometric controls on microbial carbon-use efficiency in soils. *The New Phytologist*, *196*(1), 79–91.
76. McClaugherty, C. A., & Linkins, A. E. (1990). Temperature responses of enzymes in two forest soils. *Soil Biology & Biochemistry*, *22*(1), 29–33.
77. McGill, W. B. (1996). Soil sustainability: Microorganisms, and electrons. In *Solo/Suelo'96 XIII Congresso Latino Americano de Ciéncia do Solo* (pp. 4–8).
78. Melillo, J. M., Steudler, P. A., Aber, J. D., Newkirk, K., Lux, H., Bowles, F. P., et al. (2002). Soil warming and carbon-cycle feedbacks to the climate system. *Science*, *298*(5601), 2173–2176.
79. Melillo, J. M., Frey, S. D., DeAngelis, K. M., Werner, W. J., Bernard, M. J., Bowles, F. P., et al. (2017). Long-term pattern and magnitude of soil carbon feedback to the climate system in a warming world. *Science*, *358*(6359), 101–105.
80. Monroe, J. G., Markman, D. W., Beck, W. S., Felton, A. J., Vahsen, M. L., & Pressler, Y. (2018). Ecoevolutionary Dynamics of Carbon Cycling in the Anthropocene. *Trends in Ecology & Evolution*, *33*(3), 213–225.

81. Moorcroft, P. R., Hurtt, G. C., & Pacala, S. W. (2001). A METHOD FOR SCALING VEGETATION DYNAMICS: THE ECOSYSTEM DEMOGRAPHY MODEL (ED). *Ecological Monographs*, *71*(4), 557–586.
82. Moorhead, D. L., & Sinsabaugh, R. L. (2006). A THEORETICAL MODEL OF LITTER DECAY AND MICROBIAL INTERACTION. *Ecological Monographs*, *76*(2), 151–174.
83. Moorhead, D. L., & Weintraub, M. N. (2018). The evolution and application of the reverse Michaelis-Menten equation. *Soil Biology & Biochemistry*, *125*, 261–262.
84. Moorhead, D. L., Lashermes, G., & Sinsabaugh, R. L. (2012). A theoretical model of C- and N-acquiring exoenzyme activities, which balances microbial demands during decomposition. *Soil Biology & Biochemistry*, *53*, 133–141.
85. Mooshammer, M., Wanek, W., Schnecker, J., Wild, B., Leitner, S., Hofhansl, F., et al. (2012). Stoichiometric controls of nitrogen and phosphorus cycling in decomposing beech leaf litter. *Ecology*, *93*(4), 770–782.
86. Moyano, F. E., Manzoni, S., & Chenu, C. (2013). Responses of soil heterotrophic respiration to moisture availability: An exploration of processes and models. *Soil Biology & Biochemistry*, *59*, 72–85.
87. Natali, S. M., Sañudo-Wilhelmy, S. A., & Lerdau, M. T. (2009). Plant and Soil Mediation of Elevated CO2 Impacts on Trace Metals. *Ecosystems* , *12*(5), 715–727.
88. Norby, R. J., Todd, D. E., Fults, J., & Johnson, D. W. (2001). Allometric determination of tree growth in a CO2-enriched sweetgum stand. *The New Phytologist*, *150*(2), 477–487.
89. Norby, R. J., Delucia, E. H., Gielen, B., Calfapietra, C., Giardina, C. P., King, J. S., et al. (2005). Forest response to elevated CO2 is conserved across a broad range of productivity. *Proceedings of the National Academy of Sciences of the United States of America*, *102*(50), 18052–18056.
90. Oechel, W. C., Vourlitis, G. L., Hastings, S. J., Zulueta, R. C., Hinzman, L., & Kane, D. (2000). Acclimation of ecosystem CO2 exchange in the Alaskan Arctic in response to decadal climate warming. *Nature*, *406*(6799), 978–981.
91. Pachauri, R. K., Allen, M. R., Barros, V. R., Broome, J., Cramer, W., Christ, R., et al. (2014). *Climate Change 2014: Synthesis Report. Contribution of Working Groups I, II and III to the Fifth Assessment Report of the Intergovernmental Panel on Climate Change*. (R. K. Pachauri & L. Meyer, Eds.) (p. 151). Geneva, Switzerland: IPCC.

92. Pansu, M., Sarmiento, L., Rujano, M. A., Ablan, M., Acevedo, D., & Bottner, P. (2010). Modeling organic transformations by microorganisms of soils in six contrasting ecosystems: Validation of the MOMOS model. *Global Biogeochemical Cycles*, *24*(1). Retrieved from https://onlinelibrary.wiley.com/doi/abs/10.1029/2009GB003527
93. Pendall, E., Bridgham, S., Hanson, P. J., Hungate, B., Kicklighter, D. W., Johnson, D. W., et al. (2004). Below-ground process responses to elevated CO2 and temperature: a discussion of observations, measurement methods, and models. *The New Phytologist*, *162*(2), 311–322.
94. Phillips, R. P., Finzi, A. C., & Bernhardt, E. S. (2011). Enhanced root exudation induces microbial feedbacks to N cycling in a pine forest under long-term CO2 fumigation. *Ecology Letters*, *14*(2), 187–194.
95. Pregitzer, K. S., Burton, A. J., King, J. S., & Zak, D. R. (2008). Soil respiration, root biomass, and root turnover following long-term exposure of northern forests to elevated atmospheric CO2 and tropospheric O3. *The New Phytologist*, *180*(1), 153–161.
96. Raynaud, X., & Nunan, N. (2014). Spatial ecology of bacteria at the microscale in soil. *PloS One*, *9*(1), e87217.
97. Rinnan, R., Michelsen, A., Bååth, E., & Jonasson, S. (2007). Fifteen years of climate change manipulations alter soil microbial communities in a subarctic heath ecosystem. *Global Change Biology*, *13*(1), 28–39.
98. Salazar, A., Sulman, B. N., & Dukes, J. S. (2018). Microbial dormancy promotes microbial biomass and respiration across pulses of drying-wetting stress. *Soil Biology & Biochemistry*, *116*, 237–244.
99. Schimel, D. (2001). Preface. In E.-D. Schulze, M. Heimann, S. Harrison, E. Holland, J. Lloyd, I. C. Prentice, & D. Schimel (Eds.), *Global Biogeochemical Cycles in the Climate System* (pp. xvii–xxi). San Diego: Academic Press.
100. Schimel, J. (2001). 1.13 - Biogeochemical Models: Implicit versus Explicit Microbiology. In E.-D. Schulze, M. Heimann, S. Harrison, E. Holland, J. Lloyd, I. C. Prentice, & D. Schimel (Eds.), *Global Biogeochemical Cycles in the Climate System* (pp. 177–183). San Diego: Academic Press.
101. Schimel, J. P., & Bennett, J. (2004). NITROGEN MINERALIZATION: CHALLENGES OF A CHANGING PARADIGM. *Ecology*, *85*(3), 591–602.
102. Schimel, J. P., & Schaeffer, S. M. (2012). Microbial control over carbon cycling in soil. *Frontiers in Microbiology*, *3*, 348.

103. Schimel, J. P., & Weintraub, M. N. (2003). The implications of exoenzyme activity on microbial carbon and nitrogen limitation in soil: a theoretical model. *Soil Biology & Biochemistry*, *35*(4), 549–563.

104. Schuur, E. A. G., Vogel, J. G., Crummer, K. G., Lee, H., Sickman, J. O., & Osterkamp, T. E. (2009). The effect of permafrost thaw on old carbon release and net carbon exchange from tundra. *Nature*, *459*(7246), 556–559.

105. Schwalm, C. R., Williams, C. A., Schaefer, K., Anderson, R., Arain, M. A., Baker, I., et al. (2010). A model-data intercomparison of CO2 exchange across North America: Results from the North American Carbon Program site synthesis. *Journal of Geophysical Research: Biogeosciences*, *115*(G3). Retrieved from https://agupubs.onlinelibrary.wiley.com/doi/abs/10.1029/2009JG001229

106. Serna-Chavez, H. M., Fierer, N., & Van Bodegom, P. M. (2013). Global drivers and patterns of microbial abundance in soil. *Global Ecology and Biogeography: A Journal of Macroecology*, *22*(10), 1162–1172.

107. Sihi, D., Gerber, S., Inglett, P. W., & Inglett, K. S. (2016). Comparing models of microbial–substrate interactions and their response to warming. *Biogeosciences* , *13*(6), 1733–1752.

108. Sihi, D., Davidson, E. A., Chen, M., Savage, K. E., Richardson, A. D., Keenan, T. F., & Hollinger, D. Y. (2018). Merging a mechanistic enzymatic model of soil heterotrophic respiration into an ecosystem model in two AmeriFlux sites of northeastern USA, *252*, 155–166.

109. Sihi, D., Inglett, P. W., Gerber, S., & Inglett, K. S. (2018). Rate of warming affects temperature sensitivity of anaerobic peat decomposition and greenhouse gas production. *Global Change Biology*, *24*(1), e259–e274.

110. Sihi, D., Inglett, P. W., & Inglett, K. S. (2019). Warming rate drives microbial nutrient demand and enzyme expression during peat decomposition. *Geoderma*, *336*, 12–21.

111. Sinsabaugh, R. L., Lauber, C. L., Weintraub, M. N., Ahmed, B., Allison, S. D., Crenshaw, C., et al. (2008). Stoichiometry of soil enzyme activity at global scale. *Ecology Letters*, *11*(11), 1252–1264.

112. Sinsabaugh, R. L., Manzoni, S., Moorhead, D. L., & Richter, A. (2013). Carbon use efficiency of microbial communities: stoichiometry, methodology and modelling. *Ecology Letters*, *16*(7), 930–939.

113. Somero, G. N. (1978). Temperature Adaptation of Enzymes: Biological Optimization Through Structure-Function Compromises. *Annual Review of Ecology and Systematics*, *9*(1), 1–29.

114. Somero, G. N. (2004). Adaptation of enzymes to temperature: searching for basic "strategies." *Comparative Biochemistry and Physiology. Part B, Biochemistry & Molecular Biology*, *139*(3), 321–333.

115. Steinweg, J. M., Plante, A. F., Conant, R. T., Paul, E. A., & Tanaka, D. L. (2008). Patterns of substrate utilization during long-term incubations at different temperatures. *Soil Biology & Biochemistry*, *40*(11), 2722–2728.

116. Strigul, N., Pristinski, D., Purves, D., Dushoff, J., & Pacala, S. (2008). SCALING FROM TREES TO FORESTS: TRACTABLE MACROSCOPIC EQUATIONS FOR FOREST DYNAMICS. *Ecological Monographs*, *78*(4), 523–545.

117. Sulman, B. N., Phillips, R. P., Oishi, A. C., Shevliakova, E., & Pacala, S. W. (2014). Microbe-driven turnover offsets mineral-mediated storage of soil carbon under elevated CO2. *Nature Climate Change*, *4*, 1099.

118. Suzuki, T., & Ichii, K. (2010). Evaluation of a terrestrial carbon cycle submodel in an Earth system model using networks of eddy covariance observations. *Tellus. Series B, Chemical and Physical Meteorology*, *62*(5), 729–742.

119. Tang, J., & Riley, W. J. (2014). Weaker soil carbon–climate feedbacks resulting from microbial and abiotic interactions. *Nature Climate Change*, *5*, 56.

120. Todd-Brown, K. E. O., Hopkins, F. M., Kivlin, S. N., Talbot, J. M., & Allison, S. D. (2012). A framework for representing microbial decomposition in coupled climate models. *Biogeochemistry*, *109*(1), 19–33.

121. Trasar-Cepeda, C., Gil-Sotres, F., & Leirós, M. C. (2007). Thermodynamic parameters of enzymes in grassland soils from Galicia, NW Spain. *Soil Biology & Biochemistry*, *39*(1), 311–319.

122. Van Veen, J. A., & Kuikman, P. J. (1990). Soil structural aspects of decomposition of organic matter by micro-organisms. *Biogeochemistry*, *11*(3), 213–233.

123. Vetter, Y. A., Deming, J. W., Jumars, P. A., & Krieger-Brockett, B. B. (1998). A Predictive Model of Bacterial Foraging by Means of Freely Released Extracellular Enzymes. *Microbial Ecology*, *36*(1), 75–92.

124. Wanek, W., Mooshammer, M., Blöchl, A., Hanreich, A., & Richter, A. (2010). Determination of gross rates of amino acid production and immobilization in

decomposing leaf litter by a novel 15N isotope pool dilution technique. *Soil Biology & Biochemistry*, *42*(8), 1293–1302.

125. Wang, G., & Post, W. M. (2012). A theoretical reassessment of microbial maintenance and implications for microbial ecology modeling. *FEMS Microbiology Ecology*, *81*(3), 610–617.
126. Wang, G., Post, W. M., & Mayes, M. A. (2013). Development of microbial-enzyme-mediated decomposition model parameters through steady-state and dynamic analyses. *Ecological Applications: A Publication of the Ecological Society of America*, *23*(1), 255–272.
127. Wang, G., Jagadamma, S., Mayes, M. A., Schadt, C. W., Steinweg, J. M., Gu, L., & Post, W. M. (2015). Microbial dormancy improves development and experimental validation of ecosystem model. *The ISME Journal*, *9*(1), 226–237.
128. Wang, K., Peng, C., Zhu, Q., Zhou, X., Wang, M., Zhang, K., & Wang, G. (2017). Modeling Global Soil Carbon and Soil Microbial Carbon by Integrating Microbial Processes into the Ecosystem Process Model TRIPLEX-GHG: GLOBAL SOIL CARBON AND MICROBIAL CARBON. *Journal of Advances in Modeling Earth Systems*, *9*(6), 2368–2384.
129. Wang, Y., Chen, B., Wieder, W. R., Leite, M. C., Medlyn, B. E., Rasmussen, M., et al. (2014). Oscillatory behavior of two nonlinear microbial models of soil carbon decomposition. *Biogeosciences* , *11*(7), 1817–1831.
130. Wieder, W. R., Bonan, G. B., & Allison, S. D. (2013). Global soil carbon projections are improved by modelling microbial processes. *Nature Climate Change*, *3*, 909.
131. Wieder, W. R., Allison, S. D., Davidson, E. A., Georgiou, K., Hararuk, O., He, Y., et al. (2015). Explicitly representing soil microbial processes in Earth system models: Soil microbes in earth system models. *Global Biogeochemical Cycles*, *29*(10), 1782–1800.
132. Williams, M., Rastetter, E. B., Fernandes, D. N., Goulden, M. L., Shaver, G. R., & Johnson, L. C. (1997). PREDICTING GROSS PRIMARY PRODUCTIVITY IN TERRESTRIAL ECOSYSTEMS. *Ecological Applications: A Publication of the Ecological Society of America*, *7*(3), 882–894.
133. Xu, X., Thornton, P. E., & Post, W. M. (2013). A global analysis of soil microbial biomass carbon, nitrogen and phosphorus in terrestrial ecosystems. *Global Ecology and Biogeography: A Journal of Macroecology*, *22*(6), 737–749.
134. Zaehle, S., Medlyn, B. E., & De Kauwe, M. G. (2014). Evaluation of 11 terrestrial carbon–nitrogen cycle models against observations from two temperate Free-Air CO2

Enrichment studies. *New*. Retrieved from https://nph.onlinelibrary.wiley.com/doi/abs/10.1111/nph.12697

135. Zhang, X., Niu, G.-Y., Elshall, A. S., Ye, M., Barron-Gafford, G. A., & Pavao-Zuckerman, M. (2014). Assessing five evolving microbial enzyme models against field measurements from a semiarid savannah—What are the mechanisms of soil respiration pulses? *Geophysical Research Letters*, *41*(18), 6428–6434.

	Number of pools	Key variables	Scale & resolution	Reference
Soil stocks and properties	Harmonized World Soil Database	Soil C, physical properties, top soil and subsoil (0-1m)	Global, 30 arc sec (0.008333°) resolution	FAO et al. (2012)
	ISRIC-WISE and SoilsGrid1km	Soil C, physical properties at six depths	Global, 1km resolution	Hengl et al. (2014)
Microbial biomass	Soil microbial abundance	M, soil C, physical properties	Global, 0.5° resolution	Serna-Chavez et al. (2013)
	Biome extrapolated M, N, and P	Microbial and soil C, N, and P to 1m depth	Global, 3422 data points for 14 biomes	Xu et al. (2013)
Soil respiration	Soil respiration database (SRDB)	Soil respiration, T, Q_{10}, biome	>800 studies and >3,300 records	Bond-Lamberty & Thomson (2010)

Table 1. Large-scale data sets available to parameterize and initialize global projections of *CDMZ* models. (Adapted from Table 3 in Wieder *et al.* 2015)

Model Reference	Model C Pools and Fluxes	Functional Diversity	Soil Environmental Dependency	SOC Protection (yes/no, degree, details)	Vertical Resolution	Horizontal Resolution
German *et al.* (2012)	***CM* model** *C* inflow: constant litter input, recycling of necromass; *C* outflow: decomposition (Michaelis); *M* inflow: uptake of decomposition products; *M* outflow: respiration, constant death rate.	**No**	**Temperature** Arrhenius function for Michaelis-Menten kinetic parameters. Linear function for CUE.	**No**	**No**	**5 locations** Differ in decomposition kinetics parameters and initial temperature.
Wieder *et al.* (2013)	***CMP* model** *C* inflow: constant litter input; *C* outflow: microbial decomposition (Michaelis) and constant stabilization rate (into *P*); *M* inflow: uptake of decomposition products, *M* outflow: respiration, constant death rate; *P* inflow: microbial residues and direct stabilization of *C* from litter input; *P* outflow: microbial decomposition.	**No**	**Temperature** Arrhenius function for Michaelis-Menten kinetic parameters. Linear function for CUE.	**Low** *P* is accessible to microbial decomposition and not slower than *C*.	**2 layers** 0-30cm and 30-100cm. Differ in litter inputs (65% in top layer).	**Global** Differ in litter inputs, initial temperature, Michaelis-Menten kinetic parameters.
Wieder *et al.* (2014, 2015b) MIMICS	***CMP* model** Same as Wieder *et al.* (2013).	**Two functional types for each C pool.** All affect Michaelis-Menten (reverse in Wieder *et al.*, 2018) kinetic parameters. *C* functional types also affect fraction of *C* directly stabilised and microbial CUE. *M* functional types also affect constant death rate and partitioning of necromass recycled.	**Temperature** Arrhenius function for Michaelis-Menten kinetic parameters.	**Intermediate** *P* is accessible to microbial decomposition, but slower than *C*.	**No**	**Global** Same as Wieder *et al.* (2013).
Sulman *et al.* (2014) CORPSE	***CMP* model** *C* inflow: constant litter input and turnover of *P*; *C* outflow: decomposition (reverse	**Three functional types for *C* and *P*.** Differ in litter inputs, decomposition and protection	**Temperature** Arrhenius function for reverse Michaelis-Menten V_{max} parameter. **Moisture** Non-linear	**Full** *P* is inaccessible to microbial decomposition. Its formation is not microbe-mediated, but	**No**	**Ecosystem** Differ in temperature, moisture, litter inputs, root exudate inputs, and protection

	Michaelis with *M*: *C* ratio) and protection; *M* inflow: uptake of decomposition products; *M* outflow: respiration, constant death rate; *P* inflow: protection of *C*; *P* outflow: constant turnover rate.	rates. Affect microbial uptake rate.	function for the decomposition rate.	instead is a functional type-dependent abiotic process.		rates. **Global** Model integrated into a global land model with dynamical vegetation growth and soil physical and hydrological processes.
Abramoff *et al.* (2018) MILLENIAL	***CDMP* model** *C* inflow: litter input, breakdown of *P*; *C* outflow: decomposition (double Michaelis) and protection. *D* inflow: litter input, decomposition of *C*; *D* outflow: microbial uptake, leaching, protection. *M* inflow: uptake of *D*; *M* outflow: respiration, constant death rate. *P* inflow: protection; *P* outflow: breakdown.	**Two types of *P*** Differ in formation and breakdown processes.	**Temperature** Arctangent function. **Moisture** Reverse exponential function. All processes, except litter input, are temperature and moisture dependent. **pH** Reverse exponential function for adsorption binding affinity (stronger adsorption at lower pH). **Texture (% clay)** Exponential function for the maximum sorption capacity (stronger adsorption at high % clay).	**Multiple** Two types of *P*: mineral-associated organic carbon (MAOC), and aggregate carbon (AC). MAOC inflow: adsorption of *D* following a non-linear saturating function of *D* and microbial necromass, breakdown of AC; MAOC outflow: aggregation of MAOC into AC. AC inflow: aggregation of MAOC and *C*; AC outflow: breakdown.	**No** 1m soil profile	**No**
Allison et al. (2010)	***CDMZ*** *C* inflow: constant litter input, recycling of necromass; *C* outflow: decomposition (Michaelis); *D* inflow: litter input, recycling of necromass and enzymes, decomposition; *D* outflow: microbial uptake; *Z* inflow: microbial production; *Z* outflow: constant turnover; *M* inflow: uptake of decomposition products; *M* outflow: respiration, constant death rate.	**No**	**Temperature** Arrhenius function for Michaelis-Menten V_{max} parameter. Linear function for Michaelis-Menten half-saturation constant K_M. Linear function for CUE.	**No**	**No**	**No**
Tang & Riley (2015) SUMMS	***CDMZ*** Same as Allison *et al.* (2010),	**No**	**Temperature** Arrhenius functions in	**Implicit** Mineral association with	**No**	**No**

	except microbial biomass is divided into structural biomass and reserve, and CUE is derived from the model using the dynamic energy budget theory.		competition for binding (adsorption), decomposition, uptake, and enzyme turnover.	*D* and *Z* is included implicitly as a reaction at equilibrium with the other reactions of binding for uptake and decomposition.		
Wang *et al.* (2013) MEND	***CDMZP*** Same as Allison *et al.* (2010) for *CDMZ. P* inflow: mineral-association, adsorption; *P* outflow: decomposition, desorption.	**Two types of *Z*** for the decomposition of *C* and *P*. **Two types of *P*** that differ in formation and breakdown processes.	**Temperature** Arrhenius function for Michaelis-Menten kinetic parameters, adsorption and desorption. Linear function for CUE.	**Multiple** Two types of *P*: mineral-associated organic carbon (MAOC) that can be decomposed by specific enzymes, and adsorbed *D* (AD) that is inaccessible to decomposition. MAOC inflow: mineral-association of *C*; MAOC outflow: decomposition; AD inflow: adsorption of *D* ; AD outflow: desorption.	**No**	**No**

Table 2. Structural and operational characteristics of 6 recent microbial models. Models features are presented with "yes/no" and details. *C* denotes accessible complex C compounds (litter or soil C); *D*, accessible C available for microbial uptake; *M*, microbial C biomass; *Z*, extracellular enzymatic C; *P*, protected soil C, which includes aggregate C and mineral-associated *D* or *C*, and may or may not be accessible to microbial decomposition. SOC protection qualifies as "low" when *P* is accessible to microbial decomposition at a rate that is not much lower than *C*, as "intermediate" when *P* is accessible to microbial decomposition but at a significantly lower rate than *C*, as "full" when *P* is inaccessible to microbes, and as "multiple" when there are at least one accessible and one inaccessible *P* pools. We define a process as "constant" when it occurs at a constant rate.

Eco-evolutionary dynamics of decomposition: emergence and stability of microbial cooperation for diffusive goods

Elsa Abs[*], Régis Ferrière[†], Hélène Leman[‡]

[*]ENS Paris, France, abs@biologie.ens.fr
[†]ENS Paris, France, regisf@email.arizona.edu
[‡]INRIA, ENS Lyon, France, helene.leman@ens-lyon.fr

Abstract

Microorganisms drive critical ecosystem processes by converting complex substrates into smaller compounds, that they assimilate for growth and maintenance. By relying on extracellular enzymes (exoenzymes) to perform this conversion, microbes invest in diffusive public goods—a form of cooperation that is vulnerable to 'cheaters', microbial strains that invest less and yet reap off the public benefits. To resolve how and to what degree such cooperation can evolve, we construct a spatially explicit model describing the interaction of resident strains with mutant cells, which, initially at least, occur in small, localized populations. The main difficulty here is to account for the contrasting structural and temporal scales that characterize the entities (cells, enzymes, substrates, products) and processes that affect them. The model treats the individual investment in exoenzyme production as a quantitative trait and predict its evolutionary trajectory driven by recurrent mutation and selection events. The model predicts that provided the soil diffusion rate of decomposition products is below a critical threshold. The exoenzyme production trait converges to a range of evolutionarily stable and selectively neutral values. Importantly, by responding strongly to variation in soil abiotic properties like diffusion, the adaptive evolution of exoenzyme production has the potential to reshape the macroscopic ecosystem responses, such as decomposition rate and soil carbon stock, to global environmental change.

Keywords: degradative exoenzyme, evolutionary stability, spatial structure, scaling limits, soil carbon stock, eco-evolutionary feedback, adaptive dynamics.

1 Introduction

Microorganisms drive critical ecosystem processes, such as nutrient mineralization and the decomposition of organic matter [Falkowski et al., 2008]. Many of these processes depend on the conversion of complex compounds into smaller products that microbes can assimilate for growth and maintenance. Except in environments where simple nutrients are abundant, microbes rely on extracellular enzymes (exoenzymes) to perform this conversion [Ratledge, 1994]. By doing so, they face a 'public good spatial dilemma' [Allen et al., 2013, Driscoll and Pepper, 2010]. The 'spatial dilemma' arises because exoenzymes are costly compounds [Schimel and Weintraub, 2003], with reaction products may diffuse away from the enzyme-secreting microbe and therefore benefit not only the individuals producing them, but also neighboring cells [Velicer, 2003, West et al., 2006]. Public goods are ubiquitous in microbial ecosystems. The 'spatial dilemma' over public good production arises because public goods are costly compounds that are secreted outside the cell; reaction products may diffuse away from the enzyme-secreting microbe and therefore benefit not only the individuals producing them, but also neighboring cells [Velicer, 2003, West et al., 2006]. Evolutionary theory predicts that producers of public goods are vulnerable to cheating by individuals that receive the benefits without paying the cost of production. Without some mechanism to support cooperation [Nowak, 2006], public goods production is expected to disappear under exploitation from cheaters. Nonetheless, exoenzymes are ubiquitously produced in all environments, e.g. siderophores that scavenge iron [Buckling et al., 2007, Cordero et al., 2012, Griffin et al., 2004, Julou et al., 2013], polymers that enable biofilm formation [Rainey and Rainey, 2003], and allelopathic compounds that reduce competition [Le Gac and Doebeli, 2010]. Conditions must exist that promote the evolution of exoenzyme production.

Evolutionary game theory provides a powerful framework for investigating conditions that favor exoenzyme production [Koch, 1985, Schimel and Weintraub, 2003, Sinsabaugh and Moorhead, 1994]. Evolutionary game-theoretic models have been developed to address competition between exoenzyme-producing and nonproducing (cheating) strains [Allison, 2005, Folse and Allison, 2012, Kaiser et al., 2014, 2015]. Considering the diffusivity of products, these models have highlighted the importance of habitat spatial heterogeneity for the evolution of the production mechanism. For example, organic substrates, microbes and mineral particles form a three dimensional matrix of aggregates and pore spaces of different sizes in soils [Tisdall and Oades, 1982]. For enzyme-dependent microbes, these physical properties should influence the movement of substrates, enzymes and usable products [Vetter et al., 1998], and the fate of cheating microbes [Allison, 2005, Dobay et al., 2014, Folse and Allison, 2012].

Our understanding of the evolutionary stability of diffusive public goods in general, and of degradative enzyme production in particular, remains incomplete. One limitation of previous models is their focus on two-way competition between two strains, typically a producing strain and a 'pure cheater' or non-producing strain. A key issue here is that mechanisms that promote stability

of producers against pure cheaters might fail to prevent 'erosion' of cooperation by mutant strains that produce slightly less of the public good than the wild-type, or resident strain [Ferriere et al., 2002]. Pure cheaters may go locally extinct when they do not receive enough resource produced by cooperators; however, strains that produce less, rather than none, of the public good should be less sensitive to the harm they inflict to the community [Lee et al., 2016]. On the other hand, producers may be vulnerable to pure cheaters and yet resist invasion by strains that invest only slightly less into the common good. We thus expect conditions for the evolutionary stability of cooperation to be different when considering the recurrent events of mutation of small effects and selection that shape the evolutionary trajectory of exoenzyme production.

To predict the outcome of selection on small-effect variants, we need to evaluate the population growth rate of initially rare mutant types interacting with any given resident type. To achieve this, previous models of microbe-enzyme systems need to be revisited and extended, so that invasion fitness of small-effect mutants can be computed. To describe the interaction of resident strains with mutant cells, which, initially at least, occur in small, spatially localized populations, individual-level modeling of microbe-enzyme systems is required. Previous microbe-enzyme ecological models (reviewed in Abs and Ferriere [2018], Wieder et al. [2015]) are phenomenological, rather than derived by scaling up from microscopic processes acting locally at the level of individual entities. The main difficulty here is to address the extremely different scales that characterize the entities (cells, enzymes, substrates, products) and processes that affect them. Here derive a hybrid, stochastic-deterministic model that takes this multiplicity of scales into account. By applying the hybrid model to a spatially structured habitat, we elucidate conditions that promote the evolutionary stability of enzymatic decomposition and we show that the evolution of exoenzyme production shapes the response of decomposition to environmental change.

2 Model Construction

To construct a spatially explicit model of microbe-enzyme decomposition, we focus on bacterial cells and unprotected soil organic carbon [Davidson and Janssens, 2006]. Space is modeled as a two-dimensional grid of microsites, with each microsite potentially occupied by a cell colony. Decomposition is seen as a microbial public good game, whereby individual microorganisms invest resources into the production of degradative exoenzymes. Exoenzyme molecules bind soil organic carbon (SOC) molecules and catalyse the depolymerization of SOC into dissolved organic carbon (DOC) molecules. DOC molecules occurring in a microsite may be uptaken and metabolized by cells present in the microsite, resulting in cell growth and exoenzyme production. The fraction of uptaken DOC that is invested by a cell in exoenzyme production, as opposed to cell biomass production, is denoted by φ. This is the focal trait that characterizes the microbial phenotype, for which we assume heritable variation, originating in mutation [Alster et al., 2016, Trivedi et al., 2016].

We assume that cells, enzymes, substrates (SOC) and products (DOC) are well-mixed within each microsite. Products can diffuse and offspring cells can disperse between neighboring microsites. Additional processes operating at the level of individual entities are: cell respiration, parametrized by the energetic cost of cell tissue and the energetic cost of enzyme molecules; cell death and enzyme degradation, at constant rates; cell division, determined by accrued and stored resources reaching a threshold within the cell; formation and reaction or dissociation of SOC-enzyme complexes. Additional processes operating at the level of microsites are: external inputs of SOC and DOC, losses of SOC and DOC (leaching), diffusion of DOC, random disturbances causing cell colony death and microsite 'opening' to cell dispersal. We assume nitrogen and phosphorus to be unlimiting and measure the abundance of all entities in units of carbon mass.

First we focus on the 'local' dynamics of decomposition within a microsite, where decomposition involves fluxes in and out of five local compartments: microbial cells (biomass M), enzymes (Z), SOC (C), SOC-enzyme complexes (X), and DOC (D) (Fig. 1a). To scale up the dynamics of decomposition from microscopic, stochastic processes, we take the following steps:

- We define the stochastic processes acting at the level of C, D, M, Z, X entities (molecules, cells) (Fig. 1a).
- By applying appropriate rescaling on the rates of complex (X) formation, reaction or dissociation, we reduce the stochastic model to four state variables (C, D, M, Z) (Fig. 1b).
- If all entities are in large number, the reduced stochastic model can be rescaled as a dynamical system of ordinary differential equations, similar to Schimel and Weintraub (2003) seminal "CDMZ model" of litter decomposition (see also Abs and Ferriere (2018), Wieder et al. (2015)). We obtain the scaling of the deterministic model parameters relative to the individual-level process parameters.
- When the finite, potentially small, number of bacterial cells within a microsite is taken into account, the reduced stochastic model can be rescaled as a a hybrid, stochastic-deterministic model (Piecewise Deterministic Markovian Process, or PDMP).

We then model decomposition at larger spatial scale by coupling PDMP models across the spatial grid of microsites. This forms the spatially explicit model that we use to investigate the evolutionary stability of exoenzyme production.

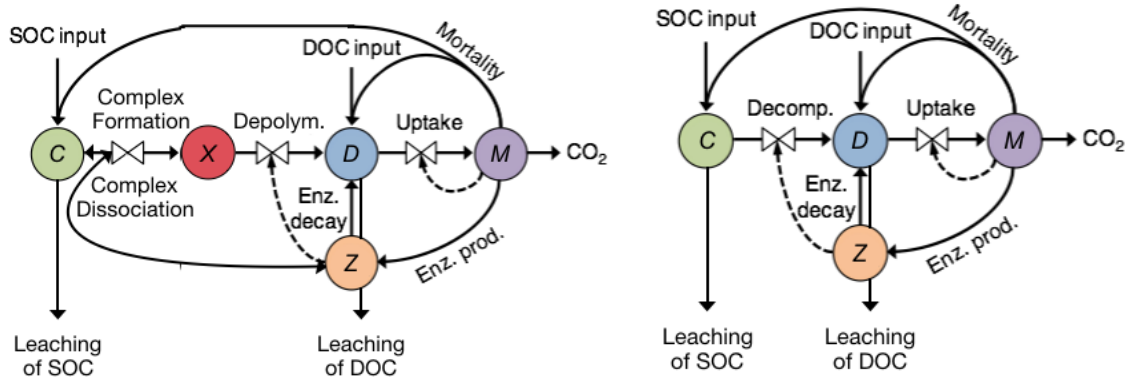

(a) (b)

Figure 1. Microbe-enzyme driven decomposition of soil organic matter: Modelled entities and processes. (a), Five-compartment model. (b), Four-compartment model. SOC, soil organic carbon. DOC, dissolved organic carbon. Arrows indicate carbon fluxes among boxes and in and out of the system.

2.1 Individual-level, stochastic processes

Fluxes in and out of C, D, M, Z, X occur in continuous time. M_t is the number of bacterial cells at time t. Z_t, C_t, D_t are the numbers of enzyme molecules, SOC molecules, and DOC molecules, respectively. X_t is the number of complexes formed by an enzyme molecule binding a DOC molecule. DOC enters the microsite at a constant rate. When a cell dies, a fraction p of the molecules released are recycled into SOC, while the rest is recycled into DOC. A fraction l of dead microbes and deactivated enzymes may be lost due to leaching.

We denote by α the structural cost of a cell, which is the number of DOC molecules contained in one cell, and by α' the energetic cost of a cell, which is the number of DOC molecules consumed to produce the energy needed for the synthesis reactions involved in the production of a cell. We denote the structural cost of one SOC molecule by β, and the structural and energetic cost of producing one molecule of enzyme by γ and γ', respectively. We assume that the energetic costs are carbon released by bacteria as CO_2 that diffuses out of the system instantaneously. We define the biomass production fraction and enzyme allocation fraction as

$$\bar{\gamma}_M := \frac{1}{\alpha + \alpha'}, \quad \bar{\gamma}_Z := \frac{1}{\gamma + \gamma'}. \tag{2.1}$$

Any event may occur at any time. The event rates (Tables 1 and 2) give an approximation of the average frequency of each event. The rates of cell growth and enzyme production depend on the cell trait φ. Cell division is the outcome of storing assimilated DOC until a threshold is reached. A parameter N scales the gradual process of consumption and storage of DOC. Thus, there can be

growth only if there is enough D to cover both the structural cost, α/N, and the energetic cost, α'/N of this growth, hence the notation $\mathbf{1}_{\{D\geq(\alpha+\alpha')/N\}}$ which equals 1 if $D \geq (\alpha+\alpha')/N$, 0 otherwise. Likewise $\mathbf{1}_{\{D\geq\gamma+\gamma'\}}$ is used for the production event of one enzyme molecule. Growth leads to cell division only if enough D has been consumed and stored.

Enzyme-substrate complexes form at rate $\bar{\lambda}$ as one enzyme molecule (e.g. cellulase) bind one SOC molecule (e.g. cellulose). A complex may either dissociate (with no reaction) at rate $\bar{\lambda}^{\varepsilon}_{-1}$, or react at rate $\bar{\mu}^{\varepsilon}$ and convert the molecule of SOC into a molecule of DOC while the enzyme is released and free again to react with new molecules of SOC.

We use K as a scaling parameter for the magnitude of the number of interacting bacteria, which by definition have access to the same (local) pool of resources. When $K = 1$, all parameter values correspond to the rates observed for a volume of soil $V = 10^{-9}$ cm^3 that we take as the baseline volume expected to contain one cell. Increasing K means that the model treats interactions as well-mixed among an increasing number of cells that occupy an increasingly large volume. As a consequence, external inputs of SOC or DOC increase with K, and the probability that two enzyme and substrate molecules encounter, that is proportional to $\bar{V}^K_{mD}$, decreases. We thus assume that there are four constant parameters, $\bar{I}_C$, $\bar{I}_D$, $\bar{V}_{mD}$ and $\bar{K}_{mU}$, such that

$$\bar{I}^K_C = K\bar{I}_C,\ \bar{I}^K_D = K\bar{I}_D,\ \bar{V}^K_{mD} = \frac{\bar{V}_{mD}}{K} \quad \text{and} \quad \bar{K}^K_{mU} = K\bar{K}_{mU} \tag{2.2}$$

where I_C is the external input of C, I_D is the external input of D, V_{mD} is the maximum decomposition rate when C is not limiting, and K_{mU} is the uptake half-saturation constant.

For K finite and fixed, we omit K from our notations and use

$$C^{\varepsilon}(t), D^{\varepsilon}(t), M^{\varepsilon}(t), Z^{\varepsilon}(t), X^{\varepsilon}(t)$$

to designate the (stochastic) number of cells, enzymes molecules, SOC molecules, complexes and DOC molecules at time t. In Appendix A we show that when K is fixed, and under the assumption that complex dissociation and the decomposition reaction of the complex are much faster than complex formation:

$$\bar{\lambda}^{\varepsilon}_{-1},\ \bar{\mu}^{\varepsilon} >> \bar{\lambda},$$

the stochastic CDMZX model can be simplified into the four-compartment stochastic CDMZ model with structure shown in Fig. 1b and events and event rates listed in Table 2.

In other words, we assume that there are two positive constant $\bar{\lambda}_{-1}$ and $\bar{\mu}$ such that

$$\bar{\lambda}^{\varepsilon}_{-1} = \frac{1}{\varepsilon}\bar{\lambda}_{-1} \quad \text{and} \quad \bar{\mu}^{\varepsilon} = \frac{1}{\varepsilon}\bar{\mu}. \tag{2.3}$$

When the scaling parameter ε is very small, the model $(C^\varepsilon, D^\varepsilon, M^\varepsilon, Z^\varepsilon, X^\varepsilon)$ can be approximated by (C, D, M, Z) where the state variables (C, D, M, Z) are driven by the stochastic CDMZ model with

$$\bar{V}_{mD} = \bar{\lambda}\frac{\bar{\mu}}{\bar{\mu} + \bar{\lambda}_{-1}}.$$

The stochastic CDMZ model can be simulated by implementing the algorithm described in Appendix B.

Table 1. Events involving enzyme-SOC complexes (X) in the CDMZX model. Individual-level events and event rates.

Event	Event rate
Formation of 1 complex X from 1 Z and 1 C: $(M, Z, C, X, D) \mapsto (M, Z-1, C-1, X+1, D)$	$\bar{\lambda}ZC$
Dissociation of 1 complex X into 1 Z and 1 C: $(M, Z, C, X, D) \mapsto (M, Z+1, C+1, X-1, D)$	$\bar{\lambda}^{\varepsilon}_{-1}X$
Depolymerization of 1 C into β D (decomposition) from the effect of Z on C in complex X $(M, Z, C, X, D) \mapsto (M, Z+1, C, X-1, D+\beta)$	$\bar{\mu}^{\varepsilon}X$

Table 2. Events and event rates in the stochastic CDMZ model. Cells are characterized by their trait value φ.

Event	Event rate
Events relative to M	
M grows and accumulates an equivalent of α/N molecules of DOC, gives birth to an offspring if its stock of carbon is equal to α $D \mapsto D - \frac{\alpha+\alpha'}{N}$	$N(1-\varphi)\bar{\gamma}_M\bar{V}_{mU}\frac{D}{\bar{K}^K_{mU}+D}\mathbf{1}_{\left\{D \geq \frac{\alpha+\alpha'}{N}\right\}}$
M dies $C \mapsto C + \lfloor(1-l)p\frac{\alpha}{\beta}\rfloor$, $D \mapsto D + \lfloor(1-l)(1-p)\alpha\rfloor$	$\bar{d}_M$
M produces 1 Z $D \mapsto D - (\gamma + \gamma')$	$\varphi\bar{\gamma}_Z\bar{V}_{mU}\frac{D}{\bar{K}^K_{mU}+D}\mathbf{1}_{\{D \geq \gamma+\gamma'\}}$
Events specific to Z, C, D	
Deactivation of 1 Z: $(M, Z, C, D) \mapsto (M, Z-1, C, D + \lfloor(1-l)\gamma\rfloor)$	$\bar{d}_Z Z$

External input of 1 C: $(M, Z, C, D) \mapsto (M, Z, C+1, D)$	$\bar{I}_C^K$
Loss of 1 C due to leaching: $(M, Z, C, D) \mapsto (M, Z, C-1, D)$	$\bar{e}_C C$
External input of 1 D: $(M, Z, C, D) \mapsto (M, Z, C, D+1)$	$\bar{I}_D^K$
Loss of 1 D due to leaching: $(M, Z, C, D) \mapsto (M, Z, C, D-1)$	$\bar{e}_D D$
Depolymerization of 1 C into β D (decomposition) through enzymatic reaction $(M, Z, C, D) \mapsto (M, Z+1, C-1, D+\beta)$	$\bar{V}_{mD}^K ZC$

2.2 Deterministic approximation and rescaling of parameters

In this subsection we assume that all bacteria initially have the same trait value, φ, and that there is no mutation (i.e. $p_{mut} = 0$), so that there is only one type of cells in the system. We show (Appendix C) that if K is large and (2.2) holds, then the stochastic CDMZ model can be approximated by the following deterministic model

$$\begin{cases} \dfrac{d\mathtt{m}}{dt} = (1-\varphi)\bar{\gamma}_M \bar{V}_{mU} \dfrac{\mathtt{d}}{\bar{K}_{mU} + \mathtt{d}} \mathtt{m} - \bar{d}_M \mathtt{m} \\ \dfrac{d\mathtt{z}}{dt} = \varphi \bar{\gamma}_Z \bar{V}_{mU} \dfrac{\mathtt{d}}{\bar{K}_{mU} + \mathtt{d}} \mathtt{m} - \bar{d}_Z \mathtt{z} \\ \dfrac{d\mathtt{c}}{dt} = \bar{I}_C - \bar{e}_C \mathtt{c} + \dfrac{\alpha}{\beta}(1-l) p \bar{d}_M \mathtt{m} - \bar{V}_{mD} \mathtt{z}\mathtt{c} \\ \dfrac{d\mathtt{d}}{dt} = \bar{I}_D - \bar{e}_D \mathtt{d} + \beta \bar{V}_{mD} \mathtt{z}\mathtt{c} + (1-l)\left[(1-p)\alpha \bar{d}_M \mathtt{m} + \gamma \bar{d}_Z \mathtt{z}\right] - \bar{V}_{mU} \dfrac{\mathtt{d}}{\bar{K}_{mU} + \mathtt{d}} \mathtt{m}, \end{cases} \tag{2.4}$$

where $\mathtt{m}$, $\mathtt{z}$, $\mathtt{c}$ and $\mathtt{d}$ give the number of cells, enzyme molecules, SOC molecules and DOC molecules predicted to occur on average around any individual cell. To set the state variables in units of carbon mass, we apply the following rescaling:

$$m = \omega_M \mathtt{m}, \quad z = \omega_Z \mathtt{z}, \quad c = \omega_C \mathtt{c}, \quad \text{and} \quad d = \omega_D \mathtt{d}$$

where m is in carbon mass unit and ω_M is the carbon mass content of one cell, and likewise for enzyme, SOC and DOC. The ω parameters are related to α, β and γ according to:

$$\alpha = \frac{\omega_M}{\omega_D}, \quad \beta = \frac{\omega_C}{\omega_D}, \quad \text{and} \quad \gamma = \frac{\omega_Z}{\omega_D}. \tag{2.5}$$

With further rescaling and notations:

$$\begin{array}{rclrclrclrcl} I_C &:=& \omega_C \bar{I}_C, & I_D &:=& \omega_D \bar{I}_D, & K_{mU} &:=& \omega_D \bar{K}_{mU}, & & & \\ V_{mD} &:=& \frac{1}{\omega_Z} \bar{V}_{mD}, & V_{mU} &:=& \frac{\omega_D}{\omega_M} \bar{V}_{mU}, & \gamma_M &:=& \frac{\omega_M}{\omega_D} \bar{\gamma}_M, & \gamma_Z &:=& \frac{\omega_Z}{\omega_D} \bar{\gamma}_Z, \\ d_M &:=& \bar{d}_M, & d_Z &:=& \bar{d}_Z, & e_C &:=& \bar{e}_C, & e_D &:=& \bar{e}_D, \end{array}$$

we obtain the following dynamical system satisfied by m, z, c and d variables measured in carbon mass unit:

$$\begin{cases} \frac{dm}{dt} = (1-\varphi)\gamma_M V_{mU} \frac{d}{K_{mU}+d} m - d_M m \\ \frac{dz}{dt} = \varphi \gamma_Z V_{mU} \frac{d}{K_{mU}+d} m - d_Z z \\ \frac{dc}{dt} = I_C - e_C c + (1-l) p d_M m - V_{mD} z c \\ \frac{dd}{dt} = I_D - e_D d + V_{mD} z c + (1-l)\left[(1-p) d_M m + d_Z z\right] - V_{mU} \frac{d}{K_{mU}+d} m. \end{cases} \tag{2.6}$$

Definitions of all parameters, units, and default values are gathered in Table D.1 of Appendix D.

2.3 Hybrid stochastic-deterministic model for small populations

A cell is 10^7 times larger than one enzyme or substrate (SOC) molecule, and 10^{10} times larger than one product (DOC) molecule. Within a given volume, the number of cells is between 10^{-5} to 10^{-10} times smaller than the number of molecules of enzyme, SOC or DOC. As a consequence, the dynamics of cells and the dynamics of enzyme, SOC and DOC do not unfold on the same scales. The events affecting Z, C and D are much faster and more numerous than events affecting M. As a consequence, we can treat the dynamics of Z, C and D as deterministic and given by the state variables z, c and d of dynamical system (2.7) over time bouts of constant cell population.

Mathematically, this can be formalized by establishing the convergence of the stochastic CDMZ model to a Piecewise Deterministic Markov Process, or PDMP (Appendix E), which is a hybrid stochastic-deterministic model. The hybrid dynamics involve random jumps of the finite cell number (driven by birth and death events) interspersed with periods of continuous, deterministic change in enzyme, SOC and DOC given by

$$\begin{cases} z'(t) = \varphi \alpha \omega_D V_{mU} \gamma_Z \frac{d}{K_{mU}+d} M - d_Z z \\ c'(t) = I_C - l_C c - V_{mD} z c \\ d'(t) = I_D - l_D d + V_{mD} z c + (1-l) d_Z z - \varphi \alpha V_{mU} \frac{d}{K_{mU}+d} M, \end{cases} \tag{2.7}$$

where M is the size of the cell population, and z, c, and d denote the amount of enzymes, SOC and DOC in carbon mass unit. Note that the mechanisms represented in the dynamical system are the events specific to Z, C, D in Table 2 and the production of enzymes (last line of the events relative to M in Table 2). The times of events related to the cell population (growth and death) remain stochastic and the rates of these events are given by the first two lines of Table 2, similarly to the stochastic CDMZ model. The simulation algorithm of the PDMP is presented in Appendix F.

We can further simplify the hybrid model by noting that when $N > 10^4$, the events of growth become as frequent as the events affecting Z, C, and D in the stochastic CDMZ model. In this case, consumption of D by cells is no longer a stochastic process but instead depends deterministically on M. Cell production thus becomes nearly deterministic, and the only remaining (slow) stochastic process is cell death. Even though the rigorous proof of this result is beyond the scope of the paper, we will adopt this approximation as we develop the spatially explicit extension of the model.

2.4 Spatial model

The spatial model retains the CDMZ functional structure and applies the approximated hybrid stochastic-deterministic model to each microsite of a large two-dimensional grid (lattice of $L \times L$ microsites). The key features added to the spatial model are diffusion of products (DOC) and dispersal of cells, both taking place between adjacent microsites.

We model the DOC diffusion between microsites by approximating a continuous diffusion with a Euler scheme in which time is discretized with a fixed time step interval, τ_{diff}. At each time step, a step of the Euler scheme associated with the diffusion equation

$$\frac{d}{dt}d(x,t) = \sigma_{\text{diff}}\Delta d(x,t)$$

is realized for the variable d, where x is the position variable. Space discretization used in the Euler scheme corresponds exactly to the habitat lattice structure.

Between two diffusion time steps, the dynamics of each microsite is calculated using the approximated hybrid stochastic-deterministic model. The DOC reserve within each cell follows

$$\frac{dS_i(t)}{dt} = \alpha(1-\varphi)\gamma_M V_{mU}\frac{d}{K_{mU}+d},$$

where S_i represents the carbon stocked at time t in the i-th cell. When $S_i(t)$ reaches α, the i-th cell divides, and both mother and daugther cells' reserve is set back to 0. The daughter cell is added to the mother cell colony with probability $1-p_{disp}$, or the new cell disperses (with probability p_{disp}) to one of the four neighbouring microsites. If empty microsites (one at least) are available in the neighborhood, the dispersing cell moves to one of them, drawn randomly. If all neighboring microsites are

occupied, there is a probability p_{open} that a 'micro-catastrophe' strikes and opens one of them, which then becomes occupied by the dispersing cell, while c and d released by the dead cells are recycled locally. If no microsite opens (with probability $1 - p_{open}$), the dispersal event is unsuccessful and the daughter cell remains in its maternal microsite. Finally, between two diffusion time steps, the random death of a cell may also happen. In this case, one cell is removed and its carbon content is recycled into c and d within the dead cell's microsite.

3 Model Analysis

3.1 Ecological dynamics

In large, well-mixed systems, ecological dynamics are driven by the deterministic model (2.6). The analytical study of (2.6) indicates that there are one or three equilibria depending on the value of φ. At the "trivial" equilibrium, there are no active microbes or enzymes ($M_{eq1} = Z_{eq1} = 0$), SOC and DOC are fixed by the balance of external inputs and leaching ($C_{eq1} = I_C/e_C$ and $D_{eq1} = I_D/e_D$). This equilibrium is always locally stable. When the other two equilibria exist, one is always unstable, and M, Z, C, D at both equilibria are all positive. Existence of the positive equilibria depends on φ belonging to a certain interval ($\varphi_{min} \leq \varphi \leq \varphi_{max}$). When the non-trivial equilibria exist, one is unstable and the other is locally stable for most values of φ and unstable (bifurcating into a limit cycle) for values of φ close to φ_{min}. For the default parameters values (Table D.1 in Appendix D), both exist when $0.01212 < \varphi < 0.9984$ and the microbial equilibrium is stable for $0.01212 < \varphi < 0.9969$.

How well does the deterministic CDMZ model capture the behavior of its stochastic counterpart? A key difference comes from the fact that a cell can grow only if there is enough D available for both the structural and the energetic costs of growth, $(\alpha + \alpha')/N$, and likewise for the production of enzyme molecules. If there is not enough D, the event is dropped, which means that the cell does not grow and no D is consumed, therefore the numbers of M, Z and D are unchanged. This does not happen in the deterministic model, which is a large population approximation of the stochastic model. In particular, since one cell is much more costly in D than one enzyme molecule (see Table D.1 in Appendix D), more events of cell division than enzyme production may be dropped, especially when N is small. As a result, a significant difference may arise between the expected investment (parameter φ) and realized investment of a cell into enzyme production versus biomass production. Figure S1 shows that at low system size K, keeping the discrepancy small between the deterministic and stochastic models across the range of feasible φ, requires outstandingly large N, so that the structural and energetic costs of growth are kept very low.

A second key difference is fluctuations in the stochastic model, which may drive the population to extinction. In contrast, for viable values of φ, strong oscillations may occur in the deterministic

model without compromising the cell population persistence (Fig. S2). In the stochastic, spatially extended system, the habitat spatial structure induces a metapopulation rescue effect, which strongly increases the probability of persistence over any given time horizon (Fig. S3).

3.2 Evolutionary suicide in well-mixed systems

In a well-mixed population, cooperation is unstable: the process of mutation-selection reduces the exoenzyme production trait φ, down to the point where the microbial population becomes unviable. This is illustrated in Fig. 2, where the system size is $K = 20$, and the ancestral cell trait value is of $\varphi = 0.5$. Without mutation, the population of bacteria stabilizes around 10 cells. With a positive probability of trait mutation ($p_{mut} = 0.1$), the mean value of the trait decreases toward the minimum viable value, leading to extinction in an instance of "evolutionary suicide" [Ferriere, 2000, Ferriere and Legendre, 2013].

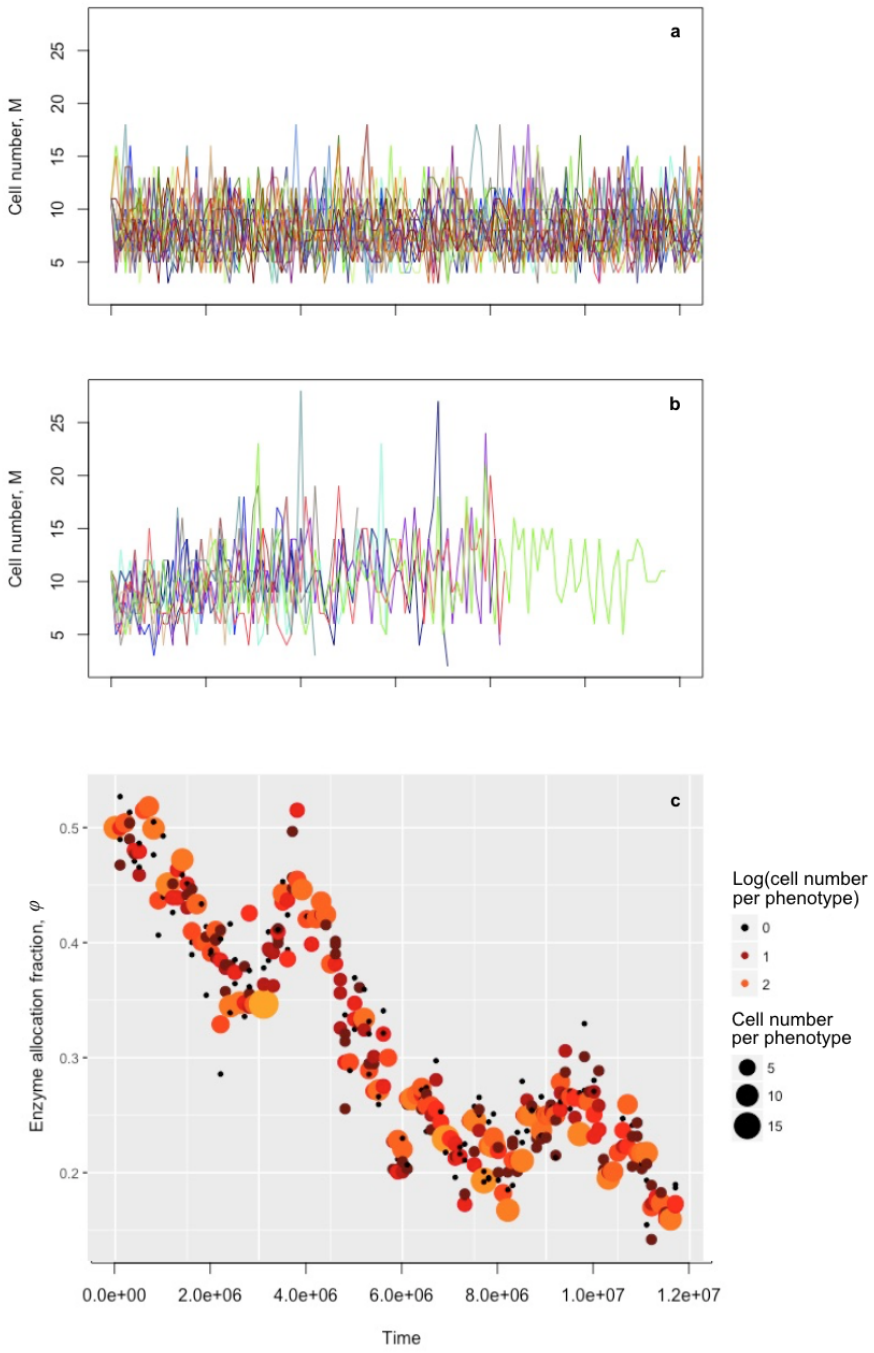

Figure 2. Dynamics of the cell population and microbial trait φ, with and without mutation. (a) Cell population dynamics without mutation. (b) Cell population dynamics with mutation. As populations evolve, they reach the minimum viable value of the enzyme production trait, φ, and go extinct. (c) Evolution of enzyme allocation fraction, φ. Ten simulation runs are shown. All constant parameters are set to the default values (Table D.1 in Appendix D), except $T_{\max} = 10^8$, ancestral φ is set to 0.5, and $p_{mut} = 0.1$ in the runs with mutation.

3.3 Spatial heterogeneity and the evolution of exoenzyme production

We now address the evolution of exoenzyme production using the spatially explicit, hybrid stochastic-deterministic model. We consider a resident, monomorphic population in which one variant cell arises by mutation. In the case where different cell genotypes can occur in the same microsite, all simulations show evolutionary suicide, as in the non-spatial model. This is expected because there is no advantage from producing exocellular enzymes – producers have to share products with cheaters in their microsite. If the original mutant successfully disperses, the spatial dynamics will keep the resident and mutant types segregated among microsites — whereas products generated by their enzymes diffuse across space. If the mutant is a stronger producer than the resident, it may invade and displace the resident genotype. Figure 3 shows an example.

Figure 4 reports variation in the long-term population growth rate of the mutant population introduced in the stationary resident population (see Appendix G for detail about simulation design). The outcome is strongly influenced by the diffusion rate. For diffusion above a critical threshold (all else being equal), there is strong selection against exoenzyme production (Fig. 4a). For diffusion below the critical threshold (Fig. 4b–4f) there is evolutionary convergence towards intermediate values of φ. At low investment in exoenzyme production, mutant with trait larger than the resident's can invade, hence directional selection for higher enzyme production. At high investment in exoenzyme production, mutant with trait smaller than the resident's can invade, hence directional selection for lower enzyme production.

Typically, there is a range of φ values for which the mutant population growth rate is close to zero, indicating a rather flat fitness landscape in this range (Table 3). Because of this flat fitness region and the system stochasticity (phenotypic variation generated by random mutations, growth rate affected by demographic stochasticity), we expect evolutionary convergence toward that range followed by sustained phenotypic fluctuations within the range, as opposed to evolutionary convergence to a single evolutionarily stable φ^* value.

Diffusion has a strong influence on selection (Fig. 4, Table 3). The range of evolutionarily attractive φ^* values decreases when σ_{diff} increases from 10^{-7} to 10^{-5}. The effect is negligible below 10^{-7}. For diffusion rates greater than 10^{-5}, evolution is always directional toward the smallest minimum viable value of φ^*, at which evolutionary suicide occurs.

Table 3. Effect of diffusion rate σ_{diff} on the evolutionary convergence of the enzyme production trait, φ. The selection gradient is close to zero across the reported ranges of φ values, which were obtained from the results displayed in Fig. 4.

Diffusion rate, σ_{diff}	Estimated range for evolutionarily convergent φ^*
10^{-4}	0
10^{-5}	0.05
10^{-6}	0.15
10^{-7}	0.15-0.2
10^{-8}	0.2-0.3
10^{-9}	0.2-0.35
10^{-10}	0.2-0.35
10^{-11}	0.2-0.3

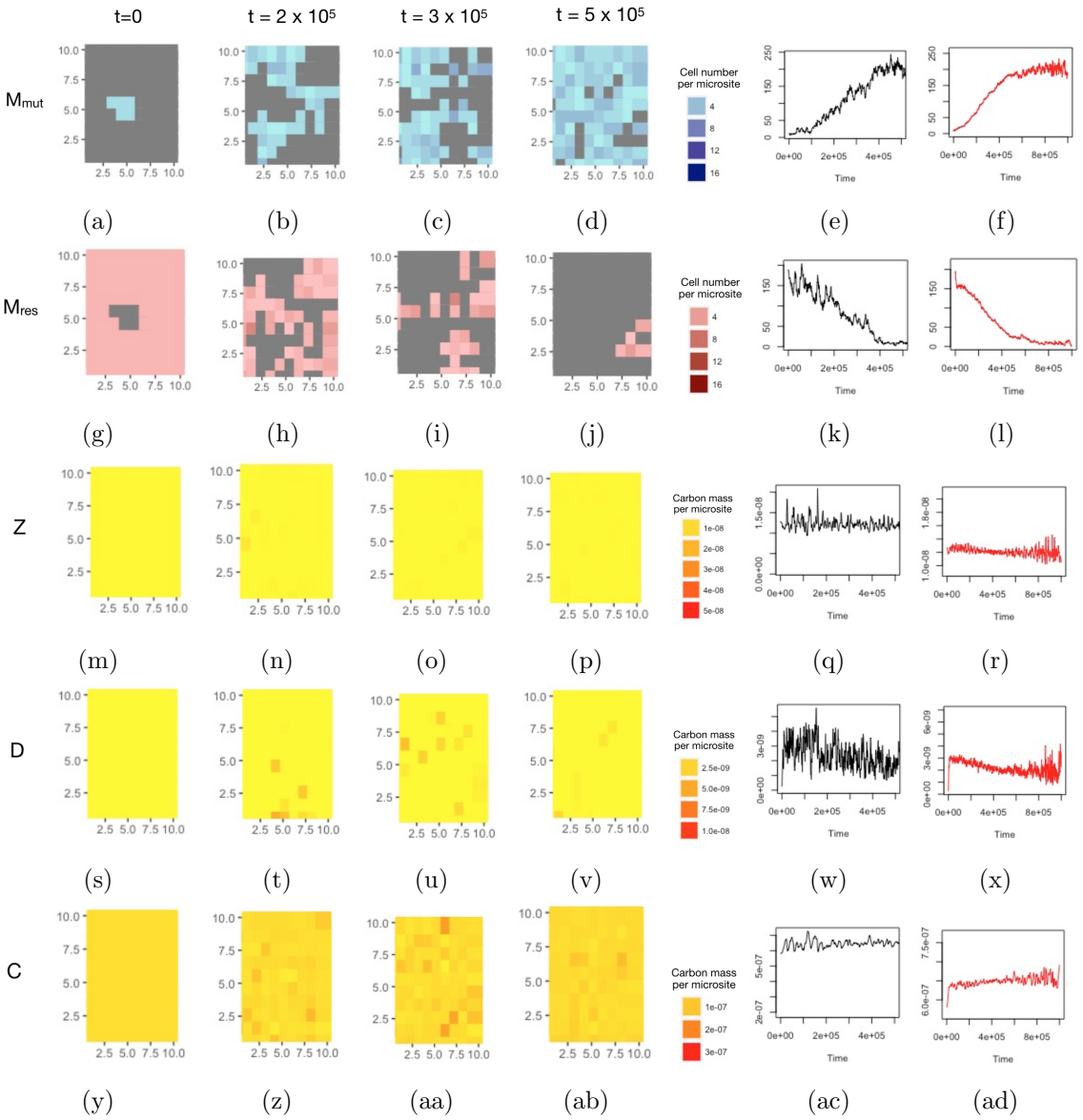

Figure 3. Spatio-temporal dynamics of invasion of a mutant cell ($\varphi_{mut} = 0.8$) into the ecosystem established by a resident cell phenotype ($\varphi_{res} = 0.75$). From top to bottom: temporal dynamics of the mutant cell population (M_{mut}), resident cell population (M_{res}), enzyme (Z), DOC (D), SOC (C). Columns 1-4: example simulation run of the spatial hybrid stochastic-deterministic model over a 10 x 10 grid of microsites, snapshots from time $t = 0$ to $t = 5 \times 10^5$. Column 5: Cross-grid aggregated dynamics of the simulation run. Column 6: Mean trajectories, averaged over 20 replicated simulation runs. All constant parameters are set to the default values (Table D.1 in Appendix D). See Appendix G for further simulation detail.

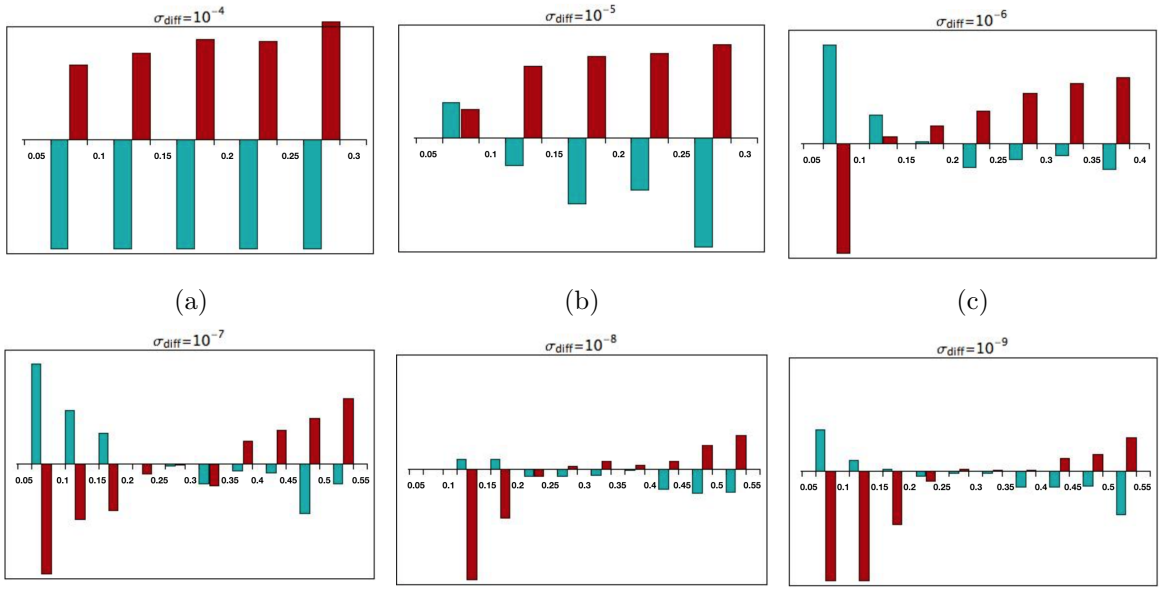

Figure 4. Selection on exoenzyme production φ, with diffusion rate σ_{diff} varying from 10^{-4} to 10^{-9}. The mutant population exponential growth rate from initial rarity (introduction in the central microsite at 5% of the abundance of the resident phenotype) is measured on the vertical axis. Red bars, Mutant φ = Resident φ - 0.05. Blue bars, Mutant φ = Resident φ + 0.05. Thin bars indicate standard deviation. All constant parameters are set to the default values (Table D.1 in Appendix D). See Appendix G for further simulation detail.

3.4 Eco-evolutionary response of decomposition to environmental change

In nature, parameters such as litter input, leaching rates, and the diffusion rate vary strongly with location, in correlation with variation in e.g. vegetation or soil type. As expected from the general theory of diffusive public goods, we find that diffusion has a major influence of the evolution of exoenzyme production. Figure 5a shows the effect of a gradient of diffusion rates that could represent spatial variation, or a temporal sequence driven by climate change. At very low diffusion rates, the range of attractive φ values remains roughly unchanged. There is a range of diffusion rates (here from 10^{-7} to 10^{-5}) over which increasing diffusion causes a significant decline in exoenzyme production (from ca. 0.25 to 0.05).

Variation in evolutionarily stable φ feeds back on the rate of decomposition (Fig. 5b, red) and soil C stock (Fig. 5c, red). Decreasing soil diffusion selects for higher exoenzyme allocation fraction (Fig. 5a) which in turn causes a strong increase in the decomposition rate (Fig. 5b, red) and a concurrently strong decrease in soil C stock (Fig. 5c, red). In comparison, predictions of decomposition rate and soil C stock are almost insensitive to the soil diffusion rate in absence of evolution (Fig. 5b, 5c, blue).

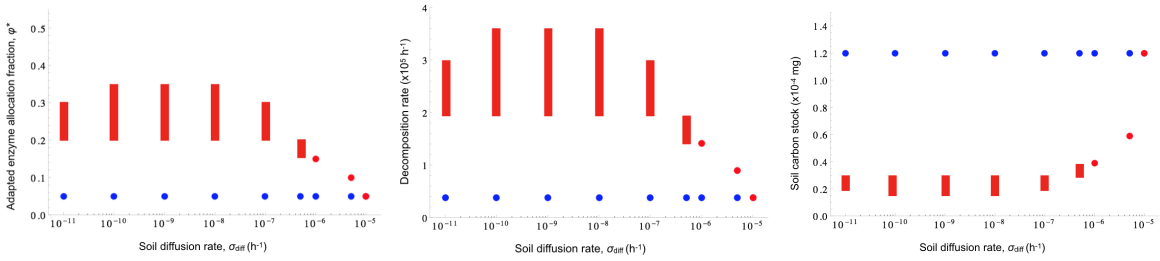

(a) (b) (c)

Figure 5. Effect of diffusion on the evolution of exoenzyme production φ, and feedback on the decomposition rate (b), and the stock of soil carbon C (c), predicted by the spatial hybrid stochastic-deterministic model. Blue, outcomes of purely ecological dynamics, in which φ is fixed to the adapted value for $\sigma_{\text{diff}} = 10^{-5}$. Red, outcomes of eco-evolutionary dynamics, in which φ evolves and adapts to the diffusion rate. In (a), a range of φ indicates evolutionarily attractive values for which the selection gradient is close to zero (Fig. 4, Table 3). Decomposition rate (b) and soil C stock (c) are then evaluated across that range. All constant parameters are set to the default values (Table D.1 in Appendix D). See Appendix G for further simulation detail.

4 Discussion

Soil microbial decomposition involves the production of exoenzymes and uptake of the products of enzyme-driven depolymerization of dead organic matter. These products form a diffusive public good, which is vulnerable to exploitation by cheaters. To elucidate conditions under which decomposition, as an outcome of microbial cooperation, is evolutionarily stable, we constructed a spatial model of soil microbe-enzyme decomposition which accounts for the finite size of microbial populations at the microscopic scale of microbial interactions.

Deterministic models of microbe-enzime driven decomposition were first introduced by Schimel and Weintraub [2003] for 'well-mixed' systems. Our work shows that Schimel and Weintraub [2003]'s model and subsequent variants (reviewed in Abs and Ferriere [2018]) are consistent with microscopic processes acting at the level of individual entities (cells, molecules). Starting from a five-compartment model including SOC and DOC molecules, microbial cells, enzyme molecules, and enzyme-SOC molecular complexes, we found that the population size of cells and molecules and some of the stochastic process rates could be rescaled to yield Schimel and Weintraub [2003] four-compartment deterministic 'CDMZ model'. As a side note, we could not find further or alternate rescaling to reduce the dimension of the system to three compartments (CDM or CMZ or DMZ). One can also prove that in all two-compartment models the equilibrium with positive cell population size is always unstable, which means that the cell population either goes extinct or grows unboundedly. Thus, the four-compartment CDMZ structure seems to be the simplest that is consistent with the individual-level processes under consideration.

The deterministic CDMZ model, however, cannot be used to capture the dynamics of a spatially explicit system in which cells and molecules interact within their local neighborhood. From the stochastic CDMZ model we obtained a hybrid stochastic-deterministic model for local populations and interactions by assuming that the size of the molecular populations (C, D, Z) is typically much larger than the size of the cellular population (M). A spatially explicit model can then be assembled by coupling hybrid models to form a grid of microsites. Microsite and grid parameters can be specified to capture the millimeter and centimeter scale, respectively. Compared to previous individual-based simulation models of decomposition [Allison, 2005, Folse and Allison, 2012, Kaiser et al., 2014, 2015], our derivation (i) recasts these model in a unified, rigorous mathematical framework, (ii) extends them by relaxing the assumption that each microsite may only be occupied by one cell. The latter is critical to address the interaction between microbial strains (genotypes) that differ in their investment in exoenzyme production. Thus, by modeling the dynamics of cell populations and decomposition within and between microsites, we can address the effect of spatially heterogeneous colony growth and colony size on the dynamics of invasion of a mutant genotype into the established population of the wild-type (resident) strain.

It has long been known that the habitat spatial structure can promote cooperation by facilitating benefit-sharing among cooperators. This was shown originally for pairwise interactions and later in the case of diffusive public goods. However, early models of diffusive public goods [Driscoll and Pepper, 2010, Ross-Gillespie et al., 2007, West and Buckling, 2003] represented space only implicitly and were therefore limited in their ability to identify conditions for the evolutionary stability of cooperation. Allison [2005] spatially explicit, individual-based simulation model of enzymatic litter decomposition backed up the expectation that the rate of products diffusion was key to the stability of cooperation. This and subsequent related models [Allison, 2012, Dobay et al., 2014, Folse and Allison, 2012, Kaiser et al., 2014, 2015], however, focused on competition among two or a small set of exoenzyme production genotypes, e.g. a producing strain and a non-producing ('pure cheater') strain. Our analysis goes a step further by predicting the evolutionary dynamics of exoenzyme production as a quantitative trait, varying continuously by random mutation of small effect.

Just like soil diffusion was identified as a critical factor for the stability of a producing strain against invasion by pure cheaters [Allison, 2005, Dobay et al., 2014], our model shows that the diffusion rate chiefly controls the evolutionarily stable investment in exoenzyme production. More precisely, all else being equal, there are lower and upper thresholds on the soil diffusion rate such that above the upper threshold, exoenzyme production is counterselected and decreases to the point where the whole system collapses; below the lower threshold, the diffusion rate has no significant influence on the evolutionarily stable level of exoenzyme production; between the thresholds, there can be a rather wide range of exoenzyme production values for which the selection gradient is very shallow; the system is thus expected to evolve stochastically within that range. Such evolutionary stochasticity might translate in strong persistent differences in decomposition rates at the centimeter scale in spite of identical ecological and biochemical conditions. It also remains to be seen whether selection could turn disruptive in these intervals of near-zero selection; disruptive selection would result in evolutionary branching, i.e. coexistence and divergence of two phenotypes, a more and a less productive strains. We did not observe evolutionary branching and coexistence in our simulations, but they could occur in regions of the parameter space that we have not yet explored. Otherwise, instances of coexistence reported by Allison [2005] and Kaiser et al. [2014, 2015] would possibly be evolutionary unstable and/or inaccessible to evolution by mutation of small effects.

Finally, our model shows how variation in evolutionarily stable exoenzyme production feeds back on ecosystem macroscopic properties such as the overall decomposition rate and soil C stock. The model predicts that if environmental change, such as variation in soil water content driven by climate change, drives changes in soil diffusion, then the microbial community may respond evolutionarily, and in return, the microorganisms' evolutionary, adaptive response may substantially impact ecosystem function. Previous models investigated how soil functional properties such as decomposition, heterotrophic respiration, and carbon stock, respond to variation in soil moisture due to variable precipitation [Homyak et al., 2018, Zhang et al., 2014]. Focusing on experimental data from semi-arid

savannah-type ecosystem subject to contrasted precipitation regimes, Zhang et al. [2014] used model-data assimilation to demonstrate the importance of water saturation as a control of enzyme activity and DOC uptake, and of the accumulation and storage of enzymes and DOC (that is temporarily inaccessible to microbes) in the dry soil pores during dry periods. Our results show that microbial evolution of exoenzyme production, in and of itself, can drive strong ecosystem responses to the effect of soil moisture variation on soil diffusion. Future work should further explore the relative effect on decomposition and heterotrophic respiration, of microbial physiological and evolutionary responses to the spatial heterogeneity of soil water distribution.

As strong ecosystem effects may result from the evolutionary adaptive response of microbial communities to changes in soil abiotic properties like diffusion, this calls for a more general investigation of the large-scale ecosystem consequences of soil microbial evolution in response to global environmental change, such as climate warming. The thermal dependence of microbe-enzyme biochemical processes involved in decomposition can radically change the global projections of soil C in response to climate change [Wieder et al., 2013]. How microbial evolutionary adaptation to warming might further change the picture warrants future research.

Data accessibility. Code and data available at the Dryad Digital Repository (http://dx.doi.org/xxx).

Authors' contributions. All authors conceived the research and developed the model. H.L. conducted mathematical analysis. E.A. and H.L. wrote code and performed simulations. All authors contributed to writing the manuscript.

Competing interests. We declare we have no competing interests.

Funding. E.A. was supported by fellowships from Ecole Doctorale Frontières du Vivant and MemoLife Laboratory of Excellence (PIA-10-LBX-54). R.F. acknowledges support from FACE Partner University Fund, CNRS Mission pour l'Interdisciplinarité, and PSL University (IRIS OCAV and PSL-University of Arizona Mobility Program). H.L. acknowledges support from CONACyT-MEXICO, CONACYT grant CB2015-01/250590, the foundation Sofía Kovalevskaia of SMM and the Chair "Modélisation Mathématique et Biodiversité" of VEOLIA-Ecole Polytechnique-MNHN-F.X.

Acknowledgements. We thank Rachel Gallery, Pierre-Henri Gouyon, Moira Hough, Laura Meredith, and Mitch Pavao-Zuckerman for discussion.

Appendix A. Reduction of the stochastic CDMZX model

Here we take $N = 1$, but the proof could be generalized $N > 1$ by introducing multiple cell stages describing the state of cell resource reserve. To reduce the CDMZX model, the main difficulty arises because we can not have classical Skorohod convergence in distribution of the process $(M^\varepsilon, Z^\varepsilon, C^\varepsilon, X^\varepsilon, D^\varepsilon, t \in [0,T])_{\varepsilon>0}$. Indeed, when ε is small, there will be some really close jumps of X^ε when a complex is formed and almost immediately dissociated or decomposed. Thus we are interested in the process

$$\mathbb{Y}^\varepsilon := (M^\varepsilon, Z^\varepsilon + X^\varepsilon, C^\varepsilon + X^\varepsilon, D^\varepsilon),$$

and we prove the following result.

Theorem 1. *Assume that (2.3) holds and that $(M^\varepsilon, Z^\varepsilon, C^\varepsilon, X^\varepsilon, D^\varepsilon)(0)$ converges in L^2 to the deterministic vector $(M_0, Z_0, C_0, 0, D_0)$, when ε goes to 0, then for any $T \geq 0$, the sequence of processes $(\mathbb{Y}^\varepsilon(t), t \in [0,T])_{\varepsilon>0}$ converges in law, in $\mathbb{D}([0,T], \mathbb{N}^4)$ endowed with the Skorohod topology, to $(M, Z, C, D)_{t\in[0,T]}$ defined by the 4-boxes model of Section 2.1 with*

$$\bar{V}_{mD} = \bar{\lambda}\frac{\bar{\mu}}{\bar{\mu} + \bar{\lambda}_{-1}},$$

and initial condition (M_0, Z_0, C_0, D_0).

Proof. **Step 1**: The first step is to prove the tightness of sequence $(\mathbb{Y}^\varepsilon)_{\varepsilon>0}$ in $\mathbb{D}([0,T], \mathbb{N}^4)$. To this aim, we denote the jumps set of process $(\mathbb{Y}^\varepsilon(t), t \in [0,T])$ by

$$\{J_j^\varepsilon\}_{j\geq 1} = \{t \in [0,T], \mathbb{Y}^\varepsilon(t-) \neq \mathbb{Y}^\varepsilon(t)\}. \tag{4.1}$$

Note that $\mathbb{Y}^\varepsilon$ is càdlàg, hence the definition (4.1). As any jump of $\mathbb{Y}^\varepsilon$ is of size 1, the tightness of $\mathbb{Y}^\varepsilon$ follows from the two conditions:

i) $\lim_{a\to+\infty} \limsup_{\varepsilon\to 0} \mathbb{P}(\|\mathbb{Y}^\varepsilon\|_\infty \geq a) = 0$,

ii) $\lim_{\delta\to 0} \limsup_{\varepsilon\to 0} \mathbb{P}(\exists j \geq 0, J_{j+1}^\varepsilon - J_j^\varepsilon \leq \delta) = 0$.

Indeed, these two conditions directly imply the two conditions of Theorem 13.2 in the book of Billingsley [2013], which ensures tightness.

To prove i), we introduce $N_{Tot}^\varepsilon = \alpha M^\varepsilon + \gamma Z^\varepsilon + \beta C^\varepsilon + (\gamma+\beta)X^\varepsilon + D^\varepsilon$ the total equivalent number of DOC molecules in the system at any time. Since the only external sources of carbon are inputs of C and D, N_{Tot}^ε is stochastically bounded from above by

$$\sup_{s\leq T} N_{Tot}^\varepsilon(s) \preceq N_{Tot}^\varepsilon(0) + \mathcal{P}((\bar{I}_D + \beta\bar{I}_C)T) =: N_{\max}^\varepsilon, \tag{4.2}$$

where $\mathcal{P}((\bar{I}_D + \beta\bar{I}_C)T)$ is a Poisson random variable with parameter $(\bar{I}_D + \beta\bar{I}_C)T$. From the assumption on the initial conditions, we deduce immediately that the random variable $N_{\max}^\varepsilon$ is L^2-integrable and that for ε sufficiently small, there exists $C_0 > 0$ such that

$$\mathbb{E}\left[N_{\max}^\varepsilon\right] + \mathbb{E}\left[(N_{\max}^\varepsilon)^2\right] \leq C_0. \tag{4.3}$$

Moreover, since α, β and γ are greater than 1, we obtain from Markov inequality,

$$\mathbb{P}(\|\mathbb{Y}^\varepsilon\|_\infty \geq a) \leq \mathbb{P}(N^\varepsilon_{\max} \geq a) \leq \frac{1}{a} C_0,$$

for any ε sufficiently small. This ends the proof of i).

We now deal with ii). Let us set $\eta > 0$. First of all, note that we can focus the study on the set $\{X^\varepsilon(0) = 0\}$. Indeed, from the assumption on the initial condition, for any ε small enough, $\mathbb{P}(X^\varepsilon(0) \geq 1) \leq \eta$. Hence

$$\mathbb{P}(\exists j \geq 0, J^\varepsilon_{j+1} - J^\varepsilon_j \leq \delta) \ \leq \ \eta + \mathbb{P}_0(\exists j \geq 0, J^\varepsilon_{j+1} - J^\varepsilon_j \leq \delta), \tag{4.4}$$

where for any set $\mathcal{A}$, $\mathbb{P}_0(\mathcal{A}) = \mathbb{P}(\mathcal{A}|X^\varepsilon(0) = 0)$. In what follows, we restrict our focus on $\{X^\varepsilon(0) = 0\}$.

Then, we count the number of jumps of $\mathbb{Y}^\varepsilon$. Note that any jump of $\mathbb{Y}^\varepsilon$ is also a jump of $(M^\varepsilon, Z^\varepsilon, C^\varepsilon, X^\varepsilon, D^\varepsilon)$. Thus, we count the jumps number of the latter. As originally done by Fournier and Méléard [2004], it is convenient to represent a trajectory of individual-based processes as the unique solution of a system of stochastic differential equations driven by Poisson point measures. To this aim, we introduce a collection of 11 independent Poisson Point Processes $(N^i(\mathrm{d}s, \mathrm{d}\theta))_{i=1,..,11}$ on $[0,\infty)^2$ with intensity $\mathrm{d}s\mathrm{d}\theta$ and independent of ε, which will be used to encode the 11 different types of events of the process $(M^\varepsilon, Z^\varepsilon, C^\varepsilon, X^\varepsilon, D^\varepsilon)$. We also denote all rates of this process by $(r^\varepsilon_i(t), t \in [0,T])_{i=1,..,11}$, i.e. these rates are respectively $(1-\varphi)\bar{\gamma}_M \bar{V}_{mU} \frac{D^\varepsilon}{K_{mU}+D^\varepsilon} M^\varepsilon \mathbf{1}_{\{D^\varepsilon \geq \alpha+\alpha'\}}$ (birth of a M), $\bar{d}_M M^\varepsilon$ (death of a M), $\varphi\bar{\gamma}_Z \bar{V}_{mU} \frac{D^\varepsilon}{K_{mU}+D^\varepsilon} M^\varepsilon \mathbf{1}_{\{D^\varepsilon \geq \gamma+\gamma'\}}$ (production of a Z), $\bar{d}_Z Z^\varepsilon$ (deactivation of a Z), $\bar{I}_C$ (appearance of a C), $\bar{e}_C C^\varepsilon$ (disappearance of a C), $\bar{I}_D$ (appearance of a D), $\bar{e}_D D^\varepsilon$ (disappearance of a D), $\bar{\lambda} Z^\varepsilon C^\varepsilon$ (formation of a X), $\bar{\lambda}^\varepsilon_{-1} X^\varepsilon$ (dissociation of a X), and $\bar{\mu}^\varepsilon X^\varepsilon$ (decomposition of a X). Note that only the events of type 1 to 8 and 11 correspond to jumps of $\mathbb{Y}^\varepsilon$. Hence, the jumps number of $\mathbb{Y}^\varepsilon$ can be bounded stochastically by

$$\sharp\{J^\varepsilon_j\} \ \preceq \sum_{i\in\{1,..,8,11\}} \int_0^T \int_{\mathbb{R}^+} \mathbf{1}_{\{\theta \leq r^\varepsilon_i(s-)\}} N^i(\mathrm{d}s, \mathrm{d}\theta). \tag{4.5}$$

The only problem comes from the last rate $\bar{\mu}^\varepsilon X^\varepsilon$, which is unbounded when ε goes to 0. However $\bar{\mu}^\varepsilon X^\varepsilon = 0$ as soon as there is no complex X in the system, and complexes are created with the encounter of a Z and a C (9-th rate). Thus, we immediately conclude that

$$\int_0^T \int_{\mathbb{R}^+} \mathbf{1}_{\{\theta \leq \bar{\mu}^\varepsilon X^\varepsilon(s-)\}} N^{11}(\mathrm{d}s, \mathrm{d}\theta) \leq \int_0^T \int_{\mathbb{R}^+} \mathbf{1}_{\{\theta \leq \bar{\lambda} Z^\varepsilon(s-) C^\varepsilon(s-)\}} N^9(\mathrm{d}s, \mathrm{d}\theta).$$

In addition with (4.5), (4.2) and (4.3), we deduce, if ε is small enough that

$$\begin{aligned}
\mathbb{P}_0(\sharp\{J^\varepsilon_j\} > n) &\leq \sum_{i=1}^9 \mathbb{P}_0\left(\int_0^T \int_{\mathbb{R}^+} \mathbf{1}_{\{\theta \leq r^\varepsilon_i(s-)\}} N^i(\mathrm{d}s, \mathrm{d}\theta) \geq \frac{n}{9}\right) \\
&\leq \frac{9}{n} T \sum_{i=1}^9 \mathbb{E}_0\left[\sup_{s\in[0,T]} r^\varepsilon_i(s)\right] \\
&\leq \frac{9T}{n}\left(\bar{I}_C + \bar{I}_D + C_1 \mathbb{E}_0\left[N^\varepsilon_{\max}\right] + \bar{\lambda}\mathbb{E}_0\left[(N^\varepsilon_{\max})^2\right]\right) \\
&\leq \frac{9T}{n} C_2 \underset{n\to+\infty}{\longrightarrow} 0,
\end{aligned} \tag{4.6}$$

with $C_1 := \bar{\gamma}_M \bar{V}_{mU} + \bar{d}_M + \bar{\gamma}_Z \bar{V}_{mU} + \bar{d}_Z + \bar{e}_C + \bar{e}_D$ and $C_2 := \bar{I}_C + \bar{I}_D + C_1 C_0 + \bar{\lambda} C_0$. We fix $n := \lfloor 9TC_2/\eta \rfloor + 1$ such that the last r.h.s. is smaller than η. Thus,

$$\begin{aligned}\mathbb{P}_0(\exists j \geq 0, J^\varepsilon_{j+1} - J^\varepsilon_j \leq \delta) \;&\leq\; \mathbb{P}_0(\sharp\{J^\varepsilon_j\} > n) + \mathbb{P}_0\left(\exists j \in \{1,..,n-1\}\; J^\varepsilon_{j+1} - J^\varepsilon_j \leq \delta,\;\; \sharp\{J^\varepsilon_j\} \leq n\right) \\ &\leq\; \eta + \sum_{j=1}^{n-1} \mathbb{P}_0(J^\varepsilon_{j+1} - J^\varepsilon_j \leq \delta)\end{aligned} \tag{4.7}$$

Moreover, for any $j \in \{1,..,n-1\}$,

$$\mathbb{P}_0(J^\varepsilon_{j+1} - J^\varepsilon_j \leq \delta) \;\leq\; \mathbb{P}_0(J^\varepsilon_{j+1} - J^\varepsilon_j \leq \delta | X^\varepsilon(J^\varepsilon_j) = 0) + \mathbb{P}_0(X^\varepsilon(J^\varepsilon_j) \geq 1) \tag{4.8}$$

The first term of the r.h.s of (4.8) can be bounding using the Markov property of $(M^\varepsilon, Z^\varepsilon, C^\varepsilon, X^\varepsilon, D^\varepsilon)$. Indeed, the two last types of events (10 and 11) can not occur after time J^ε_j and before any other jumps, since $X^\varepsilon(J^\varepsilon_j) = 0$. Hence

$$\begin{aligned}\mathbb{P}_0(J^\varepsilon_{j+1} - J^\varepsilon_j \leq \delta | X^\varepsilon(J^\varepsilon_j) = 0) &\leq \mathbb{P}_0\left(\exists i \in \{1,..,9\}, \int_0^\delta \int_{\mathbb{R}^+} \mathbf{1}_{\{\theta \leq r^\varepsilon_i(s-)\}} N^i(\mathrm{d}s, \mathrm{d}\theta) \geq 1\right) \\ &\leq \delta \sum_{i=1}^{9} \mathbb{E}_0\left[\sup_{s\in[0,T]} r^\varepsilon_i(s)\right] \leq \delta C_2 \leq \frac{\eta}{n},\end{aligned}$$

as soon as $\delta \leq \eta/(nC_2)$. Hence, with (4.7) and (4.8),

$$\mathbb{P}_0(\exists j \geq 0, J^\varepsilon_{j+1} - J^\varepsilon_j \leq \delta) \;\leq\; 2\eta + \sum_{j=1}^{n-1} \mathbb{P}_0(X^\varepsilon(J^\varepsilon_j) \geq 1). \tag{4.9}$$

To bound the second term of the r.h.s of (4.9), recall that the positive jumps of X^ε are not jumps of $\mathbb{Y}^\varepsilon$ and note that $X^\varepsilon(J^\varepsilon_j)$ may be greater than 1 only if there exists a positive jump of X^ε whose next event is of type 1 to 9 (and not of type 10 or 11). We denote the set of positive jumps of X^ε by

$$\{S^\varepsilon_\ell\}_{\ell \geq 1} = \{t \in [0,T], X^\varepsilon(t) - X^\varepsilon(t-) = 1\}.$$

The second term of the r.h.s of (4.9) can thus be bounded by

$$\sum_{j=1}^{n-1} \mathbb{P}_0(X^\varepsilon(J^\varepsilon_j) \geq 1) \leq \mathbb{P}_0\left(\exists \ell \geq 1, \min_{1\leq i\leq 9} \tau^\varepsilon_i(S^\varepsilon_\ell) \leq \min\{\tau^\varepsilon_{10}(S^\varepsilon_\ell), \tau^\varepsilon_{11}(S^\varepsilon_\ell)\}\right), \tag{4.10}$$

where for any $i = 1,..,10$, $\tau^\varepsilon_i(S^\varepsilon_\ell)$ is the first time event of type i after S^ε_ℓ, that is

$$\tau^\varepsilon_i(S^\varepsilon_\ell) := \inf\left\{t \geq S^\varepsilon_\ell, \int_{S^\varepsilon_\ell}^t \int_{\mathbb{R}^+} \mathbf{1}_{\{\theta \leq r^\varepsilon_i(s-)\}} N^i(\mathrm{d}s, \mathrm{d}\theta) \geq 1\right\}.$$

After time S^ε_ℓ and before any other event, X^ε is obviously greater than 1. The rates r^ε_{10} and r^ε_{11} can thus be bounded from below by $\bar{\lambda}^\varepsilon_{-1}$ and $\bar{\mu}^\varepsilon$ respectively, other rates can be bounded from above

using the r.v. $N^\varepsilon_{\max}$. Thus, using again (4.6), together with (4.10) and the Markov property satisfied by $(M^\varepsilon, Z^\varepsilon, C^\varepsilon, X^\varepsilon, D^\varepsilon)$, we obtain

$$\begin{aligned}\sum_{j=1}^{n-1}\mathbb{P}_0(X^\varepsilon(J_j^\varepsilon)\geq 1) &\leq \sum_{\ell=1}^{n}\mathbb{P}_0\left(\min_{1\leq i\leq 9}\tau_i^\varepsilon(S_\ell^\varepsilon)\leq \min\{\tau_{10}^\varepsilon(S_\ell^\varepsilon),\tau_{11}^\varepsilon(S_\ell^\varepsilon)\}\right)+\mathbb{P}_0(\sharp\{S_\ell^\varepsilon\}>n)\\ &\leq n\mathbb{P}_0\left(\tau\leq \mathcal{E}_{\bar\lambda_{-1}^\varepsilon+\bar\mu^\varepsilon}\right)+\eta,\end{aligned}$$

where $\mathcal{E}_{\bar\lambda_{-1}^\varepsilon+\bar\mu^\varepsilon}$ is an exponential r.v. with parameter $\bar\lambda_{-1}^\varepsilon+\bar\mu^\varepsilon$, and,

$$\tau=\inf\left\{t\geq 0,\int_0^t\int_{\mathbb{R}^+}\mathbf{1}_{\{\theta\leq \bar I_C+\bar I_D+C_1N^\varepsilon_{\max}+\bar\lambda(N^\varepsilon_{\max})^2\}}N^1(\mathrm{d}s,\mathrm{d}\theta)\geq 1\right\}.$$

Hence

$$\begin{aligned}\sum_{j=1}^{n-1}\mathbb{P}_0(X^\varepsilon(J_j^\varepsilon)\geq 1) &\leq n\int_0^\infty \mathbb{P}_0\left(\tau\leq s\right)(\bar\lambda_{-1}^\varepsilon+\bar\mu^\varepsilon)e^{-(\bar\lambda_{-1}^\varepsilon+\bar\mu^\varepsilon)s}\mathrm{d}s+\eta\\ &\leq n\varepsilon\frac{C_2}{\bar\lambda_{-1}+\bar\mu}+\eta.\end{aligned}\tag{4.11}$$

Finally, with (4.4), (4.9) and (4.11), we obtain

$$\limsup_{\varepsilon\to 0}\mathbb{P}(\exists j\geq 0, J_{j+1}^\varepsilon-J_j^\varepsilon\leq\delta)\ \leq\ 4\eta,$$

as soon as $\delta\leq\eta^2/(18TC_2^2)$ (as this implies that $\delta\leq\eta/(nC_2)$). This ends the proof of ii), and the one of the tightness of process $\mathbb{Y}^\varepsilon$.

Step 2: The second step is to identify the limit. As the sequence of processes $(\mathbb{Y}^\varepsilon)_{\varepsilon>0}$ is tight, it is sufficient to prove that any accumulation point has the same law. Let us take $(M,Z,C,D)\in\mathbb{D}([0,T],\mathbb{N}^4)$ the limit (in law) of a sub-sequence of $(\mathbb{Y}^\varepsilon)_{\varepsilon>0}$, that we denote also by $(\mathbb{Y}^\varepsilon)_{\varepsilon>0}$ for the sake of readability and we will denote (M,Z,C,D) by $\mathbb{Y}$. We first prove that $\mathbb{Y}$ is a Markov process and then characterize it by describing its jump rates. Note that $\{\mathbb{Y}^\varepsilon\}_{\varepsilon>0}$ are not Markov processes, however $\{(\mathbb{Y}^\varepsilon,X^\varepsilon)\}_{\varepsilon>0}$ are Markov processes.

To prove that $\mathbb{Y}$ is a Markov process, let us set $t>0$, a sequence of $m+m'$ times $0\leq t_1\leq ...\leq t_m\leq t\leq s_1\leq ..\leq s_{m'}$ and $m+m'+1$ vectors, $y_1,..,y_m,y_t,y_1',..,y_{m'}'\in\mathbb{N}^4$. From Dynkin's theorem, it is sufficient to prove that

$$\begin{aligned}&\mathbb{P}\Big(\mathbb{Y}(s_{m'})=y_{m'}',..,\mathbb{Y}(s_1)=y_1'|\mathbb{Y}(t)=y_t,\mathbb{Y}(t_m)=y_m,..,\mathbb{Y}(t_1)=y_1\Big)\\ &\qquad=\mathbb{P}\Big(\mathbb{Y}(s_{m'})=y_{m'}',..,\mathbb{Y}(s_1)=y_1'|\mathbb{Y}(t)=y_t\Big).\end{aligned}\tag{4.12}$$

From the convergence in law and assumptions on $X^\varepsilon(0)$, we have, for any $\varepsilon>0$,

$$\begin{aligned}&\mathbb{P}\Big(\mathbb{Y}(s_{m'})=y_{m'}',..,\mathbb{Y}(s_1)=y_1'|\mathbb{Y}(t)=y_t,..,\mathbb{Y}(t_1)=y_1\Big)\\ &\quad=\lim_{\varepsilon\to 0}\mathbb{P}_0\Big(\mathbb{Y}^\varepsilon(s_{m'})=y_{m'}',..,\mathbb{Y}^\varepsilon(s_1)=y_1'|\mathbb{Y}^\varepsilon(t)=y_t,..,\mathbb{Y}^\varepsilon(t_1)=y_1\Big)\\ &\quad=\lim_{\varepsilon\to 0}\frac{\sum_{k\geq 0}\mathbb{P}_0\Big(\mathbb{Y}^\varepsilon(s_{m'})=y_{m'}',..,(\mathbb{Y}^\varepsilon,X^\varepsilon)(t)=(y_t,k),..,\mathbb{Y}^\varepsilon(t_1)=y_1\Big)}{\sum_{k\geq 0}\mathbb{P}_0\Big((\mathbb{Y}^\varepsilon,X^\varepsilon)(t)=(y_t,k),..,\mathbb{Y}^\varepsilon(t_1)=y_1\Big)}.\end{aligned}\tag{4.13}$$

Then we prove that, for ε small enough, $X^\varepsilon(t)$ is equal to 0 with a large probability. Indeed, $(X^\varepsilon(u))_{u\le t}$ has little chance to reach 2:

$$\mathbb{P}_0(\sup_{u\le t} X^\varepsilon(u)\ge 2)\le \mathbb{P}_0\left(\exists \ell\ge 1,\ \min_{1\le i\le 9}\tau_i^\varepsilon(S_\ell^\varepsilon)\le \min\{\tau_{10}^\varepsilon(S_\ell^\varepsilon),\tau_{11}^\varepsilon(S_\ell^\varepsilon)\}\right),$$

where all terms have been defined in (4.10), and the r.h.s term has been proved to converge to 0 when ε goes to 0. It remains to prove that $X^\varepsilon(t)$ has little chance to be equal to 1 on $\{\sup_{u\le t} X^\varepsilon(u)\le 1\}$

$$\mathbb{P}_0\Big(X^\varepsilon(t)=1,\ \sup_{u\le t}X^\varepsilon(u)\le 1\Big)\le \mathbb{P}_0\Big(\exists \ell\ge 1,\ S_\ell^\varepsilon\le t<S_\ell^\varepsilon+\min\{\tau_{10}^\varepsilon(S_\ell^\varepsilon),\tau_{11}^\varepsilon(S_\ell^\varepsilon)\},\ \sup_{u\le t}X^\varepsilon(u)\le 1\Big).$$

As previously, note that there is not an infinite number of events S_ℓ^ε in $[0,T]$ and that $\{S_\ell^\varepsilon\}_{\ell>0}$ are directly correlated to the events of type 9. As $\min\{\tau_{10}^\varepsilon(S_\ell^\varepsilon),\tau_{11}^\varepsilon(S_\ell^\varepsilon)\}$ is an exponential random variable $\mathcal{E}_{\bar\lambda_{-1}^\varepsilon+\bar\mu^\varepsilon}$, we deduce,

$$\begin{aligned}
&\mathbb{P}_0(X^\varepsilon(t)=1,\{\sup_{u\le t}X^\varepsilon(u)\le 1\})\\
&\qquad\le \sum_{\ell\ge 1}\int_0^\infty \mathbb{P}_0\Big(S_\ell^\varepsilon\in]t-h,t]\Big)(\bar\lambda_{-1}^\varepsilon+\bar\mu^\varepsilon)e^{-h(\bar\lambda_{-1}^\varepsilon+\bar\mu^\varepsilon)}dh+\mathbb{P}_0\left(\sharp\{S_j^\varepsilon\}>n\right)\\
&\qquad\le n\int_0^\infty \mathbb{P}_0\Big(\int_{t-h\vee 0}^t\int_{\mathbb{R}^+}\mathbf{1}_{\{\theta\le r_9^\varepsilon(s-)\}}N^9(ds,d\theta)\ge 1\Big)(\bar\lambda_{-1}^\varepsilon+\bar\mu^\varepsilon)e^{-h(\bar\lambda_{-1}^\varepsilon+\bar\mu^\varepsilon)}dh+\eta\\
&\qquad\le n\int_0^\infty h\bar\lambda C_0(\bar\lambda_{-1}^\varepsilon+\bar\mu^\varepsilon)e^{-h(\bar\lambda_{-1}^\varepsilon+\bar\mu^\varepsilon)}dh+\eta\\
&\qquad\le \frac{n\bar\lambda C_0}{\bar\lambda_{-1}^\varepsilon+\bar\mu^\varepsilon}+\eta\le 2\eta,
\end{aligned}$$

as soon as ε is sufficiently small. In other words, $\mathbb{P}_0(X^\varepsilon(t)\ge 1)$ converges to 0 with ε. (4.13) becomes

$$\begin{aligned}
&\mathbb{P}\Big(\mathbb{Y}(s_{m'})=y'_{m'},..,\mathbb{Y}(s_1)=y'_1|\mathbb{Y}(t)=y_t,..,\mathbb{Y}(t_1)=y_1\Big)\\
&\qquad=\lim_{\varepsilon\to 0}\frac{\mathbb{P}_0\Big(\mathbb{Y}^\varepsilon(s_{m'})=y'_{m'},..,(\mathbb{Y}^\varepsilon,X^\varepsilon)(t)=(y_t,0),..,\mathbb{Y}^\varepsilon(t_1)=y_1\Big)}{\mathbb{P}_0\Big((\mathbb{Y}^\varepsilon,X^\varepsilon)(t)=(y_t,0),..,\mathbb{Y}^\varepsilon(t_1)=y_1\Big)}\\
&\qquad=\lim_{\varepsilon\to 0}\mathbb{P}_0\Big(\mathbb{Y}^\varepsilon(s_{m'})=y'_{m'},..|(\mathbb{Y}^\varepsilon,X^\varepsilon)(t)=(y_t,0),..,\mathbb{Y}^\varepsilon(t_1)=y_1\Big)\\
&\qquad=\lim_{\varepsilon\to 0}\mathbb{P}_0\Big(\mathbb{Y}^\varepsilon(s_{m'})=y'_{m'},..|(\mathbb{Y}^\varepsilon,X^\varepsilon)(t)=(y_t,0)\Big),
\end{aligned}\tag{4.14}$$

where we used the Markov property of $(\mathbb{Y}^\varepsilon,X^\varepsilon)$. Using same ideas, it is straightforward to prove that $\mathbb{P}\Big(\mathbb{Y}(s_{m'})=y'_{m'},..|\mathbb{Y}(t)=y_t\Big)$ is also equal to the last term of (4.14), hence (4.12) and the Markov property of $\mathbb{Y}$.

It remains to describe the transition rate matrix of $\mathbb{Y}$. To this aim, for any $y,y'\in\mathbb{N}^4$, we study the limits

$$\lim_{t\to 0}\mathbb{P}\Big(\mathbb{Y}(t)=y'|\mathbb{Y}(0)=y\Big).$$

From what we have seen before (notably that the events of type 1 to 8 are not really affected by the presence of the fast species X^ε), it is straightforward that, in the limiting process $\mathbb{Y}$, there exist 8

types of events with rates $(1-\varphi)\bar{\gamma}_M \bar{V}_{mU} \frac{D^\varepsilon}{\bar{K}_{mU}+D} M \mathbf{1}_{\{D\geq\alpha+\alpha'\}}$ (birth of a M), $\bar{d}_M M$ (death of a M), $\varphi\bar{\gamma}_Z \bar{V}_{mU} \frac{D}{\bar{K}_{mU}+D} M \mathbf{1}_{\{D\geq\gamma+\gamma'\}}$ (production of a Z), $\bar{d}_Z Z$ (deactivation of a Z), $\bar{I}_C$ (appearance of a C), $\bar{e}_C C$ (disappearance of a C), $\bar{I}_D$ (appearance of a D), $\bar{e}_D D$ (disappearance of a D). It remains to deal with the three last types of events. However, we have seen that when a event of type 9 occurs, an event of type 10 or 11 occurs immediately after (such that the formed complex disappears or dissociates). In the limit, both events are simultaneous and

$$\begin{aligned}
&\mathbb{P}\Big(\mathbb{Y}(t) = (m_0, z_0, c_0 - 1, d_0 + \beta) | \mathbb{Y}(0) = (m_0, z_0, c_0, d_0)\Big) \\
&= \lim_{\varepsilon\to 0} \mathbb{P}\Big(\mathbb{Y}^\varepsilon(t) = (m_0, z_0, c_0 - 1, d_0 + \beta) | \mathbb{Y}^\varepsilon(0) = (m_0, z_0, c_0, d_0)\Big) \\
&= \lim_{\varepsilon\to 0} \mathbb{P}\Big(\mathbb{Y}^\varepsilon(t) = (m_0, z_0, c_0 - 1, d_0 + \beta) | \mathbb{Y}^\varepsilon(0) = (m_0, z_0, c_0, d_0)\Big)
\end{aligned}$$

It remains to characterize the jumps rate of $\mathbb{Y}$. Let us start with a birth of a M. As done previously (see (4.13)-(4.14)), we have

$$\begin{aligned}
&\mathbb{P}\Big(\mathbb{Y}(t+h) = (m+1, z, c, d - (\alpha+\alpha'))\Big|\mathbb{Y}(t) = (m, z, c, d)\Big) \\
&\qquad = \lim_{\varepsilon\to 0} \mathbb{P}_0\Big((\mathbb{Y}^\varepsilon, X^\varepsilon)(t+h) = (m+1, z, c, d, 0)\Big|(\mathbb{Y}^\varepsilon, X^\varepsilon)(t) = (m, z, c, d, 0)\Big).
\end{aligned}$$

Using the jumps rate of $(\mathbb{Y}^\varepsilon, X^\varepsilon)$, we deduce directly

$$\mathbb{P}\Big(\mathbb{Y}(t+h) = (m+1, z, c, d-(\alpha+\alpha'))\Big|\mathbb{Y}(t) = (m, z, c, d)\Big) = (1-\varphi)\bar{\gamma}_M \bar{V}_{mU} \frac{d}{\bar{K}_{mU}+d} m \mathbf{1}_{\{d\geq\alpha+\alpha'\}} h + o(h).$$

The same can be done with the death of a M, the production of a Z, the deactivation of a Z, the (dis)appearance of a C and the (dis)appearance of a D, where the actions of the complexes do not intervene. And we find the rate given by Theorem (1) The only problem may come from the decomposition of a C into β D:

$$\begin{aligned}
&\mathbb{P}\Big(\mathbb{Y}(t+h) = (m+1, z, c-1, d+\beta)\Big|\mathbb{Y}(t) = (m, z, c, d)\Big) \\
&\quad = \lim_{\varepsilon\to 0} \mathbb{P}_0\Big((\mathbb{Y}^\varepsilon, X^\varepsilon)(t+h) = (m, z, c-1, d+\beta, 0)\Big|(\mathbb{Y}^\varepsilon, X^\varepsilon)(t) = (m, z, c, d, 0)\Big) \\
&\quad = \lim_{\varepsilon\to 0} \mathbb{P}_0\Big((\mathbb{Y}^\varepsilon, X^\varepsilon)(h) = (m, z, c-1, d+\beta, 0)\Big|(\mathbb{Y}^\varepsilon, X^\varepsilon)(0) = (m, z, c, d, 0)\Big) \\
&\quad = \lim_{\varepsilon\to 0} \mathbb{P}_0\Big(S_1^\varepsilon \leq h, \tau_{11}^\varepsilon(S_1^\varepsilon) \leq \min_{1\leq i\leq 10} \tau_i^\varepsilon(S_1^\varepsilon))\Big).
\end{aligned}$$

As we proved before that $\mathbb{P}_0\left(\min_{1\leq i\leq 9} \tau_i^\varepsilon(S_1^\varepsilon) \leq \tau_{10}^\varepsilon(S_1^\varepsilon)\right)$ converges to 0 with ε (see (4.11)), we have

$$\begin{aligned}
&\mathbb{P}\Big(\mathbb{Y}(t+h) = (m+1, z, c-1, d+\beta)\Big|\mathbb{Y}(t) = (m, z, c, d)\Big) \\
&\quad = \lim_{\varepsilon\to 0} \mathbb{P}_0\Big(S_1^\varepsilon \leq h, \tau_{11}^\varepsilon(S_1^\varepsilon) \leq \tau_{10}^\varepsilon(S_1^\varepsilon))\Big) \\
&\quad = \lim_{\varepsilon\to 0} \left(\bar{\lambda} z c \times \frac{\bar{\mu}^\varepsilon}{\bar{\mu}^\varepsilon + \bar{\lambda}_{-1}^\varepsilon} h + o(h)\right) \\
&\quad = \bar{V}_{mD} z c h + o(h).
\end{aligned}$$

□

Appendix B. Stochastic CDMZ model: simulation algorithm

Here we describe the algorithm used to simulate the stochastic CDMZ model. The algorithm is based on the ones presented for example in Champagnat et al. [2006], Fournier and Méléard [2004]. It is also known as Gillepsie algorithm [Kierzek, 2002].

The simulation starts with a given amount of M, Z, C and D at time $t = 0$. Two events can never occur at the same time. Assume that the process has been computed until the i-th event at time t_i and we explain how to compute the $i+1$-th event. We compute the total event rate which is equal to

$$r(t_i) := r_M(t_i) + r_Z(t_i) + r_C(t_i) + r_D(t_i),$$

with

$$\begin{aligned}
r_M(t_i) &:= \left[N(1-\min_\varphi)\bar{\gamma}_M\bar{V}_{mU} + \bar{d}_M + \max_\varphi \bar{\gamma}_Z\bar{V}_{mU}\right] M(t_i),\\
r_Z(t_i) &:= \left[\bar{d}_Z + \bar{V}^K_{mU}C(t_i)\right] Z(t_i),\\
r_C(t_i) &:= I^K_C + \bar{e}_C C(t_i),\\
r_D(t_i) &:= \bar{I}^K_D + \bar{e}_D D(t_i).
\end{aligned}$$

where $\max_\varphi$ (resp. $\min_\varphi$) is the maximum (resp. minimum) trait value φ that can be found among M-population at time t_i. We then simulate Δ_t, an exponential random variable with parameter $r(t_i)$, to find the time $t_{i+1} := t_i + \Delta_t$, when the possible next event occurs.

The next step is to determine which event occurs. To this aim, we simulate θ, a uniform random variable on $[0, r(t_i)]$. If $\theta \in [0, r_M(t_i)]$, the event affects 1 M. That is to say, one of the three events covered by r_M (growth of 1 M, death of 1 M or production of 1 Z by a M) may occur. Similar conclusions are drawn if θ belongs to $[r_M(t_i), r_M(t_i) + r_Z(t_i)]$, $[r_M(t_i) + r_Z(t_i), r_M(t_i) + r_Z(t_i) + r_C(t_i)]$, or $[r_M(t_i) + r_Z(t_i) + r_C(t_i), r(t_i)]$: respectively, the event affects a Z, a C or a D. We focus our explanation on the first case which is the most complex.

Assuming that $\theta \in [0, r_M(t_i)]$, the event affects 1 M. Precisely,

- if $\theta \in [0, N(1-\min_\varphi)\bar{\gamma}_M\bar{V}_{mU}M(t_i)]$, a M may grow and eventually give birth to another bacteria. The aim is now to verify if the event really occurs and to define the trait value of the new offspring. The value $N(1-\min_\varphi)\bar{\gamma}_M\bar{V}_{mU}$ has been chosen in order to overstate all individual growth rates and to consider all M equal until this step. Hence, the M that may grow and give birth is chosen uniformly at random among all M, irrespective of their trait values. Assume that the chosen M has a trait value φ. Its exact individual growth rate is thus

$$N(1-\varphi)\bar{\gamma}_M\bar{V}_{mU}\frac{D(t_i)}{\bar{K}^K_{mU} + D(t_i)}\mathbf{1}_{\left\{D(t_i) \geq \frac{\alpha+\alpha'}{N}\right\}}.$$

  We simulate θ', a uniform random variable in $[0,1]$. The event of growth really occurs if

$$\theta' \leq \frac{(1-\varphi)}{(1-\min_\varphi)}\frac{D(t_i)}{\bar{K}^K_{mU} + D(t_i)}\mathbf{1}_{\left\{D(t_i) \geq \frac{\alpha+\alpha'}{N}\right\}},$$

otherwise nothing happens and the algorithm starts again.

In the case where the event of growth occurs, an amount of α/N molecules of carbon is added to the stock of the bacteria and an amount of $(\alpha+\alpha')/N$ DOC is removed from the system, which represents the effective cost (structural and energetic costs) for the event of growth. At this time, if the stock of the bacteria reaches the size α, the bacteria splits, gives birth to a new bacteria with a stock of carbon equals to 0 and its own stock of carbon is re-initialized to 0. If an offspring arises, its trait value is the same as its parent, φ, with probability $1-p_{mut}$, and with probability p_{mut}, it is chosen through a Gaussian random variable centered in φ, with standard deviation σ_{mut}, and conditioned on staying in $[0,1]$.

- if $\theta \in [N(1-\min_\varphi)\bar{\gamma}_M \bar{V}_{mU} M(t_i), N(1-\min_\varphi)\bar{\gamma}_M \bar{V}_{mU} M(t_i) + d_M M(t_i)]$, 1 M dies. Since all M have the same individual death rate $\bar{d}_M$, 1 M is chosen uniformly randomly among all M and is removed from the population. A proportion ε of its carbon (its structural cost α and its stock) is lost out of the system by leaching and a proportion $1-\varepsilon$ is recycled. From the recycled part, a proportion p goes to C and a proportion $1-p$ goes to D.

- Finally, in the last case, 1 M may produce 1 Z. Once again, the rate has been overstated, such that the affected M is chosen uniformly and randomly among all M. If its trait value is φ, we simulate θ', a uniform random variable on $[0,1]$, and the production of 1 Z happens if

$$\theta' \leq \frac{\varphi}{\max_\varphi} \frac{D(t_i)}{\bar{K}^K_{mU} + D(t_i)} \mathbf{1}_{\{D(t_i) \geq \gamma + \gamma'\}},$$

that is, 1 Z is added to the system and $\gamma+\gamma'$ molecules of D are removed. Otherwise nothing happens.

Appendix C. Deterministic approximation of the stochastic CDMZ model

The derivation of the deterministic approximation (2.4) is based on the following lemma. Let us denote by $(M^K(t), Z^K(t), C^K(t), D^K(t))$ the number of bacteria, enzymes molecules, SOC molecules and DOC molecules given by the stochastic process presented in Section 2.1 in the case of K neighbourhoods. The following lemma can be deduced from a direct application of Chapter 11 in Ethier and Kurtz [2009].

Lemma 4.1. *Assume that (2.2) holds and that*

$$\left(\frac{M^K(0)}{K}, \frac{Z^K(0)}{K}, \frac{C^K(0)}{K}, \frac{D^K(0)}{K}\right) \underset{K\to+\infty}{\longrightarrow} (\mathtt{m}(0), \mathtt{z}(0), \mathtt{c}(0), \mathtt{d}(0)) \in [0,+\infty)^4,$$

then for any $T \geq 0$,

$$\lim_{K\to+\infty} \sup_{t\leq T} \left\| \left(\frac{M^K(t)}{K}, \frac{Z^K(t)}{K}, \frac{C^K(t)}{K}, \frac{D^K(t)}{K}\right) - (\mathtt{m}(t), \mathtt{z}(t), \mathtt{c}(t), \mathtt{d}(t)) \right\|_\infty = 0,$$

where the limit stands in probability, $\|.\|_\infty$ *denotes the* L^∞*-norm on* $\mathbb{R}^4$ *and* $(\mathtt{m}, \mathtt{z}, \mathtt{c}, \mathtt{d})$ *is the unique solution to* (2.4) *with initial condition* $(\mathtt{m}(0), \mathtt{z}(0), \mathtt{c}(0), \mathtt{d}(0))$.

For any deterministic initial condition $(\mathtt{m}(0), \mathtt{z}(0), \mathtt{c}(0), \mathtt{d}(0)) \in [0, +\infty)^4$, the solution to (2.4) is indeed unique. This uniqueness derives from the fact that the vector field is locally Lipschitz and that the solutions do not explode in finite time [Chicone, 2006]. The latter follows directly from the fact that $\frac{d}{dt}(\alpha\mathtt{m} + \gamma\mathtt{z} + \beta\mathtt{c} + \mathtt{d}) \leq \beta\bar{I}_C + \bar{I}_D$ at any time, as the only external carbon sources are the spontaneous appearances of C and D.

Appendix D. Default parameter values

The set of default parameters is derived from Allison et al. [2010], German et al. [2012], Hagerty et al. [2014], Schimel and Weintraub [2003].

The structural and energetic costs (αs and γs) are calculated from the masses and production fractions of the variables (see Equations (2.1) and (2.5)). They are not inputs of the model, and are presented here only for informative purposes.

Table D.1. Parameters of the deterministic model in biomass.

Parameter	Unit	Description	Default value
V	cm^3	microsite volume	10^{-9}
K		scaling parameter of (local) microbial population size	10
φ		exoenzyme allocation fraction	$[0, 1]$
γ_M		microbial biomass production fraction	0.3
γ_Z		exoenzyme allocation fraction	0.4
ω_M	mg	mass of 1 M cell	10^{-9}
ω_Z	mg	mass of 1 Z molecule	10^{-16}
ω_C	mg	mass of 1 C molecule	10^{-16}
ω_D	mg	mass of 1 D molecule	10^{-19}
α		structural cost in D of 1 M cell	10^{10}
α'		energetic cost in D of 1 M cell	2.33×10^{10}
β		structural cost in D of 1 C molecule	10^3
γ		structural cost in D of 1 Z molecule	10^3
γ'		energetic cost in D of 1 Z molecule	1.5×10^3
d_M	h^{-1}	microbial carbon biomass turnover rate	2×10^{-4}
d_Z	h^{-1}	enzyme carbon biomass turnover rate	2×10^{-3}
V_{mU}	h^{-1}	maximum uptake rate (in biomass)	0.42

V_{mD}	$mg^{-1}h^{-1}$	maximum decomposition rate when C is not limiting	$\frac{7\times10^{-4}}{V}$
K_{mU}	mg	uptake half-saturation constant	$0.3 \times V$
I_C	mgh^{-1}	external input of C	$5 \times 10^{-4} \times V$
I_D	mgh^{-1}	external input of D	0
e_C	h^{-1}	C leaching rate	10^{-6}
e_D	h^{-1}	D leaching rate	10^{-6}
l		fraction of dead M and Z leached instead of recycled	0
p		fraction of recycled dead M flowing into C (remaining fraction flows into D)	0.5
$T_{\max}$	h	maximum simulation time	10^6
p_{mut}		probability of mutation per cell division event	between $1/(Kln(K))$ and $1/K^2$
σ_{mut}		standard deviation of mutation effect	$[0.01 - 0.1]$

The decomposition rate V_{mD} has been calculated as $\frac{v_{max}^D}{K_m^D}$ from Allison et al. [2010]'s model. Since the stochastic model allows us to look at the behaviour of smaller populations, we reduce the soil volume to $10^{-9}cm^3$ (instead of $1cm^3$ in most models). Volume affects 3 parameters: V_{mD}, K_{mU}, and I_C. We ignore the input of D. We assumed leaching of D equal to leaching of C. Dead microbes and deactivated enzymes are recycled half into C and the other half into D. The values for p_{mut} and σ_{mut} have been chosen to respect the assumptions of the adaptive dynamics that mutations are rare and small [Geritz et al., 1998].

Concerning the change of unit from biomass to individuals (ωs), the models for M, Z, C, D are *Bacillus subtilis* ou *clausii*, cellulase, cellulose and glucose respectively. We estimated the mass of 1 D with the mass of 1 molecule of glucose, which contains 6 atoms of carbon and $m_{6.02\times10^{23}atoms\ of\ ^{12}C} = 12g$. We estimated the mass of 1 C from the approximation that 1 molecule of cellulose contains about 10^3 molecules of glucose. We estimated the mass of 1 Z by assuming that 1 molecule of cellulase contains about as much carbon as 1 molecule of cellulose. Finally, we estimated the mass of 1 M based on the results from biomass estimations of soil samples (with various methods: CFI, CFE, SIR...) that there are about 4×10^8 active individual bacteria in $1cm^3$ of bulk soil, which weight $0.1mg$ in carbon [Fierer et al., 2009].

Appendix E. Derivation of the hybrid stochastic-deterministic model

We now state and prove the theorem that justifies the approximation of the stochastic model by the PDMP. As explained above, the main idea is to use that the biomass represented by a cell is much larger than the carbon mass of a molecule of enzyme, SOC or DOC, whereas the number of cells is much smaller than the number of enzyme, SOC and DOC molecules.

To set the result rigorously, we introduce a parameter κ that gives the order of magnitude of the biomass of a cell and the number of enzymes, SOC and DOC molecules.
The structural and energetic costs of a bacteria is rewritten

$$\alpha_\kappa := \kappa\alpha \quad \text{and} \quad \alpha'_\kappa = \kappa\alpha'.$$

As previously, we set $\bar{I}_C^\kappa = \kappa\bar{I}_C$, $\bar{I}_D^\kappa = \kappa\bar{I}_D$, $\bar{V}_{mD}^\kappa = \frac{\bar{V}_{mD}}{\kappa}$, $\bar{K}_{mU}^\kappa = \kappa\bar{K}_{mU}$, and we are interested in the sequence

$$\left(M_t^\kappa, \frac{Z_t^\kappa}{\kappa}, \frac{C_t^\kappa}{\kappa}, \frac{D_t^\kappa}{\kappa}, t \geq 0\right)_{\kappa\geq 0},$$

when κ converges to ∞. A direct application of Theorem 3.1 of Crudu et al. [2012] and a change of variables similar to the one of Section 2.2 give the following theorem.

Theorem 2. *Assume that* $\left(M^\kappa(0), \omega_Z\frac{Z^\kappa(0)}{\kappa}, \omega_C\frac{C^\kappa(0)}{\kappa}, \omega_D\frac{D^\kappa(0)}{\kappa}\right)$ *converges to a deterministic vector* (M_0, z_0, c_0, d_0)*, then the sequence of processes*

$$\left(M_t^\kappa, \frac{Z_t^\kappa}{\kappa}, \frac{C_t^\kappa}{\kappa}, \frac{D_t^\kappa}{\kappa}, t \geq 0\right)$$

converges in distribution, when κ *goes to* $+\infty$*, to the distribution of a PDMP whose generator is*

$$\begin{aligned}
\mathcal{A}f(M,z,c,d) = \\
&(1-\varphi)\gamma_M V_{mU}\frac{d}{K_{mU}+d}M\mathbf{1}_{\{d\geq\omega_D(\alpha+\alpha')\}}\Big[f\left(M+1,z,c,d-\omega_D(\alpha+\alpha')\right)-f(M,z,c,d)\Big]\\
&+\bar{d}_M M\Big[f\left(M-1,z,c+(1-\varepsilon)p\alpha\omega_D, d+(1-\varepsilon)(1-p)\alpha\omega_D\right)-f(M,z,c,d)\Big]\\
&+\left(\varphi\eta\omega_D V_{mU}\gamma_Z\frac{d}{K_{mU}+d}M-d_Z z\right)\frac{\partial f(M,z,c,d)}{\partial z}\\
&+\left(I_C-l_C c-V_{mD}zc\right)\frac{\partial f(M,z,c,d)}{\partial c}\\
&+\left(I_D-l_D d+V_{mD}zc+(1-\varepsilon)d_Z z-\varphi\eta V_{mU}\frac{d}{K_{mU}+d}M\right)\frac{\partial f(M,z,c,d)}{\partial d}.
\end{aligned}$$

This approximation is justified in our context due to the large values of $\alpha_\kappa = 10^{10}$ and $\alpha'_\kappa = 2.33\cdot 10^{10}$ compared to β, γ and γ' (less than 10^4).

Appendix F. Simulation algorithm for the hybrid stochastic-deterministic model

Like in the previous algorithm presented in Appendix B, the algorithm starts with a given amount of M, z, c and d at time $t = 0$. Two stochastic events (growth or death of a bacteria) can never occur at the same time. Assume that the process has been computed until the i-th event at time t_i and we explain how to compute the $i+1$-th event. We compute the total event rate of bacteria which is equal to

$$r_M(t_i) = \left[N(1-\min_\varphi)\bar{\gamma}_M \bar{V}_{mU} + \bar{d}_M\right] M(t_i).$$

where $\max_\varphi$ (resp. $\min_\varphi$) is the maximum (resp. minimum) trait value φ that can be found among M-population at time t_i. We then simulate Δ_t, an exponential random variable with parameter $r(t_i)$, to find the time $t_{i+1} := t_i + \Delta_t$, when the next event occurs.
The next step differs significantly from the algorithm presented in Appendix B. The aim is to obtain the quantities of enzymes, SOC and DOC (resp. $z(t_{i+1})$, $c(t_{i+1})$, and $d(t_{i+1})$) in biomass at time t_{i+1}. As these quantities satisfy the dynamical system (2.7) with $M = M(t_i)$ between t_i and t_{i+1}, we use an Euler scheme to simulate the dynamics of z, c and d between times t_i and t_{i+1} and obtain the expected quantities.
It remains to determine if, at time t_{i+1}, an event really occurs to a bacteria and which one. To this aim, we proceed as the previous algorithm. We simulate a uniform random variable θ in $[0, r_M(t_i)]$.

- If $\theta \in [0, N(1-\min_\varphi)\bar{\gamma}_M \bar{V}_{mU}]$, we proceed as previously by choosing a bacteria uniformly at random among all bacteria, throwing a uniform random variable θ' in $[0,1]$ and the growth of the chosen bacteria really occurs if

$$\theta' \leq \frac{(1-\varphi)}{(1-\min_\varphi)} \frac{d(t_{i+1})}{K_{mU} + d(t_{i+1})} \mathbf{1}_{\left\{d(t_{i+1}) \geq \omega_D \frac{\alpha+\alpha'}{N}\right\}}.$$

  In this case, an amount of $\omega_D \alpha / N$ (in biomass) is added to the stock of the bacteria, and an amount of $\omega_D(\alpha+\alpha')/N$ is removed from d. If the stock of the bacteria reaches the sizes $\omega_D \alpha$, it gives birth with exact same rules as previously.

- Otherwise, a bacteria dies. It is chosen uniformly at random and removed from the population. At the same time, an amount of $(1-\varepsilon)p\omega_D\alpha$ is added to variable d and an amount of $(1-\varepsilon)(1-p)\omega_D\alpha$ is added to variable c.

Appendix G. Simulation of resident-mutant interaction in the spatial model

Microsites are initialized according to the resident stationary state for all variables M, Z, C and D. Mutants are initially located at the center of the grid (changing the initial location does not modify the final fraction of mutants in the grid). To reduce simulation time, we assume that mutants are

initially at 5% frequency in the introduction microsite. We ran simulations for (resident, mutant) pairs with +/- 0.05 difference in trait value φ . From the final frequency of mutants we compute the mutant exponential growth rate, and average over 20 simulation replicates. For values very close to zero, we re-ran simulations three times longer.

References

Elsa Abs and Régis Ferriere. Modeling microbial dynamics and soil respiration, effect of climate change. in biogeochemical cycles: Anthropogenic and ecological drivers. submitted, 2018.

Benjamin Allen, Jeff Gore, and Martin A Nowak. Spatial dilemmas of diffusible public goods. Elife, 2:e01169, 2013.

SD Allison. A trait-based approach for modelling microbial litter decomposition. Ecology letters, 15 (9):1058–1070, 2012.

Steven D Allison. Cheaters, diffusion and nutrients constrain decomposition by microbial enzymes in spatially structured environments. Ecology Letters, 8(6):626–635, 2005.

Steven D Allison, Matthew D Wallenstein, and Mark A Bradford. Soil-carbon response to warming dependent on microbial physiology. Nature Geoscience, 3(5):336, 2010.

Charlotte J Alster, Peter Baas, Matthew D Wallenstein, Nels G Johnson, and Joseph C von Fischer. Temperature sensitivity as a microbial trait using parameters from macromolecular rate theory. Frontiers in microbiology, 7:1821, 2016.

Patrick Billingsley. Convergence of probability measures. John Wiley & Sons, 2013.

Angus Buckling, Freya Harrison, Michiel Vos, Michael A Brockhurst, Andy Gardner, Stuart A West, and Ashleigh Griffin. Siderophore-mediated cooperation and virulence in pseudomonas aeruginosa. FEMS microbiology ecology, 62(2):135–141, 2007.

Nicolas Champagnat, Régis Ferrière, and Sylvie Méléard. Unifying evolutionary dynamics: from individual stochastic processes to macroscopic models. Theoretical population biology, 69(3):297–321, 2006.

Carmen Chicone. Ordinary differential equations with applications, volume 34. Springer Science & Business Media, 2006.

Otto X Cordero, Laure-Anne Ventouras, Edward F DeLong, and Martin F Polz. Public good dynamics drive evolution of iron acquisition strategies in natural bacterioplankton populations. Proceedings of the National Academy of Sciences, 109(49):20059–20064, 2012.

Alina Crudu, Arnaud Debussche, Aurélie Muller, Ovidiu Radulescu, et al. Convergence of stochastic gene networks to hybrid piecewise deterministic processes. The Annals of Applied Probability, 22 (5):1822–1859, 2012.

Eric A Davidson and Ivan A Janssens. Temperature sensitivity of soil carbon decomposition and feedbacks to climate change. Nature, 440(7081):165, 2006.

A Dobay, HC Bagheri, A Messina, R Kümmerli, and DJ Rankin. Interaction effects of cell diffusion, cell density and public goods properties on the evolution of cooperation in digital microbes. Journal of evolutionary biology, 27(9):1869–1877, 2014.

William W Driscoll and John W Pepper. Theory for the evolution of diffusible external goods. Evolution: International Journal of Organic Evolution, 64(9):2682–2687, 2010.

Stewart N Ethier and Thomas G Kurtz. Markov processes: characterization and convergence, volume 282. John Wiley & Sons, 2009.

PG Falkowski, T Fenchel, and EF Delong. The microbial engines that drive earth'92s biogeochemical cycles. Science, 320:1034–1039, 2008.

R Ferriere. Spatial structure and viability of small populations. Revue d'Ecologie-La Terre et la Vie, pages 135–138, 2000.

Regis Ferriere and Stéphane Legendre. Eco-evolutionary feedbacks, adaptive dynamics and evolutionary rescue theory. Phil. Trans. R. Soc. B, 368(1610):20120081, 2013.

Régis Ferriere, Judith L Bronstein, Sergio Rinaldi, Richard Law, and Mathias Gauduchon. Cheating and the evolutionary stability of mutualisms. Proceedings of the Royal Society of London B: Biological Sciences, 269(1493):773–780, 2002.

Noah Fierer, Michael S Strickland, Daniel Liptzin, Mark A Bradford, and Cory C Cleveland. Global patterns in belowground communities. Ecology letters, 12(11):1238–1249, 2009.

Henry Joseph Folse and Steven D Allison. Cooperation, competition, and coalitions in enzyme-producing microbes: social evolution and nutrient depolymerization rates. Frontiers in microbiology, 3:338, 2012.

Nicolas Fournier and Sylvie Méléard. A microscopic probabilistic description of a locally regulated population and macroscopic approximations. The Annals of Applied Probability, 14(4):1880–1919, 2004.

Stefan AH Geritz, Géza Mesze, Johan AJ Metz, et al. Evolutionarily singular strategies and the adaptive growth and branching of the evolutionary tree. Evolutionary ecology, 12(1):35–57, 1998.

Donovan P German, Kathleen RB Marcelo, Madeleine M Stone, and Steven D Allison. The m ichaelis–m enten kinetics of soil extracellular enzymes in response to temperature: a cross-latitudinal study. Global Change Biology, 18(4):1468–1479, 2012.

Ashleigh S Griffin, Stuart A West, and Angus Buckling. Cooperation and competition in pathogenic bacteria. Nature, 430(7003):1024, 2004.

Shannon B Hagerty, Kees Jan Van Groenigen, Steven D Allison, Bruce A Hungate, Egbert Schwartz, George W Koch, Randall K Kolka, and Paul Dijkstra. Accelerated microbial turnover but constant growth efficiency with warming in soil. Nature Climate Change, 4(10):903, 2014.

Peter M Homyak, Joseph C Blankinship, Eric W Slessarev, Sean M Schaeffer, Stefano Manzoni, and Joshua P Schimel. Effects of altered dry season length and plant inputs on soluble soil carbon. Ecology, 99(10):2348–2362, 2018.

Thomas Julou, Thierry Mora, Laurent Guillon, Vincent Croquette, Isabelle J Schalk, David Bensimon, and Nicolas Desprat. Cell–cell contacts confine public goods diffusion inside pseudomonas aeruginosa clonal microcolonies. Proceedings of the National Academy of Sciences, 110(31):12577–12582, 2013.

Christina Kaiser, Oskar Franklin, Ulf Dieckmann, and Andreas Richter. Microbial community dynamics alleviate stoichiometric constraints during litter decay. Ecology letters, 17(6):680–690, 2014.

Christina Kaiser, Oskar Franklin, Andreas Richter, and Ulf Dieckmann. Social dynamics within decomposer communities lead to nitrogen retention and organic matter build-up in soils. Nature communications, 6:8960, 2015.

Andrzej M Kierzek. Stocks: Stochastic kinetic simulations of biochemical systems with gillespie algorithm. Bioinformatics, 18(3):470–481, 2002.

Arthur L Koch. The macroeconomics of bacterial growth. Special Publications of the Society for General Microbiology[SPEC. PUBL. SOC. GEN. MICROBIOL.]. 1985., 1985.

Mickael Le Gac and Michael Doebeli. Environmental viscosity does not affect the evolution of cooperation during experimental evolution of colicigenic bacteria. Evolution: International Journal of Organic Evolution, 64(2):522–533, 2010.

William Lee, Minus van Baalen, and Vincent AA Jansen. Siderophore production and the evolution of investment in a public good: an adaptive dynamics approach to kin selection. Journal of theoretical biology, 388:61–71, 2016.

Martin A Nowak. Five rules for the evolution of cooperation. science, 314(5805):1560–1563, 2006.

Paul B Rainey and Katrina Rainey. Evolution of cooperation and conflict in experimental bacterial populations. Nature, 425(6953):72, 2003.

Colin Ratledge. Biodegradation of oils, fats and fatty acids. pages 89–141, 1994.

Adin Ross-Gillespie, Andy Gardner, Stuart A West, and Ashleigh S Griffin. Frequency dependence and cooperation: theory and a test with bacteria. The American Naturalist, 170(3):331–342, 2007.

Joshua P Schimel and Michael N Weintraub. The implications of exoenzyme activity on microbial carbon and nitrogen limitation in soil: a theoretical model. Soil Biology and Biochemistry, 35(4): 549–563, 2003.

RL Sinsabaugh and DL Moorhead. Resource allocation to extracellular enzyme production: a model for nitrogen and phosphorus control of litter decomposition. Soil biology and biochemistry, 26(10): 1305–1311, 1994.

Judith M Tisdall and J_M Oades. Organic matter and water-stable aggregates in soils. Journal of soil science, 33(2):141–163, 1982.

Pankaj Trivedi, Manuel Delgado-Baquerizo, Chanda Trivedi, Hangwei Hu, Ian C Anderson, Thomas C Jeffries, Jizhong Zhou, and Brajesh K Singh. Microbial regulation of the soil carbon cycle: evidence from gene–enzyme relationships. The ISME journal, 10(11):2593, 2016.

Gregory J Velicer. Social strife in the microbial world. Trends in microbiology, 11(7):330–337, 2003.

YA Vetter, JW Deming, PA Jumars, and BB Krieger-Brockett. A predictive model of bacterial foraging by means of freely released extracellular enzymes. Microbial ecology, 36(1):75–92, 1998.

Stuart A West and Angus Buckling. Cooperation, virulence and siderophore production in bacterial parasites. Proceedings of the Royal Society of London B: Biological Sciences, 270(1510):37–44, 2003.

Stuart A West, Ashleigh S Griffin, Andy Gardner, and Stephen P Diggle. Social evolution theory for microorganisms. Nature reviews microbiology, 4(8):597, 2006.

William R Wieder, Gordon B Bonan, and Steven D Allison. Global soil carbon projections are improved by modelling microbial processes. Nature Climate Change, 3(10):909, 2013.

William R Wieder, Steven D Allison, Eric A Davidson, Katerina Georgiou, Oleksandra Hararuk, Yujie He, Francesca Hopkins, Yiqi Luo, Matthew J Smith, Benjamin Sulman, et al. Explicitly representing soil microbial processes in earth system models. Global Biogeochemical Cycles, 29 (10):1782–1800, 2015.

Xia Zhang, Guo-Yue Niu, Ahmed S Elshall, Ming Ye, Greg A Barron-Gafford, and Mitch Pavao-Zuckerman. Assessing five evolving microbial enzyme models against field measurements from a semiarid savannah—what are the mechanisms of soil respiration pulses? Geophysical Research Letters, 41(18):6428–6434, 2014.

Electronic Supplementary Material

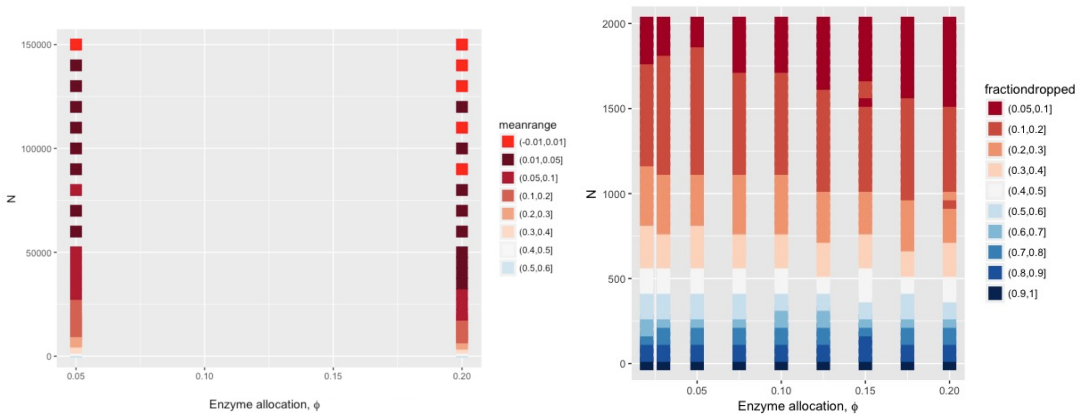

(a) K=1 (b) K=5

(c) K=10 (d) K=20

(e) K=50 (f) K=100

Figure S1. Effect of N and φ on the fraction of events dropped before the end of the simulation ($T_{\max}$ or extinction time). K increases from (a) to (f). The deterministic model (2.6) provides an accurate approximation of the PDMP model for combinations of φ for which the fraction of dropped events is less than a small threshold, e.g. 1% (bright red). All constant parameters are set to their default values, except $p = 0$ and $e_D = 10^{-2}$. Initial conditions are adjusted to the stable equilibrium of (2.6) for each value of φ, $T_{\max} = 10^6$.

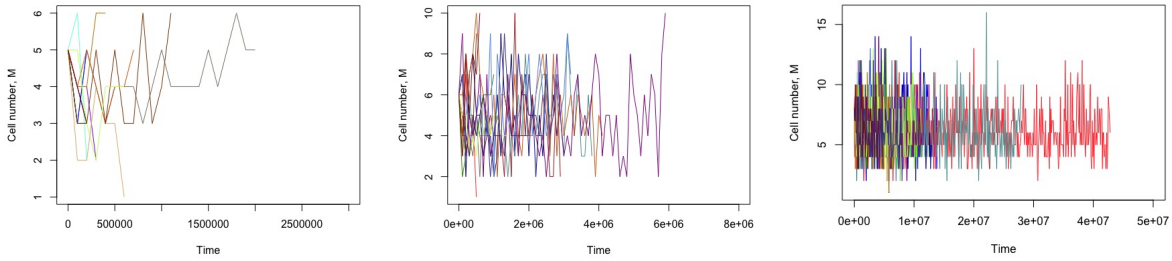

(a) K=10 (b) K=12 (c) K=15

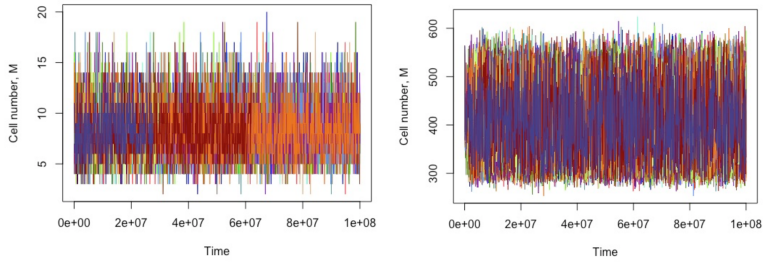

(d) K=20 (e) K=1000

Figure S2. Effect of K on the dynamics of the cell population M. The model used is the hybrid stochastic-deterministic model (approximation of the PDMP with deterministic microbial growth). Five values of K are used between 10 and 1000. For each value of K, twenty simulation runs are reported; each run is colored differently. Simulations stop when the cell population reaches zero. Parameter values: All constant parameters are set to their default values (Table D.1 in Appendix D), initial conditions are adjusted to $\varphi = 0.5$, and $T_{\max} = 10^8$.

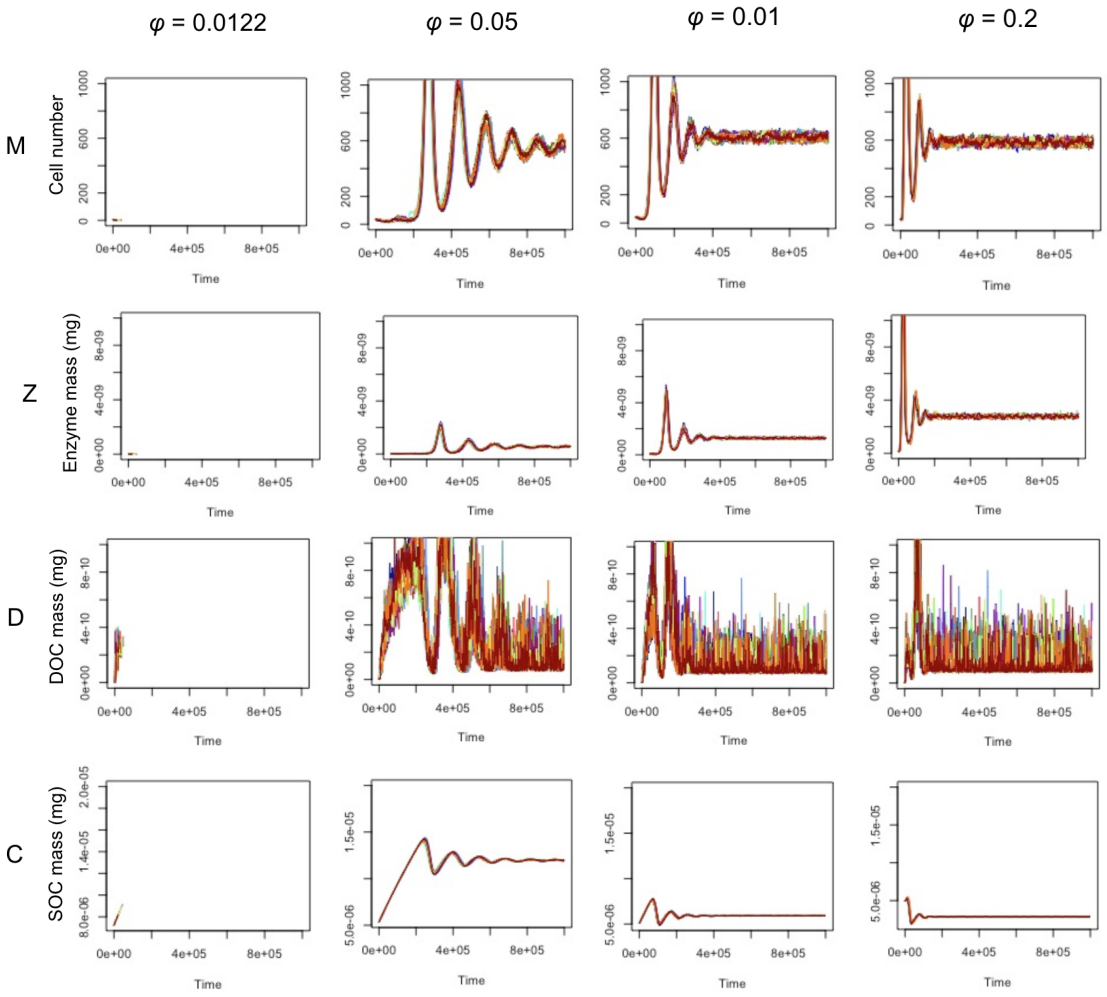

Figure S3. Aggregated dynamics of the cell population size M (in individuals), and Z, C, and D (in units of carbon mass) simulated with the spatial model in the absence of mutation. All constant parameters are set to the default values (Table D.1 in Appendix D). Parameter values specific to this model are: $K = 10$, $L = 10$, $\sigma_{\text{diff}} = 10^{-9}$, $\tau_{\text{diff}} = 10^{-3}$, $p_{disp} = 0.3$. Initial conditions are set to the steady state of the corresponding φ in the central microsites occupied by microbes, and $M = Z = D = 0$ and $C = 5 \times 10^{-5}$ in the empty microsites.

Microbial evolution reshapes soil carbon feedbacks to climate change

Elsa Abs[1,2*], Scott R. Saleska[1], Regis Ferriere[1,2,3]

[1] Department of Ecology & Evolutionary Biology, University of Arizona, Tucson, AZ 85721, USA

[2] Institut de Biologie de l'Ecole Normale Supérieure (IBENS), ENS-PSL University, CNRS, INSERM, 75005 Paris, France

[3] International Center for Interdisciplinary Global Environmental Studies (iGLOBES), CNRS, ENS-PSL University, University of Arizona, Tucson, AZ 85721, USA

*Corresponding author, abs@biologie.ens.fr

Abstract

Microbial decomposition of soil organic matter is a key component of the global carbon cycle[1,2]. As Earth's climate changes, the response of microbes and microbial enzymes to rising temperatures will largely determine the soil carbon feedback to atmospheric CO_2[3–5]. However, while increasing attention focuses on physiological and ecological mechanisms of microbial responses[6–9], the role of evolutionary adaptation to warming has been little studied. To address this gap, we develop here an eco-evolutionary model[10] of a soil microbe-enzyme system under warming[11], under three possible scenarios for the influence of temperature on microbial activity[11–15]. In the absence of microbial evolution, warming results in soil carbon loss to the atmosphere (an amplification of climate change) in all scenarios. Microbial evolutionary adaptation generally aggravates soil carbon loss in cold ecosystems, and may aggravate, buffer or even reverse carbon loss in warm ecosystems. Constraining the model with observations from five contrasting biomes[14] reveals evolutionary aggravation of soil carbon loss to be the most likely outcome, with a strong latitudinal pattern, from small evolutionary effects at low latitude to large evolutionary effects at high latitude. In all cases, local microbial competition for decomposable organic carbon, which may be shaped in part by soil texture and moisture[16,17], is a major factor of the eco-evolutionary response of microbial decomposition to warming. Accounting for evolutionary mechanisms will likely be critical for improving projections of Earth system responses to climate change.

Microorganisms are key drivers of global biogeochemical cycles[1]. In terrestrial ecosystems, soil microbes decompose organic matter, returning carbon to the atmosphere as carbon dioxide (CO_2)[2]. *In vitro* and *in situ* experiments suggest that changes in microbial decomposition with warming are an important feedback to climate[3–5]. Soil microbial populations may respond to increasing temperature through physiological mechanisms such as individual metabolic adjustment[6,7] and ecological mechanisms such as shifts in population abundance or community composition[8,9]. Given the short generation time, large population sizes and standing genetic variation of many microbial organisms, evolutionary adaptive responses of microbial populations to warming are also likely[18,19]. However, how microbial evolutionary adaptation may contribute to carbon-climate feedbacks is unknown[20].

Key to microbial decomposition of soil organic matter is the production by microbes of extracellular enzymes (exoenzymes), that diffuse locally in the soil and bind to soil organic matter compounds[21]. Because the fitness cost of exoenzyme production[22] (reduced allocation to growth, Fig. 1a) is paid by individual microbes whereas fitness benefits (larger resource pool) are enjoyed by microbial collectives[23], we expect genetic variation in exoenzyme production[24] to be under strong selection[23,25]. Our objective is to evaluate how exoenzyme production responds to selection under environmental warming, and how the evolutionary response of exoenzyme production impacts the response of soil organic carbon stock (SOC). To this end, we develop and analyze a novel eco-evolutionary model, based on ref. 13[11] (Fig. 1a), but modified to take microbial evolutionary adaptation into account.

In this novel eco-evolutionary model, the focal microbial adaptive trait is the fraction of assimilated carbon allocated to exoenzyme production[26,27], or 'exoenzyme allocation fraction', hereafter denoted by φ (the balance of assimilated carbon, $1-\varphi$, is allocated directly to microbial growth). Competition between microbial strains differing in enzyme allocation fraction φ drives adaptive evolution. The model predicts the adapted value, φ^*, of the exoenzyme allocation fraction at any given temperature; the adaptive response of the

exoenzyme allocation fraction to temperature rise; and how this response impacts the decomposition rate and SOC stock. By comparing the full eco-evolutionary (ECOEVO) response of SOC stock to the purely ecological (ECO) response in absence of evolution (in which φ is a fixed parameter that does not change), we can evaluate the contribution of microbial evolutionary adaptation (EVO effect) to the direction and magnitude of the SOC stock response to climate warming (Fig. 1b, c).

Microbial decomposition is predicted to respond to warming due to the temperature sensitivity of intra- and extra-cellular enzymatic activity[14,28,29]. In our baseline 'kinetics-only' scenario of temperature-dependent decomposition, we assume that microbial uptake parameters (maximum uptake rate and half-saturation constant) and exoenzyme kinetics parameters (maximum decomposition rate and half-saturation constant) increase with temperature[5,30]. We consider two additional scenarios for the influence of temperature on decomposition. In the microbial mortality scenario, the microbial death rate also increases with temperature[13]. This could be due to a higher risk of predation or pathogenic infection at higher temperatures, or faster microbial senescence due to higher protein turnover[13]. In the microbial growth efficiency (MGE) scenario, MGE (the fraction of carbon allocated to growth that actually contributes to microbial biomass, as opposed to being released as CO_2 via growth respiration) decreases with temperature[11,31], which could be due to higher maintenance costs at higher temperature[32].

At any given temperature, the evolutionary model predicts that the adapted value of the enzyme allocation fraction, φ^*, depends on four parameters (equation (5) in on-line Methods): MGE, mortality, maximum uptake rate, and local competitive advantage to exoenzyme producers, or 'competition asymmetry'. Among these parameters, competition asymmetry measures the differential availability of dissolved organic carbon (DOC) to different microbial strains, which may be shaped by diffusion of DOC or microbial mobility, and is thus likely influenced by soil physical properties, such as texture or moisture. For simplicity, we ignore the potential effect of temperature on the latter, and as a result, competition asymmetry is independent of temperature.

In all three scenarios of temperature dependence, the SOC non-adaptive ecological equilibrium generally decreases as temperature or exoenzyme allocation fraction increases (Fig. 1b, Extended Data Fig. 4, Supplementary Discussion). Focusing on the baseline scenario of temperature dependence, we find that the adapted enzyme allocation fraction, φ^*, always increases with increasing temperature (Fig. 1b, Extended Data Fig. 5a). Combining both results, we conclude that the ECOEVO response mediated by microbial evolution amplifies the ecology-driven loss of soil carbon due to warming (ECO response) (Fig. 1c).

The effect of evolution (EVO effect) is strong when the ECOEVO response markedly departs from the ECO response. This is predicted in cold ecosystems harboring communities of slow-growing microbes, under soil conditions that give only a small competitive edge to greater enzyme producers (Fig. 2, Extended Data Fig. 6). Strong EVO effects are robust to the other model parameters – enzyme parameters (efficiency, production) and environmental parameters (litter input, leaching) (Extended Data Figs. 6, 7, Supplementary Note 4).

We address the robustness of strong evolutionary effects (Fig. 3a) to different scenarios of temperature dependence by focusing on values of nutrient uptake parameters, litter input, and competition asymmetry that are conducive to such large EVO effects (for example, point B2 in Fig. 2b). In the temperature-dependent mortality scenario, how the direction and magnitude of the EVO effect change from the baseline scenario is entirely determined by the sensitivity of microbial mortality to warming. When mortality is moderately sensitive to temperature, the ECO and ECOEVO responses become more similar, resulting in a smaller EVO effect (Fig. 3a, b). When mortality is strongly sensitive to temperature, the ECOEVO response becomes weaker than the ECO response, which implies that evolution buffers the loss of soil carbon (negative EVO effect, Fig. 3c). Such EVO effects are predicted to be stronger in *warmer* ecosystems (higher T_0, Fig. 3c; see also Supplementary Discussion).

In the temperature-dependent MGE scenario, the direction and magnitude of the ECOEVO response to warming vary dramatically with the initial temperature T_0 (Fig. 3d). Driven by adaptive evolution, the enzyme allocation fraction increases strongly with warming in cold systems, hardly changes in temperate systems, and decreases markedly in warm systems (Extended Data Fig. 5d), with parallel effects on the decomposition rate (Extended Data Fig. 5h). As a consequence, at low T_0, aggravation of soil carbon loss by evolution is almost as severe as in the baseline scenario, even though both ECO and ECOEVO responses are weaker in this scenario (Fig. 3a, d). At higher values of T_0, the ECOEVO response becomes weaker than the ECO response or even positive (Fig. 3d), resulting in the sequestration rather than loss of soil carbon.

To illustrate how EVO effects may vary in real ecosystems, we used available data[14] on the decomposition kinetic parameters in five biomes of increasing latitude and decreasing mean annual temperature (Costa Rica, California, West Virginia, Maine, and Alaska, Fig. 4). We evaluated ECO and ECOEVO responses for each biome under three levels of competition asymmetry (as quantified by the local competitive advantage to producers, c_0) (Fig. 4a-h). Under our baseline scenario, EVO effects correlate strongly with mean annual temperature, even more so for low competition asymmetry (Fig. 4i). Stronger EVO effects occur in colder biomes, as found in the general analysis (Fig. 3a). In contrast, the ECO response does not correlate with mean annual temperature (Fig. 4a). As a result, a temperate biome such as Maine exhibits a weak ECO response that can be strongly amplified by evolution, whereas the warm Costa Rica biome shows a strong ECO response that is little affected by evolution.

These results are quantitatively attenuated but qualitatively unaffected when microbial mortality increases moderately with temperature (Fig. 4b, f, j). With a stronger effect of temperature on microbial mortality, all biomes show the evolutionary buffering effect (Fig. 4k) found in the general analysis (Fig. 3c). The intensity of evolutionary buffering is independent of the biomes' mean annual temperature, whereas it varies significantly with competition asymmetry (Fig. 4k). Under the temperature-dependent MGE scenario, ECO

and ECOEVO responses are reduced in magnitude compared to the baseline scenario (Fig. 4d, h), particularly in cold biomes. However, in these biomes, EVO effects are enhanced dramatically (Fig. 4l). Thus, in a biome as cold as Alaska, a significant ECOEVO loss of soil carbon is predicted, whereas the purely ecology-driven loss of soil carbon would be negligible (Fig. 4l).

In summary, as global warming increases environmental temperatures, our model predicts evolution of the enzyme allocation fraction, with potentially large effects on the decomposition process and SOC stock (see also Supplementary Discussion and Extended Data Figs. 9-10 for effects measured on total soil active carbon). The size of evolutionary (EVO) effects is most sensitive to MGE, microbial mortality, activation energy of uptake maximal rate, competition asymmetry, and initial temperature (Fig. 2). Evolution often aggravates the ecological loss of soil carbon in response to warming, especially in cold biomes (Figs. 1, 3). We identified two cases in which evolutionary adaptation to warming may buffer or even revert the ecology-driven loss of soil carbon: strongly temperature-dependent microbial mortality, or temperature-dependent MGE in warm ecosystems (Fig. 3). Overall, we expect evolutionary effects to vary greatly among ecosystems that differ in biotic (microbial life history and physiology) and abiotic (temperature, soil texture and moisture) characteristics.

Implications of our findings for large geographic scales, across terrestrial ecosystems, are hinted at by specifying the model for the five contrasting biomes for which exoenzyme kinetics data are available[14]. We find evolutionary aggravation of soil carbon loss to be the most likely outcome, with a strong latitudinal pattern, from small evolutionary effects at low latitude to large evolutionary effects at high latitude. In all cases, the competition asymmetry is a strong influence of the eco-evolutionary response of microbial decomposition to warming (Fig. 4). Soil texture and moisture, that may influence competition asymmetry, vary considerably among locations[14]. Predicting geographic variation in ECOEVO responses and EVO effects across large geographic scales thus calls

for more empirical data on variation in ecological (competition) traits, especially how the competitive advantage to exoenzyme producers varies with soil physical properties.

The adaptive trait-based approach we use circumvents the difficulty of prescribing critical parameters (such as the enzyme allocation fraction) and their response to environmental change. This approach can easily be extended to model (rather than assume) the adaptive dynamics of multiple microbial traits, such as growth-related traits and substrate-specific enzyme production traits, and their diversification into coexisting functional types (Supplementary Discussion). A similar approach has been used to construct a physiology-based model of feedbacks between global ocean ecosystem function and phytoplankton diversity[33]. Rather than assuming values for the multiple physiological traits characterizing each plankton species, the model let interactions among randomly parametrized species drive species sorting and emergence of the corresponding trait values. The trait-based approach for microbial communities can also facilitate model validation by leveraging genomic and metagenomic data mapped to soil microbial function[34].

Future extensions of our eco-evolutionary model will enable the mechanistic representation of below-aboveground feedbacks between soil microorganisms and vegetation, by coupling the carbon cycle with other major biogeochemical cycles, such as nitrogen and phosphorus[1]. Existing mathematical[26,35,36] and computational models[27,37,38] pave the way for such extensions. Global projections of the effect of soil microbial evolution on future climate change will become possible by coupling our eco-evolutionary model of biological decomposition with soil models that account for the chemical and physical transformations of soil carbon occurring on year-to-century timescales[5,39–41].

Given the large population size and short generation time of many microorganisms, microbial evolution should be an essential component of ecosystem models. Microbial evolutionary adaptation to warming, and its impact on the decomposition of soil organic matter, can radically change soil carbon dynamics. Empirical data suggest that natural values of enzyme allocation fraction are low[29,35] and fall in the range for which our model predicts large eco-evolutionary responses of decomposition to warming. In spite of an

increasing effort to document and understand the ecosystem impact of microbial physiological and ecological responses to climate warming[11,31,42], no Earth system model that seeks to represent the role of living organisms in climate feedbacks has yet included evolutionary mechanisms of adaptation. Our model is a critical first step. We expect projections of future climate and carbon cycle feedbacks, and their uncertainty, to be significantly impacted, from local to global scales.

Methods

We use the microbe-enzyme model of litter decomposition first introduced in ref. 11 and extend it to describe the ecological dynamics of soil organic carbon (SOC), dissolved organic carbon (DOC), microbial biomass, and extracellular enzyme abundance, given litter input, leaching rates, and soil temperature (Fig. 1a and Extended Data Fig. 1). The effect of temperature is mediated by enzymes kinetics, with exoenzymes driving the decomposition rate, and intra-cellular enzymes involved in resource uptake and microbial biomass synthesis. As temperature changes, the model predicts how the ecological equilibrium changes. The change in equilibrium SOC is what we call the ecological (ECO) response of the ecosystem.

To investigate the effect of evolutionary adaptation on decomposition, we include microbial evolution in the ecological model. Our focus is on soil bacteria (as opposed to fungi), which typically have large population size and short generation time. We assume that microbes may vary individually in their investment in exoenzymes, measured by the fraction (denoted by φ throughout the paper) of resources allocated to enzyme production. Assuming that some of this variation has a genetic basis, we derive the selection gradient and compute the evolutionarily stable value of the enzyme allocation fraction, φ^*, at any given temperature. We can then evaluate how φ^* changes as temperature increases, and how the ecosystem equilibrium changes from both the direct effect of temperature rise on enzyme kinetics, and the indirect effect mediated by microbial evolutionary adaptation to warming (Fig. 1b, c).

Ecological model

Based on ref. [11] (Fig. 1a, Extended Data Fig. 1), the ecological model has four state variables measured in unit mass of carbon: soil (non decomposed) organic carbon (SOC), C; soil decomposed soluble organic carbon (DOC), D; microbial biomass, M; and exoenzyme concentration, Z. Exoenzyme production drives the decomposition process of

SOC into DOC, which is the only source of carbon for microbes. The model accounts for microbial production and death, exoenzyme decay, recycling of dead microbes and degraded exoenzymes, SOC input from plant litter, and leaching of SOC and DOC.

Model equations. State variables C, D, M, Z obey equations (1a-d):

$$\text{(1a)} \quad \frac{dC}{dt} = I - \frac{v_{max}^{D} C}{K_m^{D}+C} Z - e_C C$$

$$\text{(1b)} \quad \frac{dD}{dt} = \frac{v_{max}^{D} C}{K_m^{D}+C} Z + d_M M + d_Z Z - \frac{v_{max}^{U} D}{K_m^{U}+D} M - e_D D$$

$$\text{(1c)} \quad \frac{dM}{dt} = (1-\varphi)\,\gamma_M \frac{v_{max}^{U} D}{K_m^{U}+D} M - d_M M$$

$$\text{(1d)} \quad \frac{dZ}{dt} = \varphi\,\gamma_Z \frac{v_{max}^{U} D}{K_m^{U}+D} M - d_Z Z$$

In equation (1a), decomposition follows from Michaelis-Menten kinetics of Z binding substrate C; there is a constant input, I, of soil organic (non decomposed) carbon from aboveground litter, and a loss due to leaching at constant rate e_C. In equation (1b), D is produced by decomposition and the recycling of dead microbial biomass and inactive enzymes; D is consumed by microbial uptake, and lost by leaching at constant rate e_D. In equation (1c), growth of microbial biomass M is driven by the rate of DOC uptake (a Monod function of D) times the fraction of uptaken DOC turned into biomass, $(1 - \varphi)\,\gamma_M$, minus microbial mortality at constant rate d_M. In equation (1d), enzyme variation is driven by the rate of DOC uptake times the fraction allocated to enzyme production, φ, and production efficiency, γ_Z, minus enzyme deactivation at constant rate, d_Z.

Ecosystem equilibria. The ecological model possesses either one globally stable equilibrium, or three equilibria (one of which is always unstable) (Extended Data Fig. 2). There are thresholds φ_{min} and φ_{max} such that the globally stable equilibrium exists for $\varphi < \varphi_{min}$ or $\varphi > \varphi_{max}$ and is given by $C = I/e_C$, $D = 0$, $M = 0$, $Z = 0$. Thus, at this equilibrium, the microbial population is extinct and no decomposition occurs. For $\varphi_{min} < \varphi < \varphi_{max}$, the

microbial population can either go extinct (then the system stabilizes at the same equilibrium as before) or persists at or around a non-trivial equilibrium, which can be solved for analytically. Note that $\varphi_{\min}$ and $\varphi_{\max}$ depend on all microbial and model parameters (Extended Data Fig. 3, Supplementary Note 1).

Effect of temperature on model parameters. Decomposition is predicted to respond to warming[5] due to the temperature sensitivity of enzymatic activity[14,28,43]. Microbial assimilation may also vary with temperature if the microbial membrane proteins involved in nutrient uptake are sensitive to warming. Following ref. 11, we assume that exoenzyme kinetics parameters (maximum decomposition rate v^D_{max} and half-saturation constant K^D_m) and microbial uptake parameters (maximum uptake rate $v^U{}_{max}$ and half-saturation constant K^U_m) follow Arrhenius relations with temperature. This defines our baseline 'kinetics-only' scenario of temperature-dependent decomposition:

$$\text{(2a)} \quad v^D_{max} = v^D_0 \, e^{-\frac{E^D_v}{R(T+273)}}$$

$$\text{(2b)} \quad K^D_m = K^D_0 \, e^{-\frac{E^D_K}{R(T+273)}}$$

$$\text{(2c)} \quad v^U_{max} = v^U_0 \, e^{-\frac{E^U_v}{R(T+273)}}$$

$$\text{(2d)} \quad K^U_m = K^U_0 \, e^{-\frac{E^U_K}{R(T+273)}}$$

where T is temperature in Celsius, R is the ideal gas constant, and the E parameters denote the corresponding activation energies.

We consider two additional scenarios for the influence of temperature on decomposition. In the temperature-dependent microbial mortality scenario[13], the microbial death rate increases with temperature. This could be due to a higher risk of predation or pathogenic infection at higher temperatures, or faster microbial senescence due to higher protein turnover[35]. In this scenario, the microbial death rate d_M depends on temperature according to

(3) $$d_M(T) = d_{M0} e^{-\frac{E_{dM}}{R(T+273)}}$$

as in ref. 13.

In the temperature-dependent microbial growth efficiency (MGE) scenario, the MGE decreases with temperature[11,13,31], possibly due to higher maintenance costs at higher temperature[32]. This is modeled by making the microbial growth efficiency γ_M vary linearly with temperature[11,12,14,15]:

(4) $$\gamma_M(T) = \gamma_{M,ref} - m\,(T - T_{ref})$$

with T_{ref} = 20 °C.

How scenarios of temperature-dependence and parameter values influence the response of equilibrium *C* to temperature is shown in Extended Data Fig. 4 and commented on in Supplementary Note 2.

Evolutionary analysis

The enzyme allocation fraction φ is a 'public good' trait: as an individual microbe produces exoenzymes, it experiences an energetic cost and obtains a benefit – access to decomposed organic carbon – that depends on its own and other microbes's production in the spatial neighborhood[44,45]. As a public good trait, φ is under strong direct negative selection: 'cheaters' that produce less or no exoenzymes, and thus avoid the cost while reaping the benefit of enzyme production by cooperative neighbors, should be at a selective advantage. In a highly diffusive environment in which exoenzymes are well mixed, φ would evolve to zero, leading to evolutionary suicide[46]. However, in a more realistic spatially distributed environment with limited exoenzyme diffusion, microbes with a given trait are more likely to interact with phenotypically similar microbes, which puts more cooperative microbes at

a competitive advantage over less cooperative strains[44,47,48]. This generates indirect positive selection on trait φ.

The trait value φ^* at which negative and positive selections balance is the evolutionarily stable microbial strategy, given by

$$(5) \qquad \varphi^*(T) = 1 - \frac{d_M}{\gamma_M \, v_{max}^U} - \frac{1}{c_0}$$

where c_0 measures the competitive advantage, due to spatially local interactions, of any given strain over a slightly less cooperative strain, or 'competition asymmetry' (Supplementary Note 3). The parameter c_0 is likely to depend on the diffusivity of DOC, which may itself vary with soil properties such as texture or water content.

As temperature rises from T_0 to T, the direction and magnitude of the microbial adaptive response is measured by $\Delta\varphi^* = \varphi^*(T) - \varphi^*(T_0)$, which depends on the scenario of temperature dependence. The eco-evolutionary (ECOEVO) response of SOC is given by

$$(6) \qquad \text{ECOEVO} = \Delta C_{\text{ECOEVO}}(T_0, T) = C(T, \varphi^*(T)) - C(T_0, \varphi^*(T_0))$$

where $C(T, \varphi)$ denotes ecological equilibrium C at temperature T, given enzyme allocation fraction φ. The ECOEVO response is to be compared with the purely ecological (ECO) response:

$$(7) \qquad \text{ECO} = \Delta C_{\text{ECO}}(T_0, T) = C(T, \varphi^*(T_0)) - C(T_0, \varphi^*(T_0))$$

in which the enzyme allocation fraction is fixed at its T_0-adapted value, $\varphi^*(T_0)$ (Fig. 1c).

We measure the magnitude of the evolutionary (EVO) effect as the difference between the ECOEVO response averaged over the temperature range (T_0, T) and the ECO response averaged over the same temperature range, normalized by the ECO response:

$$(8) \qquad EVO\ effect = \frac{\left| \int_{T_0}^{T} \Delta C_{ECOEVO}(T_0, T) - \int_{T_0}^{T} \Delta C_{ECO}(T_0, T) \right|}{\left| \int_{T_0}^{T} \Delta C_{ECO}(T_0, T) \right|}$$

This evaluation allows us to compare EVO effects across systems that differ in the magnitude of their ECO response. In all simulations we use $T = T_0 + \Delta T$ where $\Delta T = 5$ °C. In general, the ECO and ECOEVO responses are monotonic, close-to-linear functions of T over the considered temperature ranges $(T_0,\ T_0 + \Delta T)$, which makes all our comparative analyses almost insensitive to our choice of ΔT.

Parameters default values and variation range

Under the temperature-dependent kinetics-only scenario, the ecological model (equations (1) and (2)) includes seven microbial parameters (φ, γ_M, d_M, v_0^U, E_v^U, K_0^U, E_K^U), six enzyme parameters (γ_Z, d_Z, v_0^D, E_v^D, K_0^D, E_K^D) and four environmental parameters (I, e_C, e_D, T). Our set of default parameter values is derived from Allison *et al.* (2010) (Extended Data Table 1). The enzyme allocation fraction default value is 10% at 20 °C [35]. For the dependence of enzyme kinetics parameters on temperature, $v_{max}^D(T)$ and $K_m^D(T)$, we selected the Arrhenius equations that best fit data from California[14] (mean annual $T = 17$ °C) and match values at 20 °C (0.42 and 600, respectively)[11]. For the uptake kinetic parameters, we obtained $v_{max}^U(T)$ by selecting v_0^U that best fits the Arrhenius equation in ref. 11 with $E_v^U = 35$ and we obtained $K_m^U(T)$ by selecting K_0^U and E_K^U that best fit the linear relation used in ref. 11. To parametrize the temperature-dependent mortality ($d_{M,ref}$, T_{ref}) and MGE ($\gamma_{M,ref}$, m, T_{ref}) models, we used values from ref. 13 and tested two values of E_{dM} ($E_{dM} = 0$ is the enzyme only temperature-dependent model). For greater realism, we used a higher value of the exoenzyme deactivation rate (twice the value used in ref. 11) and constrained the range of all parameters in order to enhance stability and produce relative stock sizes that are consistent with empirical data, so that at equilibrium M is about 1% of C, Z is about 1% of M and D is limiting (hence close to 0 at equilibrium[49,50]),

We analysed the model sensitivity by varying parameters over two orders of magnitude (as in ref. 11) – except γ_M and γ_Z for which we used the whole range over which the non-trivial ecosystem equilibrium is stable (Extended Data Table 2). To assess the significance of our findings for real ecosystems, we focused on five biomes for which empirical data[14] could be used to constrain the model. The five biomes contrast strongly in their initial temperature, T_0, and decomposition kinetics, $v_{max}^D(T)$ and $K_m^D(T)$ for which we selected the Arrhenius equations (2) that best fit the relations used in ref. 14 (Extended Data Table 3).

References

1. Falkowski, P. G., Fenchel, T. & Delong, E. F. The microbial engines that drive Earth's biogeochemical cycles. *Science* **320,** 1034–1039 (2008).
2. Waksman, S. A. & Starkey, R. L. *The soil and the microbe*. (John Wiley And Sons; New York, 1931).
3. Frey, S. D., Lee, J., Melillo, J. M. & Six, J. The temperature response of soil microbial efficiency and its feedback to climate. *Nat. Clim. Chang.* **3,** 395 (2013).
4. Singh, B. K., Bardgett, R. D., Smith, P. & Reay, D. S. Microorganisms and climate change: terrestrial feedbacks and mitigation options. *Nat. Rev. Microbiol.* **8,** 779–790 (2010).
5. Davidson, E. A. & Janssens, I. A. Temperature sensitivity of soil carbon decomposition and feedbacks to climate change. *Nature* **440,** 165–173 (2006).
6. Bradford, M. A. *et al.* Thermal adaptation of soil microbial respiration to elevated temperature. *Ecol. Lett.* **11,** 1316–1327 (2008).
7. Tucker, C. L., Bell, J., Pendall, E. & Ogle, K. Does declining carbon-use efficiency explain thermal acclimation of soil respiration with warming? *Glob. Chang. Biol.* **19,** 252–263 (2013).
8. Creamer, C. A. *et al.* Microbial community structure mediates response of soil C decomposition to litter addition and warming. *Soil Biol. Biochem.* **80,** 175–188 (2015).
9. Wei, H. *et al.* Thermal acclimation of organic matter decomposition in an artificial forest soil is related to shifts in microbial community structure. *Soil Biol. Biochem.* **71,** 1–12 (2014).
10. Fussmann, G. F., Loreau, M. & Abrams, P. A. Eco-evolutionary dynamics of communities and ecosystems. *Funct. Ecol.* **21,** 465–477 (2007).
11. Allison, S. D., Wallenstein, M. D. & Bradford, M. A. Soil-carbon response to warming dependent on microbial physiology. *Nat. Geosci.* **3,** 336 (2010).
12. Li, J., Wang, G., Allison, S. D., Mayes, M. A. & Luo, Y. Soil carbon sensitivity to

temperature and carbon use efficiency compared across microbial-ecosystem models of varying complexity. *Biogeochemistry* **119,** 67–84 (2014).

13. Hagerty, S. B. *et al.* Accelerated microbial turnover but constant growth efficiency with warming in soil. *Nat. Clim. Chang.* **4,** 903 (2014).
14. German, D. P., Marcelo, K. R. B., Stone, M. M. & Allison, S. D. The Michaelis-Menten kinetics of soil extracellular enzymes in response to temperature: a cross-latitudinal study. *Glob. Chang. Biol.* **18,** 1468–1479 (2012).
15. Wang, G., Post, W. M. & Mayes, M. A. Development of microbial-enzyme-mediated decomposition model parameters through steady-state and dynamic analyses. *Ecol. Appl.* **23,** 255–272 (2013).
16. Vos, M., Wolf, A. B., Jennings, S. J. & Kowalchuk, G. A. Micro-scale determinants of bacterial diversity in soil. *FEMS Microbiol. Rev.* **37,** 936–954 (2013).
17. Young, I. M., Crawford, J. W., Nunan, N., Otten, W. & Spiers, A. Chapter 4 Microbial Distribution in Soils: Physics and Scaling. in *Advances in Agronomy* **100,** 81–121 (Academic Press, 2008).
18. Padfield, D., Yvon-Durocher, G., Buckling, A., Jennings, S. & Yvon-Durocher, G. Rapid evolution of metabolic traits explains thermal adaptation in phytoplankton. *Ecol. Lett.* **19,** 133–142 (2016).
19. Schaum, C.-E. *et al.* Adaptation of phytoplankton to a decade of experimental warming linked to increased photosynthesis. *Nat Ecol Evol* **1,** 94 (2017).
20. Monroe, J. G. *et al.* Ecoevolutionary Dynamics of Carbon Cycling in the Anthropocene. *Trends Ecol. Evol.* **33,** 213–225 (2018).
21. Ratledge, C. Biodegradation of oils, fats and fatty acids. in *Biochemistry of microbial degradation* (ed. Ratledge, C.) 89–141 (Springer Netherlands, 1994).
22. Harder, W. & Dijkhuizen, L. Physiological responses to nutrient limitation. *Annu. Rev. Microbiol.* **37,** 1–23 (1983).
23. Velicer, G. J. Social strife in the microbial world. *Trends Microbiol.* **11,** 330–337 (2003).

24. Trivedi, P. *et al.* Microbial regulation of the soil carbon cycle: evidence from gene-enzyme relationships. *ISME J.* **10,** 2593–2604 (2016).
25. Rainey, P. B. & Rainey, K. Evolution of cooperation and conflict in experimental bacterial populations. *Nature* **425,** 72–74 (2003).
26. Sinsabaugh, R. L. & Moorhead, D. L. Resource allocation to extracellular enzyme production: A model for nitrogen and phosphorus control of litter decomposition. *Soil Biol. Biochem.* **26,** 1305–1311 (1994).
27. Allison, S. D. A trait-based approach for modelling microbial litter decomposition. *Ecol. Lett.* **15,** 1058–1070 (2012).
28. Wallenstein, M. D., Mcmahon, S. K. & Schimel, J. P. Seasonal variation in enzyme activities and temperature sensitivities in Arctic tundra soils. *Glob. Chang. Biol.* **15,** 1631–1639 (2009).
29. Burns, R. G. *et al.* Soil enzymes in a changing environment: Current knowledge and future directions. *Soil Biol. Biochem.* **58,** 216–234 (2013).
30. Hochachka, P. W. & Somero, G. N. *Biochemical Adaptation: Mechanism and Process in Physiological Evolution*. (Oxford University Press, 2002).
31. Wieder, W. R., Bonan, G. B. & Allison, S. D. Global soil carbon projections are improved by modelling microbial processes. *Nat. Clim. Chang.* **3,** 909 (2013).
32. Sinsabaugh, R. L., Manzoni, S., Moorhead, D. L. & Richter, A. Carbon use efficiency of microbial communities: stoichiometry, methodology and modelling. *Ecol. Lett.* **16,** 930–939 (2013).
33. Follows, M. J., Dutkiewicz, S., Grant, S. & Chisholm, S. W. Emergent biogeography of microbial communities in a model ocean. *Science* **315,** 1843–1846 (2007).
34. Trivedi, P., Anderson, I. C. & Singh, B. K. Microbial modulators of soil carbon storage: integrating genomic and metabolic knowledge for global prediction. *Trends Microbiol.* **21,** 641–651 (2013).
35. Schimel, J. P. & Weintraub, M. N. The implications of exoenzyme activity on microbial carbon and nitrogen limitation in soil: a theoretical model. *Soil Biol.*

Biochem. **35,** 549–563 (2003).

36. Harte, J. & Kinzig, A. P. Mutualism and competition between plants and decomposers: implications for nutrient allocation in ecosystems. *Am. Nat.* **141,** 829–846 (1993).
37. Kaiser, C., Franklin, O., Dieckmann, U. & Richter, A. Microbial community dynamics alleviate stoichiometric constraints during litter decay. *Ecol. Lett.* **17,** 680–690 (2014).
38. Kaiser, C., Franklin, O., Richter, A. & Dieckmann, U. Social dynamics within decomposer communities lead to nitrogen retention and organic matter build-up in soils. *Nat. Commun.* **6,** 8960 (2015).
39. Abramoff, R. *et al.* The Millennial model: in search of measurable pools and transformations for modeling soil carbon in the new century. *Biogeochemistry* **137,** 51–71 (2018).
40. Bradford, M. A. *et al.* Managing uncertainty in soil carbon feedbacks to climate change. *Nat. Clim. Chang.* **6,** 751 (2016).
41. Schmidt, M. W. I. *et al.* Persistence of soil organic matter as an ecosystem property. *Nature* **478,** 49–56 (2011).
42. Treseder, K. K. *et al.* Integrating microbial ecology into ecosystem models: challenges and priorities. *Biogeochemistry* **109,** 7–18 (2012).
43. Stone, M. M. *et al.* Temperature sensitivity of soil enzyme kinetics under N-fertilization in two temperate forests. *Glob. Chang. Biol.* **18,** 1173–1184 (2012).
44. Allison, S. D. Cheaters, diffusion and nutrients constrain decomposition by microbial enzymes in spatially structured environments: Constraints on enzymatic decomposition. *Ecol. Lett.* **8,** 626–635 (2005).
45. Nadell, C. D., Drescher, K. & Foster, K. R. Spatial structure, cooperation and competition in biofilms. *Nat. Rev. Microbiol.* **14,** 589–600 (2016).
46. Ferriere, R. & Legendre, S. Eco-evolutionary feedbacks, adaptive dynamics and evolutionary rescue theory. *Philos. Trans. R. Soc. Lond. B Biol. Sci.* **368,** 20120081 (2013).

47. Durrett, R. & Levin, S. The Importance of Being Discrete (and Spatial). *Theor. Popul. Biol.* **46,** 363–394 (1994).
48. Chao, L. & Levin, B. R. Structured habitats and the evolution of anticompetitor toxins in bacteria. *Proc. Natl. Acad. Sci. U. S. A.* **78,** 6324–6328 (1981).
49. Fierer, N., Strickland, M. S., Liptzin, D., Bradford, M. A. & Cleveland, C. C. Global patterns in belowground communities. *Ecol. Lett.* **12,** 1238–1249 (2009).
50. Ladd, J. N., Amato, M., Zhou, L.-K. & Schultz, J. E. Differential effects of rotation, plant residue and nitrogen fertilizer on microbial biomass and organic matter in an Australian alfisol. *Soil Biol. Biochem.* **26,** 821–831 (1994).

End Notes

Acknowledgements We thank Rachel Gallery, Pierre-Henri Gouyon, Moira Hough, Hélène Leman, Laura Meredith, and Mitch Pavao-Zuckerman for discussion. E.A. was supported by fellowships from Ecole Doctorale Frontières du Vivant and MemoLife Laboratory of Excellence (PIA-10-LBX-54). S.R.S. was supported by a grant from the Genomic Science Program of the United States Department of Energy (DOE) (DE-SC0016440) and the University of Arizona's Agnese Nelms Haury Program in Environment and Social Justice. R.F. acknowledges support from FACE Partner University Fund, CNRS Mission pour l'Interdisciplinarité, and PSL University (IRIS OCAV and PSL-University of Arizona Mobility Program).

Author contributions R.F. conceived the study. All authors developed the model. E.A. performed the analysis. E.A. and R.F. wrote the first version of the manuscript. All authors finalized the paper.

Competing interests The authors declare no competing interests.

Additional information

Extended data is available for this paper at https://doi.org/xxx

Supplementary information is available for this paper at https://doi.org/xxx

Correspondence and requests for materials should be addressed to E.A. or R.F.

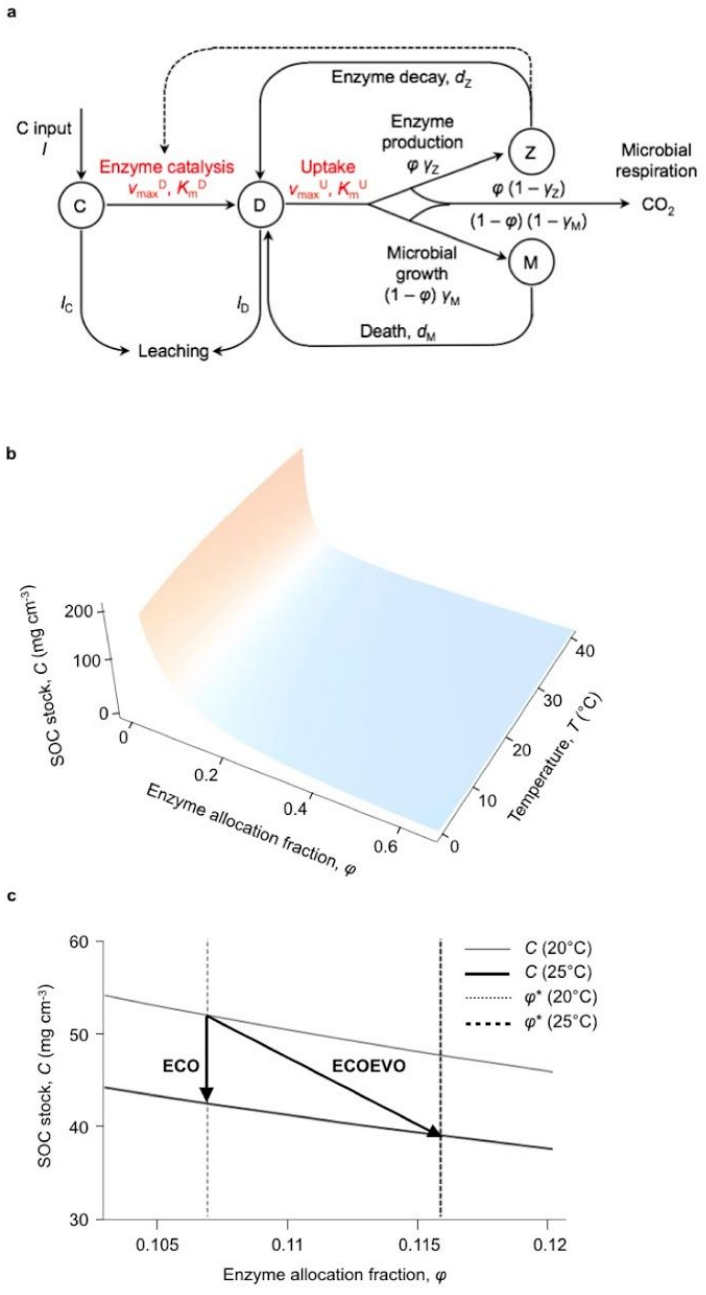

Figure 1. Effect of temperature and enzyme allocation fraction on SOC ecological equilibrium. **a**, Structure of the microbial-enzyme ecological model (see Methods for details): SOC stock is the balance of plant input, *I*, and loss by exoenzyme-mediated degradation to DOC (*D*), which in turn is allocated between (fraction φ) production of

enzymes (Z) and (fraction $1-\varphi$) growth of microbial biomass (M). **b**, Effect of temperature and enzyme allocation fraction, φ, on SOC equilibrium, C, in the baseline scenario of temperature dependence. **c**, Response of SOC ecological equilibrium, C, to a 5°C increase in temperature (from 20 °C to 25 °C) as a function of enzyme allocation fraction, φ. Parameters are set to their default values (Extended Data Table 1), except $I = 5\ 10^{-3}$, $v_0^U = 10^5$, $E_v^U = 38$ and $c_0 = 1.17$.

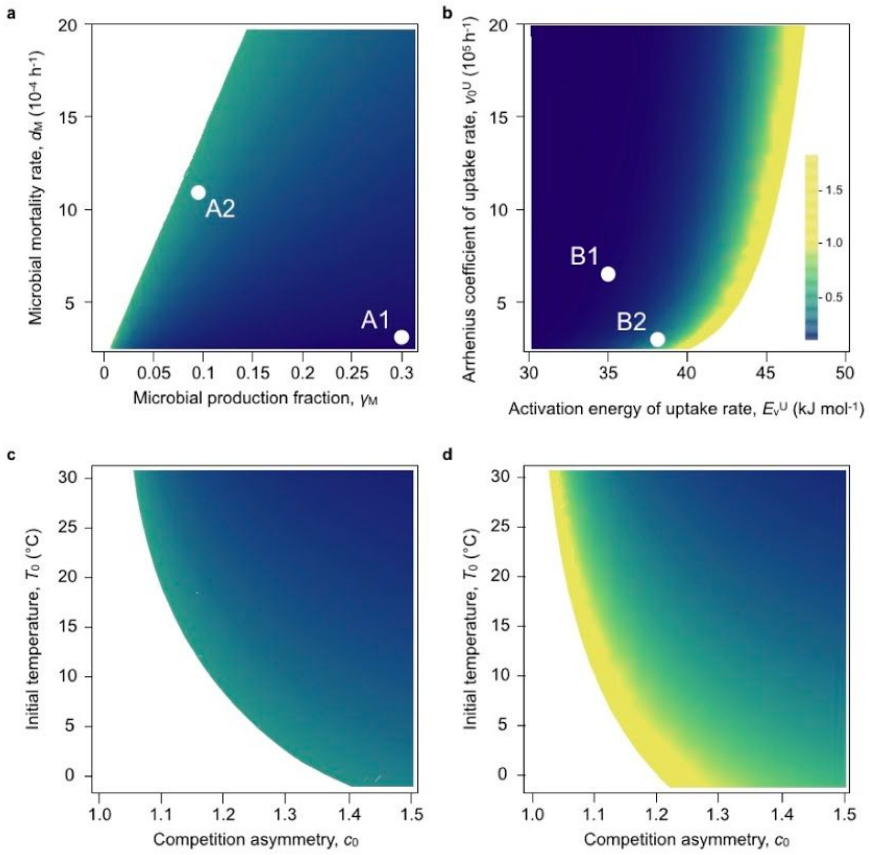

Figure 2. Effect of microbial evolutionary adaptation on the SOC equilibrium response to + 5 °C warming (EVO effect). Temperature influences enzyme kinetics only (baseline scenario of temperature dependence). **a**, Influence of microbial biomass production efficiency, γ_M, and microbial mortality rate, d_M. **b**, Influence of microbial resource acquisition traits v_0^U and E_v^U. **c-d**, Influence of competition asymmetry, c_0, and initial temperature, T_0. In all figures, constant parameters are set to their default values (Extended Data Table 1) and I is set to 5 10^{-3}. Points A1 and B1 indicate the default parameter values. Point A2 (respectively B2) exemplifies values of γ_M and d_M (resp. v_0^U and E_v^U) for which the EVO effect is strong. Panel **c** (resp. **d**) shows the influence of c_0 and T_0 on the EVO effect at A2 (resp. B2).

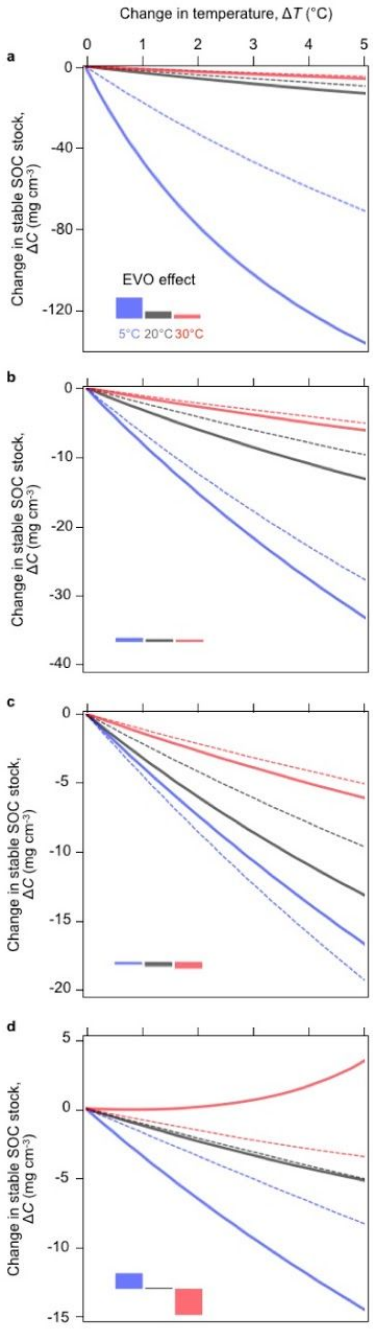

Figure 3. Ecological and eco-evolutionary responses of SOC equilibrium to warming (up to + 5 °C) for three scenarios of temperature dependence. Ecological and eco-evolutionary changes in SOC equilibrium C given by Eq. (3a) (without evolution, dashed curves) and Eq. (3b) (with evolution, plain curves) are plotted as a function of the increase in temperature. *Blue curves*, initial temperature T_0 = 5°C. *Black curves*, $T_0 = T_{\text{ref}}$ = 20°C. *Red curves*, T_0 = 30°C. *Insets*, Direction and magnitude of EVO effect (%), from - 150 % to + 150 %, color code indicates T_0 as before. **a**, Baseline scenario of temperature dependence (enzyme kinetics only). **b**, Temperature-dependent microbial turnover, with $E_{\text{dM}} = 25 < E_v^U$. **c**, Temperature-dependent microbial turnover, with $E_{\text{dM}} = 55 > E_v^U$. **d**, Temperature-dependent MGE, with m = - 0.014. Parameters values correspond to point B2 in Fig. 2 ($I = 5\ 10^{-3}$, $v_0^U = 10^5$, $E_v^U = 38$, $c_0 = 1.17$); other parameters are set to their default values (Extended Data Table 1).

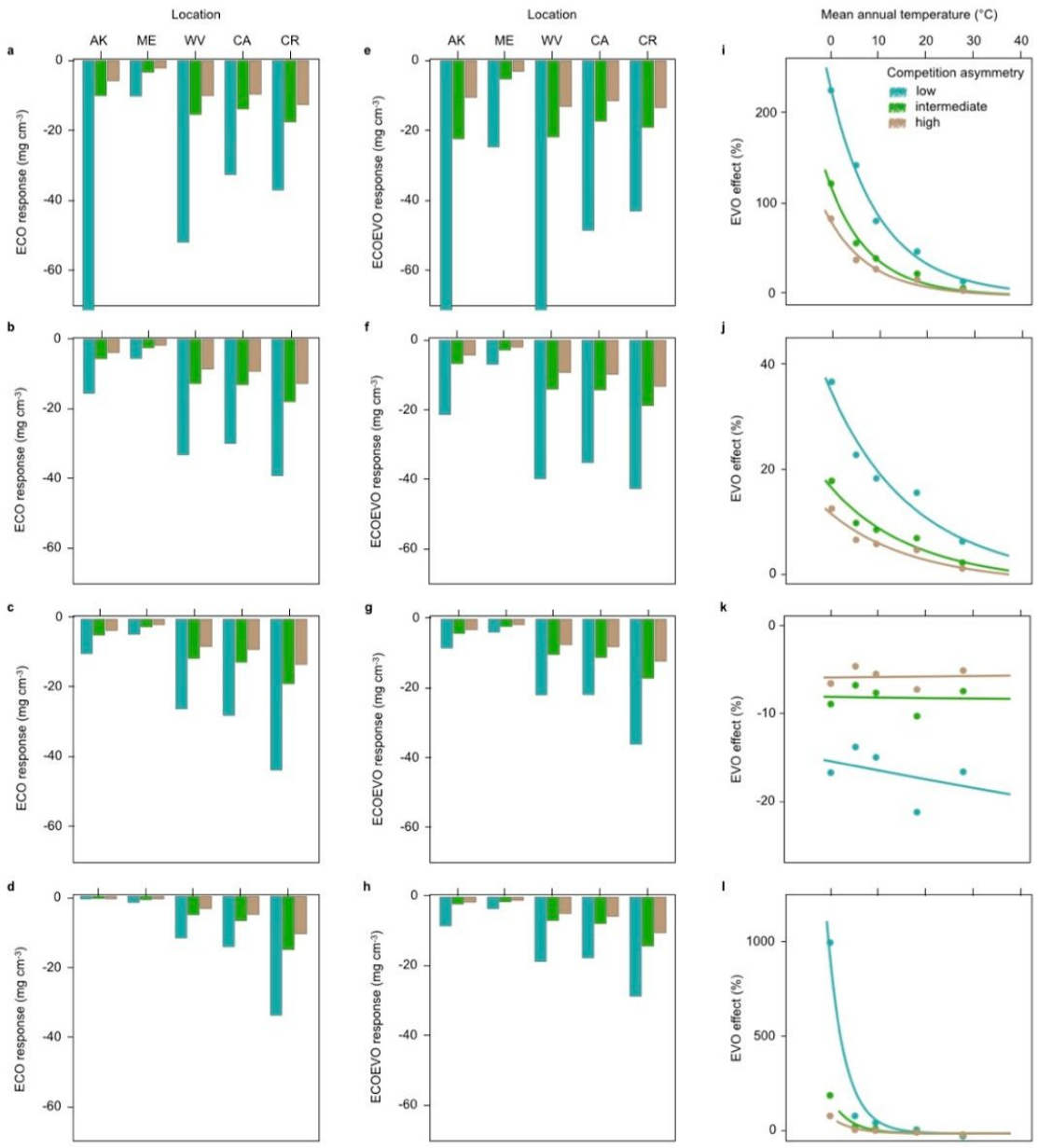

Figure 4. Ecological and eco-evolutionary responses of SOC equilibrium to + 5 °C warming predicted for five biomes. a-d, ECO response. **e-h**, ECOEVO response. **i-l,** EVO effect. AK: Alaska, boreal forest, T_0 = 0.1°C. ME: Maine, temperate forest, T_0 = 5°C. WV: West Virginia, temperate forest, T_0 = 9°C. CA: California, temperate grassland, T_0 =

17°C. CR: Costa Rica, tropical rain forest, T_0 = 26°C. First column (**a, e, i**): baseline scenario of temperature dependence. Second column (**b, f, j**): temperature-dependent microbial turnover scenario with $E_{\mathrm{dM}} = 25 < E_v^U$. Third column (*c*, *g*, *k*): temperature-dependent microbial turnover scenario with $E_{\mathrm{dM}} = 55 > E_v^U$. Fourth column (**d, h, l**): temperature-dependent MGE scenario (*m* = - 0.014). The influence of competition asymmetry, c_0, is shown. For clarity, vertical axis for ECO and ECOEVO responses are truncated at - 65 mg C cm^{-3}. Actual values for AK with c_0 = 1.17 are ECO = - 170 mg C cm^{-3} and ECOEVO = - 556 mg C cm^{-3} ; actual value for WV with c_0 = 1.17 is ECOEVO = - 92.8 mg C cm^{-3}. Parameters values correspond to point B2 in Fig. 2 ($I = 5\ 10^{-3}$, $v_0^U = 10^5$, $E_v^U = 38$, $c_0 = 1.17$); other parameters are set to their default values (Extended Data Table 1).

Extended Data Table 1. Default parameter values.

Parameter	Unit	Description	Default value
T_0, T_{ref}	°C	initial temperature	20
φ		enzyme allocation fraction	0.1
γ_M, $\gamma_{M,ref}$		microbial growth efficiency	0.3, 0.31
γ_Z		enzyme production efficiency	0.4
d_M, $d_{M,ref}$	h^{-1}	microbial mortality rate	$2\ 10^{-4}$
d_Z	h^{-1}	enzyme deactivation rate	$2\ 10^{-3}$
v_0^U	mg D cm^{-3} (mg M cm^{-3})$^{-1}$ h^{-1}	Arrhenius coefficient of uptake rate	$7.3\ 10^5$
v_0^D	mg C cm^{-3} (mg Z cm^{-3})$^{-1}$ h^{-1}	Arrhenius coefficient of decomposition rate	$1.15\ 10^6$
K_0^U	mg D cm^{-3}	Arrhenius coefficient of uptake half-saturation constant	$1.6\ 10^3$
K_0^D	mg C cm^{-3}	Arrhenius coefficient of decomposition half-saturation constant	$3.3\ 10^4$
E_v^U	kJ mol^{-1}	activation energy of uptake rate	35
E_v^D	kJ mol^{-1}	activation energy of decomposition rate	36.1
E_K^U	kJ mol^{-1}	activation energy of uptake half-saturation constant	21
E_K^D	kJ mol^{-1}	activation energy of decomposition half-saturation constant	9.7
E_{dM}	kJ mol^{-1}	activation energy of microbial turnover	0, 25, 55
I	mg C cm^{-3} h^{-1}	SOC input (litter)	$5\ 10^{-4}$
e_C	h^{-1}	SOC leaching rate	10^{-6}
e_D	h^{-1}	DOC leaching rate	10^{-2}

c_0		local competitive advantage to stronger exoenzyme producers (competition asymmetry)	1.1131
ΔT	°C	warming treatment	5

Extended Data Table 2. Sensitivity analysis of the ecological model. The table reports the absolute value of sensitivities.

Parameter	Low value	High value	Sensitivity (absolute value)				Qualitative effect on φ_{min}, φ_{max} and equilibrium C
			C	D	M	Z	
T	4.9	490	1.62	0.83	0.06	0.06	Lower φ_{min}, higher φ_{max}, C decreases especially for low values of T.
φ	0.19	0.95	0.97	1.75	1.75	0.98	C decreases especially for low values of φ.
γ_M	0.19	0.95	1.32	1	2.34	1.34	Lower φ_{min}, higher φ_{max}, C decreases especially for very high values of γ_M.
γ_Z	0.19	0.95	1.18	0	0.24	1.24	Lower φ_{min}, higher φ_{max}, C decreases strongly.
d_M	$3.8\ 10^{-6}$	$3.8\ 10^{-4}$	0.005	1	1.01	0.005	Higher φ_{min}, lower φ_{max}, C unchanged.
d_Z	$4.6\ 10^{-5}$	$4.6\ 10^{-3}$	1.05	0	0.07	1.07	Higher φ_{min}, lower φ_{max}, C increases strongly.
v_0^U	$2.1\ 10^5$	$2.1\ 10^7$	0.01	1	0.01	0.01	Lower φ_{min}, higher φ_{max}, C unchanged.
v_0^D	$5.1\ 10^5$	$5.1\ 10^7$	1.05	0	0.07	0.07	Lower φ_{min}, higher φ_{max}, C decreases strongly.
K_0^U	60	6000	0.01	1	0.01	0.01	Higher φ_{min}, lower φ_{max}, C unchanged.

K_0^D	900	$9\ 10^4$	1	0	0.08	0.08	Higher φ_{min}, lower φ_{max}, C increases strongly.
E_v^U	0.38	38	0.01	3.35	0.01	0.01	Higher φ_{min}, lower φ_{max}, C unchanged.
E_v^D	0.38	38	3.4	0	0.07	0.07	Higher φ_{min}, lower φ_{max}, C increases strongly.
E_K^U	18	1800	0.01	159	0.01	0.01	Lower φ_{min}, higher φ_{max}, C unchanged.
E_K^D	7.3	730	7.58	0	0.08	0.08	Lower φ_{min}, higher φ_{max}, C decreases strongly.
I	$2.8\ 10^{-4}$	$2.8\ 10^{-2}$	0.005	0	1.05	1.05	Lower φ_{min}, higher φ_{max}, C unchanged.
e_C	$5\ 10^{-8}$	$5\ 10^{-6}$	0.003	0	0.18	0.18	Higher φ_{min}, lower φ_{max}, C unchanged.
e_D	$3.8\ 10^{-4}$	$3.8\ 10^{-2}$	0.01	0	0.01	0.01	Higher φ_{min}, lower φ_{max}, C unchanged.
c_0	1.1	25	0.75	1	0.99	0.76	C decreases especially for low values of c_0.

Extended Data Table 3. Arrhenius parameters for the five biomes studied in German *et al.* (2012)[14].

Parameter	Location				
	Alaska (AK)	Maine (ME)	West Virginia (WV)	California (CA)	Costa Rica (CR)
T_0	0	5	9	17	26
v_0^D	$7.7\ 10^7$	$7.73\ 10^9$	$1.35\ 10^8$	$1.15\ 10^6$	$1.23\ 10^8$
E_v^D	43.7	50.6	47.2	36.1	48.9
K_0^D	$2.79\ 10^7$	$2.1\ 10^7$	$3.1\ 10^6$	$3.3\ 10^4$	$4.4\ 10^3$
E_K^D	26.2	23.8	21.4	9.7	5.2

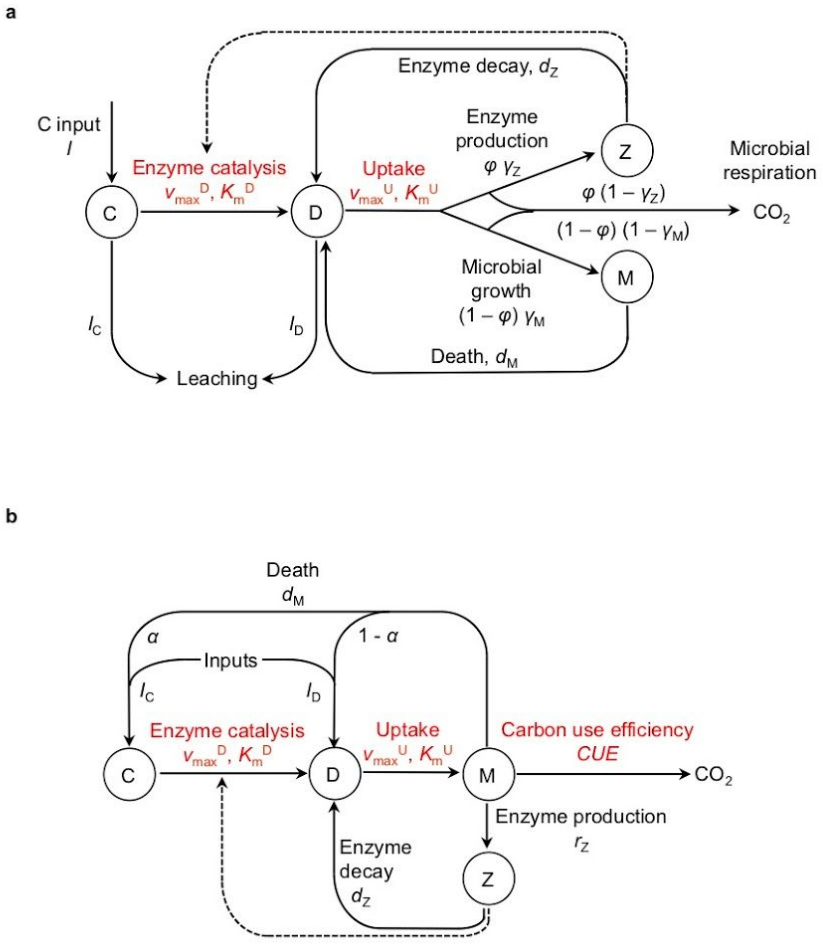

Extended Data Figure 1 | Structure of soil microbial decomposition models. a, Our model assumes dynamic allocation of assimilated carbon to enzyme production, whereas in **b**, Allison *et al.* (2010)'s model[11], enzymes are produced at a constant rate.

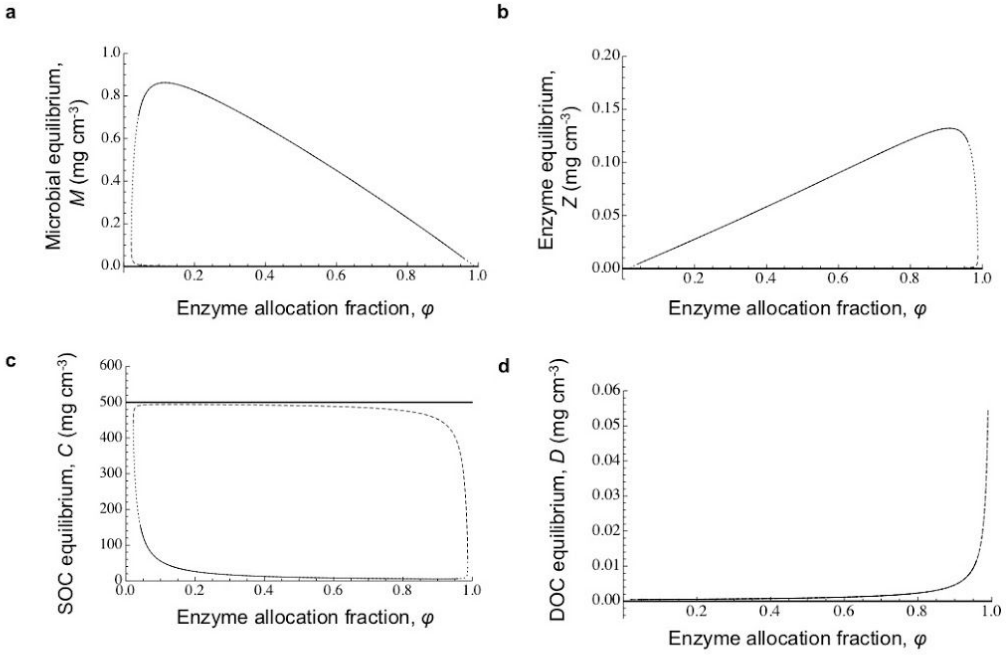

Extended Data Figure 2 | The three ecological equilibria. Effect of enzyme allocation fraction, φ, on equilibrium existence and stability. *Thick line*, trivial stable equilibrium. *Dashed curve*, unstable equilibrium. *Plain curve*, non trivial stable equilibrium. *Dotted curve*, unstable equilibrium inside stable limit cycle. **a**, Microbial biomass (M). **b**, Exoenzyme concentration (Z). **c**, SOC concentration (C). **d**, DOC concentration (D). All state variables are measured in unit mass of carbon. Parameters are set to their default values (Extended Data Table 1).

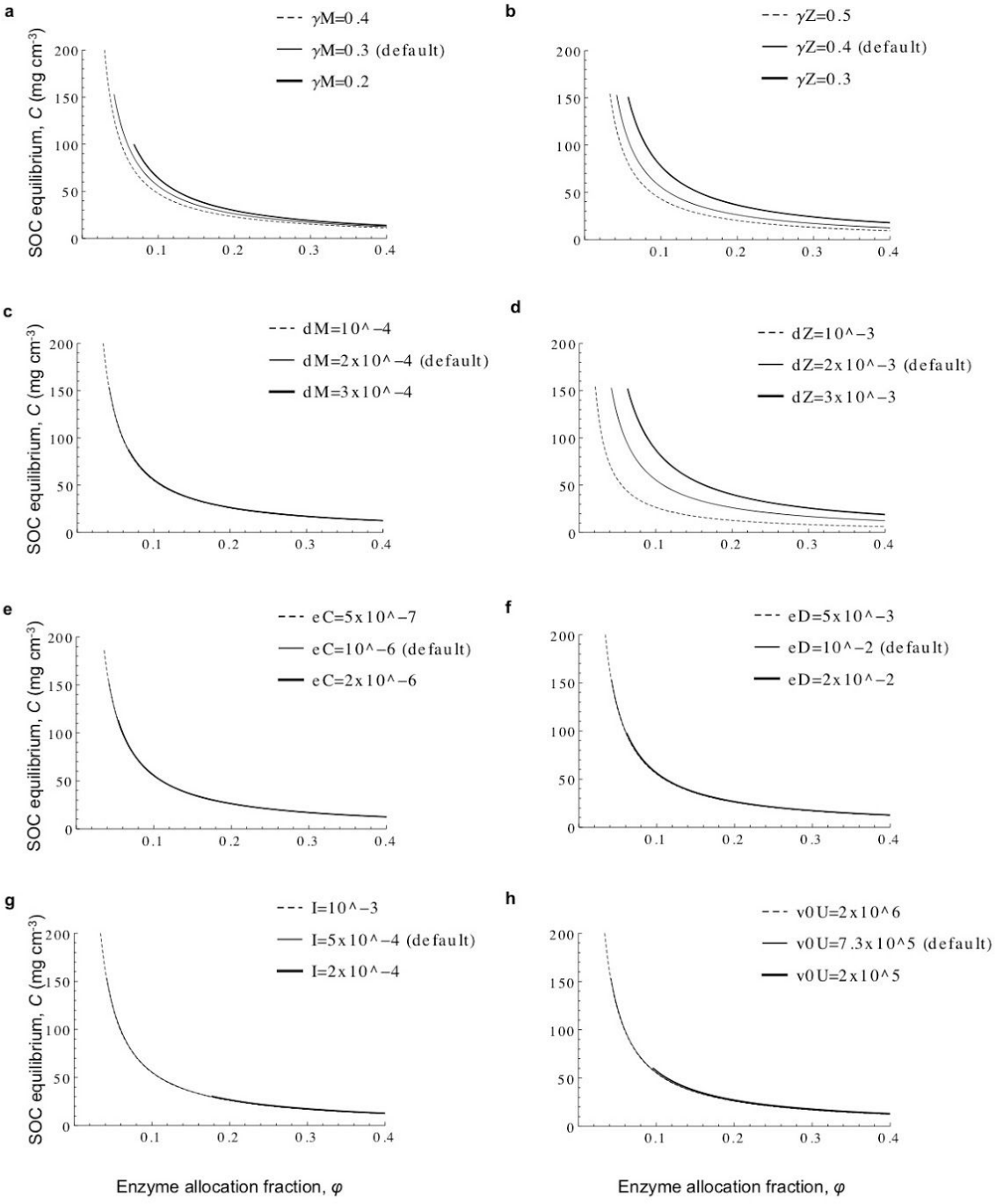
a
γM=0.4
γM=0.3 (default)
γM=0.2
b
γZ=0.5
γZ=0.4 (default)
γZ=0.3
c
dM=10^−4
dM=2x10^−4 (default)
dM=3x10^−4
d
dZ=10^−3
dZ=2x10^−3 (default)
dZ=3x10^−3
e
eC=5x10^−7
eC=10^−6 (default)
eC=2x10^−6
f
eD=5x10^−3
eD=10^−2 (default)
eD=2x10^−2
g
I=10^−3
I=5x10^−4 (default)
I=2x10^−4
h
v0U=2x10^6
v0U=7.3x10^5 (default)
v0U=2x10^5
SOC equilibrium, C (mg cm-3)
0
50
100
150
200
0.1
0.2
0.3
0.4
Enzyme allocation fraction, φ

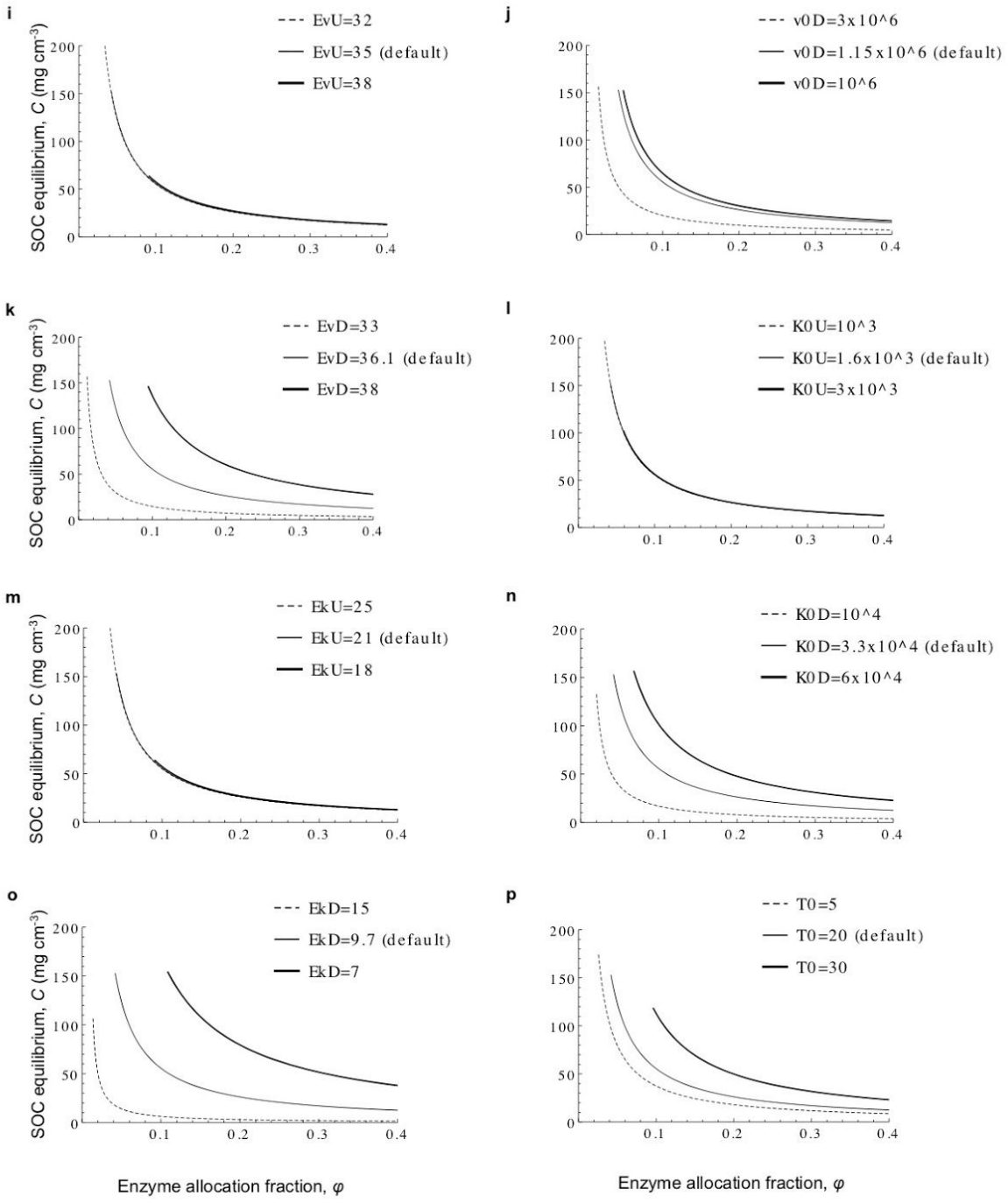

Extended Data Figure 3 | Parameter influence on the dependence of equilibrium *C* on enzyme allocation fraction, *φ*. **a**, Microbial growth efficiency, γ_M. **b**, Enzyme production efficiency, γ_Z. **c**, Microbial mortality rate, d_M. **d**, Enzyme deactivation rate, d_Z. **e**, SOC leaching

rate, e_C. **f**, DOC leaching rate, e_D. **g**, SOC input (litter), I. **h**, Arrhenius coefficient of uptake rate, v_0^U. **i**, Activation energy of uptake rate, E_v^U. **j**, Arrhenius coefficient of decomposition rate, v_0^D. **k**, Activation energy of decomposition rate, E_v^D. **l**, Arrhenius coefficient of uptake half-saturation constant, K_0^U. **m**, Activation energy of uptake half-saturation constant, E_K^U. **n**, Arrhenius coefficient of decomposition half-saturation constant, K_0^D. **o**, Activation energy of decomposition half-saturation constant, E_K^D. **p**, Initial temperature, T_0. Two parameter values (thick and dashed curves) are tested around the default value (plain curve). Other parameters are set to their default values (Extended Data Table 1).

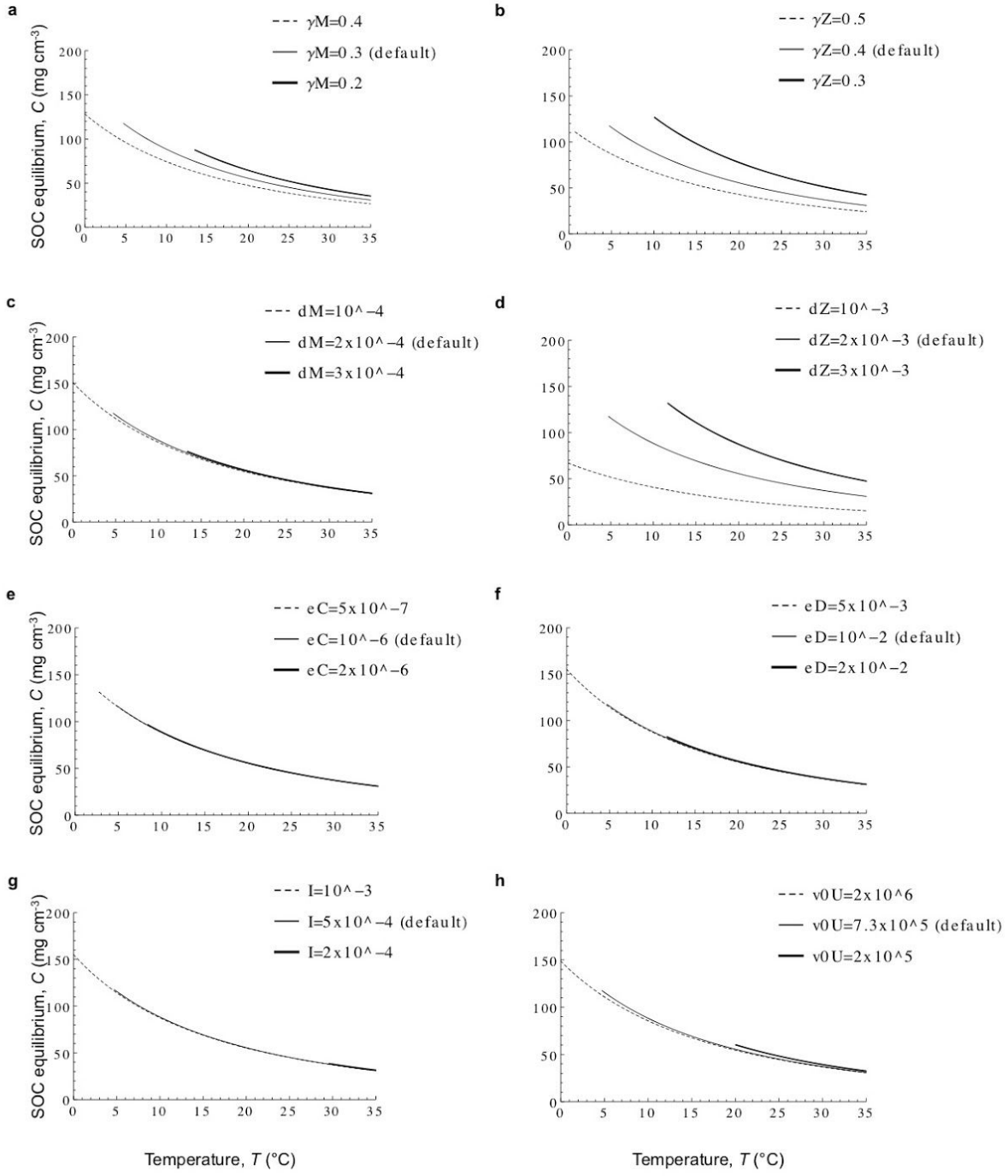
a
γM=0.4
γM=0.3 (default)
γM=0.2
b
γZ=0.5
γZ=0.4 (default)
γZ=0.3
c
dM=10^−4
dM=2x10^−4 (default)
dM=3x10^−4
d
dZ=10^−3
dZ=2x10^−3 (default)
dZ=3x10^−3
e
eC=5x10^−7
eC=10^−6 (default)
eC=2x10^−6
f
eD=5x10^−3
eD=10^−2 (default)
eD=2x10^−2
g
I=10^−3
I=5x10^−4 (default)
I=2x10^−4
h
v0U=2x10^6
v0U=7.3x10^5 (default)
v0U=2x10^5
SOC equilibrium, C (mg cm-3)
Temperature, T (°C)

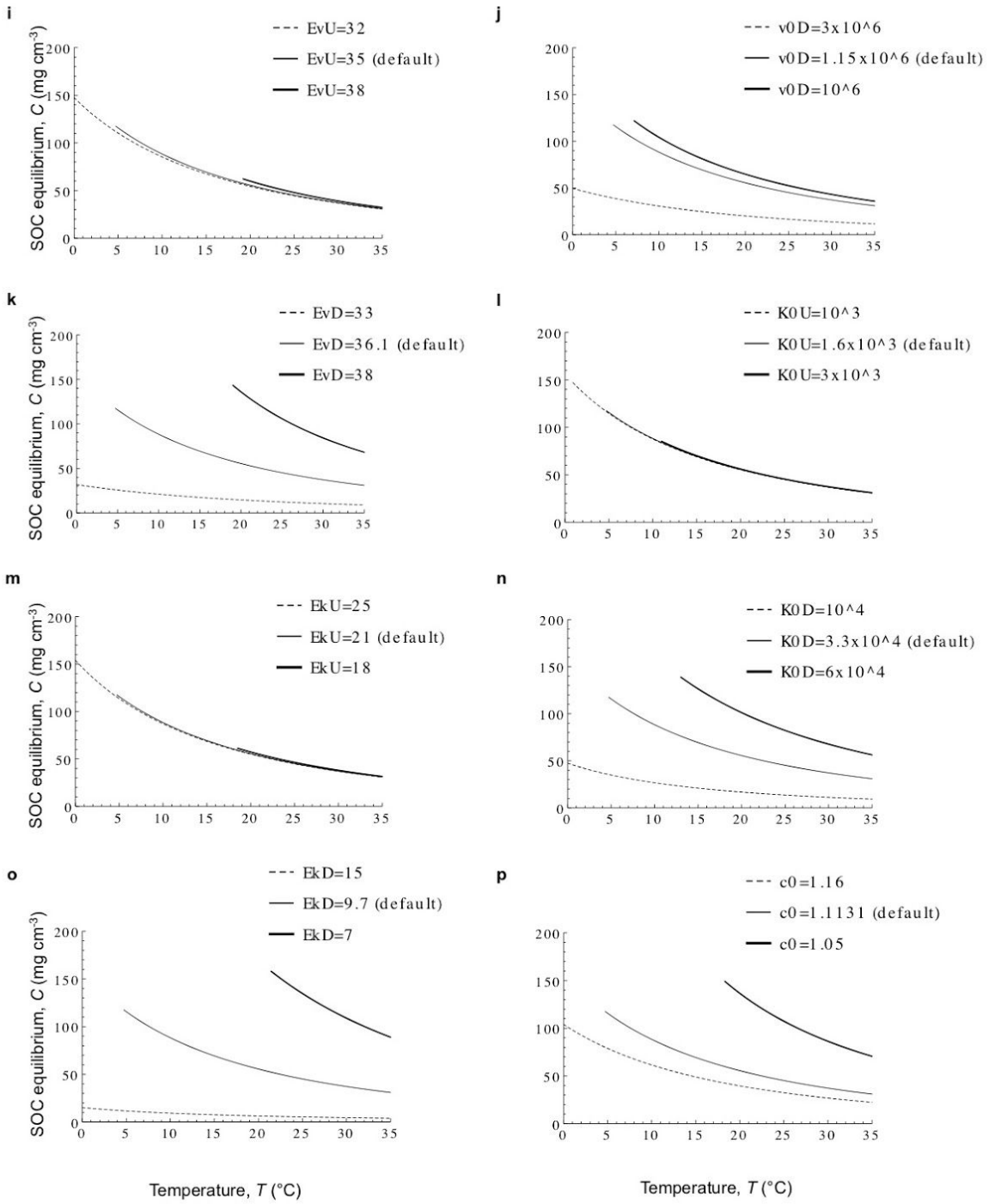

Extended Data Figure 4 | Parameter influence on the dependence of equilibrium *C* on temperature, *T*. Baseline 'kinetics-only' scenario of temperature dependence. **a**, Microbial growth efficiency, γ_M. **b**, Enzyme production efficiency, γ_Z. **c**, Microbial mortality rate, d_M. **d**,

Enzyme deactivation rate, d_Z. **e**, SOC leaching rate, e_C. **f**, DOC leaching rate, e_D. **g**, SOC input (litter), I. **h**, Arrhenius coefficient of uptake rate, v_0^U. **i**, Activation energy of uptake rate, E_v^U. **j**, Arrhenius coefficient of decomposition rate, v_0^D. **k**, Activation energy of decomposition rate, E_v^D. **l**, Arrhenius coefficient of uptake half-saturation constant, K_0^U. **m**, Activation energy of uptake half-saturation constant, E_K^U. **n**, Arrhenius coefficient of decomposition half-saturation constant, K_0^D. **o**, Activation energy of decomposition half-saturation constant, E_K^D. **p**, Competition asymmetry, c_0. Two parameter values (thick and dashed curves) are tested around the default value (plain curve). For each parameter value, enzyme allocation fraction, φ, is equal to the adapted value, φ^*, at $T = 20°C$. Other parameters are set to their default values (Extended Data Table 1).

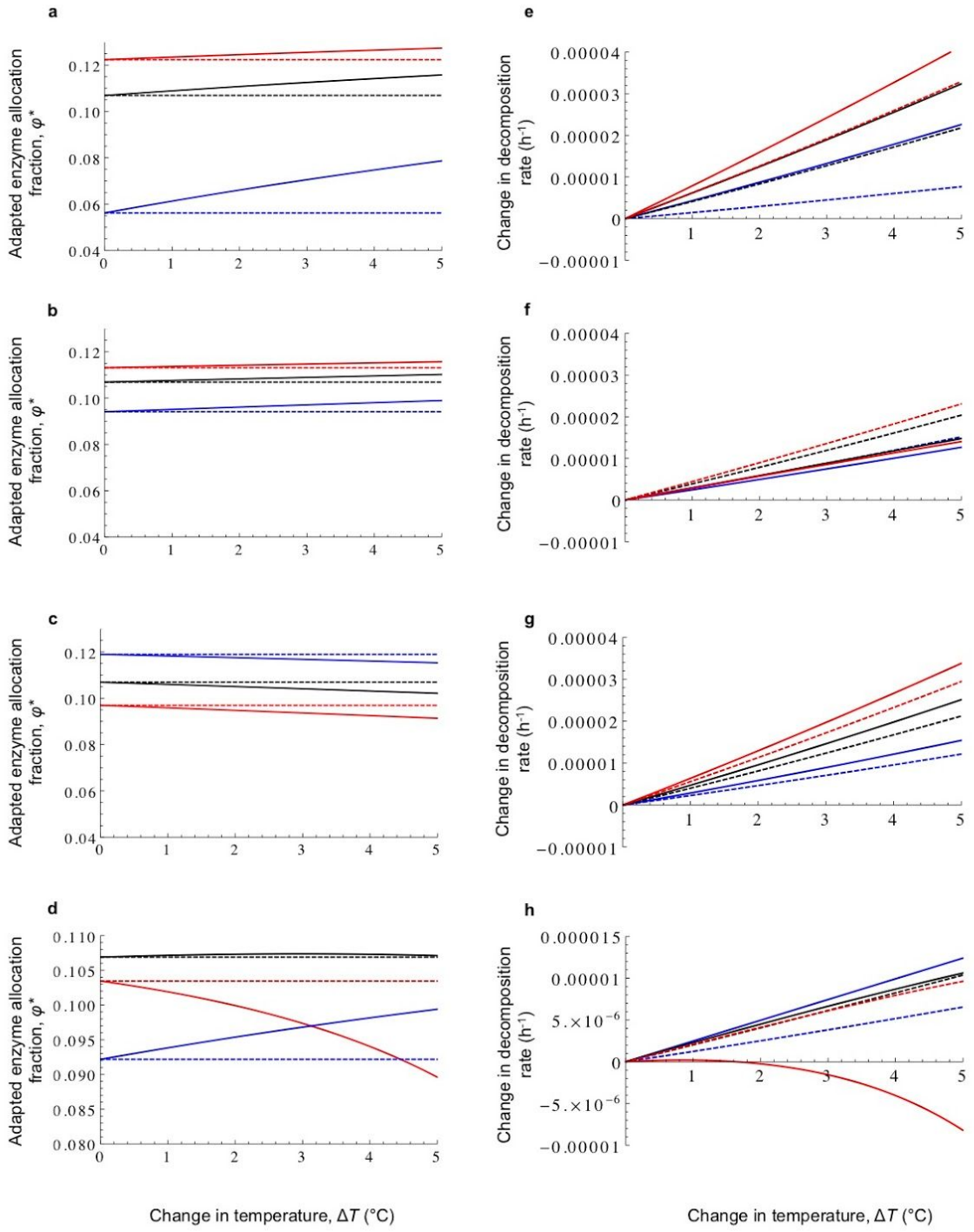

Extended Data Figure 5 | Ecological and eco-evolutionary responses of the adaptive enzyme allocation fraction, *φ (a-d), and decomposition rate (e-h) to warming for three scenarios of temperature dependence.** Ecological response (without evolution, dashed curves) and

eco-evolutionary response (with evolution, plain curves) are plotted as a function of the increase in temperature, up to + 5°C. *Blue curves*, initial temperature T_0 = 5°C. *Black curves*, $T_0 = T_{ref}$ = 20°C. *Red curves*, T_0 = 30°C. **(a, e)** Baseline 'kinetics only' scenario of temperature dependence. **(b, f)** Temperature-dependent microbial turnover, with $E_{dM} = 25 < E_v^U$. **(c, g)** Temperature-dependent microbial turnover, with $E_{dM} = 55 > E_v^U$. **(d, h)** Temperature-dependent MGE, with m = - 0.014. Parameters are set to their default values (Extended Data Table 1), except $I = 5\ 10^{-3}$, $v_0^U = 10^5$, $E_v^U = 38$, $c_0 = 1.17$.

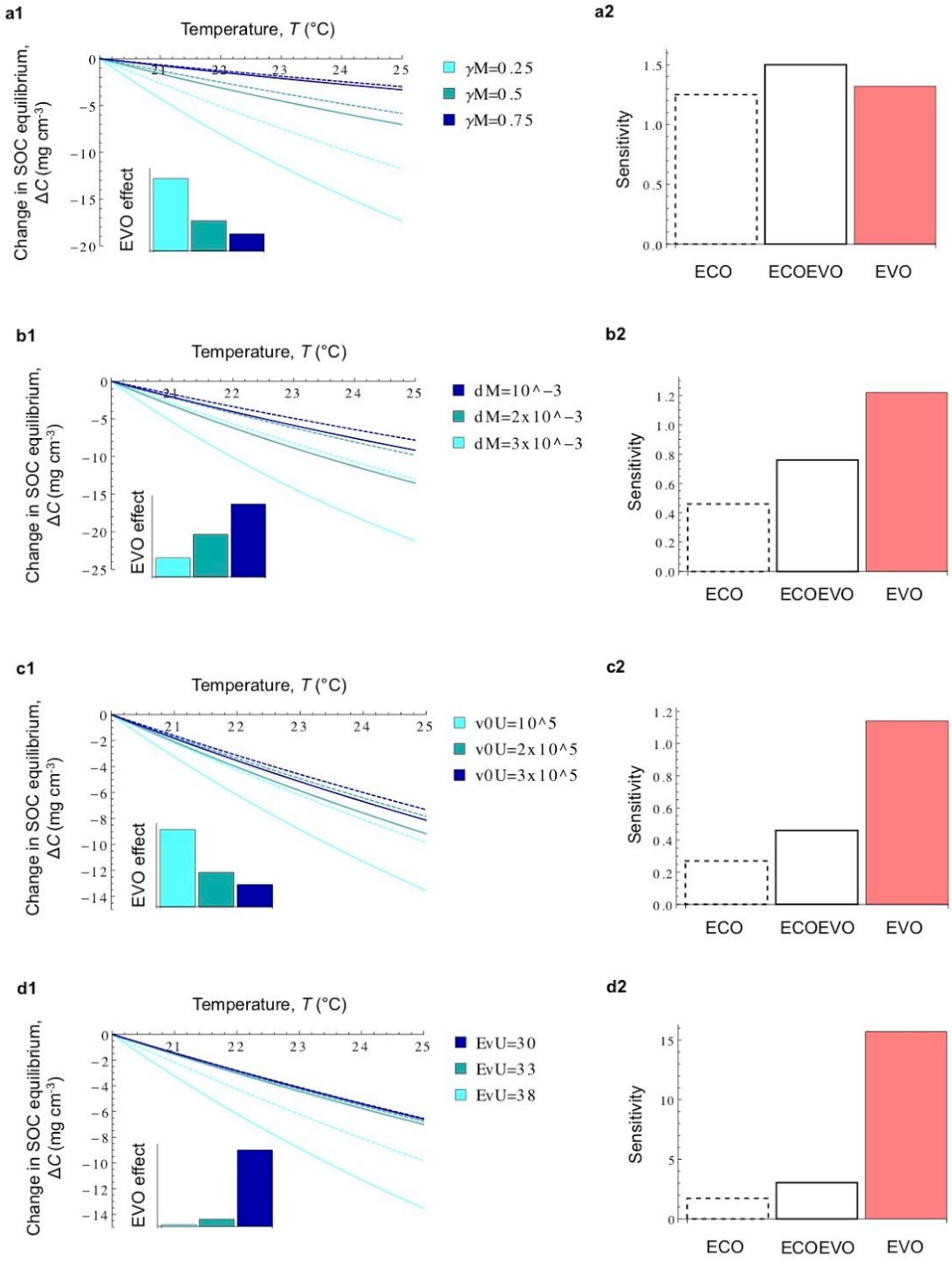
a1
Temperature, T (°C)
Change in SOC equilibrium, ΔC (mg cm-3)
γM=0.25
γM=0.5
γM=0.75
EVO effect
a2
Sensitivity
ECO
ECOEVO
EVO
b1
Temperature, T (°C)
Change in SOC equilibrium, ΔC (mg cm-3)
dM=10^-3
dM=2x10^-3
dM=3x10^-3
EVO effect
b2
Sensitivity
ECO
ECOEVO
EVO
c1
Temperature, T (°C)
Change in SOC equilibrium, ΔC (mg cm-3)
v0U=10^5
v0U=2x10^5
v0U=3x10^5
EVO effect
c2
Sensitivity
ECO
ECOEVO
EVO
d1
Temperature, T (°C)
Change in SOC equilibrium, ΔC (mg cm-3)
EvU=30
EvU=33
EvU=38
EVO effect
d2
Sensitivity
ECO
ECOEVO
EVO

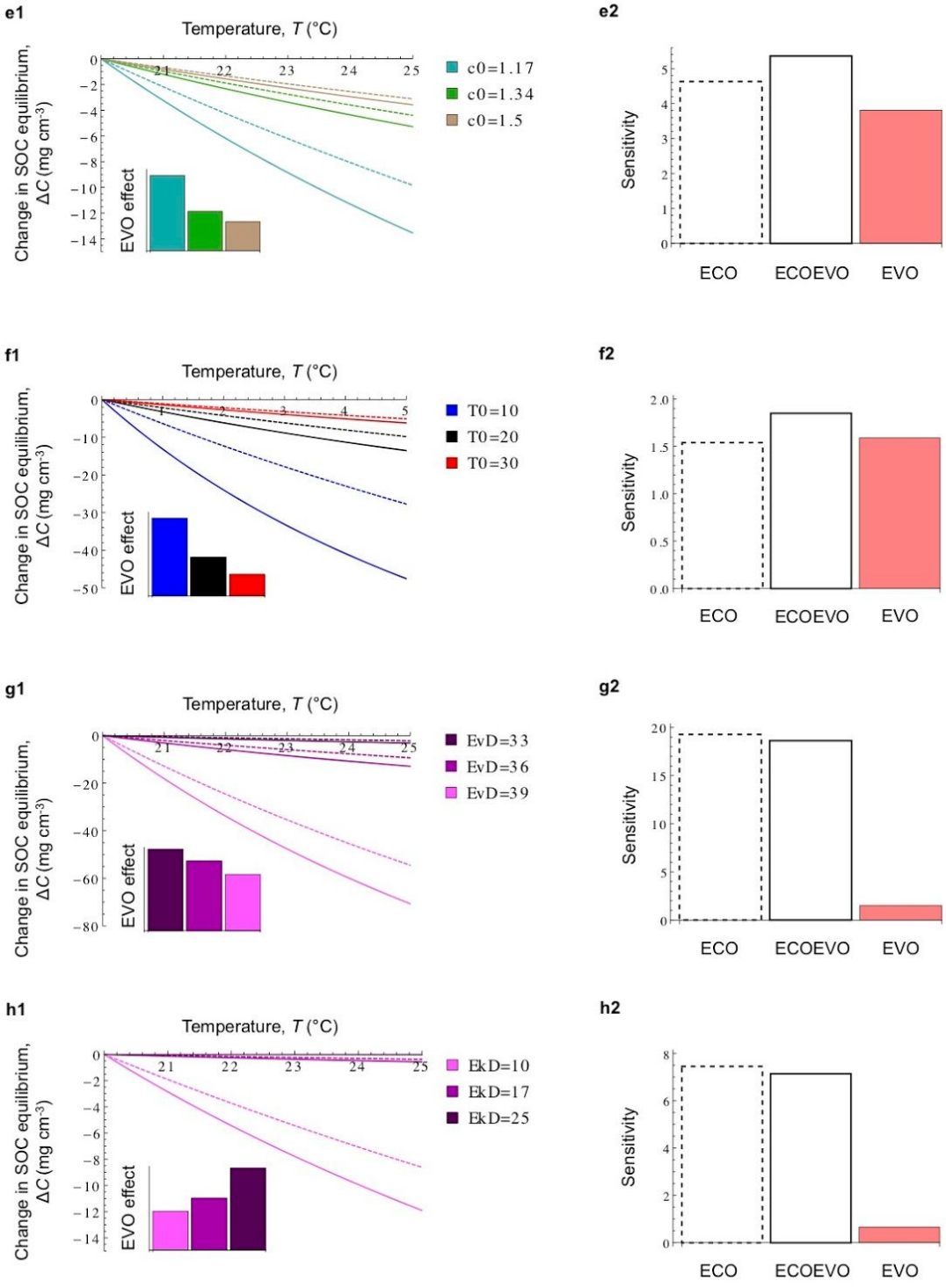
e1
Temperature, T (°C)
Change in SOC equilibrium, ΔC (mg cm-3)
c0=1.17
c0=1.34
c0=1.5
EVO effect
e2
Sensitivity
ECO
ECOEVO
EVO
f1
Temperature, T (°C)
Change in SOC equilibrium, ΔC (mg cm-3)
T0=10
T0=20
T0=30
EVO effect
f2
Sensitivity
ECO
ECOEVO
EVO
g1
Temperature, T (°C)
Change in SOC equilibrium, ΔC (mg cm-3)
EvD=33
EvD=36
EvD=39
EVO effect
g2
Sensitivity
ECO
ECOEVO
EVO
h1
Temperature, T (°C)
Change in SOC equilibrium, ΔC (mg cm-3)
EkD=10
EkD=17
EkD=25
EVO effect
h2
Sensitivity
ECO
ECOEVO
EVO

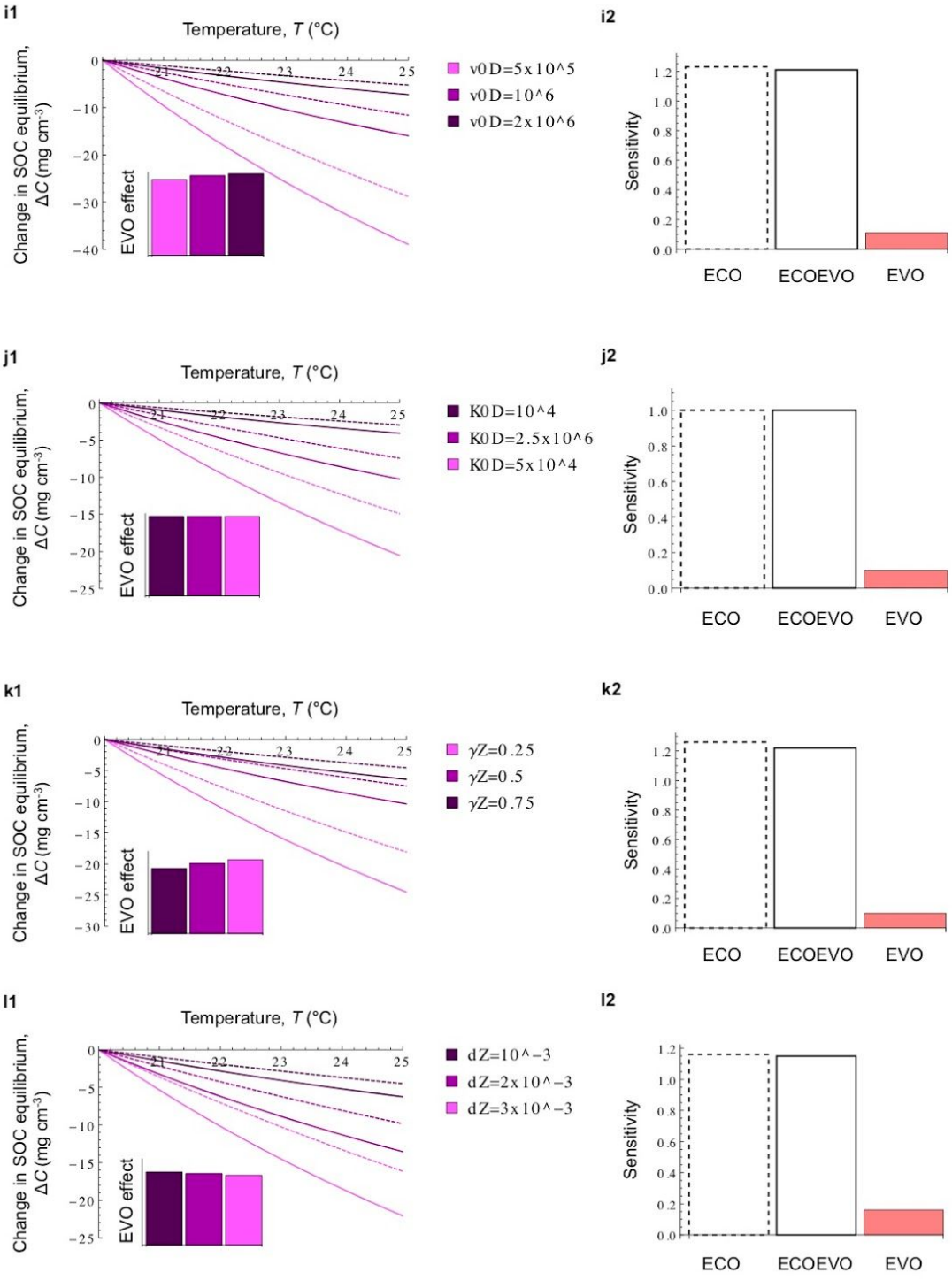
i1
Temperature, T (°C)
Change in SOC equilibrium, ΔC (mg cm-3)
EVO effect
v0D=5x10^5
v0D=10^6
v0D=2x10^6
i2
Sensitivity
ECO
ECOEVO
EVO
j1
Temperature, T (°C)
Change in SOC equilibrium, ΔC (mg cm-3)
EVO effect
K0D=10^4
K0D=2.5x10^6
K0D=5x10^4
j2
Sensitivity
ECO
ECOEVO
EVO
k1
Temperature, T (°C)
Change in SOC equilibrium, ΔC (mg cm-3)
EVO effect
γZ=0.25
γZ=0.5
γZ=0.75
k2
Sensitivity
ECO
ECOEVO
EVO
l1
Temperature, T (°C)
Change in SOC equilibrium, ΔC (mg cm-3)
EVO effect
dZ=10^-3
dZ=2x10^-3
dZ=3x10^-3
l2
Sensitivity
ECO
ECOEVO
EVO

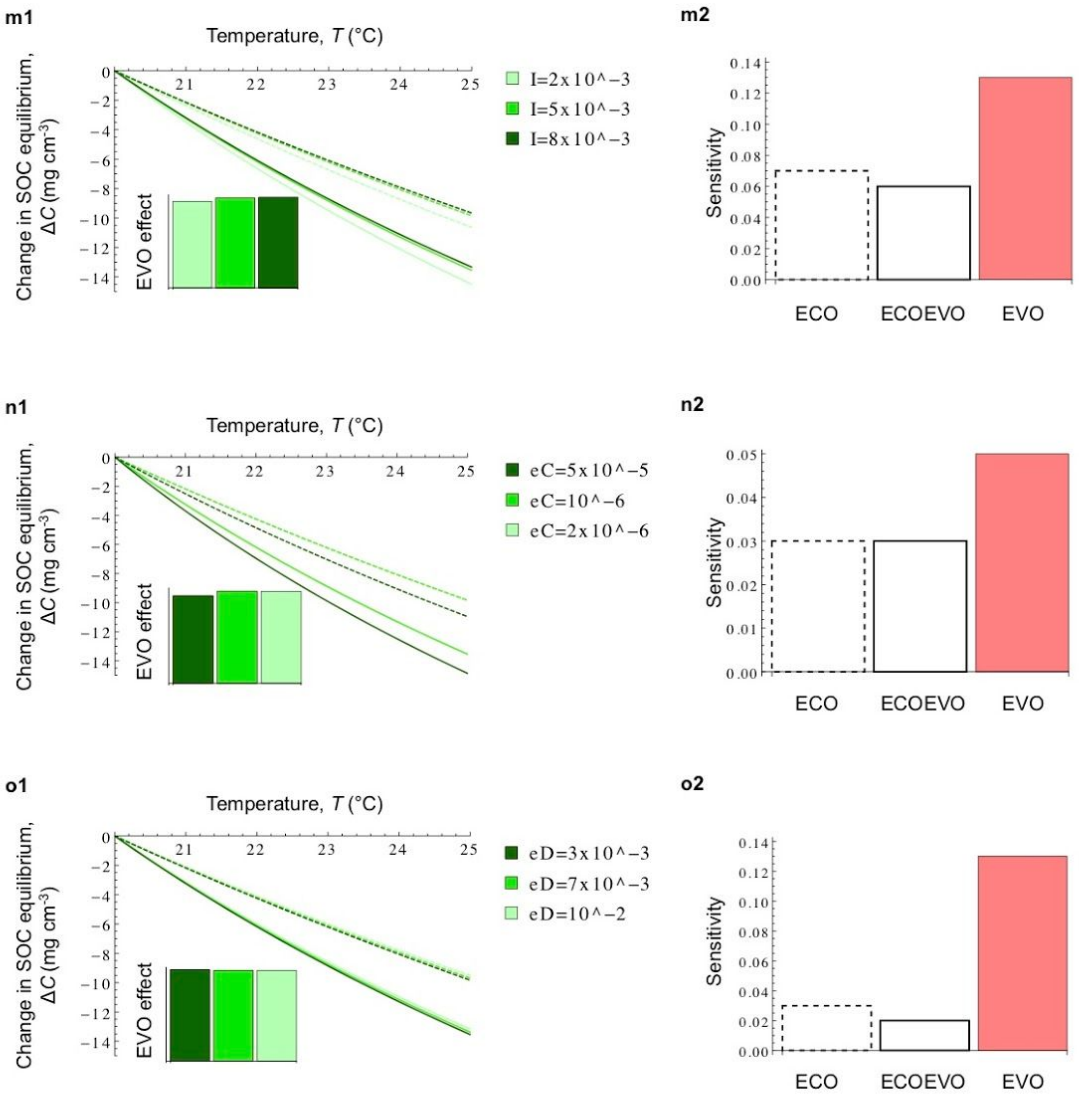

Extended Data Figure 6 | Parameter influence on the ECO response, ECOEVO response and EVO effect. Baseline 'kinetics-only' scenario of temperature dependence. *Left column*, ECO response (dashed curves), ECOEVO response (plain curves), and EVO effect (insets), for three parameters values. *Right column*, Sensitivity of ECO (dashed), ECOEVO (plain) and EVO (pink) to each parameter. Sensitivity is calculated with the minimal and maximal values tested for each parameter and is expressed in absolute value. Because we lack information about realistic range for most parameters, we show relative rather than absolute sensitivities (and the scale for the y-axis is different for each parameter). **a1-a2**, Microbial growth efficiency, γ_M.

b1-b2, Microbial mortality rate, d_M. **c1-c2**, Arrhenius coefficient of uptake rate, v_0^U. **d1-d2**, Activation energy of uptake rate, E_v^U. **e1-e2**, Competition asymmetry, c_0. **f1-f2**, Initial temperature, T_0. **g1-g2**, Activation energy of decomposition rate, E_v^D. **h1-h2**, Activation energy of decomposition half-saturation constant, E_K^D. **i1-i2**, Arrhenius coefficient of decomposition rate, v_0^D. **j1-j2**, Arrhenius coefficient of decomposition half-saturation constant, K_0^D. **k1-k2**, Enzyme production efficiency, γ_Z. **l1-l2**, Enzyme deactivation rate, d_Z. **m**, SOC input (litter), I. **n1-n2**, SOC leaching rate, e_C. **o1-o2**, DOC leaching rate, e_D. Parameters are set to their default values (Extended Data Table 1) except $I = 5\ 10^{-3}$, $v_0^U = 10^5$, $E_v^U = 38$, $c_0 = 1.17$. Darker blue indicates higher microbial performance, darker purple indicates higher enzyme performance, darker green indicates higher soil carbon retention (higher I, lower e_C, lower e_D).

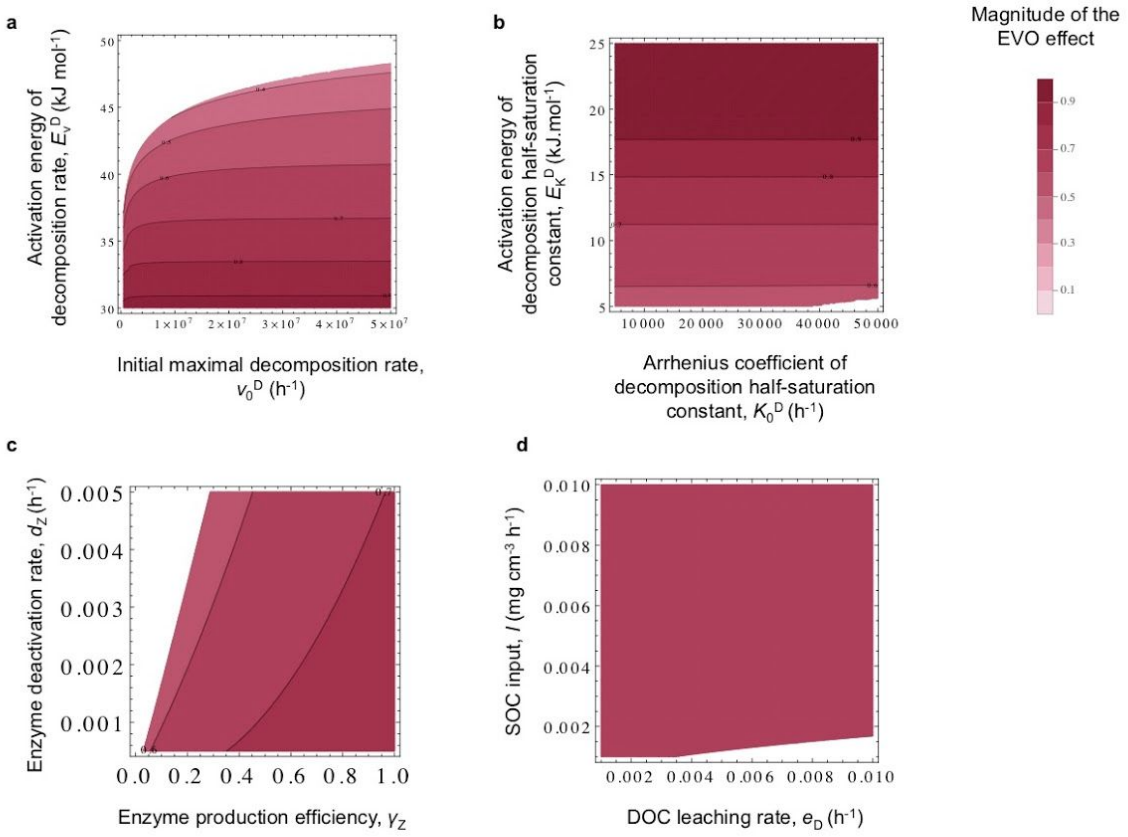

Extended Data Figure 7 | Sensitivity analysis of the EVO effect for the baseline 'kinetics-only' scenario of temperature dependence. a, Sensitivity to Arrhenius coefficient of decomposition rate, v_0^D, and activation energy of decomposition rate, E_v^D. **b**, Sensitivity to Arrhenius coefficient of decomposition half-saturation constant, K_0^D, and activation energy of decomposition half-saturation constant, E_K^D. **c**, Sensitivity to enzyme production efficiency, γ_Z, and enzyme deactivation rate, d_Z. **d**, Sensitivity to DOC leaching rate, e_D, and SOC input (litter), I. Parameters are set to their default values (Extended Data Table 1) except $I = 5\ 10^{-3}$, $v_0^U = 10^5$, $E_v^U = 38$ (point B2). The effect of e_C (not shown) is identical to the effect of e_D.

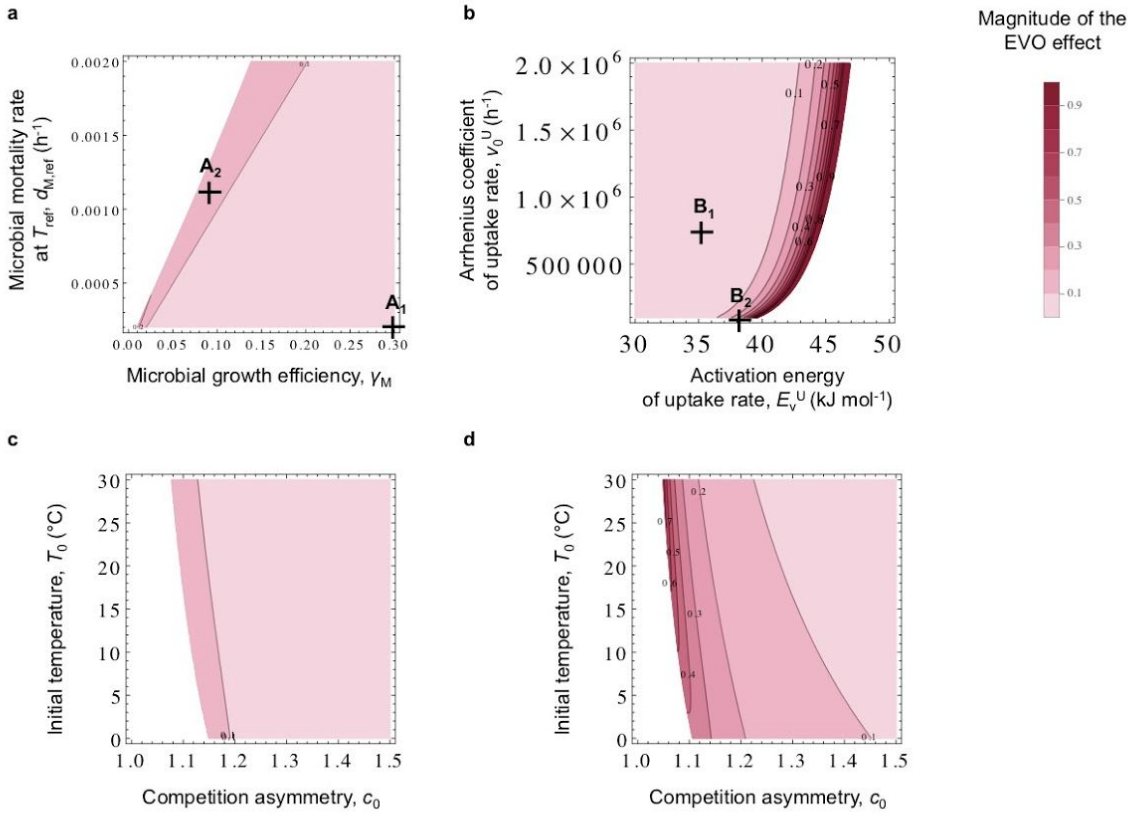
a
b
c
d
Magnitude of the EVO effect
0.9
0.7
0.5
0.3
0.1
Microbial mortality rate at T_{ref}, $d_{M,ref}$ (h^{-1})
Microbial growth efficiency, Y_M
A_2
A_1
Arrhenius coefficient of uptake rate, v_0^U (h^{-1})
Activation energy of uptake rate, E_v^U (kJ mol^{-1})
B_1
B_2
Initial temperature, T_0 (°C)
Competition asymmetry, c_0

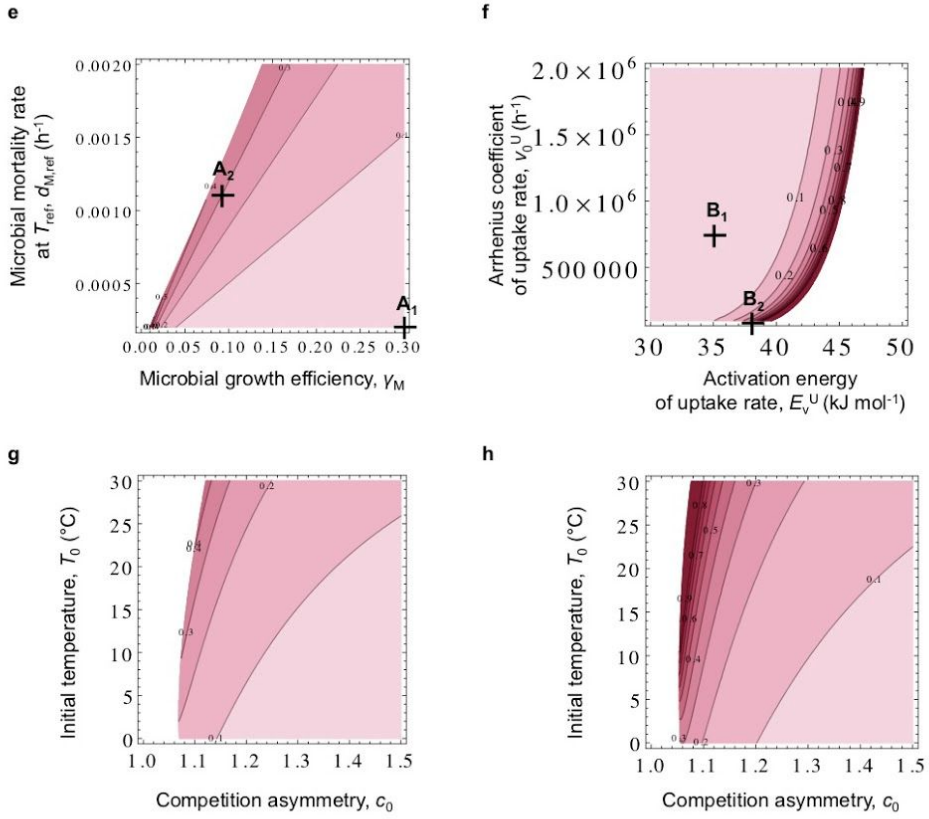
e
Microbial mortality rate at T_{ref}, $d_{M,ref}$ (h^{-1})
0.0020
0.0015
0.0010
0.0005
A_2
A_1
0.00 0.05 0.10 0.15 0.20 0.25 0.30
Microbial growth efficiency, γ_M
f
Arrhenius coefficient of uptake rate, v_0^U (h^{-1})
2.0×10^6
1.5×10^6
1.0×10^6
500 000
B_1
B_2
30 35 40 45 50
Activation energy of uptake rate, E_v^U (kJ mol^{-1})
g
Initial temperature, T_0 (°C)
30 25 20 15 10 5 0
1.0 1.1 1.2 1.3 1.4 1.5
Competition asymmetry, c_0
h
Initial temperature, T_0 (°C)
30 25 20 15 10 5 0
1.0 1.1 1.2 1.3 1.4 1.5
Competition asymmetry, c_0

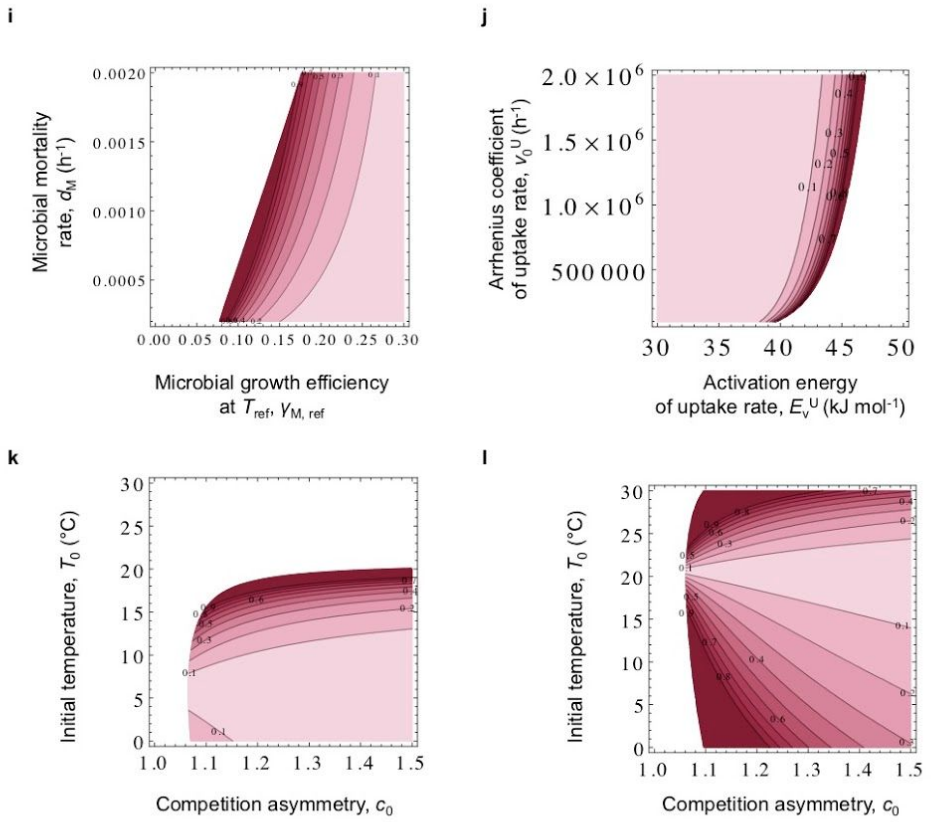

Extended Data Figure 8 | Sensitivity analysis of the EVO effect for the microbial turnover and MGE scenarios of temperature dependence. (a-d) Temperature-dependent microbial turnover, $E_{dM} = 25$. **(e-h)** Temperature-dependent microbial turnover, $E_{dM} = 55$. **(i-l)** Temperature-dependent MGE, $m = -0.014$. Parameters are set to their default values (Extended Data Table 1) except $I = 5\ 10^{-3}$. A1 = B1 = default values. A2 = default values except for γ_M and d_M. B2 = default values except for v_0^U and E_v^U. **(a, e, i)** Sensitivity to microbial growth efficiency, γ_M, and microbial mortality rate, d_M. **(b, f, j)** Sensitivity to activation energy of uptake rate, E_v^U, and Arrhenius coefficient of uptake rate, v_0^U. **(c, d, g, h, k, l)** Sensitivity to competition asymmetry, c_0, and initial temperature, T_0. Panels **(c, j, k)** (resp. **d, h, l**) show sensitivities of the EVO effect at point A2 (resp. B2) for the corresponding scenario of temperature dependence.

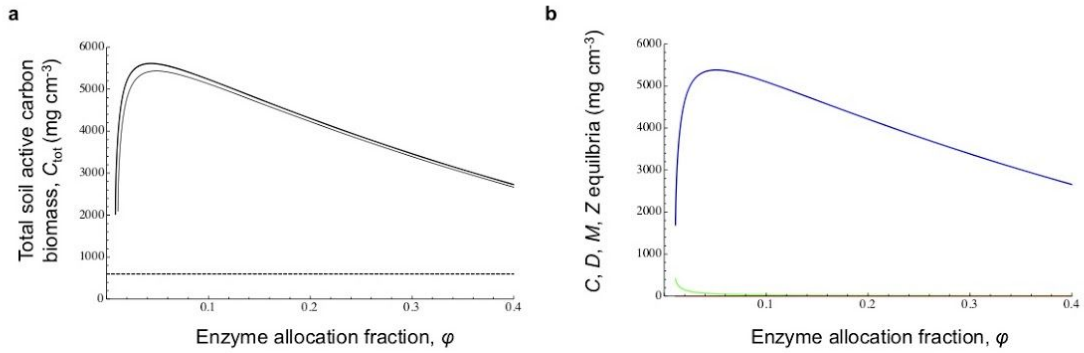

Extended Data Figure 9 | Effect of enzyme allocation fraction on total soil active carbon and its four components when microbial biomass forms the main part of active soil carbon. **a**, Total soil active carbon at 20°C (plain) and 25°C (bold) as a function of enzyme allocation fraction, φ. Note that the SOC equilibrium in the absence of microbes (dashed line) is temperature independent and always lower than the total soil active carbon. **b**, Effect of enzyme allocation fraction, φ, on the four components components of total soil active carbon at 20°C: M (blue), Z (pink), C (green), D (orange). Parameters are set to their default values (Extended Data Table 1) except $I = 3\ 10^{-3}$, $v_0^{\mathrm{U}} = 4\ 10^3$, $E_v^{\mathrm{U}} = 46$, $d_{\mathrm{M}} = 10^{-6}$, $e_{\mathrm{C}} = 5\ 10^{-6}$ and $\gamma_{\mathrm{M}} = 0.7$.

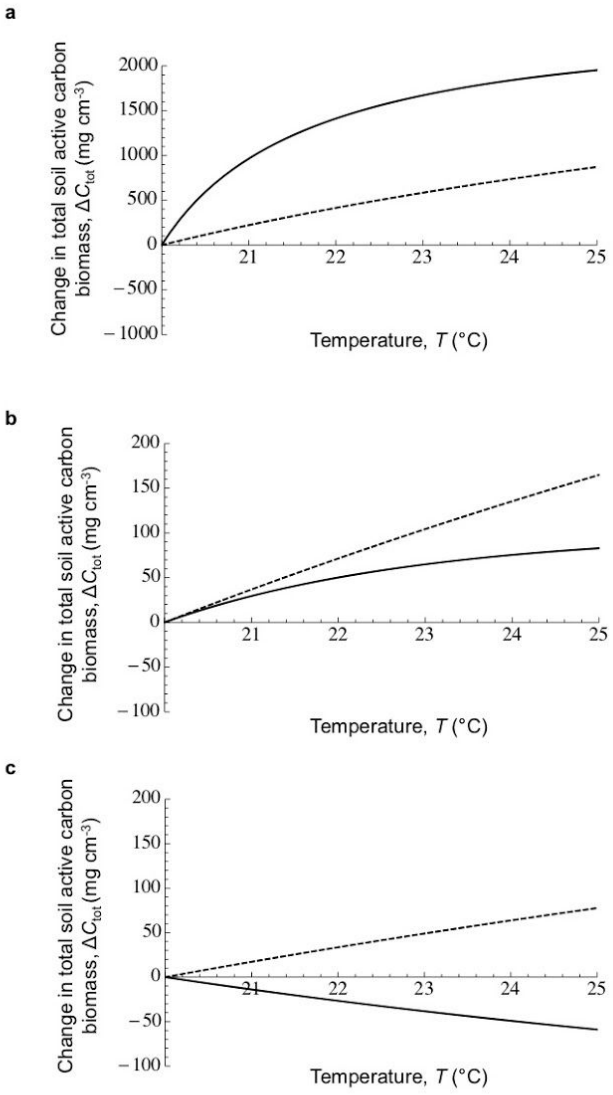

Extended Data Figure 10 | ECO and ECOEVO responses when microbial biomass forms the main part of active soil carbon for different local competitive advantage to enzyme producers (competition asymmetry). a, Small advantage ($c_0 = 1.075$). **b**, Intermediate advantage ($c_0 = 1.12$). **c**, Large advantage ($c_0 = 1.35$). Parameters are set to their default values (Extended Data Table 1) except $I = 3\ 10^{-3}$, $v_0^U = 4\ 10^3$, $E_v^U = 46$, $d_M = 10^{-6}$, $e_C = 5\ 10^{-6}$ and $\gamma_M = 0.7$.

Microbial evolution reshapes soil carbon feedbacks to climate change

Elsa Abs, Scott R. Saleska, Regis Ferriere

SUPPLEMENTARY INFORMATION

Supplementary Note 1 – Analysis of ecological model at constant temperature

At any given temperature T, depending on the enzyme allocation fraction φ, the ecological model possesses either one globally stable equilibrium, or three equilibria (one of which is always unstable) (Extended Data Fig. 2).

The globally stable equilibrium exists for $\varphi < \varphi_{\min}$ or $\varphi > \varphi_{\max}$ and is given by $M = 0$, $Z = 0$, $C = I/e_C$, $D = 0$. Thus, at this equilibrium, the microbial population is extinct and no decomposition occurs.

For $\varphi_{\min} < \varphi < \varphi_{\max}$, the microbial population can either go extinct (then the system stabilizes at the same equilibrium as before) or persists at or around a non-trivial equilibrium, which can be solved for analytically:

(S1a) $$C = \frac{1}{e_C}\frac{\alpha-\sqrt{\alpha^2-4\beta}}{2\mu}$$

(S1b) $$D = \frac{d_M K_m^U}{\lambda}$$

(S1c) $$M = \frac{\gamma_M(1-\varphi)}{d_M\delta}\frac{\left(\alpha-\Delta_M+\sqrt{\alpha^2-4\beta}\right)}{2\mu}$$

(S1d) $$Z = \frac{\gamma_Z\varphi}{d_Z\delta}\frac{\left(\alpha+\Delta_Z+\sqrt{\alpha^2-4\beta}\right)}{2\mu}$$

where

$$\alpha = \mu\left(I - e_C K_m^D\right) + \varphi\gamma_Z v_{max}^D\rho$$

$$\beta = \mu\lambda\delta d_Z I e_C K_m^D$$

$$\mu = \left(\varphi\gamma_Z v_{max}^D - d_Z\delta\right)\lambda$$

$$\Delta_M = 2d_Z\delta\rho$$

$$\Delta_Z = -2d_Z\delta\rho$$

$$\lambda = (1-\varphi)\,\gamma_M v^U_{max} - d_M$$

$$\delta = 1 - (1-\varphi)\,\gamma_M - \varphi\gamma_Z$$

$$\rho = e_C K^D_m \lambda - e_D K^U_m d_M \,.$$

Although an analytical study of the stability of the non-trivial equilibrium is out of reach, numerically we observed stability for most parameter values, based on the calculation of the Jacobian eigenvalues. Only for φ very close to φ_{min} we detected a few cases of equilibrium instability, in which case the system converges toward a small limit cycle. φ_{min} therefore provides a good approximation for the lower bound of the range of φ over which the system persists at a non-trivial equilibrium.

Boundary values, φ_{min} and φ_{max}, of existence of the non-trivial equilibrium are found where the unstable non-trivial equilibrium meets the stable non-trivial equilibrium, *i.e.* when $\alpha^2 - 4\beta = 0$, that we solved numerically. Empirical data suggest that natural values of φ are small[1,2]. The model shows that as φ decreases toward φ_{min}, equilibrium C becomes more sensitive to φ, and the smaller φ_{min}, the stronger the sensitivity of equilibrium C to φ near φ_{min}. This is true across the whole parameter set (Extended Data Fig. 3). Hereafter, unless stated otherwise, we simply use C (respectively D, M, Z) to denote equilibrium values at the non-trivial stable equilibrium of equations (1).

We performed a simple sensitivity analysis of C and existence boundaries φ_{min} and φ_{max} (Extended Data Table 2), following the scheme used by Allison *et al.* (2010)[3] (same range for each parameter in common between our study and theirs, same measure of sensitivity). All parameters affect φ_{min} and φ_{max}, whereas only microbial growth efficiency (γ_M), enzyme allocation fraction (φ), and enzyme parameters (γ_Z, d_Z, v^D_0, K^D_0, E^D_v, E^D_K) have a significant effect on C (Extended Data Fig. 3). This reflects the fact that SOC decomposition is governed by the size of the microbial pool (mostly sensitive to γ_M) and enzyme pool (shaped by φ and γ_Z), and by enzyme performance (determined by the other enzyme parameters) (Extended Data Table 2).

The lack of sensitivity of C to d_M is intriguing, because d_M has a relatively strong influence on the microbial pool (Extended Data Table 2). Both Allison *et al.* (2010)[3]and

Hagerty *et al.* (2014)[4] found a significant effect of d_M on C. This difference arises from the process driving the enzyme production. In Allison *et al.* (2010)[3] and Hagerty *et al.* (2014)[4], the enzyme production rate, r_Z (Extended Data Fig. 1b), is constant over time ('constitutive production'). Using notations similar to ours, their model reads

$$\frac{dC}{dt} = I_C - \frac{v_{max}^D C}{K_m^D + C} Z + p d_M M$$

$$\frac{dD}{dt} = I_D + \frac{v_{max}^D C}{K_m^D + C} Z + (1-p) d_M M + d_Z Z - \frac{v_{max}^U D}{K_m^U + D} M$$

$$\frac{dM}{dt} = CUE \frac{v_{max}^U D}{K_m^U + D} M - d_M M$$

$$\frac{dZ}{dt} = r_Z M - d_Z Z$$

where CUE is carbon use efficiency (*sensu* Allison *et al.* 2010[3]) and p is the fraction of microbial necromass recycled in SOC *vs*. DOC. When solving this system at equilibrium, the enzyme concentration, Z, only depends on enzyme traits (γ_M and γ_Z) and microbial abundance, M ($Z = \frac{r_Z}{d_Z} M$), which depends on microbial turnover rate ($M = \frac{CUE\,(I_D + I_C)}{(d_M + r_Z)(1 - CUE)}$). As a consequence, equilibrium Z is negatively dependent on d_M, therefore equilibrium C is positively dependent on d_M. The analytical expression of equilibrium C is (Li *et al.* 2014)[5]:

$$C = \frac{-d_Z K_m^D (I_C (d_M (1 + CUE(p-1)) + r_Z (1 - CUE)) CUE I_D p d_M)}{I_C (d_M (d_Z (1 + CUE(p-1))) + r_Z (d_Z (1 - CUE) - CUE v_{max}^D)) + CUE I_D (p d_M d_Z - r_Z v_{max}^D)}$$

To link exoenzyme production per individual microbe to the amount of assimilated resource, we substitute CUE with φCUE and r_Z with $\varphi CUE \frac{v_{max}^U D}{K_m^U + D}$. With exoenzyme production being a fraction of assimilated resource, M at equilibrium is directly inversely proportional to d_M:

$$M = \frac{(1-\varphi) CUE (I_D + I_C)}{d_M (1 - CUE)}$$

and Z becomes independent of d_M:

$$Z = \frac{\varphi d_M}{d_Z(1-\varphi)} M = \frac{\varphi CUE(I_D+I_C)}{d_Z(1-CUE)} .$$

As a consequence, C does not depend on d_M and is given by:

$$C = \frac{-d_Z K_m^D (I_C(1+CUE(p(1-\varphi)-1))+CUEI_D p(1-\varphi))}{I_C(d_Z(1+CUE(p(1-\varphi)-1)))+CUEI_D(pd_Z(1-\varphi)-v_{max}^D\varphi)} .$$

This expression was obtained in the case where the production costs of microbial biomass and exoenzymes are the same ($\gamma_Z = \gamma_M$ = CUE). Including leaching of D and C re-establishes a dependency of equilibrium C on d_M, but the sensitivity to d_M remains very low across values of leaching rates for which the equilibrium exists.

To summarize, in models where exoenzymes are produced at a constant rate per unit microbial biomass, the equilibrium exoenzyme concentration, hence the SOC equilibrium stock, are strongly dependent upon all microbial parameters, including d_M. In models like ours where exoenzyme production depends on the amount of assimilated resource, the equilibrium exoenzyme concentration and SOC stock only depend on the allocation parameters, enzyme parameters and resource input parameters, and not on d_M. However, taking evolution into account may restore a dependency of SOC equilibrium on microbial mortality, because C is strongly sensitive to the enzyme allocation fraction, φ, and the evolutionarily stable trait value φ^* itself is strongly sensitive to d_M (equation (5)).

Supplementary Note 2 – Effect of temperature on SOC equilibrium, *C*

For a given enzyme allocation fraction φ, *C* always decreases as temperature increases in the baseline scenario (Fig. 1b, Extended Data Fig. 4). In this scenario, the sensitivity of *C* to temperature is mediated chiefly by the temperature-dependence of enzyme kinetics parameters v_{max}^{D} and K_m^D (Extended Data Table 2). As *T* increases, both v_{max}^{D} and K_m^D increase, causing antagonistic effects on *C*; however, based on empirical data[6], most of the effect of warming is on v_{max}^{D}, which makes the thermal effect mediated by v_{max}^{D} prevail. As a consequence, the decomposition rate rises with temperature, hence *C* declines.

In the temperature-dependent microbial turnover scenario, the effect of temperature on decomposition and SOC stock is virtually unchanged compared to the baseline scenario. This is because the sensitivity of decomposition rate and *C* to microbial mortality d_{M} is very small (Extended Data Table 2).

The loss of soil C with warming also holds in the temperature-dependent MGE scenario. In this case, increasing *T* has antagonistic effects on decomposition mediated by v_{max}^{D} (enzyme activity increases with temperature) *vs.* γ_{M} (microbial growth decreases with temperature). However, the effect of the exponential dependence of v_{max}^{D} on *T* is stronger than the effect of the linear dependence of γ_{M} on *T*; the former thus dominates the effect of *T* on *C*, but the loss of soil C is attenuated compared to the baseline and the temperature-dependent microbial turnover scenario.

In all three scenarios, *C* is more sensitive to *T* across lower values of *T* (Fig. 3, Extended Data Fig. 4). As a consequence, the loss of soil C with warming is more pronounced in colder ecosystems.

Supplementary Note 3 – Evolutionary model

We use the framework of adaptive dynamics[7,8]. In this framework, evolution is modeled as a competition process between a 'resident strategy' (wild-type) and alternate strategies (mutants) within a set of feasible phenotypes. In a given environment (*e.g.* at a given temperature), an 'adaptation' or 'adapted value' of a trait is a phenotype that (i) when resident, no mutant can invade; (ii) can be reached by a sequence of phenotypic substitutions, whereby each step involves the replacement of a resident phenotype by a mutant phenotype. Here the phenotypic trait of interest is the enzyme allocation fraction, φ. The set of feasible phenotypes is the range ($\varphi_{\min}$, $\varphi_{\max}$) at a given temperature, for which the non-trivial ecological equilibrium exists.

3.1. Ecological interaction between resident and mutant strains

To model the competition effect of a resident phenotype, φ_{res}, on the population growth of a mutant phenotype, φ_{mut}, we extend the ecological model written for a single type (equations (1) in Methods). To account for the local nature of the interaction between rare mutant and common resident cells, we introduce a function (hereafter denoted by c) of the difference between φ_{res} and φ_{mut} to measure how local decomposition by mutant and resident cells differ from 'mean field' (average) decomposition by resident cells. Thus, for given C, D, Z, the growth of the mutant population is governed by

$$\text{(S2)} \qquad \frac{dM_{mut}}{dt} = (1-\varphi)\gamma_M \frac{v_{max}^U (1+c(\varphi_{mut}-\varphi_{res}))D_{res}}{K_m^U+(1+c(\varphi_{mut}-\varphi_{res}))D_{res}} M_{mut} - d_M M_{mut}$$

where D_{res} is the equilibrium D predicted by the ecological model applied to the sole resident phenotype φ_{res}. Here function c satisfies $c(0) = 0$, $c(z) > 0$ if $z > 0$ and $c(z) < 0$ if $z < 0$.

The underlying assumption is that each microbe has access to DOC partly as a public good and partly as a private good[9]. The public good part results from the diffusion of exoenzymes. The private good part results from local decomposition at the microscopic scale of cells and exoenzymes that they produce themselves. A mutant cell that invests more (resp. less) in exoenzyme has access to more (less) DOC than the average resident cell because the cell's private good is greater (smaller) whereas all cells share the same public good. In a spatially implicit model like ours, diffusion is not modeled, but its

effect on the accessibility of DOC to a mutant strain can be phenomenologically accounted for by putting mutant cells at a competitive advantage for DOC if the mutant phenotype invests more in exoenzyme production than the resident phenotype (i.e. $\varphi_{\text{mut}} - \varphi_{\text{res}} > 0$), or at a competitive disadvantage if the mutant phenotype invests less ($\varphi_{\text{mut}} - \varphi_{\text{res}} < 0$). This is captured phenomenologically by function c in equation (S2).

3.2. Invasion fitness and selection gradient

Mutant fitness $s(\varphi_{mut}, \varphi_{res})$ is given by the mutant population growth rate per unit biomass:

(S3) $$s(\varphi_{mut}, \varphi_{res}) = (1-\varphi)\gamma_M \frac{v_{max}^U (1+c(\varphi_{mut}-\varphi_{res}))D_{res}}{K_m^U + (1+c(\varphi_{mut}-\varphi_{res}))D_{res}} - d_M$$

The selection gradient then obtains by taking the first order derivative of the invasion fitness with respect to the mutant trait:

(S4) $$\nabla s(\varphi) = \frac{d_M}{1-\varphi}\left(\left(1-\varphi-\frac{d_M}{v_{max}^U \gamma_M}\right) c_0 - 1\right)$$

where $c_0 = c'(0)$ measures the local competitive advantage to stronger exoenzyme producers, which we call 'competition asymmetry'. Note that by definition of function c, we always have $c_0 > 0$. Variation in c_0 may be caused by different soil diffusion properties, due to *e.g.* physical texture or moisture.

3.3. Evolutionary singularity

Trait values that nullify the selection gradient are called 'evolutionary singularities'. An evolutionary singularity can be attractive or repelling, and invadable or non-invadable. Evolutionary singularities that are attractive and non-invadable represent potential end-points of evolutionary adaptation. Evolutionary singularities that are attractive and invadable can lead to evolutionary branching[8].

In a given environment (fixed parameters, constant temperature) there is at most one evolutionary singularity given by:

(S5) $$\varphi^* = 1 - \frac{d_M}{v_{max}^U \gamma_M} - \frac{1}{c_0}.$$

Existence of $\varphi^* > 0$ requires $\frac{d_M}{v_{max}^U \gamma_M} < 1$ and $c_0 > \frac{1}{\left(1-\frac{d_M}{v_{max}^U \gamma_M}\right)}$. Thus, the (cooperative) trait φ can evolve above zero only if the local competition advantage to stronger enzyme producers is large enough. The condition for φ^* to be evolutionarily stable is $c''(0) < 2\, c_0^2$ and no other condition than existence is required for φ^* to be always convergent. Here we assume that function c is such that φ^* is evolutionarily stable and attractive.

Equation (S5) shows that more cooperation (larger φ^*) should evolve in microbial populations with lower mortality, greater nutrient uptake, and/or higher MGE. When comparing microbial populations with similar life-history traits γ_M, v_{max}^U and d_M, stronger competitive advantage to exoenzyme producers (i.e. higher c_0) selects for larger φ^*.

Equation (S5) also predicts the evolutionary effect of temperature variation on enzyme production (Extended Data Fig. 5a-d). The evolutionary adaptive response of enzyme allocation fraction φ to warming is driven by the effect of temperature on v_{max}^U, d_M, and γ_M. The thermal dependence of v_{max}^U is assumed, in our baseline scenario, as a consequence of temperature-dependent enzyme kinetics. In this scenario, d_M and γ_M are constant (temperature independent); the evolutionary effect of T on φ^* is thus entirely mediated by the effect of T on v_{max}^U. Warming drives v_{max}^U up, which causes φ^* to rise (Extended Data Fig. 5a). The sensitivity of φ^* to temperature is strongest at low initial temperature T_0 (Extended Data Fig. 5a).

In the temperature-dependent turnover scenario, as the influences of d_M and v_{max}^U on φ^* are antagonistic (equation (S5)), warming causes φ^* to rise when $E_v^U > E_{dM}$, *i.e.* when d_M is not too strongly sensitive to temperature. As a consequence, the rise of φ^* is strongest in the baseline scenario (where $E_{dM} = 0$) (Extended Data Fig. 5a, b). Warming causes φ^* to decline when $E_v^U > E_{dM}$ (Extended Data Fig. 5c). The influence of T_0 on the sensitivity of φ^* to temperature observed in the baseline scenario is lost in the temperature-dependent turnover scenario (Extended Data Fig. 5c).

In the temperature-dependent MGE scenario, warming drives v_{max}^U up and γ_M down. As a consequence, warming causes a smaller increase in φ^* in this scenario (Extended Data

Fig. 5d). Here the influence of T_0 on the sensitivity of φ^* to warming is qualitatively very strong due to the different shapes of temperature dependencies of γ_M (linear) relative to v_{max}^U (exponential). As a result, at low T_0, φ^* rises with warming (because the reverse exponential of v_{max}^U dominates the linear decrease of γ_M). At high T_0, φ^* decreases in response to warming, because v_{max}^U plateaus while γ_M declines linearly (Extended Data Fig. 5d). Quantitatively, the strongest warming effect on φ^* is observed in the baseline scenario in cold ecosystems.

Supplementary Note 4 – Sensitivity analysis of ECO and ECOEVO responses and EVO effects

In the baseline scenario of temperature dependence, the EVO effect is most sensitive to microbial life-history traits γ_M, d_M (Fig. 2a, Extended Data Fig. 6a,b), v_0^U and E_v^U (Fig. 2b, Extended Data Fig. 6c, d) and environmental parameters c_0 and T_0 (Fig. 2c-d, Extended Data Fig. 6e, f). This is because these parameters influence the sensitivity of the adaptive strategy, φ^*, to temperature and/or the initial adapted value, $\varphi^*(T_0)$ (equation (5) and Supplementary Note 3), and therefore they can affect the ECOEVO response more than the ECO response, with strong EVO effects as a result (Extended Data Fig. 6a-f).

In contrast, the EVO effect is little affected by the other model parameters: enzyme parameters (efficiency, production) and environmental parameters (litter input, leaching) (Extended Data Figs. 6g-o, 7). Considering enzyme parameters, we find that less efficient enzymes lead to larger ECO and ECOEVO responses to warming (Extended Data Fig. 6g1-l1). However, the ECO and ECOEVO responses exhibit similar sensitivities to most enzyme parameters, which therefore have very little impact on the EVO effect (Extended Data Figs. 4a-c, 6i-l). Only the activation energies (E_v^D and E_K^D) have a slightly stronger impact on the ECO response than on the ECOEVO response, which results in slightly weaker EVO effects in systems with less efficient enzymes (Extended Data Figs. 6g, h, 7a, b). Finally, environmental parameters – litter input I, and leaching rates e_C and e_D – primarily affect the stability of the ecological equilibrium (via their influence on φ_{min}, Extended Data Fig. 3) and have little influence on the EVO effect (Extended Data Figs. 6m-o, 7d).

In the other scenarios of temperature dependence, the influence of parameters on the EVO effect is consistent with results shown in Fig. 2 (sensitivity analysis in the baseline scenario) and Fig. 3 (ECO and ECOEVO responses and EVO effect for the default system in the other scenarios). Thus, EVO effects are generally strong in cold ecosystems harboring communities of slow-growing microbes, under soil conditions that give only a small competitive edge to greater enzyme producer (such as in Fig. 2); EVO effets are often reduced in systems with stronger dependence of mortality d_M on

temperature; and EVO effects are strong in warm ecosystems when MGE decreases with warming, as seen in Fig. 3 (Extended Data Fig. 8).

Supplementary Discussion

Ecological responses to warming

In absence of microbial evolution, the model predicts a large loss of soil carbon with warming in systems harboring low-productivity microbes (low γ_M) secreting low-performance enzymes (high γ_Z); and in systems of high-productivity microbes (high γ_M) that synthesize high-performance enzymes (low γ_Z) but invest very little resource in their production (φ close to the minimum viable value, φ_{min}) – which is the expected adaptation to highly diffusive soils (according to equation (5)). The prediction of large ecology-driven loss of soil carbon holds even if the microbial turnover increases with warming, but is attenuated (though not reversed) if MGE decreases with warming. These results are consistent with previous ecological models of soil microbial decomposition that compared constant versus decreasing MGE with warming[3,5,6,10–17]. Note, in these models, a constant MGE (CUE in models ignoring exoenzymes dynamics, as in German *et al.* (2012)) was viewed as a microbial 'adaptation' to warming in the sense of microbes physiologically acclimating, rather than genetically evolving, to rising temperature[14,18].

Our ecological predictions, however, contrast with previous models in which microbial turnover (death rate) increases with temperature[4]. In our model, the microbial death rate has very little effect on the SOC ecological equilibrium, C, whereas Hagerty *et al.* (2014) found C to increase with higher microbial turnover. The difference stems from the rate of enzyme production being resource dependent in our model, rather than constitutive and constant as in Allison *et al.* (2010)[3] and Hagerty *et al.* (2014)[4]. Equilibrium C is determined by the decomposition rate, which is controlled by the enzyme stock, Z. When exoenzyme production is constitutive, Z is directly proportional to microbial biomass, M, and thus strongly influenced by the microbial death rate. When exoenzyme production is resource dependent, Z becomes much more sensitive to the enzyme allocation parameters, φ, γ_Z and γ_M. In our model, the temperature dependence of d_M affects the ECO response more through the dependence of $\varphi^*(T_0)$ on $d_M(T_0)$ (Eq. (2)) than the dependence of M on d_M (see Supplementary Note 1).

Evolutionary response of carbon-use efficiency (CUE)

In our formalism, the microbial strategy of resource allocation to either microbial biomass synthesis or exoenzyme production follows a standard 'Y model' of resource allocation[19]. The exoenzyme production efficiency is denoted by γ_Z, and the microbial growth efficiency (MGE), by γ_M. Thus $(1 - \gamma_Z)$ measures the energetic cost of enzyme production and $(1 - \gamma_M)$ measures the energetic cost of microbial biomass synthesis; these costs are paid through microbial respiration returning CO_2 to the atmosphere (Fig. 1a). Larger costs may ensue from the production of enzymes needed to degrade more recalcitrant carbon compounds (smaller γ_Z); or the synthesis of more complex microbial structures (smaller γ_M).

Carbon-use efficiency (CUE) has received much attention in experimental studies, prompted by the contrasted effects of warming on respiration rates and microbial biomass[13,15,20]. Previous models have highlighted the effect of CUE on soil C stock[3], from local to global scale[17]. In our framework, CUE is given by

(S6) $$\mathrm{CUE} = (1 - \varphi)\,\gamma_M + \varphi\,\gamma_Z$$

and thus appears as a compound parameter rather than a microbial trait. Our model predicts that CUE changes as the microbial trait φ evolves. Assuming constant MGE (γ_M), we find that natural selection always favors greater enzyme allocation fraction (φ) as temperature rises in the baseline scenario. From equation (S6) we conclude that CUE decreases in microbes characterized by relatively costly exoenzymes and 'cheap' tissue ($\gamma_M < \gamma_Z$), and increases otherwise. Thus, even if MGE is kept constant with respect to temperature, microbial evolutionary adaptation to warming can have mixed effects on CUE.

Influence of temperature dependence on SOC eco-evolutionary response

If MGE decreases with temperature, the direction and magnitude of the ECOEVO response to warming vary dramatically with the initial temperature T_0 (Fig. 3d, Extended Data Fig. 5d, h). The strong influence of T_0 on the ecological response of soil C to warming was noted by Li *et al.* (2014)[5] for intermediate MGE temperature sensitivity

(m = - 0.008). The outstanding eco-evolutionary response (C sequestration) predicted by our model for steeper MGE temperature dependence (m = - 0.014, Fig. 3d) are caused by the combination of $v_{max}^{U}(T)$ as an Arrhenius function with $\gamma_M(T)$ as a linear function (equations (2c, f)). While there is empirical support for this choice (reviewed in Todd-Brown *et al.* 2012), both relationships remain uncertain and warrant further experimental investigation.

If the microbial turnover increases with temperature[4], warming selects for lower enzyme allocation fraction (Extended Data Fig. 5b, c), slowing down decomposition (Extended Data Fig. 5f, g), and possibly buffering the ecology-driven loss of soil C (Fig. 3b, c). Thus, when taking microbial evolution into account, the thermal sensitivity of microbial turnover does reduce C loss but never leads to the kind of C sequestration predicted by earlier purely ecological models[4].

Ecological and eco-evolutionary responses of total soil C

Large-scale projections of soil C cycle on timescales that are long relative to the characteristic times of the processes described by our model also raise the issue of distinguishing between readily available SOM versus physio-chemically protected SOM, which decomposes more slowly[21,22]. Reinterpreting the C compartment of our model as readily available SOM removes the constraint of having M much smaller than C[23,24]. The relevant measure of soil carbon then becomes the sum of all compartments, $C_{tot} = C + M + Z + D$, called 'total soil active carbon'. We investigated how our results are changed when ECO and ECOEVO responses are defined with respect to C_{tot}, rather than C, focusing on the baseline scenario (constant MGE and constant microbial turnover).

Extended Data Fig. 9 exemplifies the case where microbial biomass is the main component of C_{tot} and total soil active carbon is higher in the presence of microbes than in their absence. This occurs because here a higher SOC leaching rate, e_C, is more than compensated by the microbial higher productivity (high MGE, γ_M, and low death rate, d_M), so that carbon is retained in the soil longer in the presence of microbes than without. In this type of high-leaching soils, the direction of the ECO response shifts

from negative (carbon loss) to positive (carbon gain). Microbial adaptive evolution can amplify, buffer or reverse this ecological response depending on the local competitive superiority of enzyme producers, c_0 (Extended Data Fig. 10). This is because microbial biomass, M, is the main carbon stock in these systems and purely ecological processes drive an approximately linear increase in M with temperature whereas M responds non-linearly to the increase in enzyme allocation fraction (Extended Data Fig. 9b).

Effect of multi-trait evolution

Our study demonstrates how a trait-based approach can be used to integrate microbial evolutionary adaptation in carbon cycle models[25]. Our focal trait, the enzyme allocation fraction, φ, is pivotal in the decomposition process. Other microbial traits that appear in our model may also respond to selection imposed by warming, such as MGE (γ_M) and the exoenzyme production efficiency (γ_Z). The γ_M trait may evolve in response to variation in environmental quality (e.g. predation or infection risk), possibly trading-off with the maximum rate of uptake or correlating with the death rate; γ_Z may evolve in response to substrate variation[26], possibly correlating with the enzyme decay rate.

Given specific assumptions about factors of and constraints on the evolution of these traits, our sensitivity analyses can be used to make qualitative predictions on how the ECOEVO response and EVO effect might be altered (Fig. 2, Extended Data Fig. 6). For example, strong EVO effects may not be affected if evolving γ_M correlates positively with d_M, whereas weak effects may become strong if γ_M trades-off with d_M. In contrast, the low sensitivity of EVO effects to γ_Z suggests that the evolution of this trait may have little impact on the response of soil C to warming.

Supplementary References

1. Schimel, J. P. & Weintraub, M. N. The implications of exoenzyme activity on microbial carbon and nitrogen limitation in soil: a theoretical model. *Soil Biol. Biochem.* **35,** 549–563 (2003).
2. Burns, R. G. *et al.* Soil enzymes in a changing environment: Current knowledge and future directions. *Soil Biol. Biochem.* **58,** 216–234 (2013).
3. Allison, S. D., Wallenstein, M. D. & Bradford, M. A. Soil-carbon response to warming dependent on microbial physiology. *Nat. Geosci.* **3,** 336 (2010).
4. Hagerty, S. B. *et al.* Accelerated microbial turnover but constant growth efficiency with warming in soil. *Nat. Clim. Chang.* **4,** 903 (2014).
5. Li, J., Wang, G., Allison, S. D., Mayes, M. A. & Luo, Y. Soil carbon sensitivity to temperature and carbon use efficiency compared across microbial-ecosystem models of varying complexity. *Biogeochemistry* **119,** 67–84 (2014).
6. German, D. P., Marcelo, K. R. B., Stone, M. M. & Allison, S. D. The Michaelis-Menten kinetics of soil extracellular enzymes in response to temperature: a cross-latitudinal study. *Glob. Chang. Biol.* **18,** 1468–1479 (2012).
7. Metz, J. A. J., Geritz, S. A. H., Meszena, G., Jacobs, F. J. A. & Heerwaarden, J. S. van. Adaptive Dynamics: A Geometrical Study of the Consequences of Nearly Faithful Reproduction. 50 (1995).
8. Geritz, S. A. H., Kisdi, E., Mesze´NA, G. & Metz, J. A. J. Evolutionarily singular strategies and the adaptive growth and branching of the evolutionary tree. *Evol. Ecol.* **12,** 35–57 (1998).
9. Driscoll, W. W. & Pepper, J. W. Theory for the evolution of diffusible external goods. *Evolution* **64,** 2682–2687 (2010).
10. Eliasson, P. E. *et al.* The response of heterotrophic CO2 flux to soil warming. *Glob. Chang. Biol.* **11,** 167–181 (2005).
11. Knorr, W., Prentice, I. C., House, J. I. & Holland, E. A. Long-term sensitivity of soil carbon turnover to warming. *Nature* **433,** 298–301 (2005).
12. Kirschbaum, M. U. F. The temperature dependence of organic-matter decomposition—still a topic of debate. *Soil Biol. Biochem.* **38,** 2510–2518 (2006).
13. Bradford, M. A. *et al.* Thermal adaptation of soil microbial respiration to elevated

temperature. *Ecol. Lett.* **11,** 1316–1327 (2008).

14. Bradford, M. A. Thermal adaptation of decomposer communities in warming soils. *Front. Microbiol.* **4,** 333 (2013).
15. Frey, S. D., Lee, J., Melillo, J. M. & Six, J. The temperature response of soil microbial efficiency and its feedback to climate. *Nat. Clim. Chang.* **3,** 395 (2013).
16. Tucker, C. L., Bell, J., Pendall, E. & Ogle, K. Does declining carbon-use efficiency explain thermal acclimation of soil respiration with warming? *Glob. Chang. Biol.* **19,** 252–263 (2013).
17. Wieder, W. R., Bonan, G. B. & Allison, S. D. Global soil carbon projections are improved by modelling microbial processes. *Nat. Clim. Chang.* **3,** 909 (2013).
18. Allison, S. D. Modeling adaptation of carbon use efficiency in microbial communities. *Front. Microbiol.* **5,** 571 (2014).
19. van Noordwijk, A. J. & de Jong, G. Acquisition and Allocation of Resources: Their Influence on Variation in Life History Tactics. *Am. Nat.* **128,** 137–142 (1986).
20. del Giorgio, P. A. & Cole, J. J. BACTERIAL GROWTH EFFICIENCY IN NATURAL AQUATIC SYSTEMS. *Annu. Rev. Ecol. Syst.* **29,** 503–541 (1998).
21. Conant, R. T. *et al.* Temperature and soil organic matter decomposition rates - synthesis of current knowledge and a way forward. *Glob. Chang. Biol.* **17,** 3392–3404 (2011).
22. Davidson, E. A. & Janssens, I. A. Temperature sensitivity of soil carbon decomposition and feedbacks to climate change. *Nature* **440,** 165–173 (2006).
23. Fierer, N., Strickland, M. S., Liptzin, D., Bradford, M. A. & Cleveland, C. C. Global patterns in belowground communities. *Ecol. Lett.* **12,** 1238–1249 (2009).
24. Ladd, J. N., Amato, M., Zhou, L.-K. & Schultz, J. E. Differential effects of rotation, plant residue and nitrogen fertilizer on microbial biomass and organic matter in an Australian alfisol. *Soil Biol. Biochem.* **26,** 821–831 (1994).
25. Wallenstein, M. D. & Hall, E. K. A trait-based framework for predicting when and where microbial adaptation to climate change will affect ecosystem functioning. *Biogeochemistry* **109,** 35–47 (2012).
26. Allison, S. D. A trait-based approach for modelling microbial litter decomposition. *Ecol. Lett.* **15,** 1058–1070 (2012).

Impact of Microbial Evolution on Soil Carbon Global Projections

Elsa Abs[1,2*], Scott R. Saleska[1], Regis Ferriere[1,2,3]

[1] Department of Ecology & Evolutionary Biology, University of Arizona,
Tucson, AZ 85721, USA

[2] Institut de Biologie de l'Ecole Normale Supérieure (IBENS),
ENS-PSL University, CNRS, INSERM, 75005 Paris, France

[3] International Center for Interdisciplinary Global Environmental Studies (iGLOBES),
CNRS, ENS-PSL University, University of Arizona, Tucson, AZ 85721, USA

*Corresponding author, abs@biologie.ens.fr

Abstract

Earth system models (ESMs) are essential tools to project future climate and carbon (C) cycle feedbacks. Recently, direct microbial control over soil C dynamics has been introduced in ESMs, thus explicitly representing microbial mechanisms of soil C cycling on the global scale. Microbial ESMs, however, do not account for the capacity of microbial populations to adapt to climate warming. Here we simulate and scale up the effect of microbial evolutionary adaptation to climate warming on global projections of soil carbon stocks. Our results confirm the expectation of a significant global aggravation of soil C loss due to microbial evolution. Colder biomes contribute relatively more to the effect of evolutionary adaptation on global soil C projections. Dormant soils, in which microbial activity is very low, tend to gain carbon initially, and even more so when the local temperature reaches a threshold at which they become active. In these regions, the negative effect of evolution on soil C may not kick in until the microbial community shifts from dormant to active, and may thus be delayed by decades. Our results argue for simulating microbial evolution in ESMs to more accurately project global soil carbon.

Introduction

Earth System models (ESMs) are used to project future climate and carbon (C) cycle feedbacks. The first generation of ESMs used simple soil C models, in which turnover rates of soil C pools are determined by first-order kinetics of enzymatic decomposition. However, first-order kinetic models neglect microbial physiological processes that transform and stabilize soil C inputs and may respond to climate warming (reviewed in Wieder et al. 2015; Abs and Ferriere, in review). Filling this gap has led to more mechanistic models of soil microbe-enzyme decomposition, which have been used to investigate the role that soil microbial communities play in shaping the response of soil C stocks to environmental change, e.g. change in soil moisture and diffusion properties in relation with patterns of precipitation (Zhang et al. 2014; Abs, Ferriere, Leman, in prep.) or change in soil temperature (Allison et al. 2010; German et al. 2012; Li et al. 2014; Abs, Saleska, Ferriere, subm.)

Wieder at al. (2013) conducted the first attempt to integrate mechanistic, small-scale microbial models of decomposition in Earth system models (ESMs). By building a temperature- dependent microbial model into the Community Land Model (CLM), they produced a "CLM microbial model" which could explain 50% of the spatial variation in observed soil C stock, contra 28-30% for the best non-microbial models. Such results indicate that explicit representation of soil microbial dynamics at the microscopic scale can significantly improve global assessment of soil carbon stocks (see Wieder et al. (2018) for further discussion). Furthermore, projections of the CLM microbial model over 2006 to 2100 predict a massive soil C loss (~300 Pg C by year 2100) in the scenario where microbial growth efficiency (MGE) is temperature-independent -- an effect that is completely offset of MGE is assumed to vary negatively with temperature. Such contrasting outcomes emphasize the importance of including microbial processes and their temperature dependence in global projections of soil carbon.

Besides the thermodynamic response of enzymatic activity to warming, decomposition may also depend on temperature via microbial adaptation (Allison 2014). In Wieder et al. (2013), the temperature-independence of MGE is interpreted as a plastic physiological response (i.e. acclimation) of microorganisms to temperature change. Given the short generation time, large population size and standing genetic variation of many microbial organisms, microbial populations are also likely to adapt *evolutionarily* to warming (Abs, Saleska, Ferriere, subm.). Using a microbe-enzyme

model of decomposition in which the fitness costs and benefits of exoenzyme production can be accounted for, Abs et al. (subm.) investigated how exoenzyme production responds to selection under environmental warming, and how the evolutionary response of exoenzyme production impacts soil organic carbon (SOC) stock. Abs et al.'s (subm.) model shows that the evolutionarily adaptive response of exoenzyme production to warming can have large effects on the decomposition process and soil C stocks. By specifying their model for five contrasting biomes for which exoenzyme kinetics parameters have been documented (German et al. 2012), Abs et al. (subm.) found evolutionary aggravation of soil C loss to be the most likely outcome, with a strong latitudinal pattern, from small evolutionary effects at low latitude to large evolutionary effects at high latitude.

Here our goal is to examine how these effects scale up to global continental Earth. To this end, we follow Wieder et al.'s (2013) approach, using Abs et al.'s (subm.) eco-evolutionary model of decomposition. We use German et al.'s (2012) parametrization of enzymatic reactions for five contrasted biomes, together with observations of soil temperature and litterfall inputs to predict the current global distribution of soil carbon. We then use soil temperature and litter input projections from an archived CMIP5 experiment for the Representative Concentration Pathway 8.5 (RCP 8.5) from 2006 to 2100, to calculate the change in soil C projected by 4.8 °C warming over the course of this century. By updating soil temperature and litter input every month, and assuming rapid convergence of the ecological model within each time interval, we obtain projections without microbial evolution, in which exoenzyme production at each location (~ 1° × 1° grid cell) remains at the initial adapted value; and projections with microbial evolution, in which exoenzyme production at each location adapts evolutionarily to the temperature change, given the concurrent change in litter input. Comparing projections from the eco-evolutionary *vs*. ecological (non-evolutionary) model upheld previous conclusions (Abs et al. subm.) about the potentially large impact of microbial evolution on the response of soil C to climate warming.

Results

We construct initial maps of soil C stock (Fig. 1) under the assumption that microbial enzyme production is locally adapted to initial temperature and litter input (estimated by averaging observed surface soil temperature and observed litter input over 15 years, from 2006 to 2021) (Fig. 2a). At many northern sites, the equilibrium of the CDMZ ecological model is unstable for the calculated value of the adapted enzyme allocation fraction, which we interpret as the microbial community being present but inactive, or 'dormant'. To these sites we assign the observed soil C stock averaged over the corresponding biome. To all other sites where the microbial community is active, the soil C stock is estimated as the sum of SOC and microbial biomass at equilibrium (in units of carbon mass per m^2 per centimeter of soil depth). The global map (Fig. 1) is in good agreement with observations from the globally gridded Harmonized World Soils Database, as reported in Wieder et al. (2013).

In the case of decomposition influenced by temperature through enzyme kinetics only, we expect adaptive evolution to promote an increase in enzyme production in response to warming (Abs et al., subm.). This effect holds at Earth scale (Fig. 2b), with the average adapted enzyme allocation fraction, φ^*, rising from ~0.015 initially to ~0.045 in 2100. This rise in enzyme production driven by microbial evolutionary adaptation has a strong impact on global projections of soil C (Fig. 3). Without evolution, warming has very little effect on global soil C, which fluctuates narrowly around 78 Pg. With evolution, the rise in enzyme production causes soil C to decline from ~78 Pg to ~72 Pg. Individual biomes vary in their ecological and eco-evolutionary responses to warming. The relative constancy of soil C predicted by the ecological model hides contrasting tendencies among biomes, with Costa Rica-type and West Virginia-type soils showing a loss of carbon (about 1 Pg each), whereas California-type and Maine-type soils show a gain of carbon (also about 1 Pg each). Microbial evolutionary adaptation offsets the carbon gains and enhances the carbon losses. We also note that although changes of soil C stock in Alaska-type biomes contribute little to global trajectories, it is in this biome that the effect of evolution (i.e. the eco-evolutionary response relative to the ecological response) is strongest.

We dissect these results further by analyzing and comparing the trajectories of sites where microbial communities were initially active ('active soils'; Fig. 4) to sites where microbial communities were initially dormant ('dormant soils'; Fig. 5). They

each initially contains about half of the global soil carbon (Figs. 1, 4, 5). Whereas the global ecological response of soil C to warming is weak (Fig. 3), we find contrasting responses of initially active vs. dormant soils (Fig. 4, 5). For initially active soils (Fig. 4), both ecological and eco-evolutionary models predict significant carbon loss (from 40 Pg to 33 Pg due to ecology only, from 40 Pg to 30 Pg due to ecology and evolution combined), and all biomes contribute to carbon loss -- each biome-specific pattern being aggravated by microbial evolution. For initially dormant soils (Fig. 5), soil C changes little in tropical (Costa Rica-type) or arctic (Alaska-type) biomes, whereas soils accrue significant carbon in the other biomes, resulting in ecology driving a global increase of soil C in initially dormant soils. Microbial evolutionary adaptation alters these patterns through a delayed, negative effect on soil C, especially in cold biomes (Maine-type and Alaska-type), which causes a reversal of the global trajectory of C stock in initially dormant soils, from early carbon gain to late carbon loss.

Discussion

Abs et al. (subm.) showed that microbial evolutionary adaptation could have large and diverse effects on the decomposition of soil organic matter, from aggravating to buffering or even reversing soil carbon loss mediated by changes in enzymatic activity. By constraining their general model with measurements of enzymatic parameters from five biomes, they concluded that microbial evolutionary adaptation to warming was more likely to cause an aggravation of soil carbon loss across biomes. Here we used Abs et al.'s model to evaluate the effect of microbial evolution on soil carbon projections at Earth terrestrial scale. Our results confirm the expectation of a significant global aggravation of soil C loss due to microbial evolution. Colder biomes contribute relatively more to the effect of evolutionary adaptation on global soil C projections. Dormant soils, in which microbial activity is very low, tend to gain carbon initially, and even more so when the local temperature reaches a threshold at which they become active. In these regions, the negative effect of evolution on soil C may not kick in until the microbial community shifts from dormant to active, and may thus be delayed by decades.

The integration of microbial models of decomposition into broad-scale ecosystem models remains challenging. Properly describing even the short-term

response of soil C dynamics to warming may raise the need to account for mechanisms such as physicochemical changes, priming, and the interaction of C and N cycles (e.g. S. Fontaine et al., 2003). In a recent study, Wieder et al. (2018) compared a first-order model (CASA-CNP) and two microbial models (MIMICS and CORPSE). The three models showed dramatically different patterns of soil carbon gains and losses despite identical litter inputs and climate forcing, with a net accumulation of soil carbon in CASA-CNP (+18.1 Pg C) and MIMICS (+24.1 Pg C), and a net loss in CORPSE (-21.7 Pg C) over the same period. Our results show that microbial evolutionary adaptation to warming may attenuate these gains or enhance the loss, and thus broaden projected ranges of soil C and increase the projections' uncertainty even further. This should not be seen as a negative outcome, as a better assessment of the uncertainties of global carbon-climate projections is a research priority (Bradford et al., 2016; Wieder et al., 2015, 2018).

Global soil carbon loss predicted by the eco-evolutionary model (Fig. 3) is the consequence of a global adaptive increase of microbial exoenzyme production (Fig. 2). Our results are thus consistent with Wieder et al.'s (2013) model including a negative dependence of microbial growth efficiency (MGE) on temperature. In our model, microorganisms pay the cost of exoenzyme production in terms of reduced growth. The global adaptive increase in exoenzyme production thus translates, in our model, in a global decline in MGE as temperature rises. Here a key difference with Wieder et al. (2013) is that this decline is an outcome of the adaptive evolutionary process, whereas Wieder et al. (2013) assumed the negative relation of MGE with temperature. The temperature sensitivity of enzyme kinetics could have further global effects that neither model has accounted for. For example, Hagerty et al. (2014) uncovered a positive effect of temperature on microbial mortality. When including this effect in their general eco-evolutionary model of decomposition, Abs et al. (subm.) found that the direction of microbial evolution in response to warming could, under some conditions, be reverted. We are currently investigating how the positive temperature-dependence of microbial mortality might alter the effect of microbial evolution on global soil C projections.

Our results highlight the importance of active vs. inactive or 'dormant' microbial populations. It is known that dormant cells are common, and sometimes dominant, in a range of ecosystems. In particular, large fractions of microorganisms may be dormant in soils (Lennon and Jones, 2011). As a general microbial trait, dormancy is expected to influence the large-scale, biogeographical processes that

structure microbial communities (Locey, 2010). Dormancy generates seed banks, which should enable the rapid recruitment of microbial populations in response to environmental change (Epstein, 2009). This points to potential long-term, large-scale effects of microbial dormancy on the response of microbial diversity and ecosystem function to global change (Lennon and Jones, 2011). Even though our model of dormancy is phenomenological (i.e. the microbial compartment is said to be dormant when there is no stable (active) microbial equilibrium), the results reported here lend weight to this view and pave the way for future studies of global ecological and evolutionary consequences of microbial dormancy.

Our goal was to evaluate the impact of evolution on projections generated by models of soil C dynamics that explicitly represent microbial biomass and exoenzyme production. Improving projections will require to overcome several shortcomings of current models, including ours. First, interactions among the carbon, nitrogen, and phosphorus cycles should be accounted for. Community-level competition for C and N sources is likely to be important for determining how microbial processes of decomposition respond to warming (Conant et al., 2011). For example, if the temperature sensitivity of key N-cycle processes are greater than some C-cycle processes, then it is possible that N availability limits microbial activity. This could influence plastic responses or evolutionary adaptations in microbial allocation to N versus C acquisition.

Furthermore, soil C-climate interaction involves timescales (year to century) over which mechanisms of soil C stabilization may not be ignored (Davidson and Janssen, 2006; Bradford et al., 2016; Abramoff et al., 2017). Soil C is stabilized by interacting with minerals (Keil & Mayer, 2014); microaggregates break down over time due to mechanical stresses or the gradual degradation of binding agents, causing carbon in chemically protected organo-mineral complexes to be slowly released (Sollins et al., 1996). So far there has been few attempts to incorporate organic-mineral interactions in microbial models of decomposition. Abramoff et al. (2018) recent work paves the way forward. They identify conditions under which their projections depart substantially from the non-microbial Century model, a long-time standard for large-scale simulations of soil C stocks. Global projections of soil carbon will be improved by using eco-evolutionary microbial models of decomposition that take slow abiotic processes of carbon stabilization into account.

Methods

Mechanistic model of microbe-enzyme decomposition and microbial adaptation to warming

We use the eco-evolutionary model of decomposition introduced in Abs et al. (subm.), derived from stochastic processes acting at the microscopic scale of microbial cells and exoenzyme, SOC, and DOC molecules (Abs, Ferriere, Leman, in prep.) The focal microbial adaptive trait is the fraction of assimilated carbon allocated to exoenzyme production, or 'exoenzyme allocation fraction', denoted by φ (the balance of assimilated carbon, $1 - \varphi$, is allocated directly to microbial growth). Competition between microbial strains differing in enzyme allocation fraction φ drives adaptive evolution. Our focus is on soil bacteria (as opposed to fungi), which typically have large population size and short generation time, thus likely to make evolution rapid on the timescale of global environmental change.

In the absence of genetic variation in φ, there is no evolution, and the system dynamics are driven by the (purely ecological) model first introduced in Allison et al. (2010), given litterfall input, leaching rates, and soil temperature, which may differ among individual locations (see below). The effect of temperature on decomposition is mediated by enzymes kinetics, with exoenzymes driving the decomposition rate, and intra-cellular enzymes involved in resource uptake and microbial biomass synthesis. As temperature changes, the model predicts how the ecological equilibrium changes. The change in equilibrium SOC is what we call the ecological (ECO) response of the ecosystem.

Assuming there is genetic variation (due to mutation) in the enzyme allocation fraction φ, The model predicts (i) the adapted value, φ^*, of the exoenzyme allocation fraction at any given temperature, given litter input and leaching rate; (ii) the adaptive response of the exoenzyme allocation fraction to temperature rise; and (iii) how this response impacts the decomposition rate and SOC stock. By comparing the full eco-evolutionary (ECOEVO) response of SOC stock to the purely ecological (ECO) response in absence of evolution (in which φ is a fixed parameter that does not change), we can evaluate the contribution of microbial evolutionary adaptation (EVO effect) to the direction and magnitude of the SOC stock response to climate warming.

Scaling up to continental ecosystems

We obtained global projections of ecosystem and evolutionary change by running the mechanistic microbial model on a grid of 1° × 1° sites across terrestrial continents. We used enzyme kinetics parameters of decomposition obtained by German et al. (2012) for five ecosystems from five contrasted 'biomes' (tropical forest in Costa Rica, grassland in California, temperate deciduous forest in West Virginia, temperate/cold coniferous forest in Maine, boreal forest in Alaska). We used the classification of terrestrial ecosystems into 13 ecoregions (excluding deserts) and clustered them into five by assigning each of them to one of the five biomes for which German et al.'s (2012) data were collected (Fig. S2).

We designed a world map of 192 points latitudinally by 288 points longitudinally, which matches the map of observed and projected soil temperature and litter input. We built the 192 x 288 raster and downloaded the geographic distribution of the 14 terrestrial ecoregions (https://worldmap.harvard.edu/data/geonode:wwf_terr_ecos_oRn), using the function "readOGR" (see code in Supplementary Material).

At each site we then parametrized the microbial decomposition model with the four kinetics parameters that German et al. (2012) measured for the corresponding biome (Fig. S3). We transformed German's exponential equations of temperature dependence into Arrhenius relationships using the same intercept values $V_{int} = 5.47$ and $K_{int} = 3.19$ for all five biomes, given that the differences between the measured values were not significant.

Soil temperature and litter flux maps

Projected soil temperature and litter input were obtained from one of the CESM models, which can be found in the PCMDI archive (http://www.cesm.ucar.edu/experiments/cesm1.0/). Following on Wieder et al. (2013), we chose the RCP8.5 scenario whose predictions span 2005 or 2006 to 2100. Among the eight ensembles available in the archive, we chose Ensemble Member #1 (as did Wieder et al. 2013), case b40.rcp8_5.1deg.001, and used the CMIP5 link. We got 27 results but narrowed them down to one by selecting the "tsl" variable (soil temperature). This returns 192 files, each one corresponding to specific variable and period of time, that we narrowed down to seven again by applying the tsl filter. We inspected the quality of the data by using the Panoply software (visualization of NetCDF data). For

example, we found that tsl_Lmon_CCSM4_rcp85_r1i1p1_200601-205002.nc and tsl_Lmon_CCSM4_rcp85_r1i1p1_205001-210012_partial.nc were interrupted after January 2008 and September 2079 respectively. We thus selected the files tsl_Lmon_CCSM4_rcp85_r1i1p1_200601-205002.nc and tsl_Lmon_CCSM4_rcp85_r1i1p1_205001-210012.nc (for some files, we downloaded a curl script that we ran from the command line). We repeated this file selection process for the second variable of interest, "fVegLitter". This is the total carbon mass flux from vegetation to litter, that we use as a proxy for litter input in our mechanistic model. We selected the data file fVegLitter_Lmon_CCSM4_rcp85_r1i1p1_200501-210012.nc, where carbon litter flux is in kg m^{-2} s^{-1} that we converted to mg cm^{-2} h^{-1} for use in our model. For both soil temperature and litter input, there is one predicted value per month (average of the number of days) and one per 11.13km (1° spatial resolution) across 192 points of latitude and 288 points of longitude.

References

1. Wieder, W. R. *et al.* Explicitly representing soil microbial processes in Earth system models: Soil microbes in earth system models. *Global Biogeochem. Cycles* **29,** 1782–1800 (2015).

2. Abs, E. & Ferriere, R. *in review* Modeling microbial dynamics and heterotrophic soil respiration – effect of climate change. In Biogeochemical Cycles: Anthropogenic and Ecological Drivers. *American Geophysical Union*
3. Zhang, X. *et al.* Assessing five evolving microbial enzyme models against field measurements from a semiarid savannah—What are the mechanisms of soil respiration pulses? *Geophys. Res. Lett.* **41,** 6428–6434 (2014).
4. Abs, E., Ferriere, R., Leman, H. *in prep* Eco-evolutionary dynamics of decomposition: microbial cooperation for diffusive goods.
5. Allison, S. D., Wallenstein, M. D. & Bradford, M. A. Soil-carbon response to warming dependent on microbial physiology. *Nat. Geosci.* **3,** 336 (2010).
6. Li, J., Wang, G., Allison, S. D., Mayes, M. A. & Luo, Y. Soil carbon sensitivity to temperature and carbon use efficiency compared across microbial-ecosystem models of varying complexity. *Biogeochemistry* **119,** 67–84 (2014).
7. German, D. P., Marcelo, K. R. B., Stone, M. M. & Allison, S. D. The Michaelis-Menten kinetics of soil extracellular enzymes in response to temperature: a cross-latitudinal study. *Glob. Chang. Biol.* **18,** 1468–1479 (2012).
8. Abs, E., Scott, S. R., Ferriere, R. *submitted* Microbial evolution reshapes soil carbon feedbacks to climate change.
9. Wieder, W. R., Bonan, G. B. & Allison, S. D. Global soil carbon projections are improved by modelling microbial processes. *Nat. Clim. Chang.* **3,** 909 (2013).
10. Wieder, W. R. *et al.* Carbon cycle confidence and uncertainty: Exploring variation among soil biogeochemical models. *Glob. Chang. Biol.* **24,** 1563–1579 (2018).
11. Allison, S. D. Modeling adaptation of carbon use efficiency in microbial communities. *Front. Microbiol.* **5,** 571 (2014).
12. Fontaine, S., Mariotti, A. & Abbadie, L. The priming effect of organic matter: a question of microbial competition? *Soil Biol. Biochem.* (2003).
13. Bradford, M. A. *et al.* Managing uncertainty in soil carbon feedbacks to climate change. *Nat. Clim. Chang.* **6,** 751 (2016).
14. Hagerty, S. B. *et al.* Accelerated microbial turnover but constant growth efficiency

with warming in soil. *Nat. Clim. Chang.* **4,** 903 (2014).

15. Lennon, J. T. & Jones, S. E. Microbial seed banks: the ecological and evolutionary implications of dormancy. *Nat. Rev. Microbiol.* **9,** 119–130 (2011).
16. Locey, K. J. Synthesizing traditional biogeography with microbial ecology: the importance of dormancy. *J. Biogeogr.* **31,** no–no (2010).
17. Epstein, S. S. Microbial awakenings. *Nature* **457,** 1083 (2009).
18. Conant, R. T. *et al.* Temperature and soil organic matter decomposition rates - synthesis of current knowledge and a way forward. *Glob. Chang. Biol.* **17,** 3392–3404 (2011).
19. Davidson, E. A. & Janssens, I. A. Temperature sensitivity of soil carbon decomposition and feedbacks to climate change. *Nature* **440,** 165–173 (2006).
20. Abramoff, R. *et al.* The Millennial model: in search of measurable pools and transformations for modeling soil carbon in the new century. *Biogeochemistry* **137,** 51–71 (2018).
21. Keil, R. G. & Mayer, L. M. Mineral matrices and organic matter. (2014).
22. Sollins, P., Homann, P. & Caldwell, B. A. Stabilization and destabilization of soil organic matter: mechanisms and controls. *Geoderma* **74,** 65–105 (1996).

End Notes

Acknowledgements We thank Abigail Swann, William Smith, William Wieder, Rachel Gallery, Pierre-Henri Gouyon, Moira Hough, Hélène Leman, Laura Meredith, and Mitch Pavao-Zuckerman for discussion. E.A. was supported by fellowships from Ecole Doctorale Frontières du Vivant and MemoLife Laboratory of Excellence (PIA-10-LBX-54). S.R.S. was supported by a grant from the Genomic Science Program of the United States Department of Energy (DOE) (DE-SC0016440) and the University of Arizona's Agnese Nelms Haury Program in Environment and Social Justice. R.F. acknowledges support from FACE Partner University Fund, CNRS Mission pour l'Interdisciplinarité, and PSL University (IRIS OCAV and PSL-University of Arizona Mobility Program).

Author contributions R.F. conceived the study. All authors developed the model. E.A. performed the analysis. E.A. and R.F. wrote the first version of the manuscript. All authors finalized the paper.

Competing interests The authors declare no competing interests.

Additional information

Supplementary figures S1-S3 are available for this paper at https://doi.org/xxx

Computer code is available for this paper at https://doi.org/xxx

Correspondence and requests for materials should be addressed to E.A. or R.F.

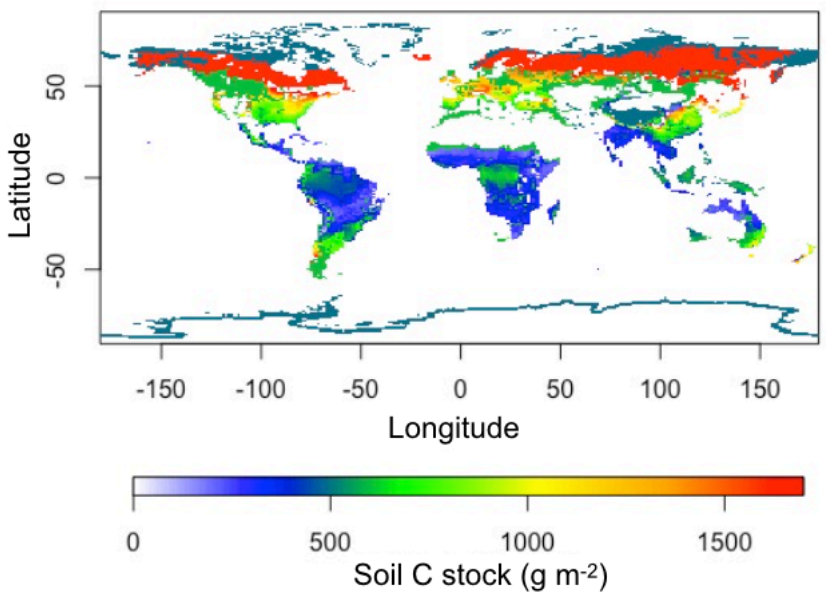

Figure 1. Initial soil carbon stocks. Soil carbon is the sum of SOC mass and microbial biomass. At each ~1° × 1° site, the enzyme allocation fraction trait, φ, takes on its value, φ^*, adapted to the local conditions (surface soil temperature and litterfall input, averaged over 15 years, from 2006 to 2021). The local carbon stock is calculated by running the corresponding microbial ecological model to equilibrium. In sites where the microbial equilibrium is unstable, we assign the observed value of the carbon stock averaged over the corresponding biome and scaled to 1 cm soil depth. See Methods for more detail.

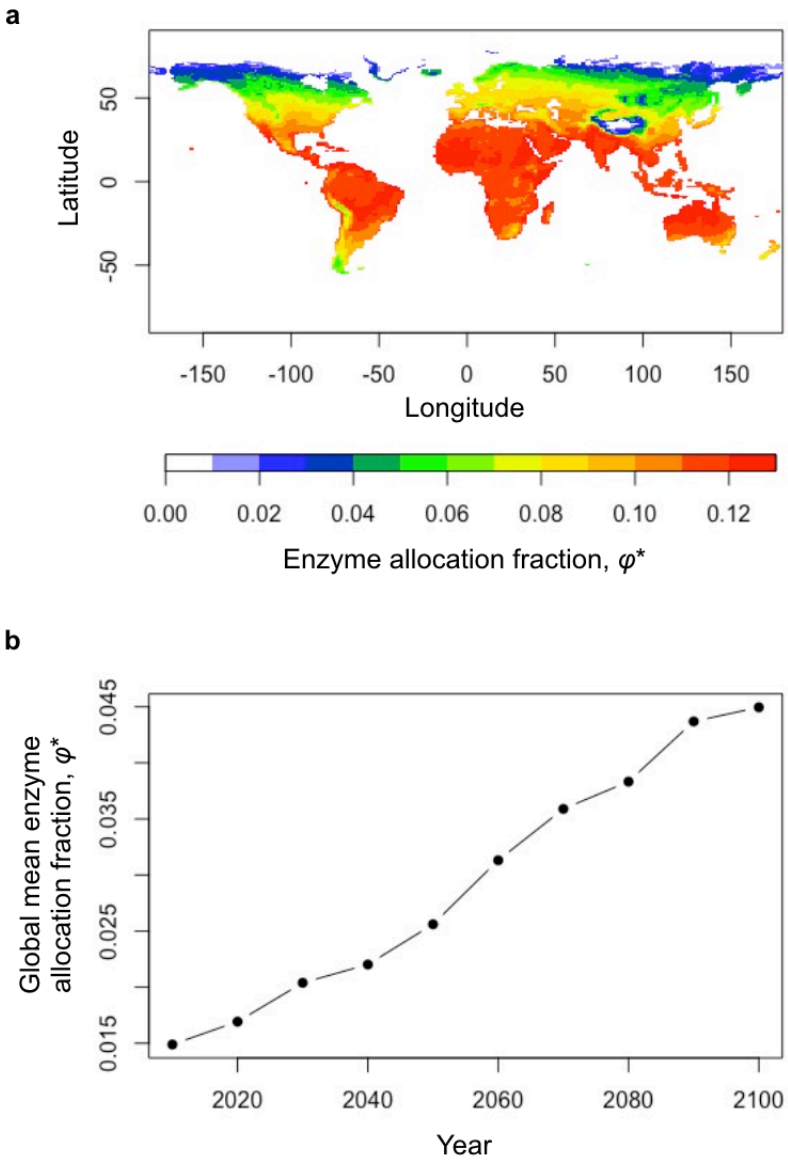

Figure 2. Adaptive evolution of the enzyme allocation fraction trait from 2010 to 2100. At each ~1° × 1° site, the enzyme allocation fraction trait, φ, takes on its value, φ^*, adapted to the local conditions (surface soil temperature and litterfall input). **a,** Spatial distribution of initial φ^* values at 1° resolution (adaptation to surface soil temperature and litterfall input averaged over 15 years, from 2006 to 2021). **b,** Global average φ^* value as a function of global mean surface soil temperature. See Methods for more detail.

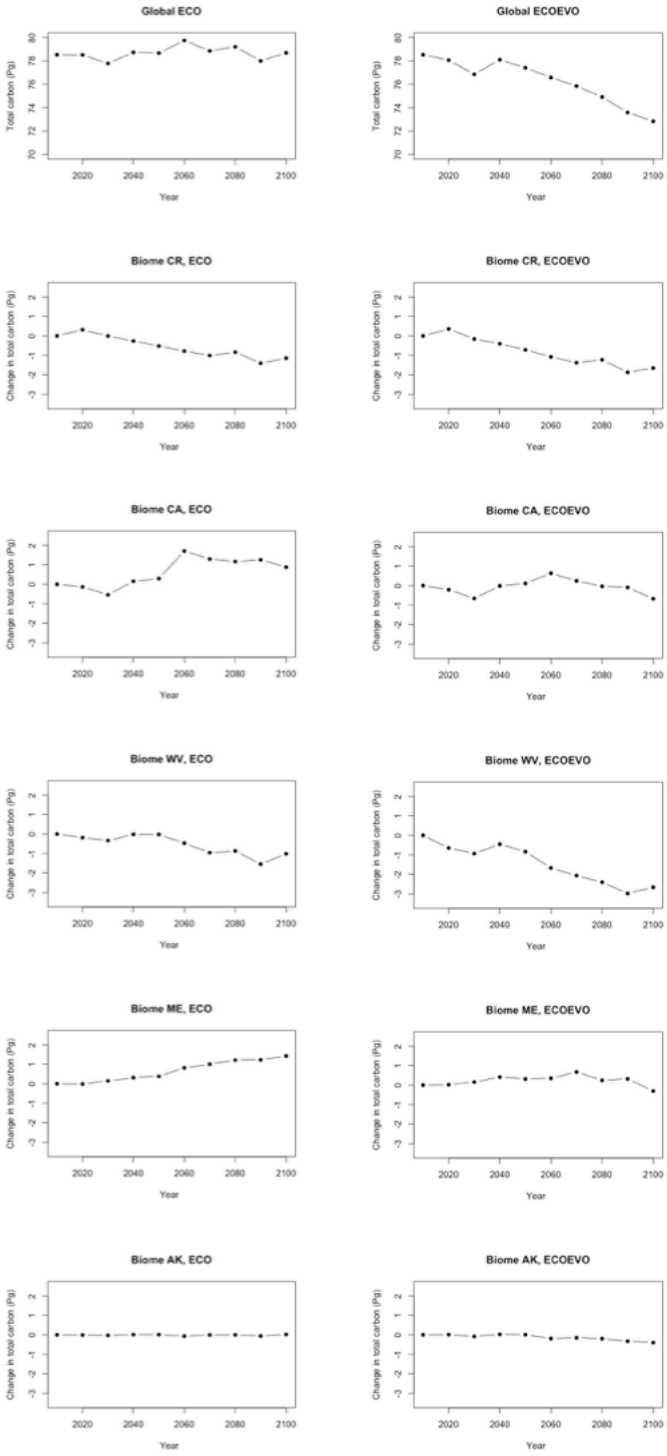

Figure 3. Global and biome-specific projections of soil carbon from 2010 to 2100. *Left*, "ECO" projections from the ecological model (no evolution; the enzyme allocation fraction trait is fixed to its value adapted to 2010 conditions). *Right*, "ECOEVO" projections from the eco-evolutionary model, including evolutionary adaptation of the enzyme allocation fraction to temperature change at each time step (monthly). See Methods for more detail.

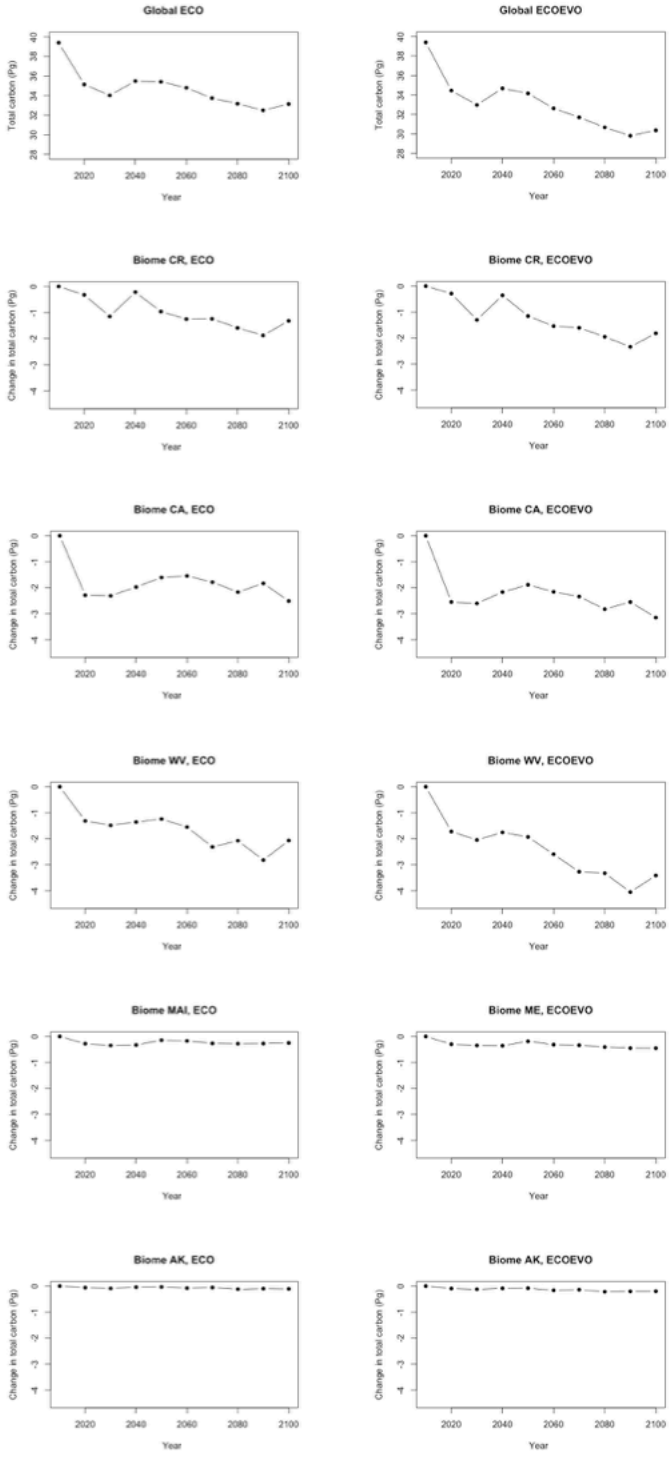

Figure 4. Global and biome-specific projections of soil carbon from 2010 to 2100 across sites that were initially microbially active. *Left*, "ECO" projections from the ecological model (no evolution; the enzyme allocation fraction trait is fixed to its value adapted to 2010 conditions). *Right*, "ECOEVO" projections from the eco-evolutionary model, including

evolutionary adaptation of the enzyme allocation fraction to temperature change at each time step (monthly). Evolutionary effect (eco-evolutionary response of soil carbon relative to the ecological response) averaged over 2020 to 2100: 28.4% in biome CR, 25.4% in biome CA, 51.5% in biome WV, 38.8% in biome ME, 111.0% in biome AK. Evolutionary effect estimated by comparing projected carbon stocks in year 2100: 37.8% in biome CR, 25.3% in biome CA, 65.2% in biome WV, 79.6% in biome ME, 82.1% in biome AK. See Methods for more detail.

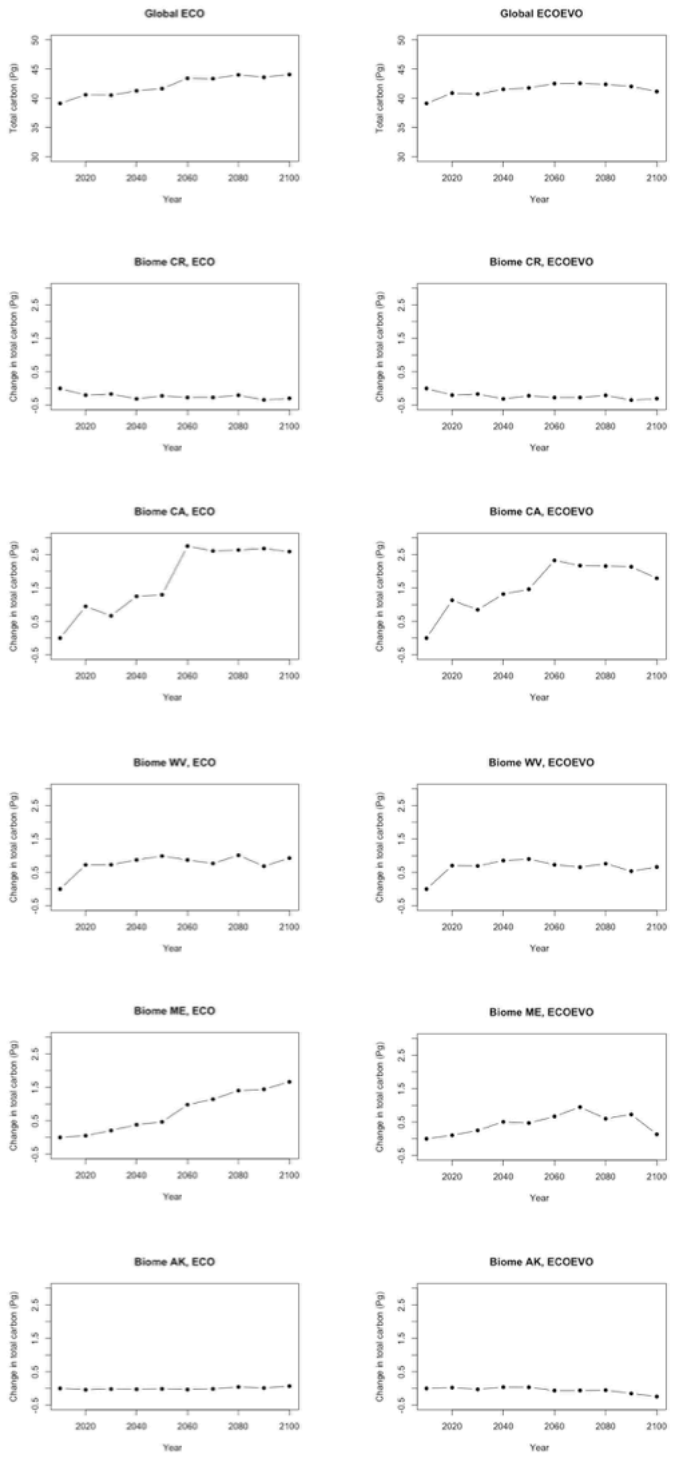

Figure 5. Global and biome-specific projections of soil carbon from 2010 to 2100 across sites that were initially microbially dormant. The initial carbon stock in each microbially dormant site is the observed value of the carbon stock averaged over the corresponding biome and scaled to 1 cm soil depth. *Left*, "ECO" projections from the ecological model (no evolution; the enzyme allocation fraction trait is fixed to its value adapted to 2010 conditions).

Right, “ECOEVO” projections from the eco-evolutionary model, including evolutionary adaptation of the enzyme allocation fraction to temperature change at each time step (monthly). See Methods for more detail.

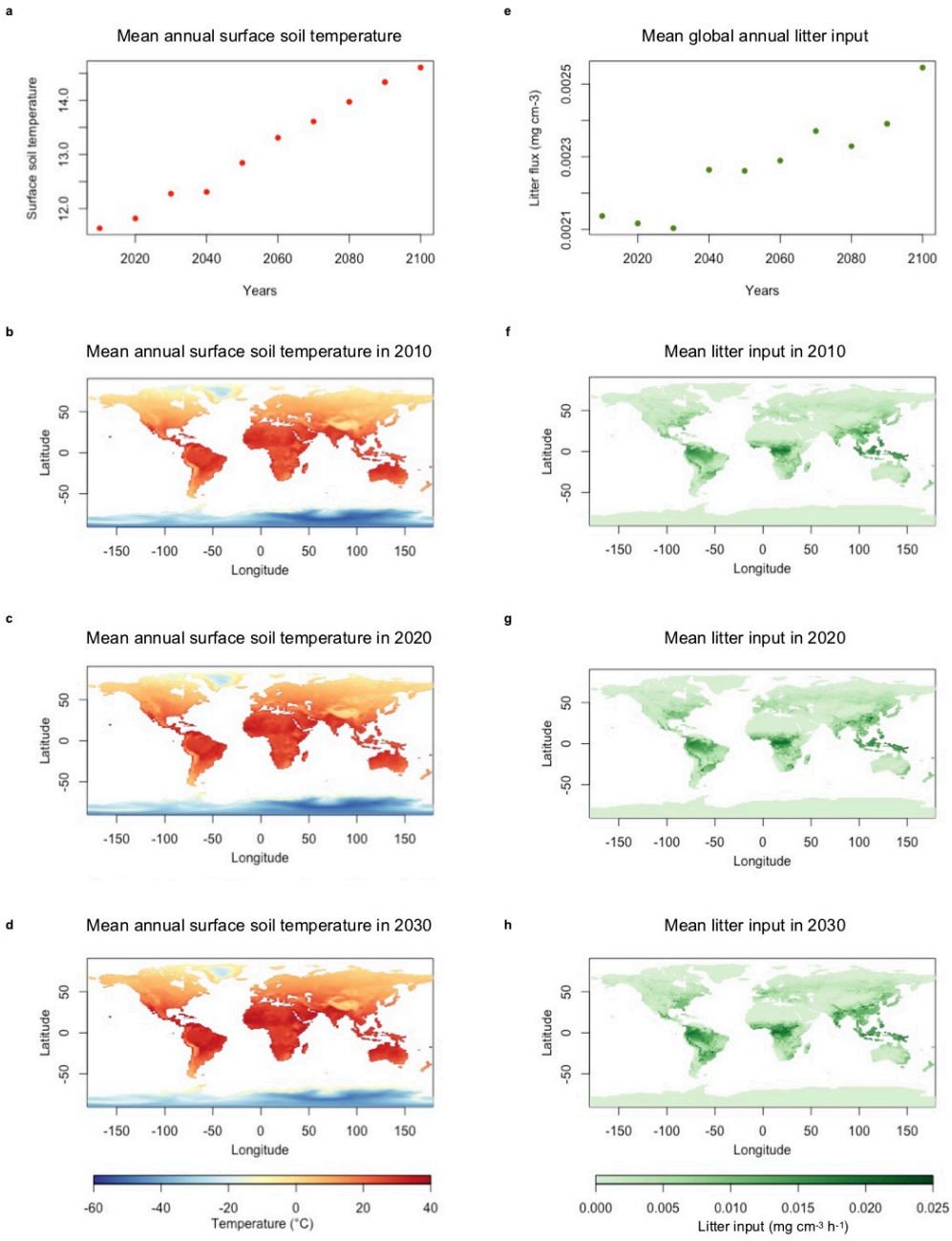

Figure S1. Model input data: projected surface soil temperature and litterfall input. Predictions from the scenario RCP8.5 of the CCSM4 model of global mean annual surface soil temperature (a-d) and litterfall input (e-h) from 2010 to 2100. See Methods for more detail.

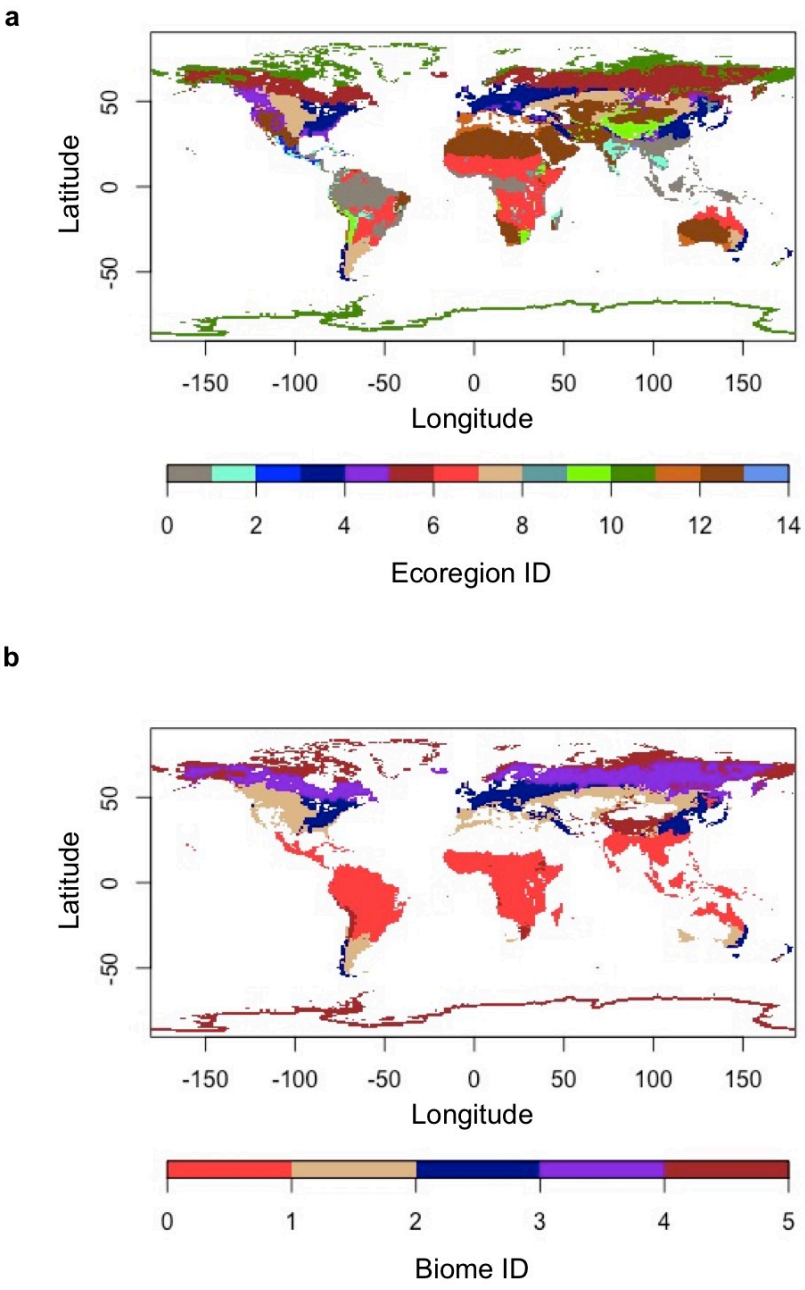

Figure S2. Earth terrestrial ecoregions (a) clustered into five biomes (b) for which enzyme kinetics parameters have been measured. The five biomes and their reference location for which enzyme kinetics were measured are tropical forest (Costa Rica), temperate grassland (California), temperate deciduous forest (West Virginia), temperate/cold coniferous forest (Maine), boreal forest/tundra (Alaska) (German et al. 2012). See Methods for more detail.

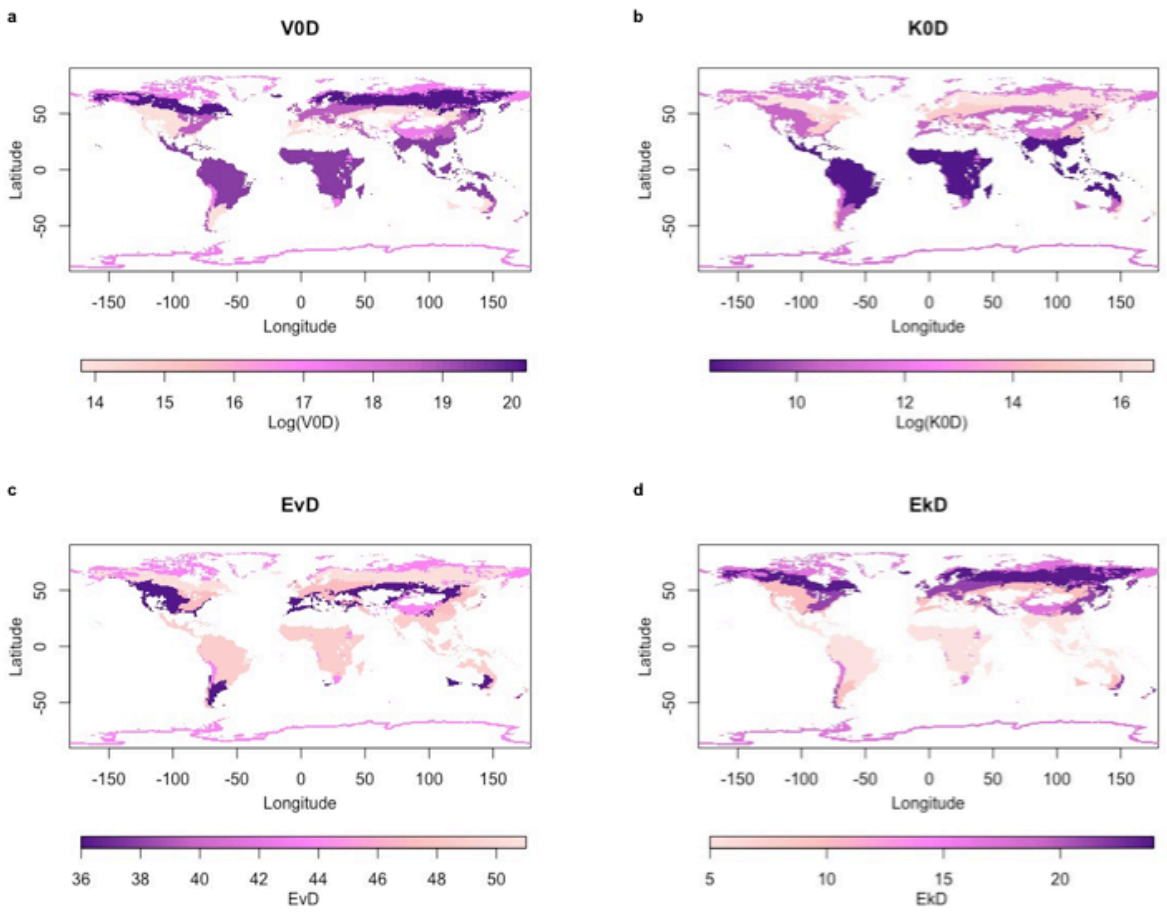

Figure S3. Biome-specific enzyme kinetics parameters. a, V0D: Arrhenius coefficient of decomposition rate. **b,** K0D : Arrhenius coefficient of decomposition half-saturation constant. **c,** EvD: activation energy of decomposition rate. **d,** EkD: activation energy of decomposition half-saturation constant. These parameters are fixed in time. See Methods for more detail.

Impact of Microbial Evolution on Soil Carbon Global Projections

Elsa Abs and Regis Ferriere

Supplementary Material: R Code used in simulations

Building the matrix of surface soil temperature from simulations data averaged over 15 years

```
#Packages
library(chron)
library(RColorBrewer)
library(lattice)
library(ncdf4)
#Open NetCDF file
ncsoiltemp = nc_open("tsl_Lmon_CCSM4_rcp85_r1i1p1_200601-205002.nc")
print(ncsoiltemp)
#Get the dimension variables (longitude, latitude, time and depth)
lon = ncvar_get(ncsoiltemp, "lon")-180
lat = ncvar_get(ncsoiltemp, "lat")
depth = ncvar_get(ncsoiltemp, "depth")
time = ncvar_get(ncsoiltemp, "time")
#Only keep 1st soil layer (surface) and transform the matrix of "soiltemp" in a 2D matrix (1 location per row, 1 monthly date per column)
B = matrix(ncvar_get(ncsoiltemp, "tsl")[,,1,], nrow = 55296, ncol = 530, byrow = FALSE)
#Average per location of surface soil temperature over 15 years (from January 2006 to December 2020 included) in °C
B2 = B[,1:180]
B3 = rowMeans(B2, na.rm=F, dims = 1)
B4 = B3-273
#Transform the list into a matrix with longitude in rows and latitude in columns
B5 = matrix(B4, nrow = 288, ncol = 192, byrow = FALSE)
B51 = B5[1:145,]
B52 = B5[146:288,]
B6 = rbind(B52,B51)
#Map Soil Temperature
par(xpd=T, mfrow=c(1,1), lwd=1, font.lab=1, font.axis=1, oma=c(3,0,0,0))
brks = seq(-60,40, by=0.1)
colfunc = colorRampPalette(c(
  "#313695","#4575b4","#74add1","#abd9e9","#e0f3f8","#ffffbf",
  "#fee090","#fdae61","#f46d43","#d73027","#a50026"))(length(brks)-1)
fields::image.plot(x=lon, y=lat, B6, ann=F, breaks=brks, horizontal=T, smallplot=c(0.16, 0.92, 0.01, 0.04),
legend.args=list(text='Temperature (°C)', side=1, font=1, line=2, cex=1), col=colfunc, xlab="Longitude",
ylab="Latitude")
mtext(side=1, text="Longitude", line=2.2, font=1)
mtext(side=2, text="Latitude", line=2.2, font=1)
title("Surface soil temperature averaged over 15 years
    (from January 2006 to December 2020 included)", outer=F)
#Save the matrix as a table
write.table(B6, file = "soilT", append = FALSE, quote = TRUE, sep = " ", dec = ".", row.names = FALSE,
col.names = FALSE)
```

Building the matrix of litter input from simulations data averaged over 15 years

```
#Packages
library(chron)
library(RColorBrewer)
library(lattice)
library(ncdf4)
#Open NetCDF file
nclitt = nc_open("fVegLitter_Lmon_CCSM4_rcp85_r1i1p1_200601-210012.nc")
print(nclitt)
#Get the dimension variables (longitude, latitude and time), with Africa placed in the center of the map
lon = ncvar_get(nclitt, "lon")-180
lat = ncvar_get(nclitt, "lat")
time = ncvar_get(nclitt, "time")
#Transform the matrix of “fVegLitter" in a 2D matrix (1 location per row, 1 monthly date per column)
A = matrix(ncvar_get(nclitt, "fVegLitter")[,,], nrow = 55296, ncol = 1140, byrow = FALSE)
#Remove absurd value
A[A > 1e+32] = NA
#Average per location of litter flux over 15 years (from January 2006 to December 2020 included) in
mg/cm3/h
A2 = A[,1:180]
A3 = rowMeans(A2, na.rm=F, dims = 1)
A4 = A3*100*3600
#Transform the list into a matrix with longitude in rows and latitude in columns
A5 = matrix(A4, nrow = 288, ncol = 192, byrow = FALSE)
A51 = A5[1:145,]
A52 = A5[146:288,]
A6 = rbind(A52,A51)
#Map litter flux matrix
par(xpd=T, mfrow=c(1,1), lwd=1, font.lab=1, font.axis=1, oma=c(3,0,0,0))
brks = seq(0,0.02, by=1e-4)
colfunc = colorRampPalette(c(
"#d9f0d3","#a6dba0","#5aae61","#1b7837","#00441b"))(length(brks)-1)
fields::image.plot(x=lon, y=lat, A6, ann=F, breaks=brks, horizontal=T, smallplot=c(0.16, 0.92, 0.01, 0.04),
legend.args=list(text='Litter flux (mg/cm3/y)',  side=1, font=1, line=2, cex=1), col=colfunc,
xlab="Longitude", ylab="Latitude")
mtext(side=1, text="Longitude", line=2.2, font=1)
mtext(side=2, text="Latitude", line=2.2, font=1)
title("Litter flux averaged over 15 years
    (from January 2006 to December 2020 included)", outer=F)
#Save the matrix as a table
write.table(A6, file = "litt15y", append = FALSE, quote = TRUE, sep = " ",  dec = ".", row.names = FALSE,
col.names = FALSE)
```

Calibrate value of leaching, eC, per biome and build global map of eC

```
#Calculate value of eC per biome
eC_CR = A6[101,91]/1100
eC_CA = A6[61,150]/1000
eC_WV = A6[77,136]/900
eC_ME = A6[46,153]/900
eC_AK = A6[17,171]/1800
#Save list of eC as a table
biomes_eC = matrix(c(eC_CR,eC_CA,eC_WV,eC_ME,eC_AK), nrow=1)
write.table(biomes_eC, file = "biomes_eC", append = FALSE, quote = TRUE, sep = " ", dec = ".",
row.names = FALSE, col.names = FALSE)
#Get biomes table
biomes_df = read.table('bio5_newreso',sep= " ",dec='.',header=F)
biomes = as.matrix(biomes_df)
#Get eC table
eCbiomes_df = read.table('biomes_eC',sep= " ",dec='.',header=F)
eCbiomes = as.matrix(eCbiomes_df)
#Convert biomes into eC
eC = biomes
#CR=1, CA=2, WV=3, ME=4, AK=5
eC[which(eC==1)] = eCbiomes[1]
eC[which(eC==2)] = eCbiomes[2]
eC[which(eC==3)] = eCbiomes[3]
eC[which(eC==4)] = eCbiomes[4]
eC[which(eC==5)] = eCbiomes[5]
#Save the matrix as a table
write.table(eC, file = "eC_table", append = FALSE, quote = TRUE, sep = " ", dec = ".", row.names = FALSE,
col.names = FALSE)
```

Building the matrix of Earth's five terrestrial biomes from Earth's 14 ecoregions map

```
#Packages
library(raster)
library(rgdal)
library(chron)
library(RColorBrewer)
library(lattice)
library(ncdf4)
#Create a raster of longitude and latitude in the same dimension as surface soil temperature and litter
flux
world = raster(nrows=192, ncols=288)
#Get file containing the terrestrial ecoregions
s1 = shapefile("~/Desktop/Abby/wwf_terr_ecos_oRn/wwf_terr_ecos_oRn")
#Transform the "biome" data from vectors to raster
```

```
biomes = rasterize(s1, world, "BIOME", fun='last', background=NA, mask=FALSE, update=FALSE,
updateValue='all', filename="", na.rm=TRUE)
#Plot map of biomes
plot(biomes)
#Remove Antarctica and Greenland biomes
biomes[biomes > 15] = NA
#Plot new map of 14 biomes
brks = seq(0, 14, by=1)
mycols = colors()[c(7,8,26,30,31,32,33,37,42,47,51,52,56,62)]
plot(biomes, breaks=brks, col=mycols)
#Convert the raster into a matrix and transpose the matrix to have the same coordinates order as for
litter flux and soil temperature
biomesmat = as.matrix(biomes)
biomesmat2 = biomesmat[ nrow(biomesmat):1, ]
biomesmat3 = t(biomesmat2)
#Plot the map from the matrix
par(xpd=T, mfrow=c(1,1), lwd=1, font.lab=1, font.axis=1, oma=c(3,0,0,0))
brks = seq(0, 14, by=1)
mycols = colors()[c(7,8,26,30,31,32,33,37,42,47,51,52,56,62)]
longit = c(1:288)-180
#Get the matrix of coordinates from the litter flux data (or soil temperature)
nclitt = nc_open("fVegLitter_Lmon_CCSM4_rcp85_r1i1p1_200501-210012.nc")
lon = ncvar_get(nclitt, "lon")-180
lat = ncvar_get(nclitt, "lat")
fields::image.plot(x=lon, y=lat, biomesmat3, ann=F, breaks=brks,
        horizontal=T, smallplot=c(0.11, 0.85, 0.01, 0.04),
        legend.args=list(text='Biome ID',
                side=1, font=1, line=2, cex=1),
        col=mycols,
        xlab="Longitude", ylab="Latitude")
mtext(side=1, text="Longitude", line=2.2, font=1)
mtext(side=2, text="Latitude", line=2.2, font=1)
title("Earth 14 terrestrial biomes", outer=F)
#Locate German's 5 locations
points(-145,64, pch = 16)
points(-70,45, pch = 16)
points(-80,39, pch = 16)
points(-115,34, pch = 16)
points(-85,8, pch = 16)
#Convert 14-biomes-Earth to 5-biomes-Earth with NA in desert biome
biomesmat5 = biomesmat3
#Decisions for clustering: CR=1, CA=2, WV=3, ME=4, AK=5
biomesmat5[which(biomesmat5==1)] = 1
biomesmat5[which(biomesmat5==2)] = 1
biomesmat5[which(biomesmat5==3)] = 1
biomesmat5[which(biomesmat5==4)] = 3
biomesmat5[which(biomesmat5==5)] = 4
biomesmat5[which(biomesmat5==6)] = 5
```

```
biomesmat5[which(biomesmat5==7)] = 1
biomesmat5[which(biomesmat5==8)] = 2
biomesmat5[which(biomesmat5==9)] = 1
biomesmat5[which(biomesmat5==10)] = 5
biomesmat5[which(biomesmat5==11)] = 5
biomesmat5[which(biomesmat5==12)] = 2
biomesmat5[which(biomesmat5==13)] = NA
biomesmat5[which(biomesmat5==14)] = 1
#Map 5-biomes-Earth
par(xpd=T, mfrow=c(1,1), lwd=1, font.lab=1, font.axis=1, oma=c(3,0,0,0))
brks = seq(0, 5, by=1)
mycols = colors()[c(33,37,30,31,32)]
fields::image.plot(x=lon, y=lat, biomesmat5, ann=F, breaks=brks,
        horizontal=T, smallplot=c(0.11, 0.85, 0.01, 0.04),
        legend.args=list(text='Biome ID',
                side=1, font=1, line=2, cex=1),
        col=mycols,
        xlab="Longitude", ylab="Latitude")
mtext(side=1, text="Longitude", line=2.2, font=1)
mtext(side=2, text="Latitude", line=2.2, font=1)
title("Earth 5 terrestrial biomes", outer=F)
#Save the matrix as a table
write.table(biomesmat5, file = "bio5_newreso", append = FALSE, quote = TRUE, sep = " ", dec = ".",
row.names = FALSE, col.names = FALSE)
```

Building the matrix of enzyme kinetic parameters from the five biomes

```
#Get table of 5 terrestrial biomes and transform it into a matrix
biomes_df = read.table('bio5_newreso',sep= " ",dec='.',header=F)
biomes = as.matrix(biomes_df)
#Convert biomes into EvD
EvD = biomes
#CR=1, CA=2, WV=3, ME=4, AK=5
EvD[which(EvD==1)] = 48.9
EvD[which(EvD==2)] = 36.1
EvD[which(EvD==3)] = 47.2
EvD[which(EvD==4)] = 50.6
EvD[which(EvD==5)] = 43.7
#Save the matrix as a table
write.table(EvD, file = "EvD_table", append = FALSE, quote = TRUE, sep = " ", dec = ".", row.names =
FALSE, col.names = FALSE)
#Convert biomes into EkD
EkD = biomes
#CR=1, CA=2, WV=3, ME=4, AK=5
EkD[which(EkD==1)] = 5.2
EkD[which(EkD==2)] = 9.7
EkD[which(EkD==3)] = 21.4
```

```
EkD[which(EkD==4)] = 23.8
EkD[which(EkD==5)] = 17
#Save the matrix as a table
write.table(EkD, file = "EkD_table", append = FALSE, quote = TRUE, sep = " ", dec = ".", row.names =
FALSE, col.names = FALSE)
#Convert biomes inro V0D
V0D = biomes
#CR=1, CA=2, WV=3, ME=4, AK=5
V0D[which(V0D==1)] = 2.8e+8
V0D[which(V0D==2)] = 1.15e+6
V0D[which(V0D==3)] = 1.34e+8
V0D[which(V0D==4)] = 5.86e+8
V0D[which(V0D==5)] = 3.07e+7
#Save the matrix as a table
write.table(V0D, file = "V0D_table", append = FALSE, quote = TRUE, sep = " ", dec = ".", row.names =
FALSE, col.names = FALSE)
#Convertir biomes en K0D
K0D = biomes
#CR=1, CA=2, WV=3, ME=4, AK=5
K0D[which(K0D==1)] = 4.5e+3
K0D[which(K0D==2)] = 3.3e+4
K0D[which(K0D==3)] = 5.3e+6
K0D[which(K0D==4)] = 1.5e+7
K0D[which(K0D==5)] = 8.7e+4
#Save the matrix as a table
write.table(K0D, file = "K0D_table", append = FALSE, quote = TRUE, sep = " ", dec = ".", row.names =
FALSE, col.names = FALSE)
#Map V0D (log scale)
V0Dlog = log(V0D)
par(xpd=T, mfrow=c(1,1), lwd=1, font.lab=1, font.axis=1, oma=c(3,0,0,0))
brks = seq(13.8,20.2, by=0.1)
colfunc = colorRampPalette(c(
  "mistyrose","rosybrown1","orchid1","orchid3","purple4"))(length(brks)-1)
fields::image.plot(x=lon, y=lat, V0Dlog, ann=F, breaks=brks,
                horizontal=T, smallplot=c(0.16, 0.92, 0.01, 0.04),
                legend.args=list(text='Log(V0D)',
                                 side=1, font=1, line=2, cex=1),
                col=colfunc,
                xlab="Longitude", ylab="Latitude")
mtext(side=1, text="Longitude", line=2.2, font=1)
mtext(side=2, text="Latitude", line=2.2, font=1)
title("V0D predicted from Biomes (Log scale)", outer=F)
#Map EvD
par(xpd=T, mfrow=c(1,1), lwd=1, font.lab=1, font.axis=1, oma=c(3,0,0,0))
brks = seq(36,51, by=0.1)
colfunc = colorRampPalette(c(
  "purple4","orchid3","orchid1","rosybrown1","mistyrose"))(length(brks)-1)
fields::image.plot(x=lon, y=lat, EvD, ann=F, breaks=brks,
```

```
            horizontal=T, smallplot=c(0.16, 0.92, 0.01, 0.04),
            legend.args=list(text='EvD',
                  side=1, font=1, line=2, cex=1),
            col=colfunc,
            xlab="Longitude", ylab="Latitude")
mtext(side=1, text="Longitude", line=2.2, font=1)
mtext(side=2, text="Latitude", line=2.2, font=1)
title("EvD from Biomes", outer=F)
#Map K0D (log scale)
K0Dlog = log(K0D)
par(xpd=T, mfrow=c(1,1), lwd=1, font.lab=1, font.axis=1, oma=c(3,0,0,0))
brks = seq(8.4,16.6, by=0.1)
colfunc = colorRampPalette(c(
  "purple4","orchid3","orchid1","rosybrown1","mistyrose"))(length(brks)-1)
fields::image.plot(x=lon, y=lat, K0Dlog, ann=F, breaks=brks,
            horizontal=T, smallplot=c(0.16, 0.92, 0.01, 0.04),
            legend.args=list(text='Log(K0D)',
                  side=1, font=1, line=2, cex=1),
            col=colfunc,
            xlab="Longitude", ylab="Latitude")
mtext(side=1, text="Longitude", line=2.2, font=1)
mtext(side=2, text="Latitude", line=2.2, font=1)
title("K0D predicted from Biomes (Log scale)", outer=F)
#Map EkD
par(xpd=T, mfrow=c(1,1), lwd=1, font.lab=1, font.axis=1, oma=c(3,0,0,0))
brks = seq(5,24, by=0.1)
colfunc = colorRampPalette(c(
  "mistyrose","rosybrown1","orchid1","orchid3","purple4"))(length(brks)-1)
fields::image.plot(x=lon, y=lat, EkD, ann=F, breaks=brks,
            horizontal=T, smallplot=c(0.16, 0.92, 0.01, 0.04),
            legend.args=list(text='EkD',
                  side=1, font=1, line=2, cex=1),
            col=colfunc,
            xlab="Longitude", ylab="Latitude")
mtext(side=1, text="Longitude", line=2.2, font=1)
mtext(side=2, text="Latitude", line=2.2, font=1)
title("EkD from Biomes", outer=F)
```

Present SOCeco predicted with fixed enzyme parameters (from biomes) and surface soil temperature and litter flux averaged over 15 years

```
#Packages
library(chron)
library(RColorBrewer)
library(lattice)
library(ncdf4)
library(rootSolve)
```

```
library(deSolve)
library(matrixcalc)
#Get surface soil temperature table
soilT_df <- read.table('soilT',sep= " ",dec='.',header=F)
soilT <- as.matrix(soilT_df)
#Get litter flux table
litt_df <- read.table('litt15y',sep= " ",dec='.',header=F)
litt <- as.matrix(litt_df)
#Get V0D table
V0D_df <- read.table('V0D_table',sep= " ",dec='.',header=F)
V0D <- as.matrix(V0D_df)
#Get EvD table
EvD_df <- read.table('EvD_table',sep= " ",dec='.',header=F)
EvD <- as.matrix(EvD_df)
#Get K0D table
K0D_df <- read.table('K0D_table',sep= " ",dec='.',header=F)
K0D <- as.matrix(K0D_df)
#Get EkD table
EkD_df <- read.table('EkD_table',sep= " ",dec='.',header=F)
EkD <- as.matrix(EkD_df)
#Fixed parameter values
eC = 1e-5
eD = 1e-2
dM = 2e-4
dZ = 2e-3
V0U = 1e+5
EvU = 38
K0U = 1.6e+3
EkU = 21
gM = 0.31
gZ = 0.4
phieco = 0.1
#Mathematical expression that does not depend on any matrix
deltaeco = 1 - (1-phieco)*gM - phieco*gZ
#Initialization
AA = matrix(0L, nrow=288, ncol=192)
VmD = AA
KmD = AA
VmU = AA
KmU = AA
K1 = AA
K2 = AA
K3 = AA
K4 = AA
K5 = AA
K6 = AA
deltaMeco = AA
deltaZeco = AA
```

```
Ceco = AA
Deco = AA
Meco = AA
Zeco = AA
param = c(0,0,0,0,0,0,0,0,0,0,0,0)
eig = c(0,0,0,0)
Csol = AA
#Initialization for the system of differential equations
ICp = 0
VmDp = 0
KmDp = 0
eCp = 0
eDp = 0
dMp = 0
dZp = 0
VmUp = 0
KmUp = 0
gMp = 0
gZp = 0
phiecop = 0
#Differential equations of the model
eqn <- function (t, state, pars)
{
  with (as.list(c(state, pars)),  {
    dSOC <- ICp - VmDp*SOC*ENZ / (KmDp+SOC) - eCp*SOC
    dDOC <- VmDp*SOC*ENZ / (KmDp+SOC) - VmUp*DOC*MBC / (KmUp+DOC) - eDp*DOC + dZp*ENZ +
dMp*MBC
    dMBC <- gMp*(1-phiecop)*VmUp*DOC*MBC / (KmUp+DOC) - dMp*MBC
    dENZ <- gZp*phiecop*VmUp*DOC*MBC / (KmUp+DOC) - dZp*ENZ
    list(c(dSOC, dDOC, dMBC, dENZ))
  })
}
#Calculation of SOC stock
for(i in 1:dim(AA)[1]) {
  for(j in 1:dim(AA)[2]) {
    #Calculation of VmD, KmD, VmU, KmU
    VmD[i,j] = V0D[i,j]*exp(-EvD[i,j]/(8.314e-3*(soilT[i,j]+273)))
    KmD[i,j] = K0D[i,j]*exp(-EkD[i,j]/(8.314e-3*(soilT[i,j]+273)))
    VmU[i,j]= V0U*exp(-EvU/(8.314e-3*(soilT[i,j]+273)))
    KmU[i,j] = K0U*exp(-EkU/(8.314e-3*(soilT[i,j]+273)))
    #Calculation of intermediary mathematical expressions
    K1[i,j] = (1-phieco)*gM*VmU[i,j] - dM
    K2[i,j] = eC*KmD[i,j]*K1[i,j] - eD*KmU[i,j]*dM
    K3[i,j] = (phieco*gZ*VmD[i,j] - dZ*deltaeco)*K1[i,j]
    K4[i,j] = K3[i,j]*(litt[i,j]-eC*KmD[i,j]) + phieco*gZ*VmD[i,j]*K2[i,j]
    K5[i,j] = K3[i,j]*K1[i,j]*deltaeco*dZ*litt[i,j]*eC*KmD[i,j]
    deltaMeco[i,j] = 2*dZ*deltaeco*K2[i,j]
    deltaZeco[i,j] = -2*dZ*deltaeco*K2[i,j]
```

```
   #Condition 1: NA stays NA
   if (is.na(K4[i,j]^2 - 4*K5[i,j]) == TRUE) {
    Csol[i,j] = NA
   }else{
    #Condition 2: steady states have to be non imaginary
    if (K4[i,j]^2 - 4*K5[i,j] >= 0) {
     #Calculation of Meco, Zeco, Ceco, Deco
     Ceco[i,j] = (K4[i,j] - (K4[i,j]^2 - 4*K5[i,j])^(1/2)) / (2*eC*K3[i,j])
     Deco[i,j] = dM*KmU[i,j] / K1[i,j]
     Meco[i,j] = (gM*(1-phieco))*(K4[i,j] - deltaMeco[i,j] + (K4[i,j]^2 - 4*K5[i,j])^(1/2)) /
(2*dM*K3[i,j]*deltaeco)
     Zeco[i,j] = (gZ*phieco)*(K4[i,j] + deltaZeco[i,j] + (K4[i,j]^2 - 4*K5[i,j])^(1/2)) / (2*dZ*K3[i,j]*deltaeco)
     param = c(eCp = eC, eDp = eD, dMp = dM, dZp = dZ, VmUp = VmU[i,j],
           KmUp = KmU[i,j], gMp = gM, gZp = gZ, phiecop = phieco,
           ICp = litt[i,j], VmDp = VmD[i,j], KmDp = KmD[i,j])
     #Meco, Zeco, Ceco, Deco have to be positive and all the real parts of the eigenvalues negative
     if (Ceco[i,j] >= 0 & Deco[i,j] >= 0 & Meco[i,j] >= 0 & Zeco[i,j] >= 0 &
        all(Re(eigen(jacobian.full(y = c(SOC = Ceco[i,j], DOC = Deco[i,j], MBC = Meco[i,j], ENZ = Zeco[i,j]),
                    func = eqn, parms = param))$values) <= 0)) {
      Csol[i,j] = Ceco[i,j]
     } else {
      Csol[i,j] = litt[i,j] / eC
     }
    }
    else {
     Csol[i,j] = litt[i,j] / eC
    }
   }
  }
}
#Map of present SOC stock predicted by the ECO model (with simulations data averaged over 15 years)
in g/m2
Csolu = Csol*10
#Get the matrix of coordinates from the litter flux data (or soil temperature)
nclitt = nc_open("fVeglitter_Lmon_CCSM4_rcp85_r1i1p1_200501-210012.nc")
lon = ncvar_get(nclitt, "lon")-180
lat = ncvar_get(nclitt, "lat")
par(xpd=T, mfrow=c(1,1), lwd=1, font.lab=1, font.axis=1, oma=c(3,0,0,0))
#Color function scaled using the SOCecoevo predictions
brks = seq(0, 6723, by=0.1)
colfunc = colorRampPalette(c(
  "white","blue","green","yellow","orange","red"))(length(brks)-1)
fields::image.plot(x=lon, y=lat, Csolu, ann=F, breaks=brks,
           horizontal=T, smallplot=c(0.16, 0.92, 0.01, 0.04),
           legend.args=list(text='SOCeco (g m-2)',
                  side=1, font=1, line=2, cex=1),
           col=colfunc,
           xlab="Longitude", ylab="Latitude")
```

```
mtext(side=1, text="Longitude", line=2.2, font=1)
mtext(side=2, text="Latitude", line=2.2, font=1)
title("SOCeco with fixed enzyme parameters (from biomes)
    and litter flux and surface soil temperature
    averaged over 2006-2021", outer=F)
```

Present SOCecoevo predicted with fixed enzyme parameters (from biomes) and surface soil temperature and litter flux averaged over 15 years

Same packages and tables to get as for SOCeco

```
#Fixed parameter values
eC = 1e-5
eD = 1e-2
dM = 2e-4
dZ = 2e-3
V0U = 1e+5
EvU = 38
K0U = 1.6e+3
EkU = 21
gM = 0.31
gZ = 0.4
c0 = 1.17
#Initialization
AA = matrix(0L, nrow=288, ncol=192)
VmD = AA
KmD = AA
VmU = AA
KmU = AA
phiecoevo = AA
deltaecoevo = AA
K1 = AA
K2 = AA
K3 = AA
K4 = AA
K5 = AA
K6 = AA
deltaMecoevo = AA
deltaZecoevo = AA
Cecoevo = AA
Decoevo = AA
Mecoevo = AA
Zecoevo = AA
param = c(0,0,0,0,0,0,0,0,0,0,0,0)
eig = c(0,0,0,0)
Csol = AA
#Initialization for the system of differential equations
ICp = 0
```

```
VmDp = 0
KmDp = 0
eCp = 0
eDp = 0
dMp = 0
dZp = 0
VmUp = 0
KmUp = 0
gMp = 0
gZp = 0
phip = 0
#Differential equations of the model
eqn <- function (t, state, pars)
{
  with (as.list(c(state, pars)),  {
    dSOC <- ICp - VmDp*SOC*ENZ / (KmDp+SOC) - eCp*SOC
    dDOC <- VmDp*SOC*ENZ / (KmDp+SOC) - VmUp*DOC*MBC / (KmUp+DOC) - eDp*DOC + dZp*ENZ +
dMp*MBC
    dMBC <- gMp*(1-phip)*VmUp*DOC*MBC / (KmUp+DOC) - dMp*MBC
    dENZ <- gZp*phip*VmUp*DOC*MBC / (KmUp+DOC) - dZp*ENZ
    list(c(dSOC, dDOC, dMBC, dENZ))
  })
}
#Calculation of SOC stock
for(i in 1:dim(AA)[1]) {
  for(j in 1:dim(AA)[2]) {
    #Calculation of VmD, KmD, VmU, KmU
    VmD[i,j] = V0D[i,j]*exp(-EvD[i,j]/(8.314e-3*(soilT[i,j]+273)))
    KmD[i,j] = K0D[i,j]*exp(-EkD[i,j]/(8.314e-3*(soilT[i,j]+273)))
    VmU[i,j] = V0U*exp(-EvU/(8.314e-3*(soilT[i,j]+273)))
    KmU[i,j] = K0U*exp(-EkU/(8.314e-3*(soilT[i,j]+273)))
    #Calculation of phiecoevo
    phiecoevo[i,j] = 1 - dM / (VmU[i,j]*gM) - 1/c0
    #Calculation of delatecoevo
    deltaecoevo[i,j] = 1 - (1-phiecoevo[i,j])*gM - phiecoevo[i,j]*gZ
    #Calculation of intermediary mathematical expressions
    K1[i,j] = (1-phiecoevo[i,j])*gM*VmU[i,j] - dM
    K2[i,j] = eC*KmD[i,j]*K1[i,j] - eD*KmU[i,j]*dM
    K3[i,j] = (phiecoevo[i,j]*gZ*VmD[i,j] - dZ*deltaecoevo[i,j])*K1[i,j]
    K4[i,j] = K3[i,j]*(litt[i,j]-eC*KmD[i,j]) + phiecoevo[i,j]*gZ*VmD[i,j]*K2[i,j]
    K5[i,j] = K3[i,j]*K1[i,j]*deltaecoevo[i,j]*dZ*litt[i,j]*eC*KmD[i,j]
    deltaMecoevo[i,j] = 2*dZ*deltaecoevo[i,j]*K2[i,j]
    deltaZecoevo[i,j] = -2*dZ*deltaecoevo[i,j]*K2[i,j]
    #Condition 1: NA stays NA
    if (is.na(K4[i,j]^2 - 4*K5[i,j]) == TRUE) {
      Csol[i,j] = NA
    }else{
      #Condition 2: steady states have to be non imaginary
```

```
    if (K4[i,j]^2 - 4*K5[i,j] >= 0) {
      #Meco, Zeco, Ceco, Deco have to be positive and all the real parts of the eigenvalues negative
      Cecoevo[i,j] = (K4[i,j] - (K4[i,j]^2 - 4*K5[i,j])^(1/2)) / (2*eC*K3[i,j])
      Decoevo[i,j] = dM*KmU[i,j] / K1[i,j]
      Mecoevo[i,j] = (gM*(1-phiecoevo[i,j]))*(K4[i,j] - deltaMecoevo[i,j] + (K4[i,j]^2 - 4*K5[i,j])^(1/2)) /
(2*dM*K3[i,j]*deltaecoevo[i,j])
      Zecoevo[i,j] = (gZ*phiecoevo[i,j])*(K4[i,j] + deltaZecoevo[i,j] + (K4[i,j]^2 - 4*K5[i,j])^(1/2)) /
(2*dZ*K3[i,j]*deltaecoevo[i,j])
      param = c(eCp = eC, eDp = eD, dMp = dM, dZp = dZ, VmUp = VmU[i,j],
            KmUp = KmU[i,j], gMp = gM, gZp = gZ, phip = phiecoevo[i,j],
            ICp = litt[i,j], VmDp = VmD[i,j], KmDp = KmD[i,j])
      if (Cecoevo[i,j] >= 0 & Decoevo[i,j] >= 0 & Mecoevo[i,j] >= 0 & Zecoevo[i,j] >= 0 &
        all(Re(eigen(jacobian.full(y = c(SOC = Cecoevo[i,j], DOC = Decoevo[i,j], MBC = Mecoevo[i,j], ENZ =
Zecoevo[i,j]),
                           func = eqn, parms = param))$values) <= 0)) {
       Csol[i,j] = Cecoevo[i,j]
      } else {
       Csol[i,j] = litt[i,j] / eC
      }
    }
    else {
      Csol[i,j] = litt[i,j] / eC
    }
   }
  }
}
#Map of present SOC stock predicted by the ECOEVO model (with simulations data averaged over 15
years) in g/m2
Csolu = Csol*10
#Get the matrix of coordinates from the litter flux data (or soil temperature)
nclitt = nc_open("fVeglitter_Lmon_CCSM4_rcp85_r1i1p1_200501-210012.nc")
lon = ncvar_get(nclitt, "lon")-180
lat = ncvar_get(nclitt, "lat")
par(xpd=T, mfrow=c(1,1), lwd=1, font.lab=1, font.axis=1, oma=c(3,0,0,0))
brks = seq(0, 6723, by=0.1)
colfunc = colorRampPalette(c(
  "white","blue","green","yellow","orange","red"))(length(brks)-1)
fields::image.plot(x=lon, y=lat, Csolu, ann=F, breaks=brks,
            horizontal=T, smallplot=c(0.16, 0.92, 0.01, 0.04),
            legend.args=list(text='SOCecoevo (g m-2)',
                        side=1, font=1, line=2, cex=1),
            col=colfunc,
            xlab="Longitude", ylab="Latitude")
mtext(side=1, text="Longitude", line=2.2, font=1)
mtext(side=2, text="Latitude", line=2.2, font=1)
title("SOCecoevo with fixed enzyme parameters
    and litter flux and surface soil temperature
    averaged over 2006-2021", outer=F)
```